UNIVERSITY OF SOUTHAMPTON

FACULTY OF NATURAL AND ENVIRONMENTAL SCIENCES

School of Chemistry

Lithium/Sulfur Batteries: An Electrochemical Study

by

Saddam Mohammed Al-Mahmoud

Thesis for the degree of Doctor of Philosophy

July_2015

UNIVERSITY OF SOUTHAMPTON

ABSTRACT

FACULTY OF NATURAL AND ENVIRONMENTAL SCIENCES

School of Chemistry

Thesis for the degree of Doctor of Philosophy

LITHIUM/SULFUR BATTERIES: AN ELECTROCHEMICAL STUDY

Saddam Mohammed Al-Mahmoud

The lithium/sulfur battery has been investigated as an attractive candidate for the rechargeable energy storage system, since it can potentially deliver a much higher energy than a typical lithium-ion battery of the same weight. In this work, sulfur/acetylene black composite electrodes were prepared by the ball milling method and studied cells with various electrolyte systems. A significant impact of the electrolyte viscosity on the electrochemical performance of the cells was explained in terms of the electrolyte penetration into the sulfur electrode structure, the diffusion rate of lithium salts and the dissolution rate of the solid active materials. Sulfur/acetylene black (AB) composites were also prepared using a direct precipitation method. The smaller particles of sulfur, as well as the well-distributed AB on the surface of sulfur particles resulting from the precipitation method was found to provide a more uniform and conductive S/AB composite with a larger surface area. The resulting electrodes showed less degradation on cycling than those prepared by milling method.

A simple quantitative one-dimensional model of the initial self-discharge has been developed in terms of diffusion of a polysulfide shuttle species. Despite the simplicity of the model, it reproduces very well the decrease in the open circuit potential of the cells under a range of experimental conditions (varying the number of separators between the electrodes, the amount of AB in the sulfur electrode and the pre-saturation of the electrolyte with sulfur). The model provides a detailed understanding of the mechanism of self-discharge, quantifying the two main causes of sulfur loss from the positive electrode: dissolution followed by diffusion down a concentration gradient and direct reaction with polysulfides arriving from the lithium electrode.

Galvanostatic Intermittent Transient Technique (GITT) measurements were conducted to study the diffusion behaviour in Li/S cells. Analysis of the transient voltage change during and after current pulses was performed at different states of discharge/charge. The relaxation time was optimised to avoid errors due to poor equilibration at short times and self-discharge during longer periods.

Finally, the effect of the shuttle reaction on the electrochemical performance of Li/S cells was investigated using a lithium ion conducting glass ceramic (LICGC) separator in an effort to eliminate the self-discharge. This resulted in a higher discharge capacity and more accurate GITT results, showing that better controlled diffusion conditions can be achieved in a Li/S cell containing LICGC separator.

Table of Contents

List of tables

List of figures

DECLARATION OF AUTHORSHIP

I, Saddam Mohammed Al-Mahmoud declare that this thesis and the work presented in it are my own and has been generated by me as the result of my own original research.

Lithium/sulfur batteries: an electrochemical study

I confirm that:

1. This work was done wholly or mainly while in candidature for a research degree at this University;
2. Where any part of this thesis has previously been submitted for a degree or any other qualification at this University or any other institution, this has been clearly stated;
3. Where I have consulted the published work of others, this is always clearly attributed;
4. Where I have quoted from the work of others, the source is always given. With the exception of such quotations, this thesis is entirely my own work;
5. I have acknowledged all main sources of help;
6. Where the thesis is based on work done by myself jointly with others, I have made clear exactly what was done by others and what I have contributed myself;
7. None of this work has been published before submission.

Signed: .....

Date:.....

Acknowledgements

"In the Name of Allah, the Most Beneficent, the Most Merciful"

I would like to express my deep gratitude to my research supervisor Professor John R. Owen, for his enthusiastic encouragement and valuable and constructive suggestions during the planning and development of this research work. Without his supervision and constant help this dissertation would not have been possible. I would also like to offer my very great appreciation to my co-supervisor Dr Nuria Garcia-Araez, for her professional guidance and valuable help and advice during this project.

Special thanks should be given to Dr Andrew L. Hector for his useful and constructive recommendations and to Dr Guy Denuault for his help in doing the simulations used in this work. I am particularly grateful for the assistance given by Mrs Chun Borodzicz during the application and the registration at the university.

My greatest thanks are also extended to my colleagues in the Owen group. The assistance and advice provided by them were greatly appreciated. I take this opportunity to express gratitude to all of the School of Chemistry members for their help and support. I would also like to gratefully acknowledge the Higher Committee for Education Development in Iraq (HCED) for their financial support, during the majority of this work.

Finally, I owe a debt of gratitude to my mother, my wife, my lovely daughters, and all my family members who provided their support and encouragement throughout my study.

Definitions and Abbreviations

AB	Acetylene Black
CV	Cyclic voltammetry
DMC	Dimethyl carbonate
DME	1,2-dimethoxyethane
DOD	Depth of discharge
DOL	1,3-dioxolane
EC	Ethylene carbonate
EMS	Ethyl methyl sulfone
EIS	Electrochemical impedance spectroscopy
GF	Glass fibre
GITT	Galvanostatic intermittent titration technique
Li/S	Lithium/sulfur
$LiNO_3$	Lithium nitrate
LICGC	Lithium ion conducting glass ceramic
$LiCF_3SO_3$	Lithium trifluoromethanesulfonate
$LiClO_4$	Lithium perchlorate
$LiCoO_2$	Lithium cobalt oxide
$LiFePO_4$	Lithium iron phosphate
$LiPF_6$	Lithium hexafluorophosphate
LiTFSI	Lithium bis(Trifluoromethanesulfonyl)Imide
MCF	Mesoporous carbon foams
MPG	Multichannel potentiostat galvanostat
MWCNTs	Multi walled carbon nanotubes

OCV	Open circuit voltage
PAN	Polyacrilonitrile
PANI	Polyaniline
PC	Propylene carbonate
PPY	Polypyrrole
PTFE	Polytetrafluoroethylene
PTH	Polythiophene
PV	Photovoltaic
rpm	Round per minute
(s)	Solid
(soln.)	Solution
SEI	Solid electrolyte interface
SEM	Scanning electron microscopy
TEGDME	Tetraethylene glycol dimethyl ether
THF	Tetrahydrofuran
TX-100	Triton X-100
wt	Weight
wt%	Weight ratio

Chapter 1:

Aims, Introduction and Background

1.1 Aims and objectives

The aim of this project was to advance the technology of ambient temperature, non-aqueous lithium/sulfur batteries by improving understanding of the underlying science. The objectives were

- to investigate the discharge performance of lithium/sulfur cells in different electrolyte systems based on a binary organic solvents mixture, and to better understand how the electrolyte component affects the electrochemical performance for the lithium/sulfur battery.
- to investigate the effects of different methods to prepare the sulfur/acetylene black electrode composite in order to enhance the electrochemical stability and cycle life performance of the battery.
- to investigate the shuttle mechanism of the battery self-discharge using a simple quantitative model that incorporates 1-D diffusion of the shuttle species and thus better understand of the main causes of sulfur lost at the positive electrode.
- to study the lithium/sulfur cells using GITT technique, by performing discharge with current interruptions while measuring the potential *vs.* time throughout, and analysing the resulting transients to categorize the changes during discharge.
- to investigate the use of lithium ion conducting glass ceramic separator in order to prevent the self-discharge and to better understand of the electrochemical performance for the lithium sulfur battery.

1.2 Lithium ion batteries

1.2.1 Background

Since the middle of the last century, the growing global demand for energy, the concern about the depletion of traditional energy sources, such as oil, coal and natural gas, and the environmental impacts resulting from their use, have led to improved alternative sources of energy which are renewable and non-harmful to the environment such as wind and solar energy. The low costs of production and maintenance, simple operation, high efficiency and long lifetime are the most unique requirements for storage systems used with renewable energy applications such as solar.[1] To fulfil these requirements, work began on the development of different types of batteries such as lead-acid and lithium ion batteries.[2]

Rydh & Sanden stated that the energy required for production and transport of lithium ion batteries is less than that for lead-acid batteries.[3] The reason is that the specific energy (the energy stored per unit weight) of lead-acid batteries is small relative to that for lithium ion batteries, because the low atomic weight and higher voltage of lithium leads to higher specific energy. Moreover, lifetimes of lead-acid batteries are limited and less than that for lithium ion batteries, which means that lead-acid batteries should be replaced more often, resulting in raising the cost of production and transportation. In addition, the lithium ion batteries has less loss of energy, i.e. the highest energy efficiency (charge-discharge) compared with all other types of batteries.[2] A low efficiency will increase the cost because low battery efficiency results in a larger PV array and charger.[3]

The low cost and the availability of lead-acid batteries around the world make them the most common batteries in the renewable energy applications,[2] however, the low specific energy and lifetime has lead researchers to look for alternative batteries that can meet these requirements. Lithium ion batteries are considered as one of the most promising electrochemical storage systems. Due to high specific capacity and long lifetime (for example $LiFePO_4$ have a theoretical capacity of 170 $mAh.g^{-1}$),[4–7] lithium ion batteries can be coupled to renewable energy sources like solar and wind,[8,9] and to power the

next generation of portable electronic devices including laptops and mobile phones, as well as power systems for electric vehicle applications.[10]

Lithium metal, due to its highest specific capacity, had been used in the earliest compositions of rechargeable lithium cells as the negative electrode materials with chalcogenides as positives.[5] Irregular precipitation of metallic lithium on the negative electrode during cycling led to generation of lithium dendrites. Dendrite growth on the lithium surface could penetrate the separator and resulting in short circuiting of the cell.[11] In order to solve the safety concern arises from lithium dendrite formation, research was shifted towards replacing lithium metal electrode by an insertion material that can provide a host for lithium ions. This can be represented in Figure 1.1, which shows clearly the dendrite formation at the surface of lithium metal using the metallic lithium electrode (a), and the effect of replacing lithium metal by an insertion material to eliminate the dendrite growth (b).

Lithium cobalt oxide ($LiCoO_2$) as a positive electrode with carbon as a negative electrode is the first commercial rechargeable lithium ion battery which was introduced by Sony in 1991.[12] The expression lithium-ion battery refers to a battery in which the mobile lithium ions exchange between two host lattices in the positive and negative electrodes.

$LiCoO_2$ was used as the positive electrode in the most common rechargeable lithium ion batteries that was widely used in the market. The toxicity and high cost of elemental cobalt led to a search for other positive insertion compounds such as lithium iron phosphate ($LiFePO_4$), which considered to be the most attractive candidate as a cathode for rechargeable lithium ion batteries, due to its low cost, nontoxicity and environmentally acceptance.[13]

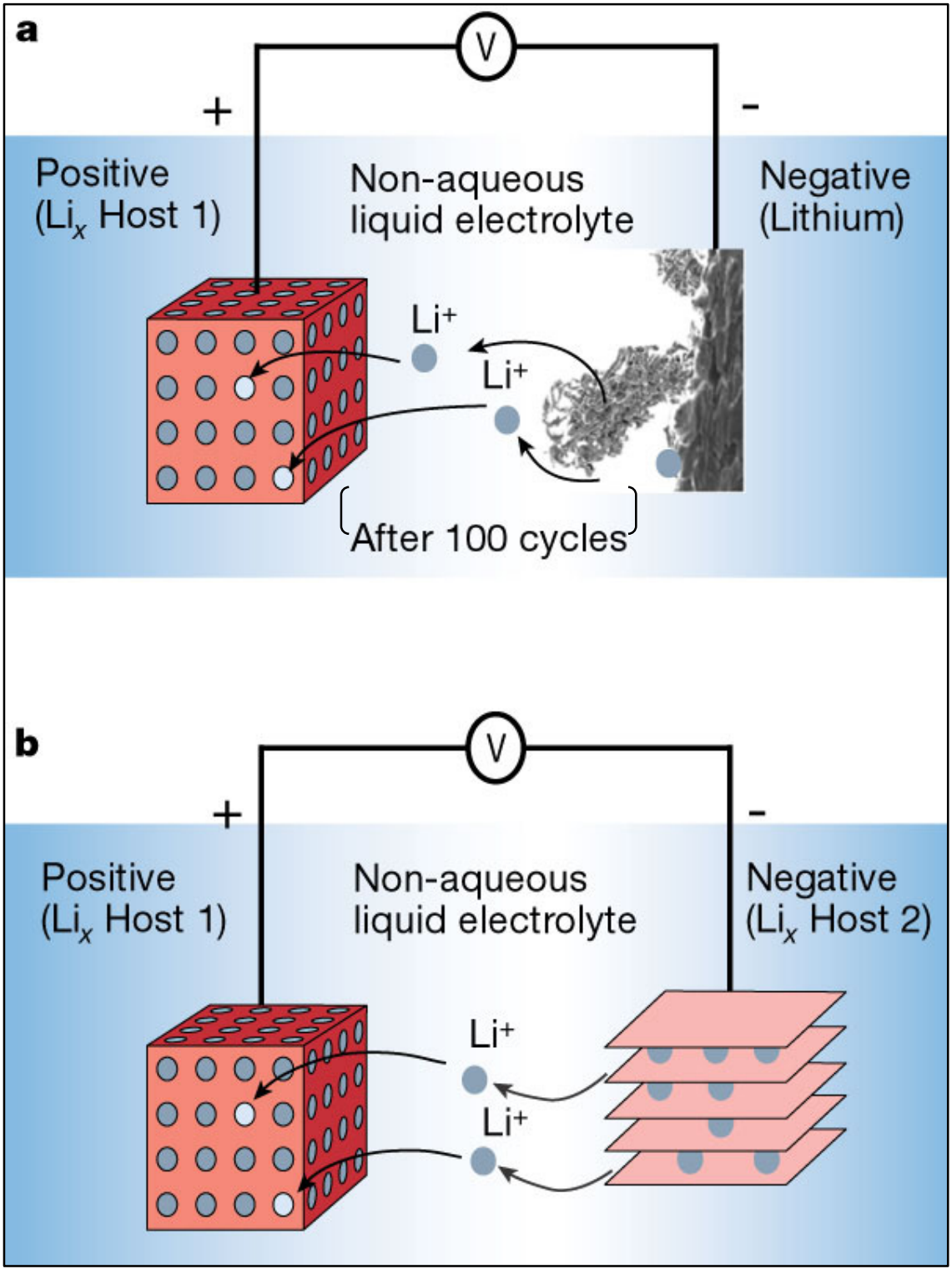

Figure 1.1 Schematic representation of (a) Rechargeable Li metal battery, and (b) Rechargeable Li ion battery, showing the occurrence and the avoidance of dendritic of lithium plating in the former. Reproduced from ref.[8] with permission from Macmillan Publishers Ltd.

1.2.2 General cell chemistry

Rechargeable lithium ion batteries consists of a positive electrode formed by a lithium transition-metal oxide or phosphate, combined with carbon as a negative electrode material, separated by an electrolyte solution consisting of a lithium salt in a mixed organic solvents.[14] A convenient electrolyte that is used in lithium ion batteries must have high chemical stability, suitable ionic conductivity, low cost and satisfying safety requierments.[14] An electrolyte consists of an inorganic lithium salt dissolved in organic solvents which enable lithium ion transfer between positive and negative electrodes.[8]

Common Lithium salts used frequently in electrolytes of lithium ion batteries should be inert towards the cell components with a high solubility in the organic solvents, such as lithium hexafluorophosphate ($LiPF_6$),[15,16] lithium perchlorate ($LiClO_4$),[17] lithium tetrafluoroborate ($LiBF_4$),[18,19] lithium hexafluoroarsenate ($LiAsF_6$),[20,21] and Lithium bis(trifluoromethane sulfonyl) imide (LiTFSI).[22] Combining of two or more organic solvents is often used to improve the properties of the electrolyte. Main organic solvents used in lithium ion batteries are ethylene carbonate (EC), propylene carbonate (PC), diethyl carbonate (DEC), dimethyl carbonate (DMC), and 1,2-dimethoxyethane (DME).[23]

Lithium ion cells operate on the basis of intercalation reaction which involves the extraction/insertion of lithium ions between the two electrodes.[14,24] The chemical reactions that take place in the electrodes in lithium ion cell, using for example $LiCoO_2$ as a positive electrode and carbon as a negative electrode, can be simply demonstrated by the following equations:[25]

Charge process

Positive electrode $LiCoO_2 \rightarrow CoO_2 + Li^+ + e^-$ (1.1)

Negative electrode $6C + Li^+ + e^- \rightarrow LiC_6$ (1.2)

Discharge process

Positive electrode $CoO_2 + Li^+ + e^- \rightarrow LiCoO_2$ (1.3)

Negative electrode $LiC_6 \rightarrow 6C + Li^+ + e^-$ (1.4)

When the cell charge (equations 1.1 and 1.2), the lithium ions are extracted from the positive electrode and migrate through the electrolyte to intercalate in the carbon negative electrode. During the discharge (equations 1.3 and 1.4), the lithium ions move back to the positive electrode from the negative electrode.[14,26] This reaction causes a flow of electrons used to power an electric device (Figure 1.2).

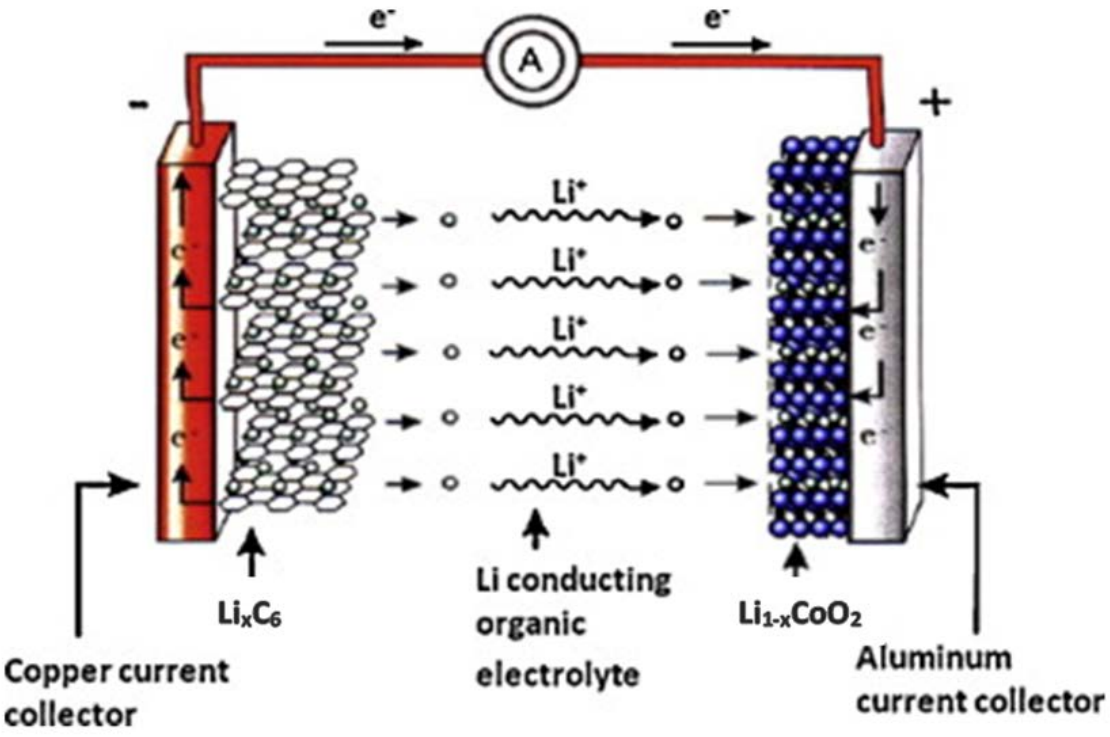

Figure 1.2 Scheme of a common lithium ion battery. Reproduced from ref. [27] with permission from Elsevier.

1.3 Lithium/sulfur batteries

The lithium sulfur (Li/S) batteries has received a considerable attention in the last decades, because its higher theoretical specific energy (about 2600 Wh/kg) and a theoretical capacity of 1672 $mAh.g^{-1}$ (based on complete reduction of sulfur).[28–32] Li/S batteries hold the potential to revolutionize the rechargeable energy storage market, since they can potentially deliver a much higher energy than lithium ion batteries of the same weight.[33–41] In addition, sulfur is inexpensive, naturally abundant and nontoxic, making elemental sulfur a very attractive as a cathode material in rechargeable lithium batteries.[28,42,43] Currently, Li/S batteries are successfully commercialised for certain applications, but improvements at the level of cell performance is required to extremely increase their contribution in the market.

1.3.1 Basic Li/S cell chemistry

Li/S cell generally consists of sulfur/conducting material composite as a positive electrode and lithium metal as a negative electrode, separated by an organic liquid electrolyte. Li/S cell operation is different from Lithium ion cells which based on intercalation reaction. The reduction of elemental sulfur during discharge is a very complicated, and considered as a multistep electrochemical process.[28,44–46] Lithium ions are expected to react with elemental sulfur (S_8) at the positive electrode to first produce high order lithium polysulfide (Li_2S_8), which is soluble in the electrolyte. After that, further reduction of long chain lithium polysulfide will occur to produce shorter chain lithium polysulfides (Li_2S_n, $8 > n > 2$). Lithium disulfide Li_2S_2 and then lithium sulfide Li_2S, both have been assumed to precipitate to form electrode passivation will be generated near the end of the discharge.[45,46]

The main reduction steps of sulfur can be represented by the following equations:[47,48]

$$S_{8(s)} + 2\,Li^+ + 2\,e^- \rightarrow Li_2S_{8(soln.)} \quad (1.5)$$

$$Li_2S_{8(soln.)} + 2\,Li^+ + 2\,e^- \rightarrow 2\,Li_2S_{4(soln.)} \quad (1.6)$$

$$Li_2S_{4(soln.)} + 4\,Li^+ + 4\,e^- \rightarrow Li_2S_{2(s)} + 2\,Li_2S_{(s)} \quad (1.7)$$

$$Li_2S_{2(s)} + 2\,Li^+ + 2\,e^- \rightarrow 2\,Li_2S_{(s)} \quad (1.8)$$

These are quite simple processes to describe the intermediate species that formed during sulfur reduction process. Different techniques has been used in order to reveal details related to these processes such as UV-Vis spectroscopy[48,49,50], operando X-ray absorption near-edge spectroscopy (XANES)[51], and ^{7}Li NMR[52]. The overall reaction is represented in the equation (1.9):[48,53]

$$S_{8(s)} + 16\,Li^+ + 16\,e^- \rightarrow 8\,Li_2S_{(s)} \quad (1.9)$$

1.3.2 Li/S cell discharge process

Several reports have described the discharge process as a two reduction stages corresponding to the formation of dissolved S_4^{2-} at the end of the first stage, and the solid products Li_2S_2 and Li_2S generated at the second stage.[47,54–57] Yamin *et al.*[28] indicated the irreversibility of the redox mechanism of sulfur, by observing one anodic peak and up to three cathodic peaks in the CV results of sulfur and polysulfide in THF solution. They assumed that the anodic peak corresponds to the oxidation of all polysulfides to elemental sulfur, and the three cathodic peaks might be related to the formation of S_6^{2-}, S_5^{2-}, and S^{2-}.

An important recent report on sulfur discharge in TEGDME/DOL by Barchasz *et al.*[50] proposes a possible mechanism for sulfur reduction consisting of three steps. During the first reduction step long polysulfide chains were produced at (2.4−2.2 V vs. Li^+/Li), such as S_8^{2-} and S_6^{2-}. $S_3^{\bullet-}$ radical can also be found in solution attributed to disproportionation of S_6^{2-} as shown in the equation below:

$$S_6^{2-} \rightarrow 2\,S_3^{\bullet-} \quad (1.10)$$

Further reduction of long chain polysulfides will produce S_4^{2-} during the second reduction step (2.15−2.1 V vs. Li^+/Li). Finally, short polysulfide species, such as S_3^{2-}, S_2^{2-}, and S^{2-}, are generated at the end of the reduction process (2.1 and 1.9 V vs. Li^+/Li). They shows that the potential depend not only on the main oxidation state but also the speciation of the sulfur. The potential varies between 2.4 V and 2.1 V as the oxidation state of the solution phase changes from -0.25 (S_8^{2-}) to -0.5 (S_4^{2-}). And the species S_8^{2-}, S_6^{2-} and S_4^{2-} have been detected. On the other hand in the long plateau region at 2.0 V, the partly soluble and insoluble species S_2^{2-}, S^{2-} are reported.[50]

1.3.3 Challenges in Li/S batteries

Although, lithium sulfur batteries have many advantages, there are several drawbacks that limit the commercialization of lithium sulfur batteries. First of all, the electrically insulating nature of elemental sulfur (5 x 10^{-30} S/cm at 25°C),[47,56] leads to low utilization of sulfur in the cathode. Therefore, sulfur needs to be in intimate contact with a conductive material (such as carbon) in order to enable electron transport to the reduction sites at the electrode-electrolyte interface. The added conductive material has a negative impact on the total energy density of Li/S battery, compared with the theoretical value calculated on the basis of pure elemental sulfur.

The second factor is that the reduction of elemental sulfur involves the generation of intermediate species of lithium polysulfides (Li_2S_n, $8 \geq n \geq 3$), which are highly soluble in most liquid electrolyte used in Li/S batteries.[37] High order lithium polysulfides can dissolve in the electrolyte solution[49] and diffuse to the lithium negative electrode, and react with the lithium anode forming insoluble products (Li_2S_2 and Li_2S), which will precipitate on the Li anode resulting in loss of active material and rapid capacity fading during cycling.[58] Also, transporting of soluble lithium polysulfide species between the cathode and anode will initiate the shuttle mechanism in the Li/S cell as will be explained in the next section.

Thirdly, part of the sulfur is removed from the electrochemical processes as a result of insoluble lithium sulfide precipitation on the sulfur cathode during discharge, preventing contact between remaining active sulfur and the electrolyte and blocking the ionic conduction pathway. This passivation layer causes a premature end of the discharge, by preventing the further reduction of sulfur.[54,,57,59] Also, part of Li_2S left in the cathode in a form that is not easily reoxidized on charging process, which can be considered as irreversible loss of the active material. The remaining Li_2S does not participate in electrochemical oxidation, as a result of the loss in the electronic contact with the conductive materials. Therefore, incomplete charge is then would lower the capacity at the next discharge.[57,60]

Finally, the sulfur cathode suffers from a variation in the volume during cycling of Li/S cell. A large volume expansion (~80%) from that of the initial sulfur active material occurs during discharging the cell, due to the different densities of sulfur and lithium sulfide (2.07 and 1.66 g/cm^3, respectively) and generates stress in the cathode. This devastates its structural stability and leads to loss of electrical contact with the current collector or the conductive material, which can cause a rapid capacity decline and limited cycling stability.[34,61–63]

1.3.4 The shuttle reaction

Mikhaylik *et al.*,[55] investigated the shuttle reaction that causes charge loss resulted from electrons carried cross the electrolyte by soluble polysulfide species due to the change in the oxidation state during discharge/charge process. The shuttle mechanism is a cyclic process comes from the formation of lithium polysulfides with high oxidation state (e.g. Li_2S_8) at the cathode during the discharge, which dissolve into the electrolyte and migrate to the lithium anode and react directly with the lithium to transform to lower oxidation state polysulfides.

These polysulfides with low oxidation state diffuses back due to concentration gradient[64] carrying electrons to the sulfur cathode where they are reoxidized to polysulfides with higher oxidation state, which then returns to the anode again to take more electrons, and the cycle continuous according to the scheme bellow (Figure 1.3). The dissolution of polysulfides led to not only rapid capacity fading resulted from insoluble products precipitation on the anode, but also low charge and discharge efficiency due to the polysulfides shuttling through the electrolyte.[64,65]

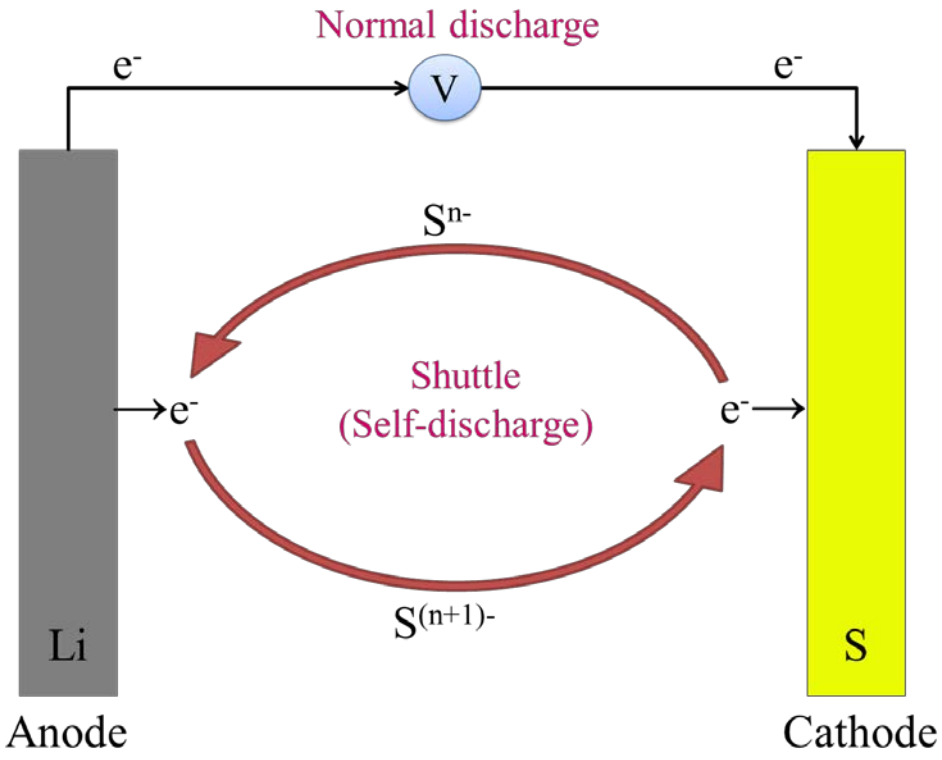

Figure 1.3 Scheme of the shuttle reaction in Li/S cell.

1.3.5 The sulfur/conducting materials composite electrode

In order to enhance the electrical conduction properties of elemental sulfur, sulfur must be incorporated within well-distributed conducting materials as the elementary substance in the cathode. Several conductive polymers have been used to prepare sulfur/polymer composites, such as polyaniline (PANI),[66,67] polyacrilonitrile (PAN),[68,69] polythiophene (PTh),[70] and polypyrrole (PPY).[71–74] Conductive polymers has attracted significant interest due to their electrochemical stabilities and their favourable morphologies.[70,75] Conductive polymers acts as a conducting additive and a strong adsorbing agent which effectively improve the electrochemical performance and cycle life of the Li/S cells.[76,77] However, a large amount of the conductive polymer should be added into the sulfur cathode in order to trap polysulfide species efficiently, resulting in low sulfur loading in the electrode.[78]

Major attempts have been devoted on the development of carbon-based sulfur composites in order to enhance the electrochemical performance of Li/S cells.[79] An optimal carbon matrix for sulfur/carbon composites requires to have (1) high electrical conductivity, (2) electrochemical affinity for sulfur, (3) small pores with small outlets to accommodate polysulfide species, (4) good accessibility of liquid electrolyte to active material, and (5) stable structure to tolerate the stress formed by the volume variation of the active material during cycling.[37]

Intensive investigations on different carbon materials as conductive additives for Li/S cell have been made. Nazar *et al.* utilized sulfur with highly ordered mesoporous carbon (CMK-3), which has a uniform pore diameter and high conductivity, and it has the potential of reaching a high capacity of using sulfur as an electrode (1320 $mAh.g^{-1}$ of S) with a good cycling stability.[80] Mesoporous carbon can reserve elemental sulfur in its pores and thus enhance the electrical conductivity and reduce the polysulfide shuttling.[81] Zhang *et al.* stated that a high utilization of sulfur active material was successfully achieved by encapsulating sulfur in the mesoporous carbon foams (MCF) framework, which provides an effective trapping for sulfur in the MCF host.[82]

Graphene showed high specific capacity and relatively good cycling stability, due to its good electrical conductivity, strong mechanical property, high surface area and good chemical stability.[62,83,84] Using graphene in the sulfur composite is very effective in confining the polysulfides , supposedly preventing their diffusion out of the graphene structure, and can accommodate the volume expansion of the electrode during the discharge process.[85–90]

Multi walled carbon nanotubes (MWCNTs) can provide an effective electronically conductive network, thus it can be an attractive choice as a conductive additive for sulfur cathode.[91–93] Ahn *et al.* shows that the sulfur-MWCNTs composite deliver a high discharge capacity of about 1355 $mAh.g^{-1}$ of S, which is 81% of the sulfur utilization, and two discharge plateaus were observed at around 2.45 and 2.05 V corresponding to the formation of lithium polysulfides (Li_2S_n, $4 \leq n \leq 8$) and insoluble products (Li_2S_n, $n < 4$), respectively. In addition, 63% of the capacity retention was measured after 30 cycles. They indicated that the well-dispersed sulfur-MWCNTs composite prepared via direct precipitation method will provide an excellent conductive cathode material resulting in improve the electrochemical performance of Li/S cell.[94]

However, graphene, mesoporous carbon and carbon nanotubes showed a high capacity and good cycle performance by enhancement of electrical contact and reduce the shuttle mechanism, these materials are very expensive compared with acetylene black which is very economical for use in Li/S batteries. Acetylene black have a good conductivity and absorbing ability,[95] and is often used as conductive matrix in the electrode by incorporating sulfur by ball-milling[96–100] and thermal treatment[45,95,101] to obtain sulfur/acetylene black composites.

Choi *et al.* investigates the effect of sulfur particle size on the sulfur utilization in the Li/S battery.[102] The results show that sulfur with smaller particle size assist to reach a higher utilization of sulfur. Also, they introduce a model for the cathode structure showing that the pores that form after the complete dissolution of solid sulfur into the electrolyte during the discharge process has a significant effect on the sulfur utilization. Smaller pores resulted from smaller particle size of sulfur would have the more favourable structure for confining and absorbing the soluble lithium polysulfide species, and enhance the utilizing of the carbon black as an electrochemical reaction sites.[102]

1.3.6 The electrolyte system

The nature of the solvent as well as the composition of mixed solvents is very important to stabilize the capacity and cycle life performance of the Li/S cell.[103] Intensive investigations on the using sulfolane in Li/S battery were done by Kolosnitsyn *et al.*.[52,104,105] They found that electrolyte based on sulfolane can be very interesting in lithium sulfur battery due to its moderate electrical conductivity and high electrochemical stability.[105]

Ether based solvents such as tetraethylene glycol dimethyl ether (TEGDME)[50,56,106–108] and 1, 3-Dioxolane (DOL)[109–115] are the most commonly used solvents in Li/S battery. TEGDME considered to be an attractive organic solvent for Li/S cell, due to its high solvating ability.[116] Adding DOL to the electrolyte will increase the ionic conductivity as a result of decreasing the viscosity of the electrolyte.[116,117]

Choi *et al.* investigated the effect of liquid electrolyte content on cycle performance of Li/S cell, and found that the liquid electrolyte content in the cell has a significant effect on the enhance the first discharge capacity and cycle life performance.[118]

The study by Chang *et al.* focus on the discharge behaviour of the Li/S battery with the electrolyte system based on a binary solvent mixture of TEGDME and DOL.[116] It reports that ether type solvent has a high solubility of polysulfide ions in the electrolyte solution. They state that the electrolyte requirement cannot be achieved by a single solvent, and using electrolyte system based on a binary solvent mixture is a very important to achieve the successful operation of Li/S battery.[116]

Gao *et al.* also investigated the effect of liquid electrolytes on the electrochemical performance of Li/S batteries.[119] These electrolytes consists of different lithium salts ($LiClO_4$, $LiPF_6$,or $LiCF_3SO_3$) dissolved in the organic carbonate solvents (eg. ethylene carbonate, propylene carbonate, and diethyl carbonate) and ethers such as 1,3-dioxolane (DOL), 1,2-dimethoxyethane (DME), ethyl methyl sulfone (EMS), and tetra ethylene glycol dimethyl ether (TEGDME). The results show that the first discharge capacity of about 1000 $mAh.g^{-1}$ of S was achieved by the electrolytes based on ethereal solvents, and two discharge plateaus was observed at around 2.4 and 2.1 V corresponds to the formation of long chain lithium polysulfides and insoluble products (Li_2S_2 and

Li_2S), respectively. For the carbonate-based electrolyte, only one voltage plateau was observed at around 2.4 V. and no further discharge reaction was occur afterward. They also observed that the discharge and charge capacity for the cells using different lithium salt in the electrolyte are almost the same. And it indicates that the lithium salt has no important effects in the electrochemical performance of lithium sulfur cell.[119]

In addition, it was reported recently that adding some additives such as lithium nitrate ($LiNO_3$) to the electrolyte solution can enhance Li/S battery performance.[120] Lithium nitrate suppressed the shuttle mechanism by forming a protective surface film on the lithium metal anode to avoid further reaction with lithium polysulfides.[120,121] However, deep discharge should not be lower than 1.7 V for a long cycle life Li/S cell in order to avoid the reduction of $LiNO_3$.[122,123]

1.3.7 The negative electrode

The highest specific capacity of about 3842 $mAh.g^{-1}$ for lithium metal,[124] make it an ideal anode material for Li/S batteries. However, the disparate passivation layer formed on the lithium surface as a result of its reaction with most of the electrolyte media during charge, which eventually may extend to the generation of lithium dendrites all across the cell.[36] The safety concern arises from lithium dendrite formation during charge as mentioned earlier, and the low coulombic efficiency exhibited using lithium anode[125,] led to search for an alternative anode materials that can replace metallic lithium in Li/S batteries.

One way to avoid the safety issue is by replacing elemental sulfur with Li_2S as the cathode.[35] In this case, a high-capacity such as tin[126,127] or silicon[128] can be utilized instead of the metallic lithium anode, because lithium is stored in the Li_2S cathode.[36,128]

1.3.8 Separators and membranes

Different kinds of separators were used such as Glass fibre separators and various kinds of polyolefins with different porosity and pore sizes (e.g. Celgard 2200, 2300, 2400, 2500), which considered the typical choices in in Li/S batteries. However, any clear motivation for the particular choice of separator is rarely given in the studies and the effect of the separator on the Li/S cell performance is often predominantly neglected.[39]

One of the major challenges in Li/S batteries remains the polysulfide shuttle between the sulfur cathode and Lithium anode. One approach to solve this problem is using ion selective Nafion-based membrane by coating Celgard separator with lithiated thin Nafion. In this case, the separators act not only to preserve the physical integrity of the cells but also it has the potential to inhibit the transfer of polysulfide anions between the electrodes.[129] using ion selective Nafion-based membrane shows a greatly improved cycling stability of Lithium Sulfur cells.[130]

Other approach is by adding barrier layers between the sulfur cathode and the separator. Zhou *et.al.* utilizes graphene membrane as barrier layer, which shows a great promise to enhance the cyclability of Li/S batteries. They states that graphene membrane not only acts as a good current collector but also capable of suppressing the polysufide shuttle when used as barrier layer between the sulfur cathode and separator in Li/S batteries.[63] More recently, lithium ion conducting glass ceramic (LICGC) separator has been used in the Li/S cells.[131] LICGC separator is only permeable to lithium ions; therefore, it can become an ideal candidate to eliminate the polysulfide shuttle in Li/S system.[132]

1.4 References

(1) Jossen, A.; Garche, J.; Sauer, D. U. *Sol. Energy* **2004**, *76*, 759–769.

(2) Perrin, M.; Saint-Drenan, Y. M.; Mattera, F.; Malbranche, P. *J. Power Sources* **2005**, *144*, 402–410.

(3) Rydh, C. J.; Sandén, B. a. *Energy Convers. Manag.* **2005**, *46*, 1957–1979.

(4) Takahashi, M. *Solid State Ionics* **2002**, *148*, 283–289.

(5) Whittingham, M. S. *Chem. Rev.* **2004**, *104*, 4271–301.

(6) Shin, H. C.; Cho, W. Il; Jang, H. *J. Power Sources* **2006**, *159*, 1383–1388.

(7) Huang, Y.; Goodenough, J. B. *Chem. Mater.* **2008**, *20*, 7237–7241.

(8) Tarascon, J. M.; Armand, M. *Nature* **2001**, *414*, 359–67.

(9) Daniel, C. *JOM* **2008**, *60*, 43–48.

(10) Franco, A. A. *RSC Adv.* **2013**, *3*, 13027–13058.

(11) Ellis, B. L.; Lee, K. T.; Nazar, L. F. *Chem. Mater.* **2010**, *22*, 691–714.

(12) Armand, M.; Tarascon, J.-M. *Nature* **2008**, *451*, 652–657.

(13) A. K. Padhi, K. 5. Nanjundaswamy, and J. B. G. *J. Electrochem. Soc.* **1997**, *144*.

(14) Wakihara, M. *Mater. Sci. Engeneering* **2001**, *33*, 109–134.

(15) Webber, A. **1991**, *138*, 2586–2590.

(16) Takami, N. *J. Electrochem. Soc.* **1992**, *139*, 1849.

(17) Uchida, I. *J. Electrochem. Soc.* **1995**, *142*, L139.

(18) Zhang, S. S.; Xu, K.; Jow, T. R. *J. Electrochem. Soc.* **2002**, *149*, A586.

(19) Zhang, S. S.; Xu, K.; Jow, T. R. *Electrochem. commun.* **2002**, *4*, 928–932.

(20) Aurbach, D.; Ein-Eli, Y. **1995**, *142*, 1746–1752.

(21) Mengeritsky, E.; Dan, P.; Weissman, I.; Zaban, A.; Aurbach, D. *J. Electrochem. Soc.* **1996**, *143*, 2110–2116.

(22) Xu, K.; Day, D. N.; Angell, C. A. *J. Electrochem. Soc.* **1996**, *143*, L209.

(23) Xu, K. *Chem. Rev.* **2004**, *104*, 4303–4417.

(24) *Advances in Lithium-Ion Batteries*; Schalkwijk, W. va; Scrosati, B., Eds.; Kluwer Academic/Plenum: New York, 2002.

(25) Zhang, P.; Yokoyama, T.; Itabashi, O.; Suzuki, T. M.; Inoue, K. *Hydrometallurgy* **1998**, *47*, 259–271.

(26) Bruce, P. G. *Solid State Ionics* **2008**, *179*, 752–760.

(27) Scrosati, B.; Garche, J. *J. Power Sources* **2010**, *195*, 2419–2430.

(28) Yamin, H.; Forenshtein, A.; Penciner, J.; Sternberg, Y.; Peled, E. *J. Electrochem. Soc.* **1988**, *135*, 1045.

(29) Peled, E. *J. Electrochem. Soc.* **1989**, *136*, 1621.

(30) Marmorstein, D.; Yu, T. .; Striebel, K. .; McLarnon, F. .; Hou, J.; Cairns, E. . *J. Power Sources* **2000**, *89*, 219–226.

(31) Fanous, J.; Wegner, M.; Grimminger, J.; Andresen, A.; Buchmeiser, M. R. *Chem. Mater.* **2011**, *23*, 5024–5028.

(32) Choi, N.-S.; Chen, Z.; Freunberger, S. a; Ji, X.; Sun, Y.-K.; Amine, K.; Yushin, G.; Nazar, L. F.; Cho, J.; Bruce, P. G. *Angew. Chem. Int. Ed. Engl.* **2012**, *51*, 9994–10024.

(33) Evers, S.; Nazar, L. F. *Acc. Chem. Res.* **2013**, *46*, 1135–1143.

(34) Yin, Y.-X.; Xin, S.; Guo, Y.-G.; Wan, L.-J. *Angew. Chemie Int. Ed.* **2013**, *52*, 2–18.

(35) Yang, Y.; Zheng, G.; Cui, Y. *Chem. Soc. Rev.* **2013**, *42*, 3018–3032.

(36) Bresser, D.; Passerini, S.; Scrosati, B. *Chem. Commun. (Camb).* **2013**, *49*, 10545–10562.

(37) Manthiram, A.; Fu, Y.; Su, Y. *Acc. Chem. Res.* **2013**, *46*, 1125–1134.

(38) Barghamadi, M.; Kapoor, a.; Wen, C. *J. Electrochem. Soc.* **2013**, *160*, A1256–A1263.

(39) Scheers, J.; Fantini, S.; Johansson, P. *J. Power Sources* **2014**, *255*, 204–218.

(40) Gao, J. *J. Phys. Chem. Lett.* **2014**, *5*, 882–885.

(41) Song, M.-K.; Cairns, E. J.; Zhang, Y. *Nanoscale* **2013**, *5*, 2186–204.

(42) Rauh, R. D.; Abraham, K. M.; Pearson, G. F.; Surprenant, J. K.; Brummer, S. B. *J. Electrochem. Soc.* **1979**, *126*, 523.

(43) Wang, C.; Chen, J.; Shi, Y.; Zheng, M.; Dong, Q. *Electrochim. Acta* **2010**, *55*, 7010–7015.

(44) Jung, Y.; Kim, S. *Electrochem. commun.* **2007**, *9*, 249–254.

(45) Barchasz, C.; Leprêtre, J.-C.; Alloin, F.; Patoux, S. *J. Power Sources* **2012**, *199*, 322–330.

(46) Diao, Y.; Xie, K.; Xiong, S.; Hong, X. *J. Electrochem. Soc.* **2012**, *159*, A421.

(47) Shim, J.; Striebel, K. a.; Cairns, E. J. *J. Electrochem. Soc.* **2002**, *149*, A1321.

(48) Teran, A. A.; Balsara, N. P. *Macromolecules* **2011**, *44*, 9267–9275.

(49) Rauh, R. D.; Shuker, F. S.; Marston, J. M.; Brummer, S. B. *J. inorg. nucl. Chem.* **1977**, *39*, 1761–1766.

(50) Barchasz, C.; Molton, F.; Duboc, C.; Leprêtre, J.-C.; Patoux, S.; Alloin, F. *Anal. Chem.* **2012**, *84*, 3973–80.

(51) Cuisinier, M.; Cabelguen, P.-E.; Evers, S.; He, G.; Kolbeck, M.; Garsuch, A.; Bolin, T.; Balasubramanian, M.; Nazar, L. F. *J. Phys. Chem. Lett.* **2013**, *4*, 3227–3232.

(52) See, K. A.; Leskes, M.; Gri, J. M.; Britto, S.; Matthews, P. D.; Emly, A.; Ven, A. Van Der; Wright, D. S.; Morris, A. J.; Grey, C. P.; Seshadri, R. *J. Am. Chem. Soc.* **2014**, *136*, 16368−16377.

(53) Ji, X.; Nazar, L. F. *J. Mater. Chem.* **2010**, *20*, 9821.

(54) Kolosnitsyn, V. S.; Karaseva, E. V; Seung, D. Y.; Cho, M. D. *Russ. J. Electrochem.* **2002**, *38*, 1314–1318.

(55) Mikhaylik, Y. V.; Akridge, J. R. *J. Electrochem. Soc.* **2004**, *151*, A1969.

(56) Ryu, H.-S.; Ahn, H.-J.; Kim, K.-W.; Ahn, J.-H.; Lee, J.-Y. *J. Power Sources* **2006**, *153*, 360–364.

(57) Cheon, S.-E.; Ko, K.-S.; Cho, J.-H.; Kim, S.-W.; Chin, E.-Y.; Kim, H.-T. *J. Electrochem. Soc.* **2003**, *150*, A796.

(58) Kolosnitsyn, V. S.; Karaseva, E. V. *Russ. J. Electrochem.* **2008**, *44*, 506–509.

(59) Cheon, S.-E.; Choi, S.-S.; Han, J.-S.; Choi, Y.-S.; Jung, B.-H.; Lim, H. S. *J. Electrochem. Soc.* **2004**, *151*, A2067.

(60) Cheon, S.-E.; Ko, K.-S.; Cho, J.-H.; Kim, S.-W.; Chin, E.-Y.; Kim, H.-T. *J. Electrochem. Soc.* **2003**, *150*, A800.

(61) Yang, Y.; Yu, G.; Cha, J. J.; Wu, H.; Vosgueritchian, M.; Yao, Y.; Bao, Z.; Cui, Y. *ACS Nano* **2011**, *5*, 9187–93.

(62) Huang, X.; Sun, B.; Li, K.; Chen, S.; Wang, G. *J. Mater. Chem. A* **2013**, *1*, 13484.

(63) Zhou, G.; Pei, S.; Li, L.; Wang, D.-W.; Wang, S.; Huang, K.; Yin, L.-C.; Li, F.; Cheng, H.-M. *Adv. Mater.* **2013**, *26*, 625–631.

(64) Guo, J.; Xu, Y.; Wang, C. *Nano Lett.* **2011**, *11*, 4288–94.

(65) Akridge, J.; Mikhaylik, Y.; White, N. *Solid State Ionics* **2004**, *175*, 243–245.

(66) Xiao, L.; Cao, Y.; Xiao, J.; Schwenzer, B.; Engelhard, M. H.; Saraf, L. V; Nie, Z.; Exarhos, G. J.; Liu, J. *Adv. Mater.* **2012**, *24*, 1176–81.

(67) Zhou, W.; Yu, Y.; Chen, H.; Disalvo, F. J.; Abruña, H. D. *J. Am. Chem. Soc.* **2013**, *135*, 16736–16743.

(68) Wang, J.; Yang, J.; Wan, C.; Du, K.; Xie, J.; Xu, N. *Adv. Funct. Mater.* **2003**, *13*, 487–492.

(69) Yu, X. G.; Xie, J. Y.; Yang, J.; Huang, H. J.; Wang, K.; Wen, Z. S. *J. Electroanal. Chem.* **2004**, *573*, 121–128.

(70) Wu, F.; Chen, J.; Chen, R.; Wu, S.; Li, L.; Chen, S.; Zhao, T. *J. Phys. Chem.* **2011**, *115*, 6057–6063.

(71) Fu, Y.; Manthiram, A. *RSC Adv.* **2012**, *2*, 5927.

(72) Zhang, Y.; Bakenov, Z.; Zhao, Y.; Konarov, A.; Doan, T. N. L.; Malik, M.; Paron, T.; Chen, P. *J. Power Sources* **2012**, *208*, 1–8.

(73) Sun, M.; Zhang, S.; Jiang, T.; Zhang, L.; Yu, J. *Electrochem. commun.* **2008**, *10*, 1819–1822.

(74) Shi chao, Z.; Lan, Z.; Jinhua, Y. *J. Power Sources* **2011**, *196*, 10263–10266.

(75) Wei, W.; Wang, J.; Zhou, L.; Yang, J.; Schumann, B.; NuLi, Y. *Electrochem. commun.* **2011**, *13*, 399–402.

(76) Wang, J.; Chen, J.; Konstantinov, K.; Zhao, L.; Ng, S. H.; Wang, G. X.; Guo, Z. P.; Liu, H. K. *Electrochim. Acta* **2006**, *51*, 4634–4638.

(77) Qiu, L.; Zhang, S.; Zhang, L.; Sun, M.; Wang, W. *Electrochim. Acta* **2010**, *55*, 4632–4636.

(78) Zhang, S. S. *J. Power Sources* **2013**, *231*, 153–162.

(79) Fedorková, A.; Oriňáková, R.; Čech, O.; Sedlaříková, M. *Int. J. Electrochem. Sci.* **2013**, *8*, 10308–10319.

(80) Ji, X.; Lee, K. T.; Nazar, L. F. *Nat. Mater.* **2009**, *8*, 500–6.

(81) Jayaprakash, N.; Shen, J.; Moganty, S. S.; Corona, A.; Archer, L. A. *Angew. Chem.* **2011**, *123*, 6026–6030.

(82) Tao, X.; Chen, X.; Xia, Y.; Huang, H.; Gan, Y.; Wu, R.; Chen, F.; Zhang, W. *J. Mater. Chem. A* **2013**, *1*, 3295–3301.

(83) Wang, J.-Z.; Lu, L.; Choucair, M.; Stride, J. a.; Xu, X.; Liu, H.-K. *J. Power Sources* **2011**, *196*, 7030–7034.

(84) Cao, Y.; Li, X.; Aksay, I. a; Lemmon, J.; Nie, Z.; Yang, Z.; Liu, J. *Phys. Chem. Chem. Phys.* **2011**, *13*, 7660–7665.

(85) Wang, H.; Yang, Y.; Liang, Y.; Robinson, J. T.; Li, Y.; Jackson, A.; Cui, Y.; Dai, H. *Nano Lett.* **2011**, *11*, 2644–7.

(86) Park, M.-S.; Yu, J.-S.; Kim, K. J.; Jeong, G.; Kim, J.-H.; Jo, Y.-N.; Hwang, U.; Kang, S.; Woo, T.; Kim, Y.-J. *Phys. Chem. Chem. Phys.* **2012**, 6796–6804.

(87) Ji, L.; Rao, M.; Zheng, H.; Zhang, L.; Li, Y.; Duan, W.; Guo, J.; Cairns, E. J.; Zhang, Y. *J. Am. Chem. Soc.* **2011**, *133*, 18522–5.

(88) Hsieh, C.-T.; Pai, C.-T.; Chen, Y.-F.; Chen, I.-L.; Chen, W.-Y. *J. Taiwan Inst. Chem. Eng.* **2014**, *45*, 1501–1508.

(89) Yu, M.; Yuan, W.; Li, C.; Hong, J.-D.; Shi, G. *J. Mater. Chem. A* **2014**, *2*, 7360.

(90) Liu, Y.; Guo, J.; Zhang, J.; Su, Q.; Du, G. *Appl. Surf. Sci.* **2015**, *324*, 399–404.

(91) Han, S.-C.; Song, M.-S.; Lee, H.; Kim, H.-S.; Ahn, H.-J.; Lee, J.-Y. *J. Electrochem. Soc.* **2003**, *150*, A889.

(92) Yuan, L.; Yuan, H.; Qiu, X.; Chen, L.; Zhu, W. *J. Power Sources* **2009**, *189*, 1141–1146.

(93) Jia-jia, C.; Xin, J.; Qiu-jie, S.; Chong, W.; Qian, Z.; Ming-sen, Z.; Quan-feng, D. *Electrochim. Acta* **2010**, *55*, 8062–8066.

(94) Ahn, W.; Kim, K.-B.; Jung, K.-N.; Shin, K.-H.; Jin, C.-S. *J. Power Sources* **2012**, *202*, 394–399.

(95) Zhang, B.; Lai, C.; Zhou, Z.; Gao, X. P. *Electrochim. Acta* **2009**, *54*, 3708–3713.

(96) Choi, Y.-J.; Chung, Y.-D.; Baek, C.-Y.; Kim, K.-W.; Ahn, H.-J.; Ahn, J.-H. *J. Power Sources* **2008**, *184*, 548–552.

(97) Zhao, X.; Kim, D.-S.; Ahn, H.-J.; Kim, K.-W.; Jin, C.-S.; Ahn, J.-H. *J. Korean Electrochem. Soc.* **2010**, *13*, 169–174.

(98) Liu, G.; Su, Z.; He, D.; Lai, C. *Electrochim. Acta* **2014**, *149*, 136–143.

(99) Liu, X.; Shan, Z.; Zhu, K.; Du, J.; Tang, Q.; Tian, J. *J. Power Sources* **2015**, *274*, 85–93.

(100) Kang, S.-H.; Zhao, X.; Manuel, J.; Ahn, H.-J.; Kim, K.-W.; Cho, K.-K.; Ahn, J.-H. *Phys. Status Solidi* **2014**, *211*, 1895–1899.

(101) Li, F.; Lu, W.; Niu, S.; Li, B. *New Carbon Mater.* **2014**, *29*, 309–315.

(102) Choi, Y. S.; Kim, S.; Choi, S. S.; Han, J. S.; Kim, J. D.; Jeon, S. E.; Jung, B. H. *Electrochim. Acta* **2004**, *50*, 833–835.

(103) Kim, S.; Jung, Y.; Lim, H. S. *Electrochim. Acta* **2004**, *50*, 889–892.

(104) Kolosnitsyn, V. S.; Karaseva, E. V; Amineva, N. A.; Batyrshina, G. A. *Russ. J. Electrochem.* **2002**, *38*, 329–331.

(105) Kolosnitsyn, V. S.; Sheina, L. V.; Mochalov, S. E. *Russ. J. Electrochem.* **2008**, *44*, 575–578.

(106) Zhang, S. S. *J. Electrochem. Soc.* **2013**, *160*, A1421–A1424.

(107) Islam, M. M.; Bryantsev, V. S.; van Duin, a. C. T. *J. Electrochem. Soc.* **2014**, *161*, E3009–E3014.

(108) Gu, M.; Lee, J.; Kim, Y.; Kim, J. S.; Jang, B. Y.; Lee, K. T.; Kim, B.-S. *RSC Adv.* **2014**, *4*, 46940–46946.

(109) Etacheri, V.; Geiger, U.; Gofer, Y.; Roberts, G. a.; Stefan, I. C.; Fasching, R.; Aurbach, D. *Langmuir* **2012**, *28*, 6175–6184.

(110) Weng, W.; Pol, V. G.; Amine, K. *Adv. Mater.* **2013**, *25*, 1608–15.

(111) Wu, H. Bin; Wei, S.; Zhang, L.; Xu, R.; Hng, H. H.; Lou, X. W. D. *Chem. Eur. J.* **2013**, *19*, 10804–10808.

(112) Zhao, X. Y.; Tu, J. P.; Lu, Y.; Cai, J. B.; Zhang, Y. J.; Wang, X. L.; Gu, C. D. *Electrochim. Acta* **2013**, *113*, 256–262.

(113) Peng, Z.; Fang, W.; Zhao, H.; Fang, J.; Cheng, H.; Doan, T. N. L.; Xu, J.; Chen, P. *J. Power Sources* **2015**, *282*, 70–78.

(114) Moreno, N.; Caballero, A.; Hernán, L.; Morales, J. *Carbon N. Y.* **2014**, *70*, 241–248.

(115) Xu, C.; Wu, Y.; Zhao, X.; Wang, X.; Du, G.; Zhang, J.; Tu, J. *J. Power Sources* **2015**, *275*, 22–25.

(116) Chang, D.-R.; Lee, S.-H.; Kim, S.-W.; Kim, H.-T. *J. Power Sources* **2002**, *112*, 452–460.

(117) Kim, H.-S.; Jeong, C.-S. *Bull. Korean Chem. Soc.* **2011**, *32*, 3682–3686.

(118) Choi, J.-W.; Kim, J.-K.; Cheruvally, G.; Ahn, J.-H.; Ahn, H.-J.; Kim, K.-W. *Electrochim. Acta* **2007**, *52*, 2075–2082.

(119) Gao, J.; Lowe, M. A.; Kiya, Y.; Abruna, D. *J. Phys. Chem.* **2011**, *115*, 25132–25137.

(120) Aurbach, D.; Pollak, E.; Elazari, R.; Salitra, G.; Kelley, C. S.; Affinito, J. *J. Electrochem. Soc.* **2009**, *156*, A694.

(121) Liang, X.; Wen, Z.; Liu, Y.; Wu, M.; Jin, J.; Zhang, H.; Wu, X. *J. Power Sources* **2011**, *196*, 9839–9843.

(122) Zhang, S. S. *Electrochim. Acta* **2012**, *70*, 344–348.

(123) Zhang, S. S. *J. Electrochem. Soc.* **2012**, *159*, A920–A923.

(124) Kraytsberg, A.; Ein-Eli, Y. *J. Power Sources* **2011**, *196*, 886–893.

(125) Liang, X.; Wen, Z.; Liu, Y.; Zhang, H.; Huang, L.; Jin, J. *J. Power Sources* **2011**, *196*, 3655–3658.

(126) Hassoun, J.; Scrosati, B. *Angew. Chem. Int. Ed. Engl.* **2010**, *49*, 2371–4.

(127) Hassoun, J.; Sun, Y.-K.; Scrosati, B. *J. Power Sources* **2011**, *196*, 343–348.

(128) Yang, Y.; McDowell, M. T.; Jackson, A.; Cha, J. J.; Hong, S. S.; Cui, Y. *Nano Lett.* **2010**, *10*, 1486–91.

(129) Jin, Z.; Xie, K.; Hong, X.; Hu, Z.; Liu, X. *J. Power Sources* **2012**, *218*, 163–167.

(130) Huang, J.-Q.; Zhang, Q.; Peng, H.-J.; Liu, X.-Y.; Qian, W.-Z.; Wei, F. *Energy Environ. Sci.* **2014**, *7*, 347.

(131) Lu, Y.-C.; He, Q.; Gasteiger, H. a. *J. Phys. Chem. C* **2014**, *118*, 5733–5741.

(132) Hagen, M.; Dörfler, S.; Althues, H.; Tübke, J.; Hoffmann, M. J.; Kaskel, S.; Pinkwart, K. *J. Power Sources* **2012**, *213*, 239–248.

Chapter 2:

Experimental techniques

2.1 Preparation of the electrode and cell fabrication

2.1.1 Composite electrodes prepared by ball milling method

Ball milling is one of the most popular methods that has been used to prepare active materials. The vigorous treatment that leads to gain high density materials, the reproducibility of the results due to the efficiency of the process, the simplicity to achieve large scale preparation of homogeneous electrode materials, are regarded as the main advantages that make the ball milling process widely utilized in the preparation of electrode materials.[1]

The ball milling operation for the electrode material was performed in a ball mill (RETSCH MM 200, Germany) in order to decrease the particle size. The container used to mill the active material consists of a 10 ml sealed stainless steel grinding jar and a 10 mm diameter stainless steel ball. The ball milling procedure was conducted continuously for 30 min at a speed of 1200 rpm. As the container rotates, the ball movement from one side to the other will grind the material and hence reduce the particle size.

2.1.2 Composite electrodes prepared by a precipitation method

Direct precipitation is another method that has been used for the preparation of electrode materials in lithium/sulfur cells. By using this method, sulfur (100 MESH, Sigma-Aldrich) can be mixed with acetylene black (Chevron Phillips Chemical Company LP, specific surface area 76 m^2/g, mean particle size 42 nm) homogeneously to provide a more effective conductive network and thus enhance the electrical conduction properties of sulfur.

A sulfur suspension can be prepared using this method by mixing of 26 mM sodium thiosulfate with an aqueous solution of 1% surfactant, and a solution of 1.1 M of hydrochloric acid was then added to this mixture slowly (ca. 2 min.) The major role of the surfactant used is to lower the size of sulfur particles by limiting both the particle growth and the tendency towards agglomeration.[2] After 1 min., acetylene black was then added to the sulfur suspension under vigorous magnetic stirring. The precipitate was then filtered under vacuum and then dried.

2.1.3 The cell fabrication

Cell construction was done by using S/AB composites. The positive electrode was prepared according to the following steps: 90 wt% S/AB composite was ground thoroughly in a mortar then mixed with 10 wt% polytetrafluoroethylene (PTFE, 6C-N, Dupont) as a binder until it formed a thick felt like film; next, the film was placed between two aluminum foils and rolled into a 80-90 μm thick sheet using a rolling mill (Durston, 100 mm) at room temperature, then cut into 1 cm diameter pellets using hole puncher with a mass range of 7.5 – 8 mg and dried at 50 ºC under vacuum overnight; finally it was moved and stored in an argon-filled glove box (MBraun).

The typical cell used for the battery materials test is shown in Figure 2.1. The test cell was assembled in an argon-filled glove box; the test cell is composed of S/AB composite with sulfur loading of about 1.7 g/cm^2 as the positive electrode and an excess of lithium metal (99.99%, Rockwood lithium GmbH) as the negative electrode (approximately 100 μm thick with an area of 1 cm^2) separated by two glass fibre separators (GF/F grade, Whatman) sandwiched together, and soaked with 0.125 ml of electrolyte. The cell was sealed by screwing down the lid on the cell. The spring below the current collector piston ensures good contact between the electrodes and the electrolyte, while the Viton ring ensures there is no short circuits in the cell by keeping both current collectors separate.

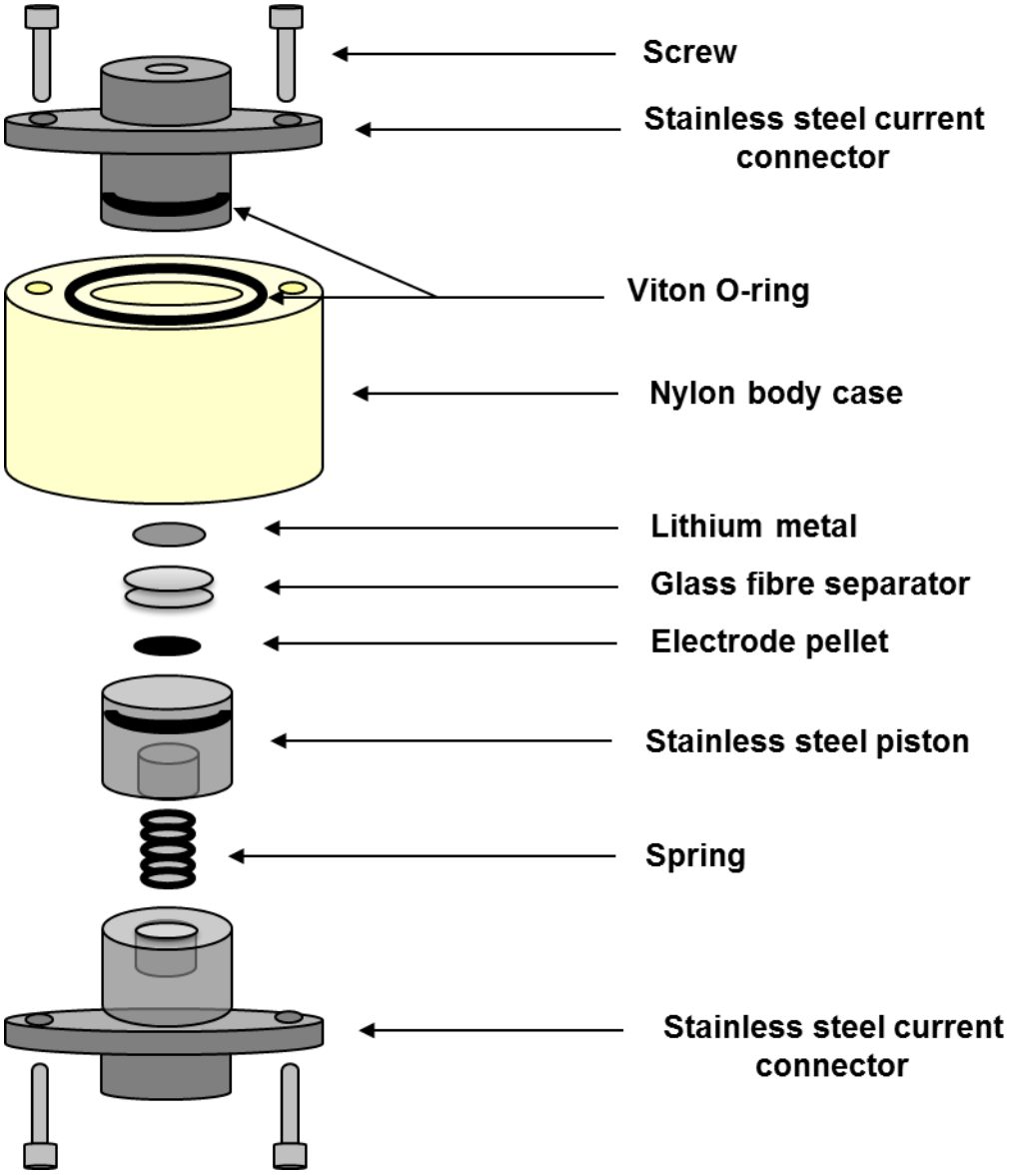

Figure 2.1 Cell construction for testing of battery materials.

2.2 Electrochemical techniques

All electrochemical experiments were carried out inside a thermostat chamber controlled at 25 ºC.

2.2.1 Cyclic voltammetry

Cyclic voltammetry (CV) is one of the most powerful electrochemical techniques that has been widely used for obtaining preliminary information about electrochemical processes. CV is the measure of the current response that results from the applied potential over a given potential range. The rate of potential change with time is defined as the potential scan rate (v). The potential of the electrode is scanned linearly between two values of limited potential range (V_1 and V_2) where an electrode reaction occurs,[3] at a constant scan rate starting from an initial value V_i, as shown in Figure 2.2.

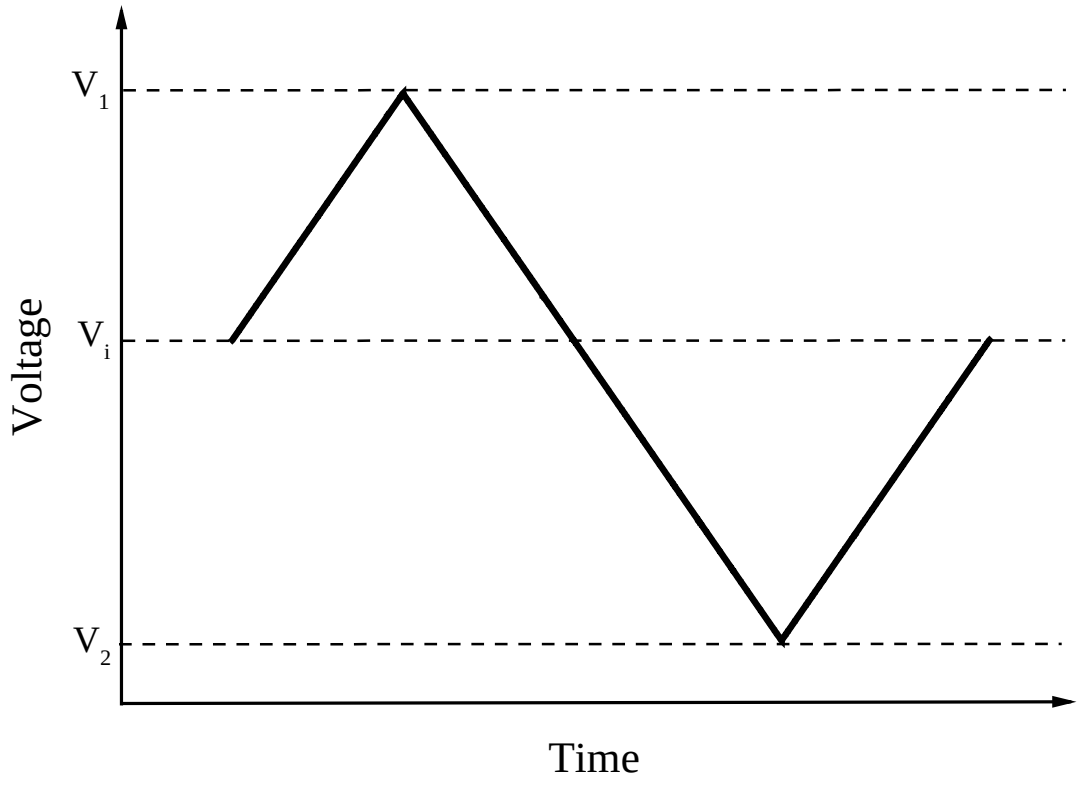

Figure 2.2 Cyclic voltammetry showing the potential-time waveform.

The potential can be swept forward and backward with time depending on the initial sweep direction. Sweeping the potential in a positive direction (forward sweep) can be used to study oxidation reactions. On the other hand, sweeping the potential in a negative direction (backward sweep) can be used to study reduction reactions. The cycle can be repeated, and the number of cycles and the scan rate can be controlled in the experimental setup.

The data obtained which represents the current response resulted from electrochemical reaction is generally plotted as a function of the applied potential, as shown in Figure 2.3. The cyclic voltammogram below shows two current peaks corresponding to the reduction or cathodic peak (I_{pc}), and oxidation or anodic peak (I_{pa}), of a reversible electron transfer reaction:

$$Red - e^- \rightleftarrows Ox \tag{2.1}$$

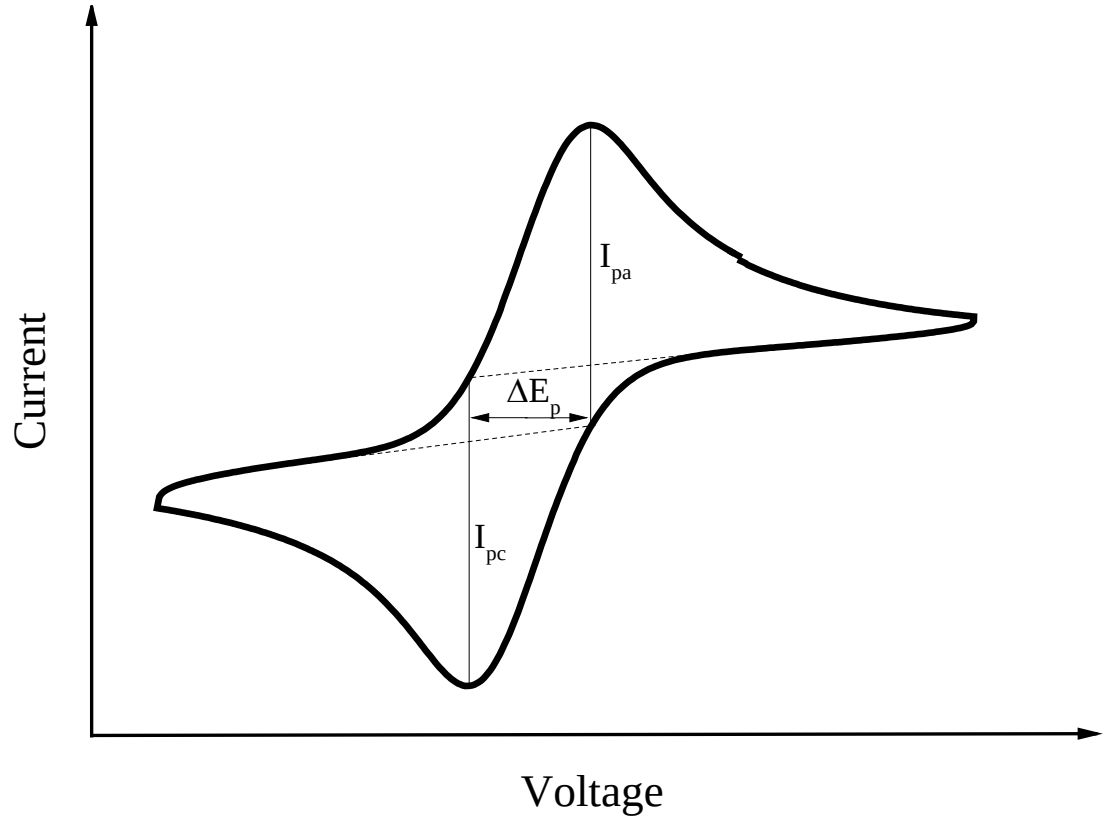

Figure 2.3 Cyclic voltammogram showing the shape of the response.

The peak current (i_p) is generally described by the Randles-Sevcik equation (at 25 ºC) which shows the dependency of the peak current on the square root of the scan rate:

$$i_p = 2.69 \times 10^5 \, n^{3/2} A D^{1/2} C v^{1/2} \quad (2.2)$$

This equation supposes a reversible redox couple and the changes in concentrations of oxidised and reduced forms at the electrode surface are directly correlated to potential changes, as determined by the Nernst equation:

$$E = E° + \frac{RT}{nF} \ln \frac{[Ox]}{[Red]} \quad (2.3)$$

The potential difference between the oxidation and reduction peaks ($E_{pa} - E_{pc}$) is equal to 59/*n* mV, which indicates the reversibility of the redox couple. Deviation from the ideal CV described above can be caused by slow electrode kinetics where the reaction rate constant is small. A larger peak separation would be observed, which indicates a non-reversible redox couple.

In Li/S cell there are many different reactions occurs during reduction/oxidation of S/Li_2S. Therefore, more than one peak was expected to be observed during each process.

A general CV experiment consists of a low concentration of the reactants with a concentrated supporting electrolyte. Therefore, the effect of the IR drop is negligible. On the other hand, in Li/S cell, the concentration of the reactants is similar or might be larger than the concentration of the supporting electrolyte. Using fast scan rate would cause the current to be limited by the IR drop. Therefore, The CV studied in this project was performed using slow scan rate in order to reduce the IR effect.

The CV was carried out at a potential scan rate of 0.1 mV/s and using a potential limit between 1.5 and 3 V (vs Li/Li^+). One different problem arises if the scan rate is very slow, when convection disturbs the diffusion field and causes a distortion of the results from what would be expected from the simple analysis based on semi-infinite boundary condition. In this case, using a separator in the cell may be useful to hold the electrolyte in order to avoid any convection that might be generated during scanning the potential slowly.

2.2.2 Galvanostatic cycling

Galvanostatic cycling is an important method for studying the electrochemical behaviour of battery materials upon cycling. A constant current is applied to the cell within a range of limited potential, to record a potential response as a function of time. The cell is discharged by applying a negative current to the working electrode, with a decline in the corresponding cell potential. On the other hand, applying a positive current to the working electrode will charge the cell with an increase in cell potential. This can be represented in Figure 2.4, which shows the applied current as a function of time (a), and the potential response during that time (b), during a galvanostatic discharge/charge of Li/S cell.

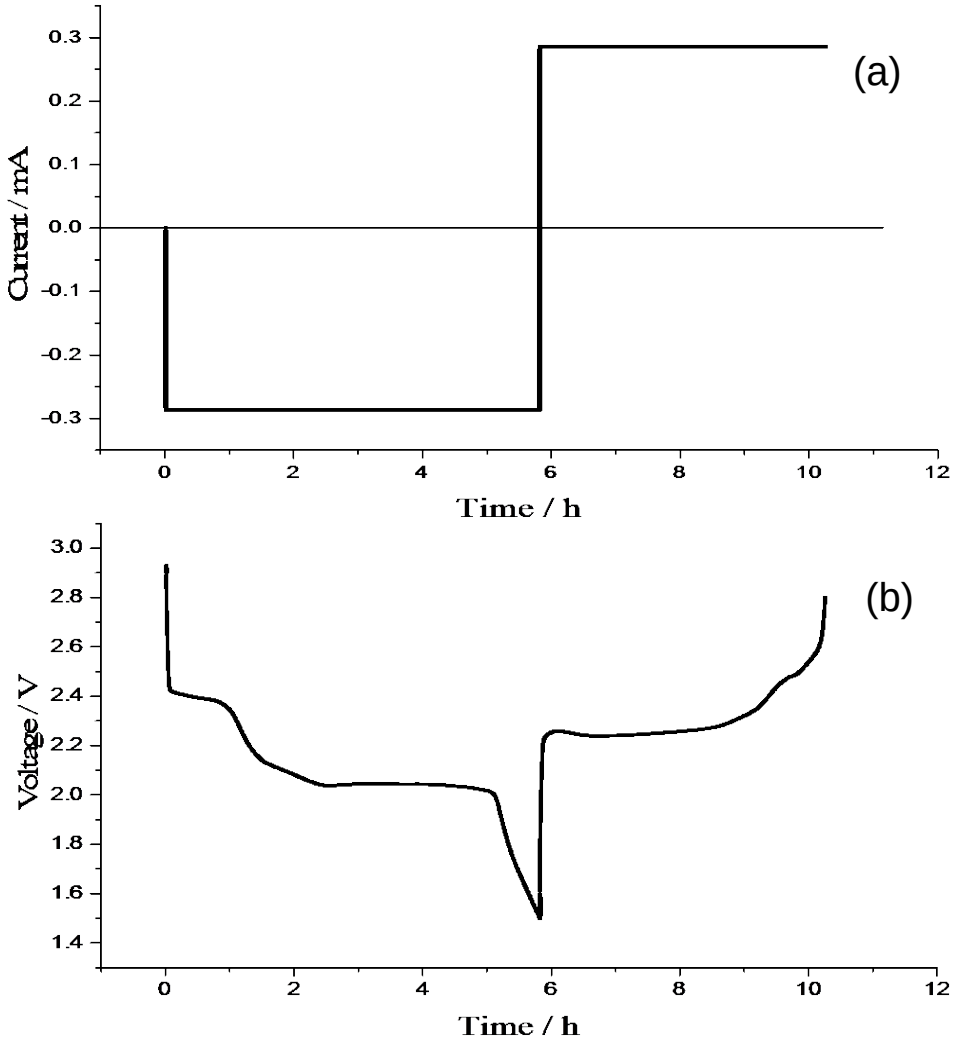

Figure 2.4 Schematic representation of galvanostatic cycling of Li/S cell showing (a) applied current vs. time, and (b) voltage response vs. time.

The C rate can be defined as the rate at which a battery is discharged and charged relative to its specific capacity. For example, one C rate means a complete charge or discharge of the cell in one hour. A charge rate at C/10 would charge the battery in ten hours, while a charge rate at 10 C would charge the battery in six minutes. The cycle life of active material can be illustrated from plotting the specific capacity as a function of cycle number.

The applied current (I) for the corresponding C rate (C_r) can be calculated from equation 2.4,

$$I = C_r \times Q_A \tag{2.4}$$

where Q_A is the capacity of the active material in the electrode (mAh), and can be obtained using equation 2.5, as follows,

$$Q_A = m_A \times Q_{Th} \tag{2.5}$$

where Q_{Th} is the theoretical capacity of the active material ($mAh.g^{-1}$), and m_A is the mass of the active material in the electrode (g).

The results were also displayed as differential capacity (dQ/dV) which was reproduced from the 1st discharge/charge profiles of the cells using EC-Lab software. This shows the effective pseudo capacitance of the redox reaction in units of Farad. The display resembles a cyclic voltammogram taken at a very slow scan rate because,

$$\frac{dQ}{dV} = \frac{dQ}{dt}\frac{dt}{dV} = \frac{1}{v}\frac{dQ}{dt} \tag{2.6}$$

where υ = scan rate, and *dQ/dt* = current.

The cells were galvanostatically discharged and charged using MPG (BioLogic Science Instruments). All the specific capacity values in the present work were calculated on the basis of sulfur mass, and repeated experiments show that specific capacity that been used is about ± 50 $mAh.g^{-1}$ of S.

2.2.3 Galvanostatic intermittent titration technique

The galvanostatic intermittent titration technique (GITT) is a useful electrochemical technique that has been widely used to obtain the diffusion coefficient of lithium ions in electrode materials.[4,5] It consists of measuring the voltage transient resulting from disconnecting the current.[6] It was carried out for the Li−S cells using MPG (BioLogic Science Instruments) at 25 °C. A series of constant current pulses was applied to the cell within a range of limited potential, to record a potential response as a function of time. Each pulse was followed by open circuit relaxation, in which no current passes within the cell.

During the discharge, a negative current is applied to the cell for a certain time (*τ)*. The initial rapid decrease in the cell voltage is attributed to the IR drop; and then the voltage slowly decreases with time, in order to preserve a constant concentration gradient at the surface as required by Fick's constant current. During open circuit relaxation time, there is no current passing through the cell. The potential quickly increases to a value corresponding to the IR drop. Afterwards, it slowly increases until the cell is reach the OCV, as shown in Figure 2.5. This alteration of current pulse followed by open circuit relaxation time is repeated until a cut-off voltage of the cell is reached. In contrary, a positive current is applied to the cell during the charge, and the reverse process is performed.

The interpretation of the curved regions is usually made according to Fick's laws of diffusion. Through a series of assumptions and simplifications, the diffusion coefficient *D* can be determined from the following equation when using a small current:[4,7]

$$D = \frac{4}{\pi}\left(\frac{m_B V_m}{M_B S}\right)^2 \left(\frac{\Delta E_s}{\tau\left(\frac{dE}{d\sqrt{t}}\right)}\right)^2, \quad t \ll \frac{L^2}{D} \tag{2.7}$$

where V_m is the molar volume of the compound, M_B is the molecular weight of the active material, m_B is the mass of the active material, S is the total contact area between the electrolyte and the electrode, ΔE_s is the change of the steady-state voltage of the cell resulting from the current pulse, L is the electrode thickness, and τ is the time interval for which a constant current is applied.

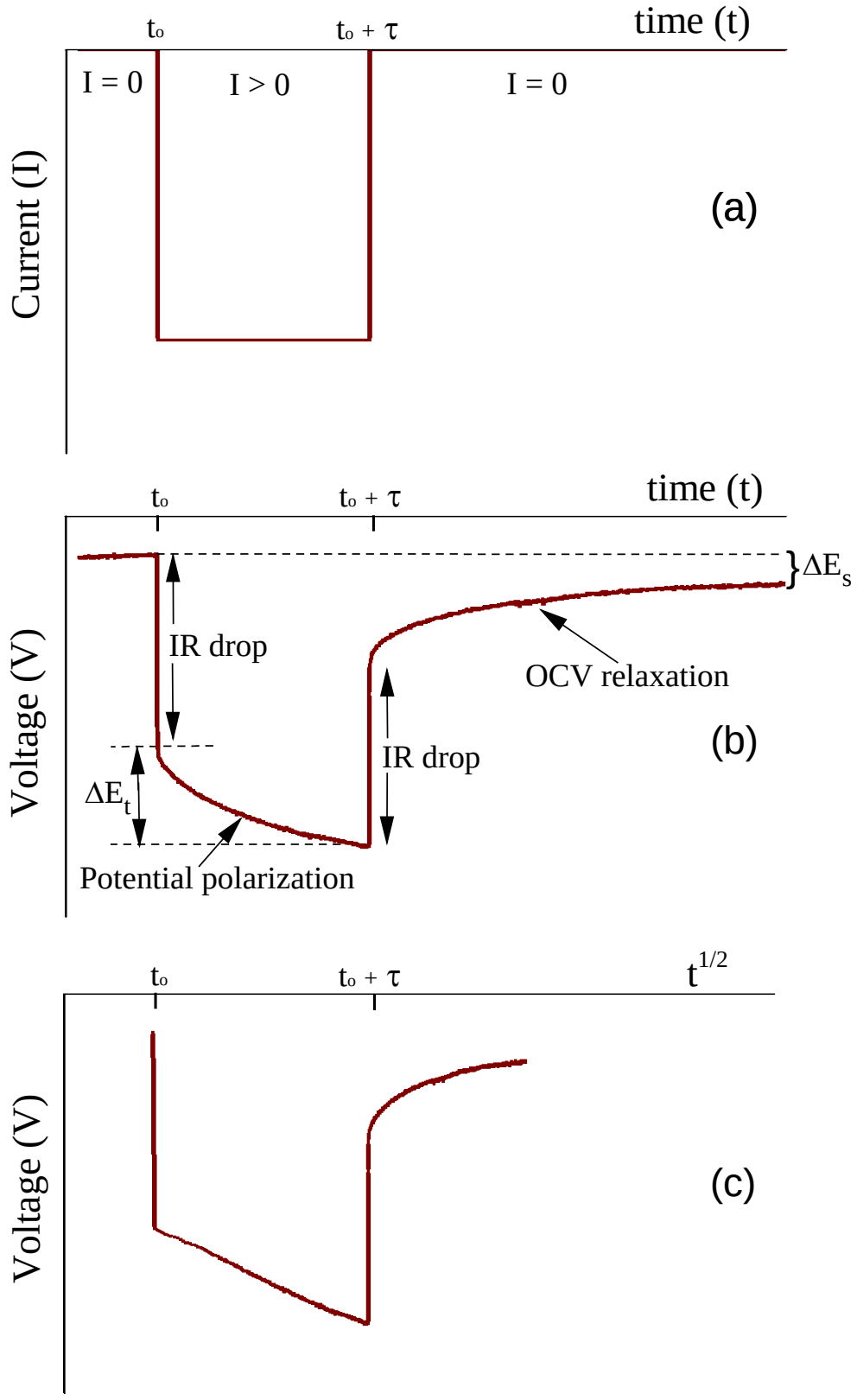

Figure 2.5 Schematic representation of single step of the GITT in the Li/S cell (a) applied current vs. time, (b) voltage response vs. time, and (c) voltage response vs. $t^{1/2}$.

If the reaction is diffusion controlled, then E versus $t^{1/2}$ should shows a straight line behaviour over the entire time period of current pulse, as shown in Figure 2.5 (c). then Eq. (2.7) can be further simplified as:[7]

$$D = \frac{4L^2}{\pi\tau}\left(\frac{\Delta E_s}{\Delta E_t}\right)^2 \tag{2.8}$$

where ΔE_t is the total change of the cell voltage during the current pulse, after subtracting the IR drop.

2.2.4 Open Circuit Voltage

Open circuit voltage (OCV) is a useful electrochemical technique that has been used in the battery test. OCV can be defined as the voltage of the battery under equilibrium conditions, and is directly connected to the state of charge of the battery.[8]

OCV consists of a certain period of time when no current or voltage is applied in or out of the working electrode. This duration is generally used as preconditioning time for equilibration of the electrochemical cell. At equilibrium state, it can be supposed that the battery voltage will stabilize to a particular value, which represents the value of the OCV.

2.2.5 Electrochemical impedance spectroscopy

Electrochemical impedance spectroscopy (EIS) is a relatively widely used as a standard characterization method for describing the electrochemical behaviour of materials and their interfaces with electronically conducting electrodes.[9] The impedance spectroscopy can be determined by applying a sinusoidal voltage perturbation to the system, and record the sinusoidal current response for each frequency. The impedance Z can be represented in the equation below:

$$Z = R + jX$$

$$= Z' + jZ'' \qquad (2.9)$$

where the resistance is the real part R, and the reactance is the imaginary part X, and they usually displayed in the Nyquist plot as Z' and Z'', respectively. j is the Imaginary unit.

The standard equivalent circuit used to illustrate the behaviour of simple electrochemical systems is known as the Randles circuit,[10] shown in Figure 2.6.

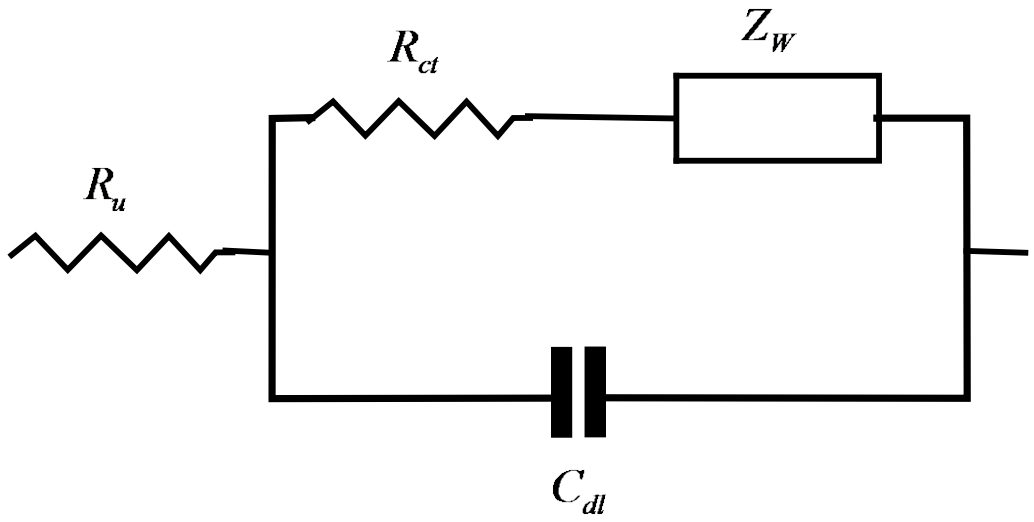

Figure 2.6 Equivalent circuit diagram for the Randles circuit.

The typical Nyquist plot of a Randles circuit consist of a combination of a semicircle and a straight slopping line at low frequency, as shown in Figure 2.7. The semicircle is referred to the double layer capacitance C_{dl} and the charge transfer resistance R_{ct}. The straight slopping line at low frequency end is described as Warburg impedance Z_W, which is usually used to describe diffusion in an electrochemical system. The R_u is known as the uncompensated resistance, which is normally attributed to the electrolyte resistance, electrode surfaces and cell components.[11]

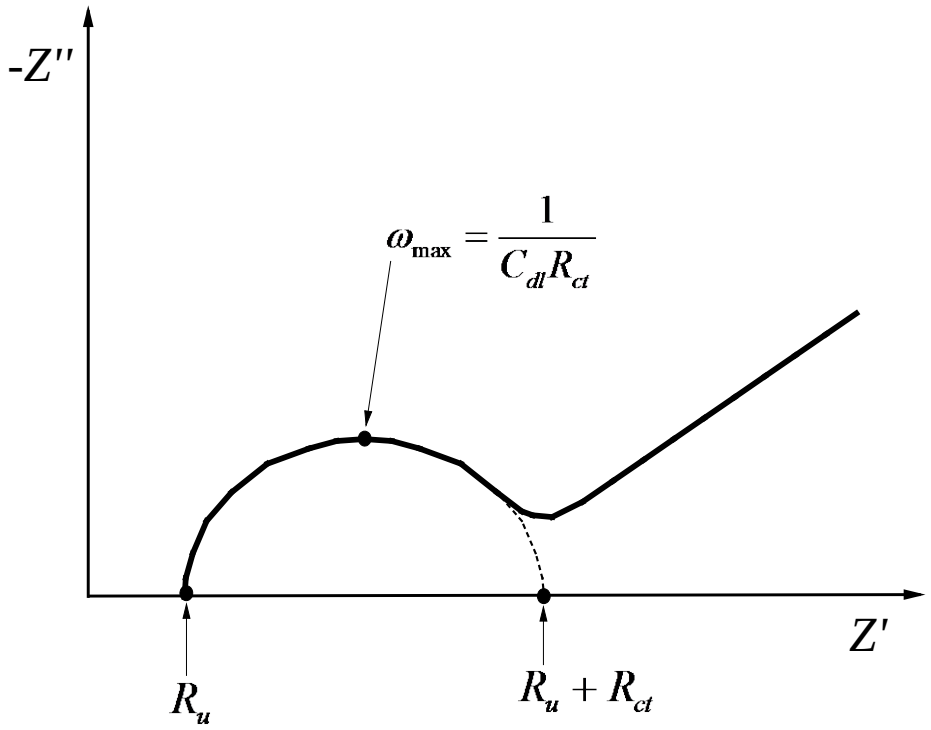

Figure 2.7 Typical Nyquist plot of the Randles circuit.

2.3 Scanning electron microscopy

Scanning electron microscopy (SEM) is a powerful technique that generates signals at the surface of a solid sample. These signals are containing information about the topography and composition of the sample, resulting from the interaction between the electrons from the focused beam and the atoms in the sample. The reflected secondary electrons that are produced from scanning the electron beam over the sample are collected by a detector and transformed into an image.

SEM allows a much higher resolution than traditional optical microscopes; it can obtain a resolution of 1 nanometer. The electron beam can be accelerated in a vacuum between 1-200 kV. Because of the nature of the technique, insulating materials produce unclear images, so materials to be analysed using SEM must be electrically conductive. In this work, SEM images have been obtained using Philips XL30 microscope.

2.4 References

(1) Liu, G.; Su, Z.; He, D.; Lai, C. *Electrochim. Acta* **2014**, *149*, 136–143.

(2) Chaudhuri, R. G.; Paria, S. *J. Colloid Interface Sci.* **2010**, *343*, 439–46.

(3) Pletcher, D. *A First Course in Electrode Processes*; 2nd ed.; RSC Publishing: Cambridge, 2009.

(4) Weppner, W.; Huggins, R. A. *J. Electrochem. Soc.* **1977**, *124*, 1569–1578.

(5) Markevich, E.; Levi, M. D.; Aurbach, D. *J. Electroanal. Chem.* **2005**, *580*, 231–237.

(6) Mennola, T.; Mikkola, M.; Noponen, M.; Hottinen, T.; Lund, P. *J. Power Sources* **2002**, *112*, 261–272.

(7) Wen, C. J.; Boukamp, B. A.; Huggins, R. A.; Weppner, W. *J. Electrochem. Soc.* **1979**, *126*, 2258–2266.

(8) Snihir, I.; Rey, W.; Verbitskiy, E.; Belfadhel-Ayeb, A.; Notten, P. H. L. *J. Power Sources* **2006**, *159*, 1484–1487.

(9) Barsoukov, E.; Macdonald, J. R. *Impedance Spectroscopy*; 2nd ed.; John Wiley & Sons, Inc., Hoboken, New Jersey., 2005.

(10) Randles, J. E. B. *Discuss. Faraday Soc.* **1947**, *1*, 11–19.

(11) Zhang, S. S.; Xu, K.; Jow, T. R. *Electrochim. Acta* **2004**, *49*, 1057–1061.

Chapter 3:

The effect of electrolyte on the electrochemical performance of Li/S cells

3.1 Introduction

The nature of the solvent as well as the composition of mixed solvents is very important to stabilize the capacity and cycle life performance of the Li/S cell.[1] The electrolyte requirements that can fulfil a successful operation of a Li/S battery are high ionic conductivity, good polysulfide solubility, low viscosity, electrochemical stability, chemical stability toward lithium, and high flash point.[2] The electrolyte requirement cannot be achieved by a single solvent[3], and using an electrolyte system based on a binary solvent mixture is very important to achieve the successful operation of Li/S battery.[2]

This chapter looks at the electrochemical performance of a sulfur/acetylene black composite prepared by ball milling, in different electrolyte systems based on a binary solvent mixture. The moderate dielectric constant and high electrochemical stability of sulfolane make it a particularly interesting solvent for use in Li/S battery.[4] Due to the high solvating power, tetraethylene glycol dimethyl ether (TEGDME) is considered to be an attractive organic solvent for Li/S cell.[2] Adding 1,3-dioxolane (DOL) to the electrolyte will increase the ionic conductivity as a result of decreasing the viscosity of the electrolyte.[2,5]. The viscosity difference between these electrolytes explains the results in terms of their penetration into the sulfur electrode structure as well as the dissolution rate of the solid material and the diffusion rate of the lithium ion, which can connected to the conductivity (λ) according to the Nernst-Einstein relation:

$$\lambda = \frac{z^2 F^2 D}{RT} \tag{3.1}$$

where D is the diffusion coefficient, z is the charge number of the ion, F is the Faraday constant, R is the gas constant, and T is the absolute temperature.

3.2 Experimental details

3.2.1 Preparation of the electrode

To prepare the sulfur/acetylene black (1:3) composite by the ball milling method, first, the sublimed sulfur (100 MESH, Sigma-Aldrich) was dried under vacuum at 50 ºC for 24h before use. 0.1 of sulfur was then mixed with 0.3 g of acetylene black (Chevron Phillips Chemical Company LP, specific surface area 76 m^2/g, mean particle size 42 nm). The mixture was ground in a mortar and ball milled to prepare S/AB composite with a weight ratio S:AB = 1:3. The ball-milling procedure was conducted continuously for 30 min at a speed of 1200 rpm in a ball mill (RETSCH MM 200, Germany) with using a 10 ml stainless steel grinding jar, and a 10 mm diameter stainless steel ball. The composite was then dried at 50 ºC under vacuum for one day. The positive electrode was prepared as described in chapter 2, and sulfur loading in each electrode was about 1.7 mg/cm^2.

3.2.2 Preparation of the electrolytes

Two salts were used in this study, lithium hexafluorophosphate ($LiPF_6$, Sigma-Aldrich), and lithium bis(trifluoromethane sulfonyl) imide (LiTFSI, Sigma-Aldrich). The salts were dried under vacuum at 140°C for 24 h before use. Tetra ethylene glycol dimethyl ether (TEGDME, 99%, Sigma-Aldrich) was dried under vacuum at 100°C for 48 h before use. 1,3-Dioxolane (DOL, 99.8% Sigma-Aldrich) and sulfolane (99% Sigma-Aldrich) were used as received. Three electrolytes were prepared by dissolving lithium salts into the desired solvents in an argon filled glove box. These electrolyte solutions consisting of:

1M $LiPF_6$ dissolved in a (1:1) mixture of TEGDME and sulfolane.

1M LiTFSI dissolved in a (1:1) mixture of TEGDME and sulfolane.

1M LiTFSI dissolved in a (1:1) mixture of TEGDME and DOL.

All ratios are based on volume. In all electrochemical testing, cells were assembled as described in Chapter 2. All cells were cycled at 25 ºC.

3.3 The effect of electrolyte on cell potential and capacity

3.3.1 Cyclic voltammetry

Cyclic voltammograms of lithium/sulfur cells tested with 0.1 mV s^{-1} scan rate in the voltage range of 1.5 to 3.0 V vs. Li/Li^+ are shown in figure 3.1. The CV measurements were performed using very slow scan rates to minimise diffusion limitations, and therefore gave more symmetrical shapes than those typically seen with faster scans. For the cells that use $LiPF_6$ in TEGDME/sulfolane and LiTFSI in TEGDME/sulfolane (Figure 3.1 (a) & (b)), their peak potentials are almost the same and there are clearly two main cathodic peaks. The first peak represents the transformation of elemental sulfur to lithium polysulfides (Li_2S_n, 8 > n > 2) at around 2.32V. The second peak at around 1.85 V corresponds to the formation of Li_2S_2 and Li_2S at the end of the reduction process.[6,7] During the anodic sweep, two oxidation peaks are observed which represent the reverse transformation of lithium sulfide to Li_2S_4 at 2.43 V, which then will oxidize to elemental sulfur at 2.61V.[8]

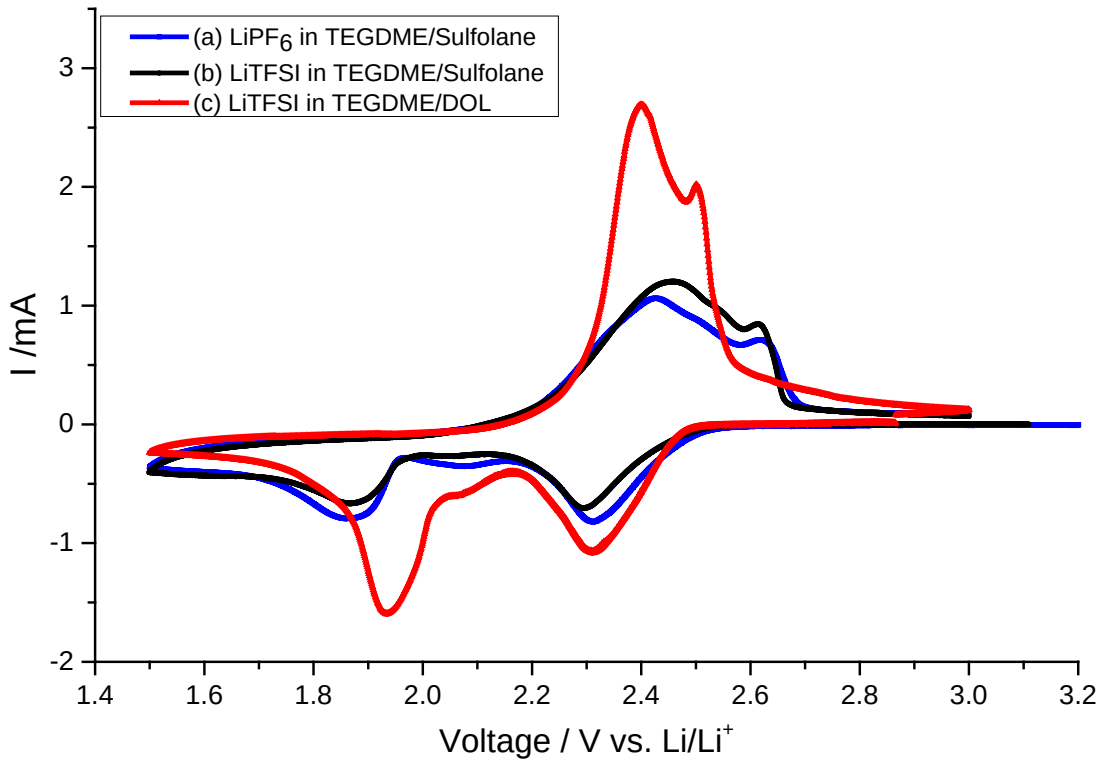

Figure 3.1 Cyclic voltammograms obtained in different liquid electrolytes for sulfur/AB (1:3) composite prepared by ball milling, using potential sweep from 1.5 to 3.0 V at 0.1 $mV.s^{-1}$ scan rate.

On the other hand, the electrolyte based on the DOL solvent shows different values of the peak potentials (Figure 3.1 (c)). The second cathodic peak was slightly shifted to a higher potential at around 1.93 V, and the anodic peaks were shifted to a lower potential at around 2.4 V and 2.5 V, which results in better reversibility of the sulfur in the cell. In addition, a weak peak or shoulder is shown at 2.05 V, particularly for the electrolyte containing DOL, which could be related to the reduction of high order lithium polysulfides to lower order lithium polysulfide Li_2S_4. This is in agreement with the sulfur reduction/oxidation mechanism reported recently.[9]

The total charge was calculated by integrating the area under the peak and then the integrated area was divided by the scan rate. The total charge under the reduction peaks was -5.6, -5.11, and -7.28 coulomb, while the total charge under the oxidation peaks was 3.64, 3.95, and 5.94 coulomb for the cells containing 1M $LiPF_6$ in TEGDME/sulfolane, 1M LiTFSI in TEGDME/sulfolane, and 1M LiTFSI in TEGDME/DOL, respectively. The total charge under reduction peaks is more than the total charge under the oxidation peaks for all cells, which indicates the low efficiency of the cells. Moreover, the cell with electrolyte containing DOL can deliver higher charge than that uses sulfolane-based electrolytes.

The theoretical charge can be calculated by applying Faraday's law:

$$Q = nmF \tag{3.2}$$

Where n is the number of electrons, m is the number of moles of sulfur, and F is the Faraday's constant (96485 C/mol). The theoretical charge of about 9.5 C was calculated based on the amount of sulfur in the electrode, which is higher than that determined from CV measurements. This indicates that the san rate is not slow enough to convert all the sulfur in the cathode.

3.3.2 Galvanostatic discharge

The S/AB electrodes were galvanostatically discharged and charged between 1.5 and 2.8 V vs. Li/Li^+ at a current density of 167.2 $mA.g^{-1}$ of S (C rate of 0.1 h^{-1}), with different electrolytes, assuming a theoretical capacity of 1672 $mAh.g^{-1}$ of S.

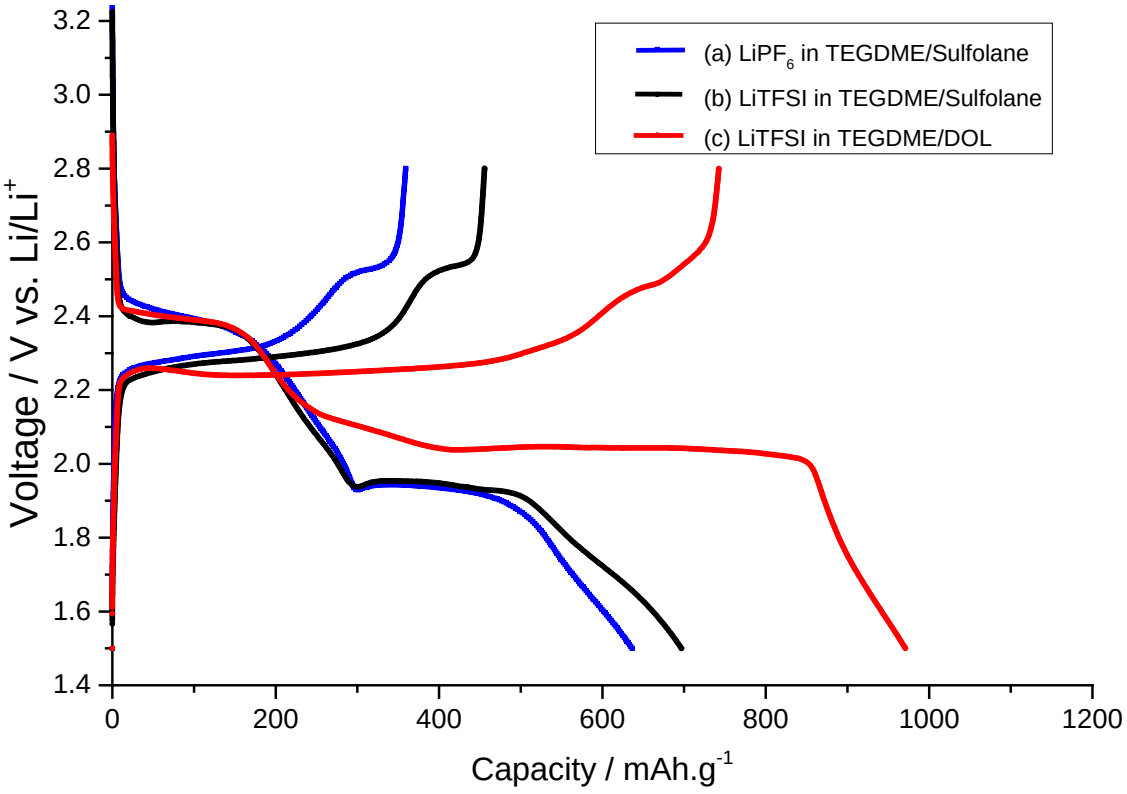

Figure 3.2 Discharge/charge profiles measured with a C rate of 0.1 h^{-1} for S/AB (1:3) composite prepared by ball milling, using different electrolytes (a) 1M $LiPF_6$ in TEGDME/sulfolane, (b) 1M LiTFSI in TEGDME/sulfolane and (c) 1M LiTFSI in TEGDME/DOL.

Figure 3.2 represents the discharge/charge capacity of Li/S cells using 1M $LiPF_6$ in TEGDME/sulfolane, 1M LiTFSI in TEGDME/sulfolane and 1M LiTFSI in TEGDME/DOL. The initial discharge of the cells produces a capacity of 640 and 695 $mAh.g^{-1}$ of S for 1M of $LiPF_6$ in TEGDME/sulfolane and 1M of LiTFSI in TEGDME/sulfolane, respectively. The initial discharge capacities are almost the same and there is no significant difference in the discharge capacity results with the change of lithium salt. This means that changing the salt did not affect the capacity. This is in agreement with what has been reported, that lithium salt has no significant effects on the electrochemical performance of the Li/S cell.[10]

Moreover, two plateaus are clearly shown in the discharge curve of the sulfolane-based electrolytes, which is similar to those reported earlier,[11,12] corresponding to the two reduction stages of elemental sulfur to the soluble lithium polysulfides and then to the solid state lithium sulfide. On the other hand, the capacity produced on the initial discharge of the electrolyte containing DOL is higher than the capacity produced by electrolytes containing sulfolane (see Figure 3.2 (c)). The initial discharge of the cell produces a capacity of about 970 $mAh.g^{-1}$ of S, which is about 40% higher than that produced by any other cells. Also, two plateaus and a shoulder are clearly shown in the discharge curve (Figure 3.2 (c)), and are related to the three reduction steps reported recently.[9]

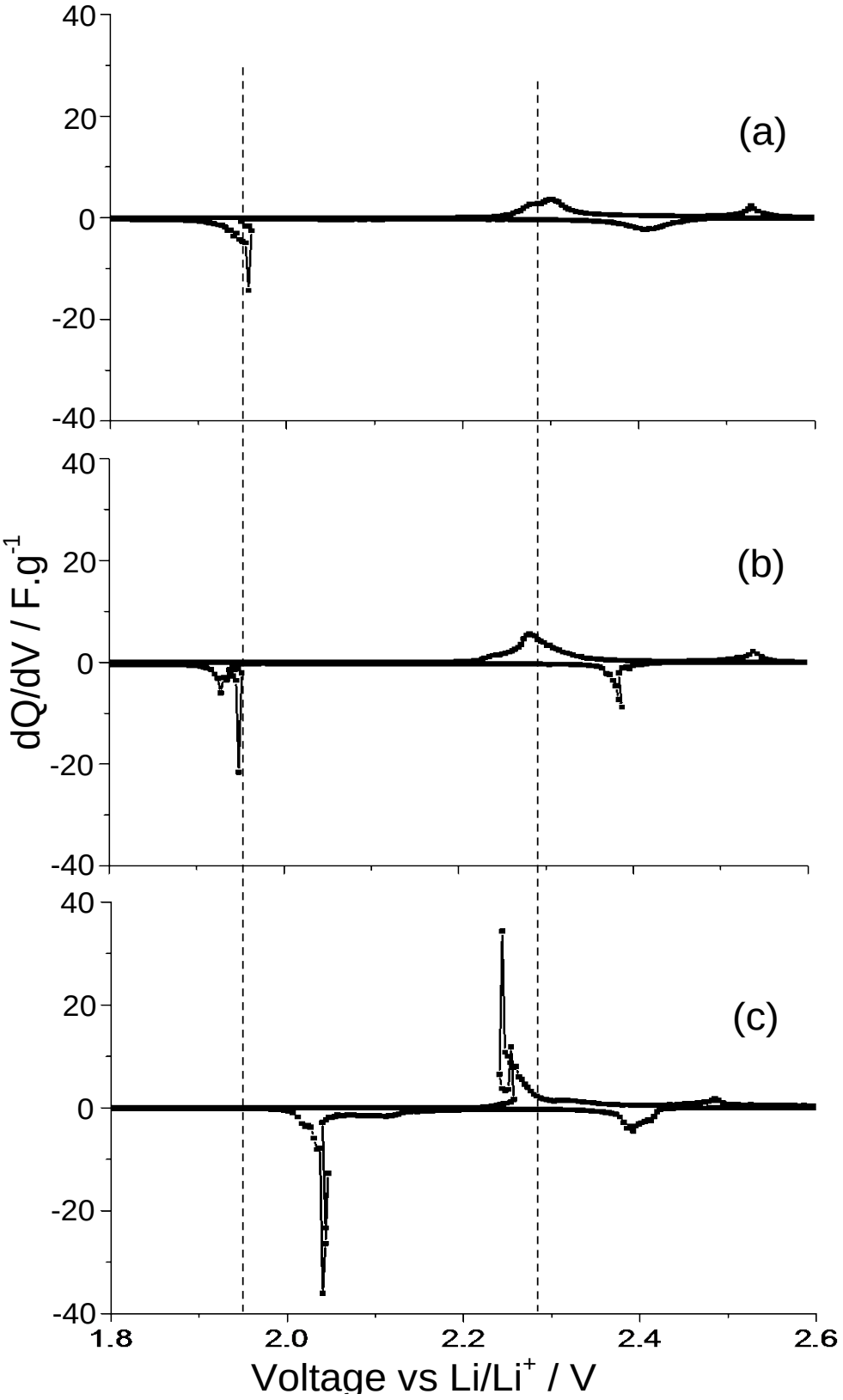

Figure 3.3 Differential capacity vs. voltage for sulfur electrodes reproduced from the 1st discharge/charge curves in different electrolytes (a) 1M $LiPF_6$ in TEGDME/sulfolane, (b) 1M LiTFSI in TEGDME/sulfolane and (c) 1M LiTFSI in TEGDME/DOL.

The differential capacity (dQ/dV) versus voltage for sulfur electrodes with different electrolytes during the first discharge/charge are presented in Figure 3.3. The differential capacity curve is obtained by differentiating the capacity-voltage curve in Figure 3.2. The differential capacity curve shows a number of peaks, and each peak corresponds to the potential plateau. The peaks for the electrolytes containing sulfolane, as shown in Figure 3.3 (a) and (b), are almost at the same potentials. The plot in Figure 3.3 (c) for the electrolyte containing DOL is more symmetrical and the peak for the lower discharge plateau is significantly shifted to a higher potential, and the peak for the lower charge plateau is significantly shifted to a lower potential. This is in agreement with the reported result that electrolytes have an important effect on the discharge behaviour of the Li/S cell.[3]

This can be explained by knowing that the viscosity of the electrolyte medium in the cathode will increase with the formation of soluble lithium polysulfides, resulting in the low lithium ion diffusion inside the cathode.[2] As a consequence, the generation of solid reduction products will be more likely at the surface of the cathode. Forming a thick layer of solid lithium sulfide at the surface of the cathode means no more reduction of soluble polysulfides can occur resulting in diminished sulfur utilization. It is known that the viscosity of DOL is less than that for sulfolane, and adding DOL decreases the viscosity of the electrolyte, and as a result increases the ionic conductivity.[2] The low viscous electrolyte might be able to increase the diffusion rate of lithium ion and the dissolution rate of the solid material (elemental sulfur and lithium sulfide), resulting in an improvement of reversibility of the electrode and helping the cell to reach the maximum sulfur utilization.

3.4 The effect of electrolyte on cycle life performance

The cycle life performance of S/AB (1:3) composite cycled versus metallic lithium negative electrode at a rate of 0.1 h^{-1} in different electrolytes is given in Figure 3.4. The initial discharge of the cells shows a capacity of 640, 695 and 970 $mAh.g^{-1}$ of S in $LiPF_6$ in TEGDME/sulfolane, LiTFSI in TEGDME/sulfolane and LiTFSI in TEGDME/DOL, respectively. In subsequent cycles, the discharge capacity was rapidly decreased at the 2nd cycle, and then the capacity fading was relatively slow and remained relatively stable after the 5th cycle. It can be observed that the cells with electrolytes containing sulfolane showed slower capacity decay than the one with DOL, and a capacity of 280, 313 and 290 $mAh.g^{-1}$ of S was attained at 20 cycles (a capacity retention of 44, 45, 30% respectively).

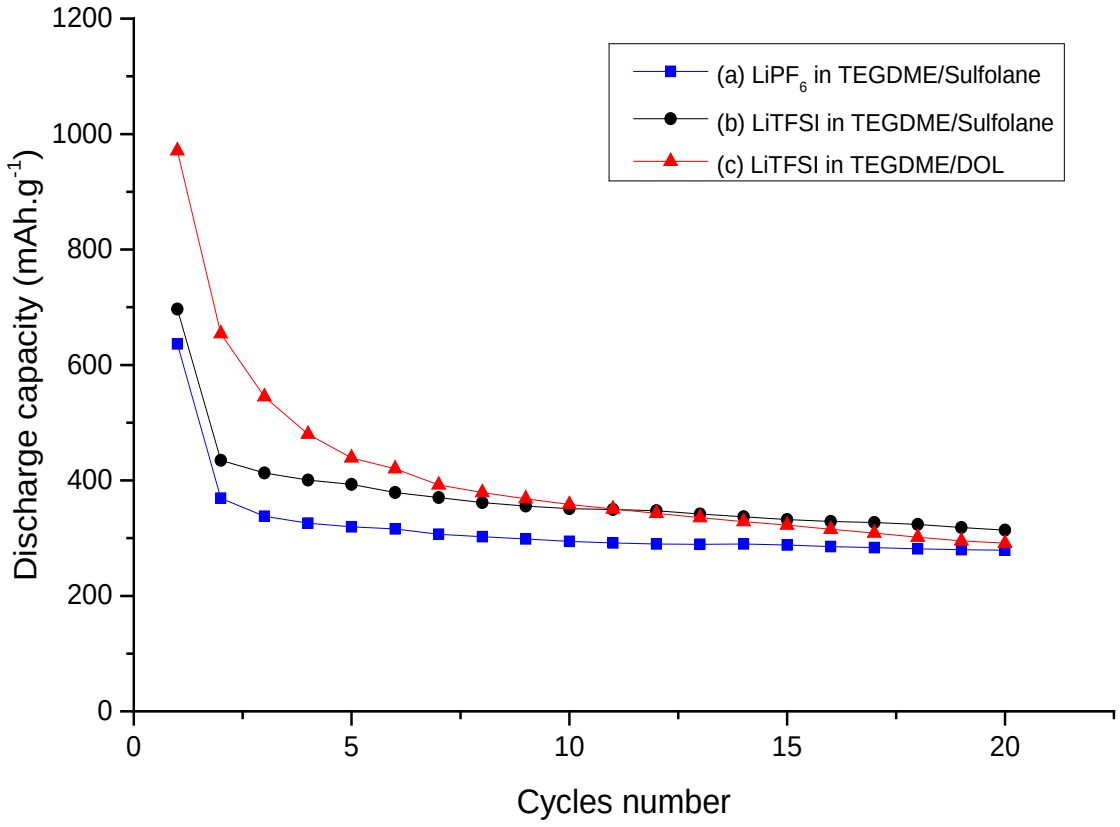

Figure 3.4 Cycle performance of S/AB (1:3) composite prepared by ball milling at a C rate of 0.1 h^{-1}, using different electrolyte (a) 1M $LiPF_6$ in TEGDME/sulfolane, (b) 1M LiTFSI in TEGDME/sulfolane and (c) 1M LiTFSI in TEGDME/DOL.

Although, the electrolyte containing DOL can obtain a higher discharge capacity than the other electrolytes, the capacity fading was faster than the other cells that contained sulfolane, and shows a gradual decrease in the capacity after 5th cycle. This is dependent on the mobility of the polysulfide species through the solvent electrolyte which can be related to the viscosity of the electrolyte, as mentioned before. The electrolyte containing DOL had less viscosity than the other electrolytes which contain sulfolane, allowing more high order polysulfide species to be able to diffuse between the two electrodes; hence there is an increase in the shuttle mechanism, in addition to the reaction of polysulfide species with the lithium electrode to produce insoluble polysulfide which will precipitate on the surface of the anode,[13,14] resulting in a loss of sulfur utilization and a rapid decrease in the capacity over the subsequent cycles.

3.5 The effect of electrolyte at different C rate

The discharge performance of the S/AB (1:3) composite prepared by ball milling measured at different C rates, using 1M $LiPF_6$ in TEGDME/Sulfolane, 1M LiTFSI in TEGDME/Sulfolane and 1M LiTFSI in TEGDME/DOL are shown in Figures 3.5, 3.6 and 3.7, respectively.

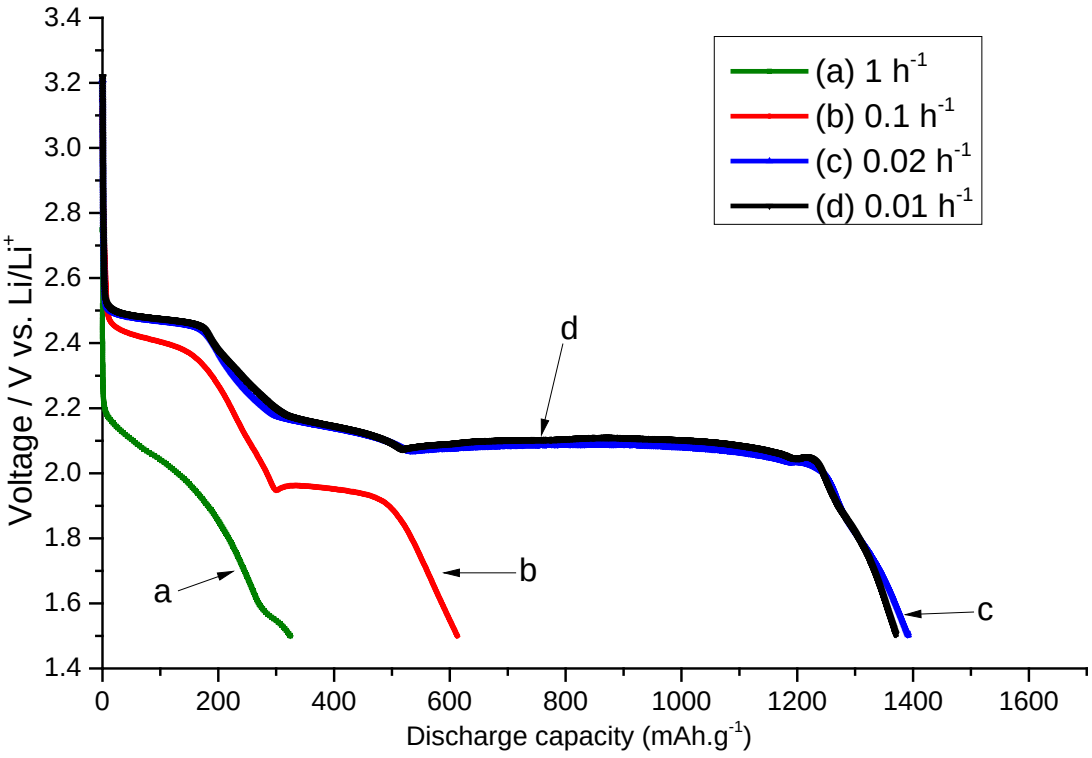

Figure 3.5 Discharge profiles measured for S/AB (1:3) composite prepared by ball milling, using 1M $LiPF_6$ in TEGDME/sulfolane, at a C rate of (a) 1 h^{-1}, (b) 0.1 h^{-1}, (c) 0.02 h^{-1} and (d) 0.01 h^{-1}.

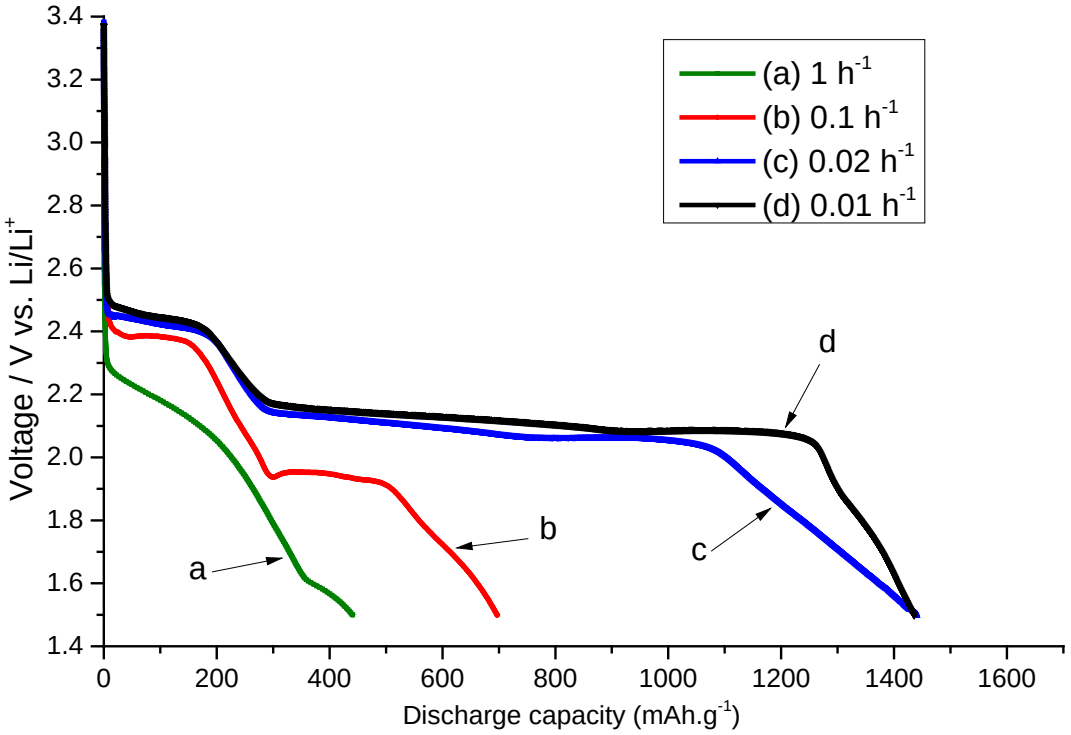

Figure 3.6 Discharge profiles measured for S/AB (1:3) composite prepared by ball milling, using 1M LiTFSI in TEGDME/sulfolane, at a C rate of (a) 1 h^{-1}, (b) 0.1 h^{-1}, (c) 0.02 h^{-1} and (d) 0.01 h^{-1}.

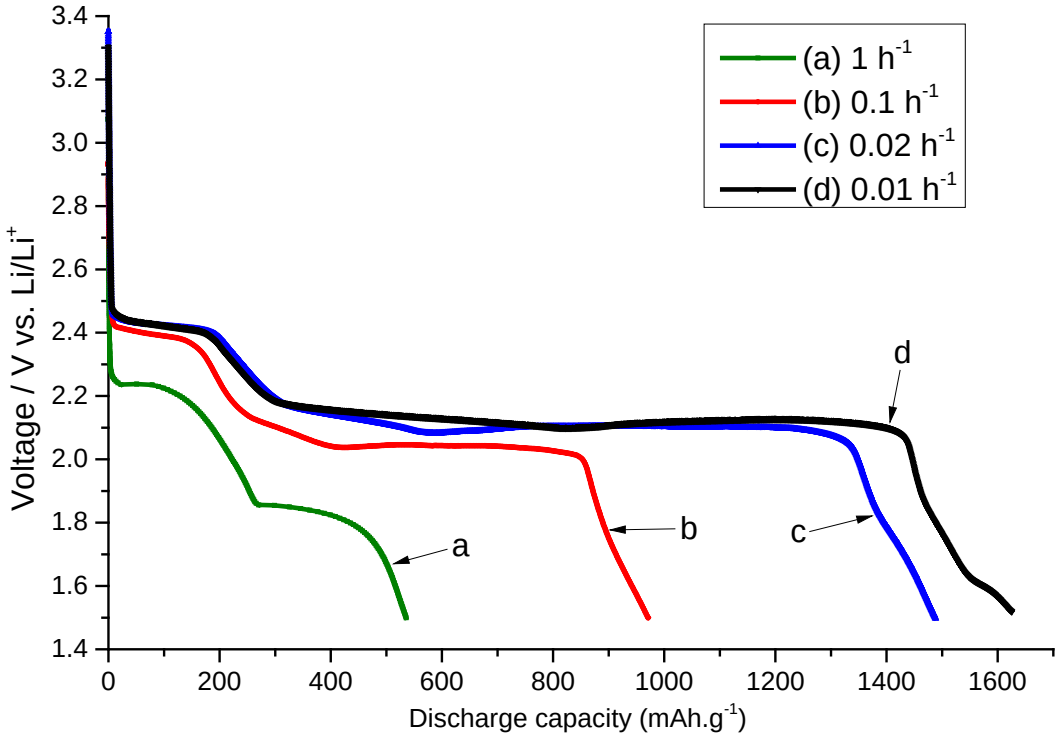

Figure 3.7 Discharge profiles measured for S/AB (1:3) composite prepared by ball milling, using 1M LiTFSI in TEGDME/DOL, at a C rate of (a) 1 h^{-1}, (b) 0.1 h^{-1}, (c) 0.02 h^{-1} and (d) 0.01 h^{-1}.

All cases shows scan rate dependence, and there is IR drop (voltage loss) at the high discharge rate. Also, the discharge potential decreased as the rate of discharge was increased. The IR drop increased due to creating the greater initial resistance in the cell resulting from applying a larger current at a higher discharge rate, and this makes the discharge curve have a low voltage, i.e. less than 2.3 V for first plateau and 1.8 V for the second. Also, only 32% of the sulfur was utilized when the cell was discharged at the high discharge rate of 1 h^{-1} (based on the theoretical specific capacity 1672 $mAh.g^{-1}$ of S); less than 550 $mAh.g^{-1}$ of S discharge capacity was obtained for the electrolyte containing DOL, and less than that for the other electrolytes based on sulfolane.

On the other hand, decreasing the discharge rate helps to decrease the IR drop, and the discharge capacity increased to reach the highest values of 1370, 1435, and 1625 $mAh.g^{-1}$ of S at a C rate of 0.01 h^{-1} by using $LiPF_6$ in TEGDME/sulfolane, LiTFSI in TEGDME/sulfolane and LiTFSI in TEGDME/DOL, respectively. As reported before, the high discharge efficiency was found at extremely low discharge rates.[15]

The effect of the discharge rate on sulfur utilization in different electrolytes is more easily visualised in Figure 3.8. It is clear that the sulfur utilization increased for all the electrolytes with a decrease in the discharge rate. Also, it shows that decreasing the discharge rate from a rate corresponding to 0.02 h^{-1} to a rate of 0.01 h^{-1} does not have a large impact on the sulfur utilization of the cells using electrolytes containing sulfolane. Sulfur utilization stabilized at 82% (1370 $mAh.g^{-1}$ of S) and 85% (1435 $mAh.g^{-1}$ of S) after the discharge rate of 0.02 h^{-1} for the cells uses $LiPF_6$ in TEGDME/sulfolane, and LiTFSI in TEGDME/sulfolane, respectively. In comparison, the capacity continued to increase for the electrolyte containing DOL to reach about 97% of the sulfur utilization at a C rate of 0.01 h^{-1}.

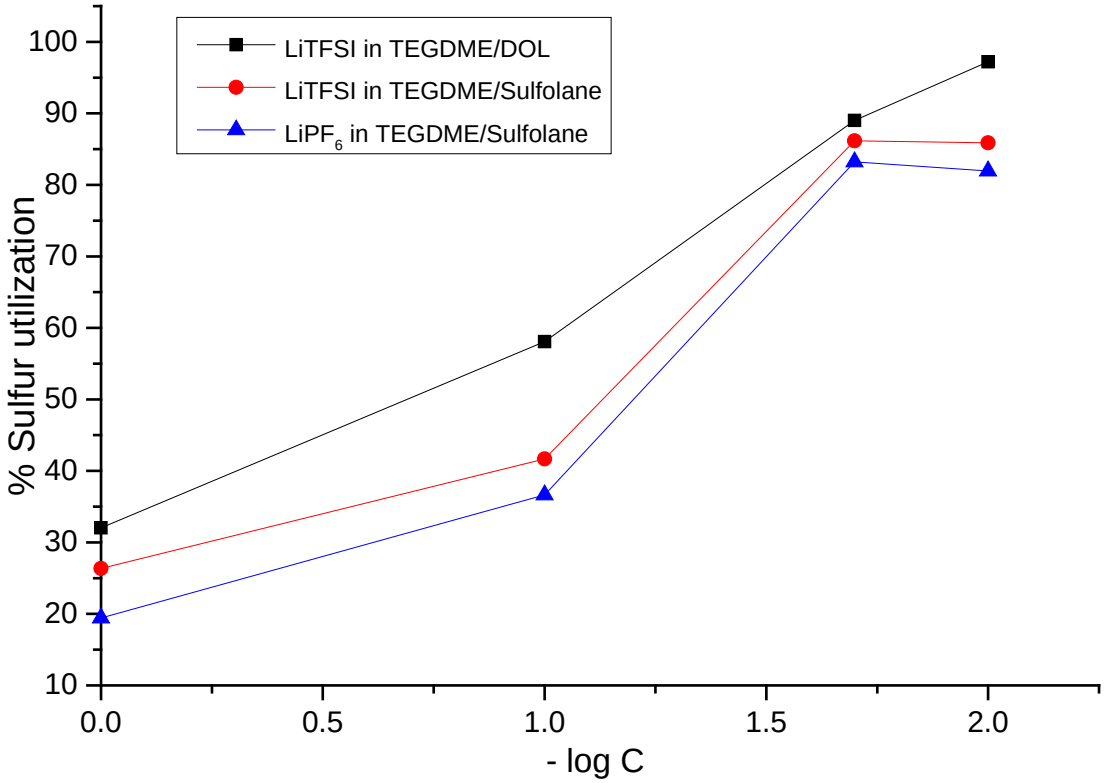

Figure 3.8 Sulfur utilization ratio for S/AB (1:3) composite prepared by ball milling vs. - log C rate using different electrolytes.

When the discharge rate decreased to 0.02 h^{-1}, the capacity was increased for all cells, because there will then be enough time for lithium ions to move and penetrate the sulfur electrode. Thus more sulfur can participate in the reaction. Decreasing the discharge rate from 0.02 h^{-1} to 0.01 h^{-1} did not affect the capacity for the electrolytes containing sulfolane; this might be related to the deposition of a thick layer of solid Li_2S_2 and Li_2S on the surface of the electrolyte which will diminish the reduction to reach the theoretical capacity. On contrary, the low viscosity of the electrolyte containing DOL might be able to delay the precipitation of solid product on the surface of the electrode, and thus reach the highest capacity (1625 $mAh.g^{-1}$ of S), which is very close to the theoretical capacity of sulfur.

3.6 Conclusion

The electrochemical performance of S/AB (1:3) composite prepared by ball milling, in different electrolyte systems containing 1M of $LiPF_6$ in TEGDME/sulfolane, 1M of LiTFSI in TEGDME/sulfolane, and 1M of LiTFSI in TEGDME/DOL was investigated. The results show that the performance of Li/S cells can be influenced by the electrolyte applied to the system. Electrolytes containing sulfolane behave in a similar way, and there is no significant difference in their CVs and discharge capacity curves. This indicates that changing the lithium salt has no significant effect on the electrochemical performance of the Li/S cells, while the electrolyte containing DOL, shows the highest discharge capacity and better reversibility.

The viscosity difference between these electrolytes would affect their penetration into the sulfur electrode structure, and by using sulfolane, which is more viscous, makes it hard for the ions to penetrate the electrode and would be expected to reduce the migration of ions between the electrodes in the cell. On the other hand, the low viscosity of DOL could increase the diffusion rate of the lithium ions and the dissolution rate of the solid material, resulting in enhanced reversibility of the electrode and increased sulfur utilization.

In addition, the effect of the discharge rate on the electrochemical performance of Li/S cells in different electrolytes was investigated. It revealed that the IR drop was affected by the discharge rate of the cell. Higher discharge rates, due to the larger current being applied, created greater initial resistance in the cell resulting in a higher IR drop.

Decreasing the rate of discharge would affect the sulfur utilization in the cell. The sulfur utilization increased as the rate of discharge was decreased. This clearly demonstrated that a rate of discharge contributes to the diffusion and penetration time of lithium ions into the cathode. Decreasing the rate of discharge would allow more time for lithium ions to move and penetrate the sulfur electrode and thus increase the utilization of active material.

The highest discharge capacity was obtained for cells with electrolyte containing DOL at different C rates. The utilization of sulfur was stabilized at a discharge rate of 0.02 h^{-1} for electrolytes containing sulfolane. The deposition of a thick layer of lithium sulfide

on the surface of the sulfur electrode resulted from the high viscosity of electrolytes containing sulfolane would accelerate the end of the discharge, thus reducing the use of active material. In comparison, the low viscosity of the electrolyte containing DOL reduces the deposition of lithium sulfide, and delays the end of the discharge and as a result increases the utilization of sulfur as well as the capacity to reach about 97% of the theoretical capacity at a discharge rate of 0.01 h^{-1}.

3.7 References

(1) Kim, S.; Jung, Y.; Lim, H. S. *Electrochim. Acta* **2004**, *50*, 889–892.

(2) Chang, D.-R.; Lee, S.-H.; Kim, S.-W.; Kim, H.-T. *J. Power Sources* **2002**, *112*, 452–460.

(3) Choi, J.-W.; Kim, J.-K.; Cheruvally, G.; Ahn, J.-H.; Ahn, H.-J.; Kim, K.-W. *Electrochim. Acta* **2007**, *52*, 2075–2082.

(4) Kolosnitsyn, V. S.; Sheina, L. V.; Mochalov, S. E. *Russ. J. Electrochem.* **2008**, *44*, 575–578.

(5) Kim, H.-S.; Jeong, C.-S. *Bull. Korean Chem. Soc.* **2011**, *32*, 3682–3686.

(6) Ryu, H.-S.; Ahn, H.-J.; Kim, K.-W.; Ahn, J.-H.; Lee, J.-Y. *J. Power Sources* **2006**, *153*, 360–364.

(7) Wu, F.; Wu, S. X.; Chen, R. J.; Chen, S.; Wang, G. Q. *Chinese Chem. Lett.* **2009**, *20*, 1255–1258.

(8) Kolosnitsyn, V. S.; Karaseva, E. V; Amineva, N. A.; Batyrshina, G. A. *Russ. J. Electrochem.* **2002**, *38*, 329–331.

(9) Barchasz, C.; Molton, F.; Duboc, C.; Leprêtre, J.-C.; Patoux, S.; Alloin, F. *Anal. Chem.* **2012**, *84*, 3973–80.

(10) Gao, J.; Lowe, M. A.; Kiya, Y.; Abru, D. *J. Phys. Chem.* **2011**, *115*, 25132–25137.

(11) Shim, J.; Striebel, K. a.; Cairns, E. J. *J. Electrochem. Soc.* **2002**, *149*, A1321.

(12) Kolosnitsyn, V. S.; Karaseva, E. V. *Russ. J. Electrochem.* **2008**, *44*, 506–509.

(13) Kolosnitsyn, V. S.; Karaseva, E. V; Seung, D. Y.; Cho, M. D. *Russ. J. Electrochem.* **2002**, *38*, 1314–1318.

(14) Cheon, S.-E.; Ko, K.-S.; Cho, J.-H.; Kim, S.-W.; Chin, E.-Y.; Kim, H.-T. *J. Electrochem. Soc.* **2003**, *150*, A796.

(15) Peled, E. *J. Electrochem. Soc.* **1989**, *136*, 1621.

Chapter 4:

Electrochemical performance of S/AB composites prepared by precipitation method

4.1 Introduction

The direct precipitation method is an inexpensive and easy synthesis method which can provide nanoparticle size of sulfur.[1] By using this method sulfur can be dispersed with acetylene black (AB) homogeneously to provide more effective conductive network and thus enhance the utilization of sulfur. The reaction formula for the preparation of sulfur is as follows:

$$Na_2S_2O_{3(aq.)} + 2HCL_{(aq.)} \rightarrow 2NaCL_{(aq.)} + SO_{2(g)} + S_{(s)} + H_2O_{(l)} \qquad (4.1)$$

In this chapter, the direct precipitation method will be utilized to prepare S/AB composites, to investigate the effect of the amount of AB on the electrochemical performance of S/AB composites. In addition, to study the effects of different methods to prepare the S/AB composites on the electrochemical stability and cycle life performance of Li/S battery.

4.2 Experimental details

4.2.1 Preparation of the composite using precipitation method

1.5 g of sodium thiosulfate (99.5%, Sigma Aldrich) was completely dissolved in 230 ml of deionized water to which 10 ml of 1% Triton X-100 (Polyethylene glycol tert-octylphenyl ether, BDH Chemicals Ltd) aqueous solution was added. A solution of 1 ml of hydrochloric acid (34%, Fisher Scientific) in 9 ml deionized water was slowly added (drop by drop) to the sodium thiosulfate solution with stirring (ca. 2 min.). After one minute, AB (Chevron Phillips Chemical Company LP, specific surface area 76 m^2/g, mean particle size 42 nm) was then added into the sulfur suspension under vigorous magnetic stirring. After 3 hrs, the product was filtered under vacuum using 0.22 µm filter paper. After filtration, the precipitated S/AB was washed several times with deionized water. Finally, the S/AB composite was dried in an oven at 80 ºC overnight then dried at 50 ºC under vacuum for 24 hrs. The amount of AB that has been added was varied in order to obtain S/AB composites in different weight ratios.

For comparison, the S/AB composite was prepared following the same steps as above, but by changing the addition of AB to be before adding the HCl solution.

4.2.2 Preparation of the composite using ball milling method

S/AB composite (30 wt% S) was prepared as described in Chapter 3 using the ball milling method, but by changing the weight ratio of S/AB to be 1:2.

In all electrochemical testing, cells were assembled as described in Chapter 2, using 0.125 ml of 1 M of LiTFSI in TEGDME:DOL (1:1) as an electrolyte. All cells were cycled at 25 ºC.

4.3 The effect of surfactant and AB on the sulfur particle size

Sulfur was prepared using direct precipitation method in order to produce a smaller particle size. To study the effect of the surfactant on the sulfur particle size, Sulfur particles were prepared with and without adding the surfactant. The SEM images of sulfur particles prepared by precipitation method with and without adding the surfactant were presented in Figure 4.1.

The Sulfur particles that prepared without adding Triton X-100 (Figure 4.1a), have a larger particle size (> 10 μm), and agglomerated particles can be observed clearly. Chaudhuri and Paria states that sulfur particles have a tendency towards grain growth and agglomeration rather than discrete particles.[1] Increasing the number of sulfur particles during the reaction will increase the density of this particles in the solution led to more agglomeration will resulted from the collision between the particles.

(a) (b)

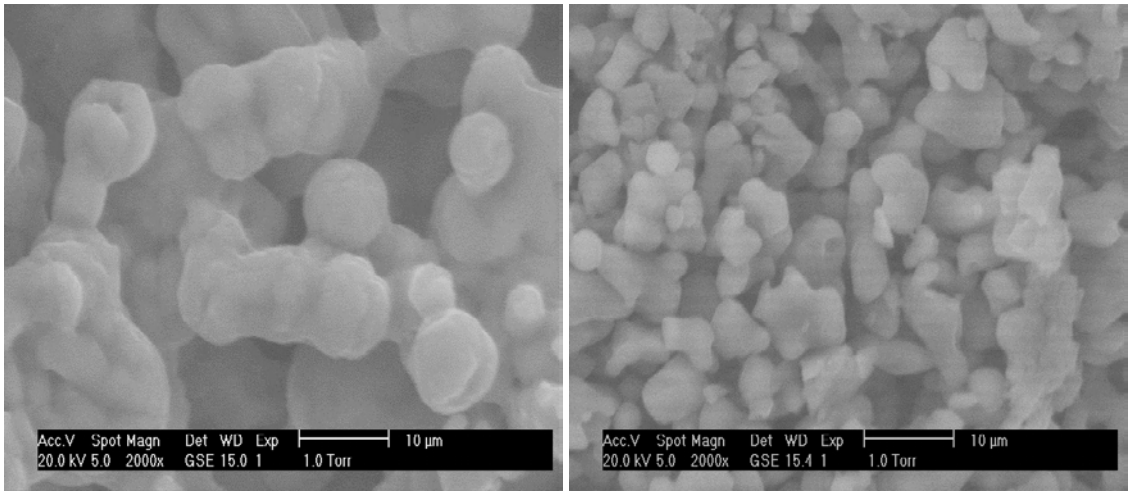

Figure 4.1 SEM images of sulfur particles prepared by precipitation method a) without TX-100, b) with TX-100.

Figure 4.1b presents the sulfur particles generated in the presence of the surfactant TX-100. It shows that adding the surfactant can significantly reduce the sulfur particle diameter to less than 10 μm. The surfactant molecules will be adsorbed on the particle surface through its hydrophobic group and prevent the growth as well as the agglomeration of particles.

The scheme of Figure 4.2 suggests that the role of the surfactant is to prevent the increase of sulfur particle size by coating on the sulfur particles due to its adsorption property, and reducing the growth and the agglomeration tendency of the particles.

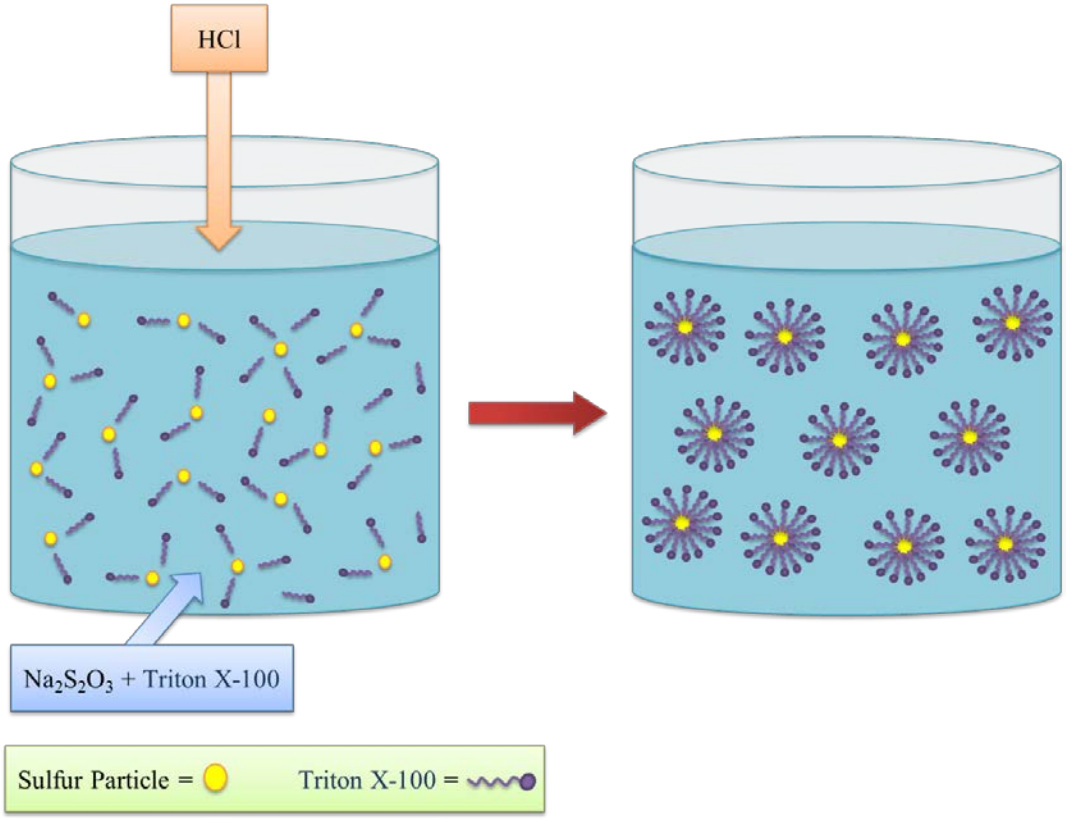

Figure 4.2 - Schematic diagram shows how addition of surfactant prevents grain growth and agglomeration of sulfur particles.

The SEM images of S/AB composites prepared by precipitation method are shown in Figure 4.3. One composite was prepared by adding AB to the solution before the generation of colloidal sulfur (Figure 4.3a), and the other composite was prepared by adding AB to the solution after the generation of colloidal sulfur (Figure 4.3b). It shows that the average size of sulfur particles that prepared by adding AB before the reaction between sodium thiosulfate and hydrochloric acid, is considerably larger than the average size of the particles that prepared by adding AB after the reaction (Figure 4.3b). This suggests that adding AB before the reaction may contributes in increasing the sulfur particle size by providing nucleation sites for facilitating crystal growth.

On the other hand, adding the AB directly after producing the sulfur particles gives a smaller particles size. Adding AB after generation of colloidal sulfur can contributes in preventing the crystal growth of sulfur particles by surrounding the sulfur particles and then stops further increase in the particles size.

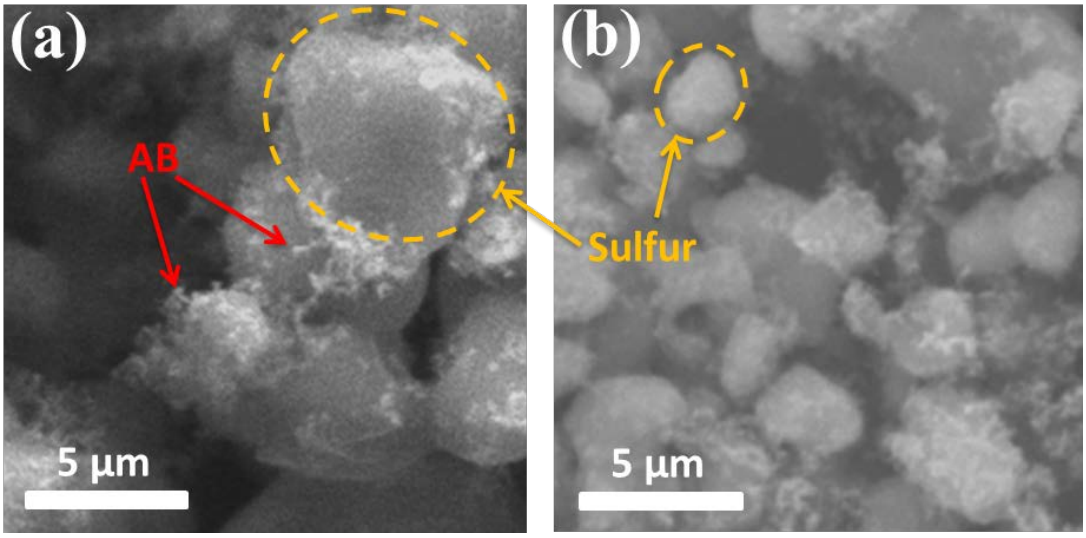

Figure 4.3 SEM images of S/AB composites prepared by precipitation method, by adding AB a) before, and b) after 3minutes of the reaction.

Using the surfactant and adding AB after the reaction gives smaller particles of sulfur, and this resulting in increased the surface area. A larger surface area gives better electrical contact with AB conductor, and led to a greater utilization of active material.

4.4 Galvanostatic cycling of S/AB electrodes

The S/AB electrodes with varied weight ratio of sulfur were galvanostatically discharged and charged between 1.5 and 2.8 V vs. Li/Li^+ at a current density of 167.2 $mA.g^{-1}$ (C rate of 0.1 h^{-1}), with 1M of LiTFSI in TEGDME/DOL using the theoretical capacity of 1672 $mAh.g^{-1}$ of S. The highest discharge capacity of about 1278 $mAh.g^{-1}$ of S was achieved using 30 wt.% sulfur, and the lowest discharge capacity of about 383 $mAh.g^{-1}$ of S was obtained by 72 wt.% sulfur, as shown in Figure 4.4.

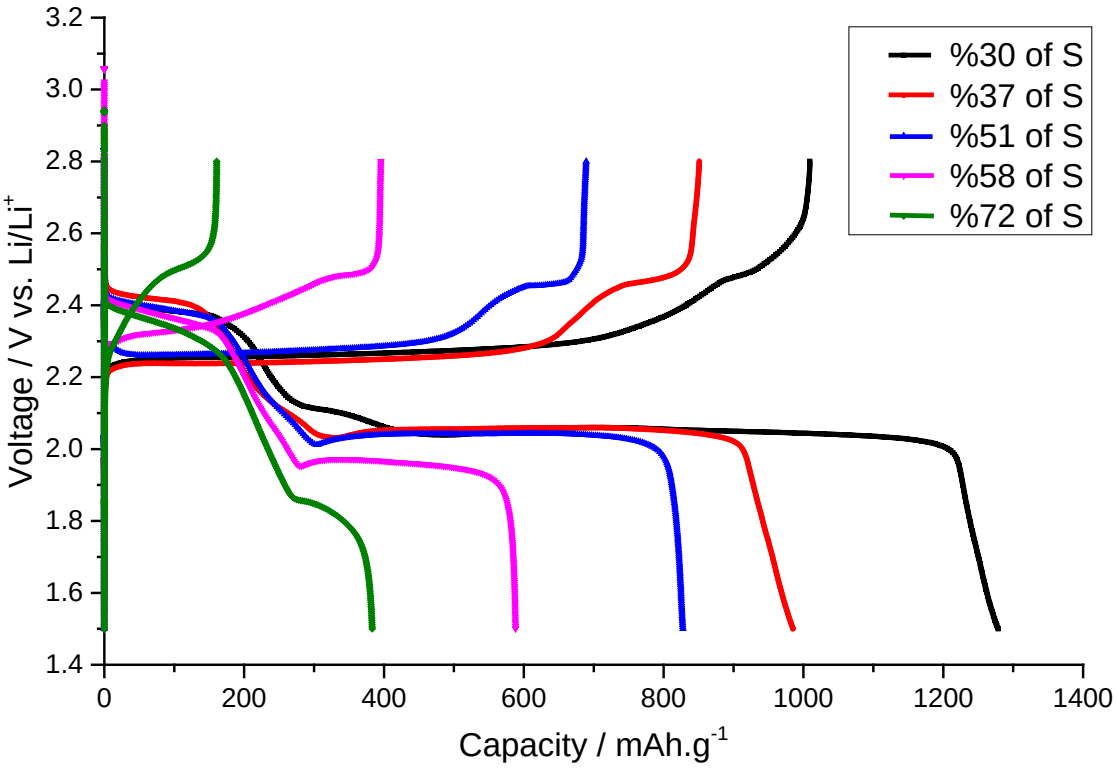

Figure 4.4 Discharge/charge profiles for S/AB composites prepared by precipitation method, using1M of LiTFSI in TEGDME/DOL at a C rate of 0.1 h^{-1} using 72, 58, 51, 37, and 30 weight ratio of sulfur.

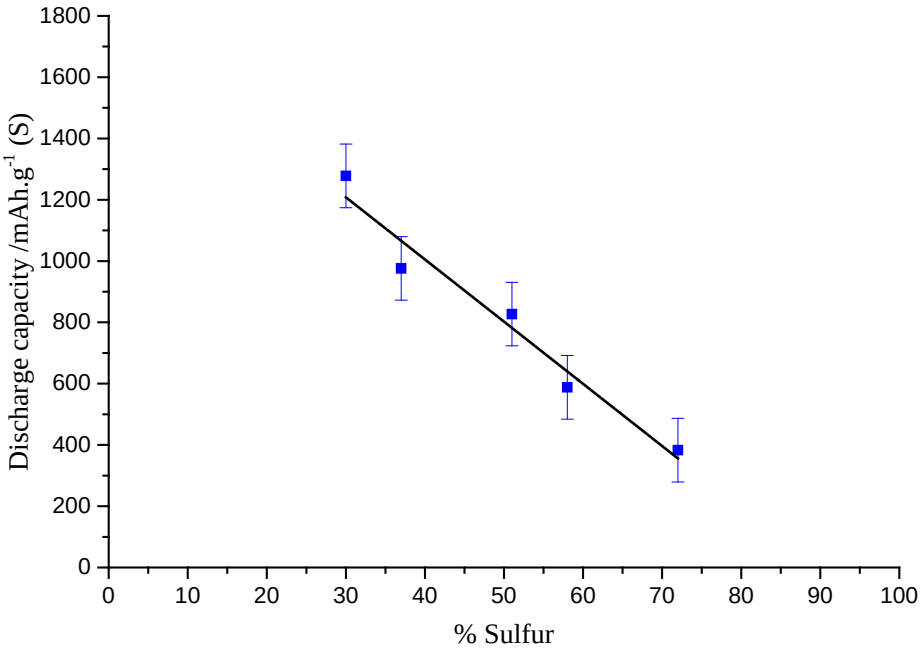

Figure 4.5 Discharge capacity of S/AB composites prepared by precipitation method, using1M of LiTFSI in TEGDME/DOL at a C rate of 0.1 h^{-1} using different weight percentage of sulfur.

The 1st discharge capacity of S/AB electrodes versus the weight percentage of sulfur to the total mass of the electrode was plotted in Figure 4.5, in order to analyse the large improvement in the discharge capacity with the decrease in sulfur content. It can be seen that the discharge capacity increases when the sulfur content decreases. In other words, as the AB fraction in the composites increases the discharge capacity increases. This can be attributed to the fact that sulfur is highly electrically insulator, and needs to remain in intimate contact with a conductor to gain high performance. The AB content as a conducting material significantly improves the capacity of the sulfur electrode as a result of increase the contact area between sulfur and acetylene black.[2] So that, adding more AB to the electrode does enhance the discharge capacity by enhances the electronic conductivity of the electrode. Moreover, as the AB content increases, the electrode surface area is also increases, and the passivation layer formed from the deposition of insoluble products (Li_2S_2 and Li_2S) at the end of the discharge will be thinner,[3] thus increases the capacity as delaying the end of discharge. This indicates that sulfur utilization is affected by the percentage of active mass in the electrode.

4.4.1 Comparison of the first plateau lengths of the first discharge curves

The first plateau in the discharge curve can be related to the reaction of elemental sulfur at the cathode with lithium ions to form high order polysulfide (Li_2S_8). The first plateau length of the first discharge with varying the weight ratio of AB to the total mass of the electrode is presented in Figure 4.6. It can be observed that there is no significant change in the first plateau length for all the cells, and it almost deliver the same discharge capacity of about 160 $mAh.g^{-1}$ of S. This indicates that increasing the amount of AB in the electrode had no effect on the first plateau length, and the contribution of the first plateau in the first discharge capacity is independent on the amount of AB in the electrode.

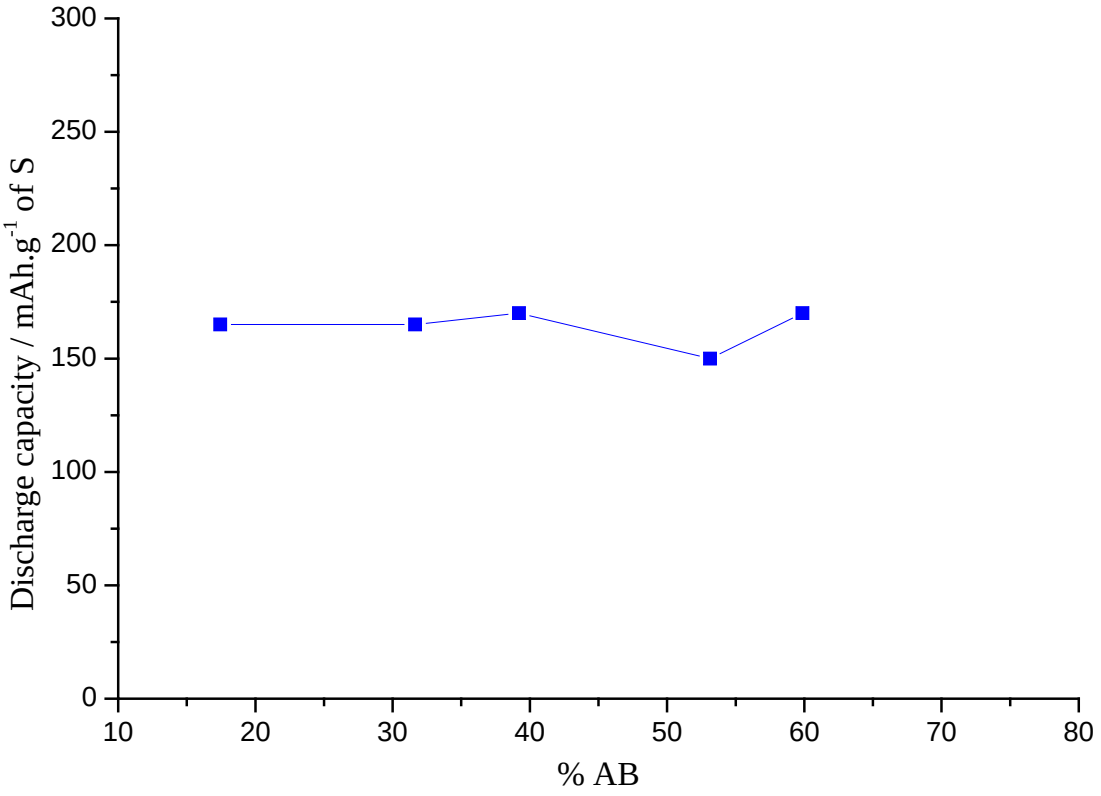

Figure 4.6 1st plateau length of the 1st discharge verses % acetylene black.

4.4.2 Comparison of the second plateau lengths of the first discharge curves

The second plateau in the discharge curve can be attributed to the reduction of low order lithium polysulfides to produce solid products Li_2S_2 and Li_2S. Figure 4.7 displays the second plateau length of the first discharge with varying the weight ratio of AB to the total mass of the electrode. It is clearly seen that there is a direct relationship between the 2nd plateau length and the amount of AB. The 2nd plateau length decreases with decreasing the weight ratio of AB in the electrode.

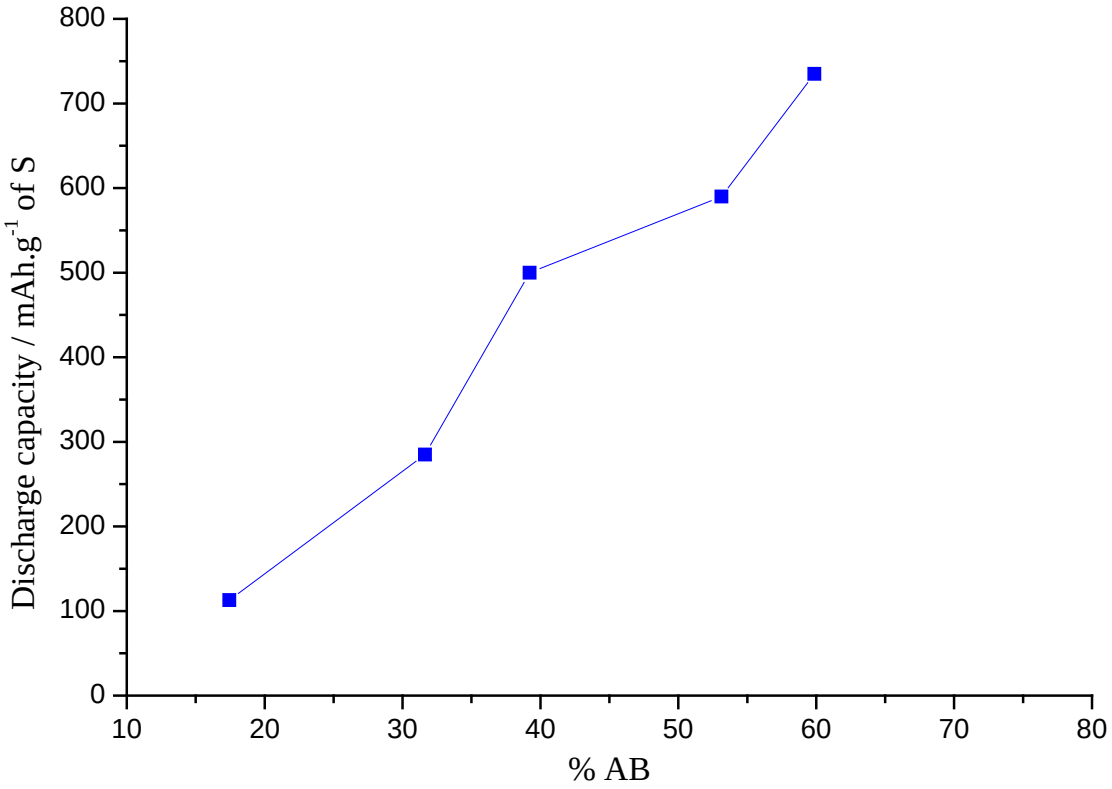

Figure 4.7 2nd plateau length of the 1st discharge verses % acetylene black.

As mentioned before, the electrode surface area would be affected by the AB content. Decreasing the AB as the sulfur amount increases, should reduce the surface area of the electrode. The passivation layer formed from the deposition of insoluble products at the cathode surface will increases, and will prevent further reduction of polysulfides and accelerate the end of the discharge, thus will shortening the second plateau length. This indicates that the contribution of the third plateau in the first discharge capacity is significantly affected by the amount of AB in the electrode.

4.5 Comparison between S/AB composites prepared by precipitation and ball milling methods

4.5.1 Cyclic voltammetry

Cyclic voltammograms of S/AB composites (30 wt% S) prepared by precipitation and ball milling methods, using 1M of LiTFSI in TEGDME/DOL as an electrolyte tested with 0.1 $mV.s^{-1}$ scan rate are shown in Figure 4.8. It can clearly see that there are two reduction peaks and shoulder. The first peak represents the transformation of sulfur to long chain lithium polysulfides at 2.31V, and the shoulder is related to the reduction of long chain lithium polysulfides to lower order lithium polysulfides species (eg, Li_2S_4) at 2.1 V, and the second peak at around 1.9 V corresponds to reduction of Li_2S_4 to form solid state Li_2S_2 and Li_2S. Also, two oxidation peaks could be observed at 2.41 and 2.54V represent the reverse transformation of lithium sulfide to Li_2S_4 and then to elemental sulfur.[4]

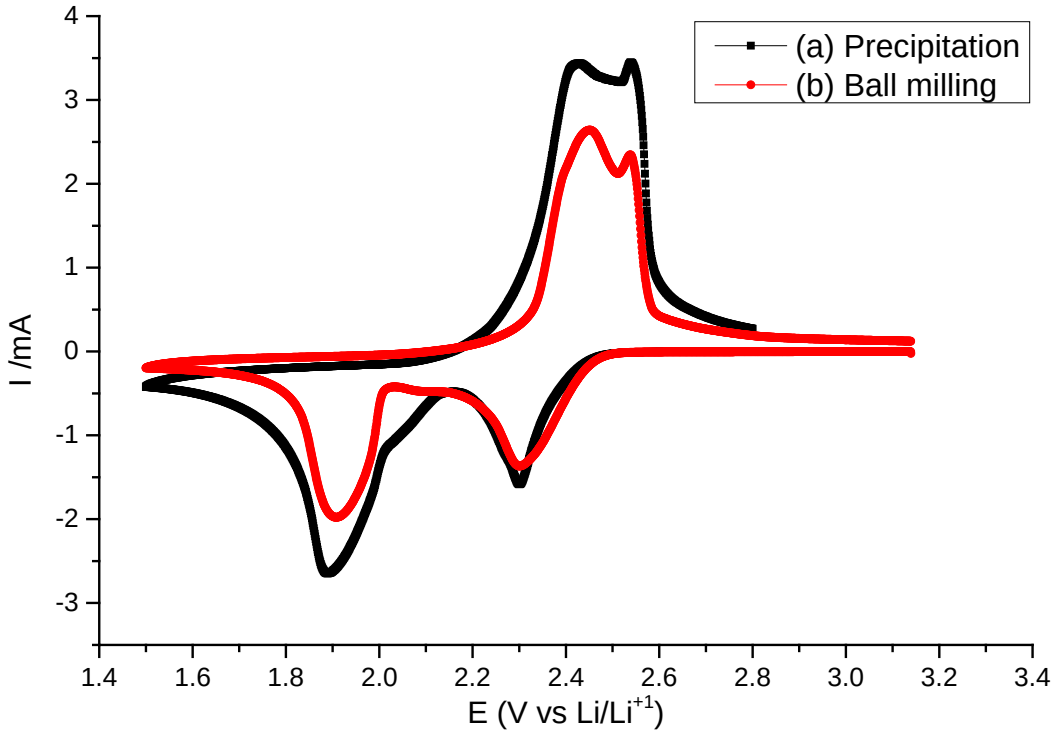

Figure 4.8 Cyclic voltammograms obtained for S/AB composites (30 wt% S) prepared by (a) precipitation and (b) Ball milling method, using LiTFSI in TEGDME/DOL, using 0.1 $mV.s^{-1}$ scan rates.

The potential difference between the second reduction peak and first oxidation peak is very high, indicating that this process is electrochemically irreversible, while the potential difference between the first reduction peak and second oxidation peak is much closer to reversible. The area under the peak was integrated and then was divided by the scan rate in order to calculate the charge under the peaks. The total charge under the reduction peaks was -10.77 and -7.27 coulomb, while the total charge under the oxidation peaks was 9.1 and 6.32 coulomb, for S/AB composites (30 wt% S) prepared by precipitation and ball milling methods, respectively. These results displays that the total charge under reduction peaks is more than the total charge under the oxidation peaks, which indicates the low efficiency of the cells. Moreover, it shows that the composite prepared using precipitation method can deliver higher charge than that prepared via ball milling method.

Based on the amount of sulfur in the electrode, a theoretical charge of about 14 C was calculated using Faraday's law, which is higher than that determined from CV measurements. This indicates that the san rate is not slow enough to convert all the sulfur in the cathode.

4.5.2 Discharge capacity

The SEM images of the S/AB composites (30 wt% S) prepared by precipitation and ball milling methods are presented in Figure 4.9. It is clearly shown that the particles of the composite prepared by precipitation method have uniform particles with the particle size below 5 µm (Figure 4.9 a). While the particles of the composite prepared by ball milling method are irregular, with the particle size more than 10 µm (Figure 4.9 b).

(a) (b)

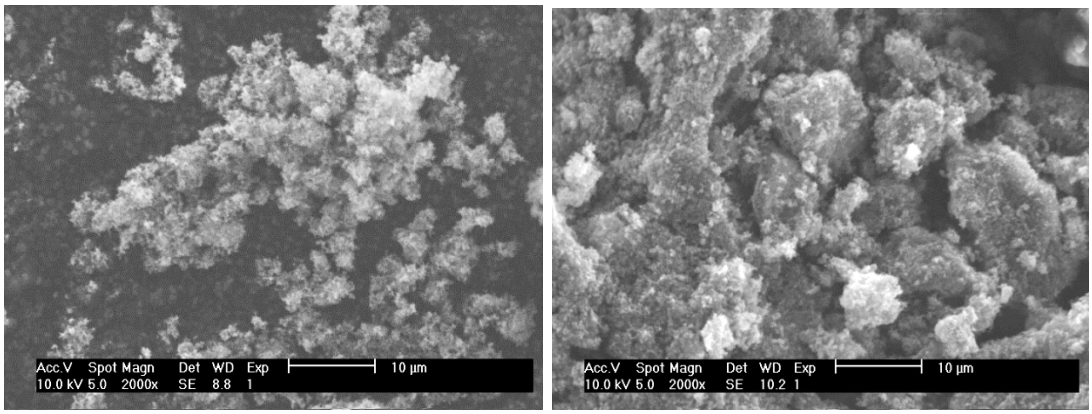

Figure 4.9 SEM images of S/AB composites (30 wt% S) prepared by a) Precipitation, and b) Ball milling methods.

Figure 4.10 displays the first discharge/charge profile of S/AB composites (30 wt% S) prepared by precipitation and ball milling methods at the current density of 167.2 mA/g (C rate of 0.1 h^{-1}), using 1M of LiTFSI in TEGDME/DOL as an electrolyte. Figure 4.10 (a) shows that the discharge capacity for the composite prepared by precipitation method is 1280 $mAh.g^{-1}$ of S (which corresponded to 75.5 % of sulfur utilization based on the theoretical capacity of sulfur 1672 $mAh.g^{-1}$), While it produces a capacity of about 800 $mAh.g^{-1}$ of S (about 48 % of sulfur utilization) for the composite prepared by ball milling method (Figure 4.10 b). The discharge capacity for the composite prepared via the precipitation method is about 37% higher than that uses ball milling method.

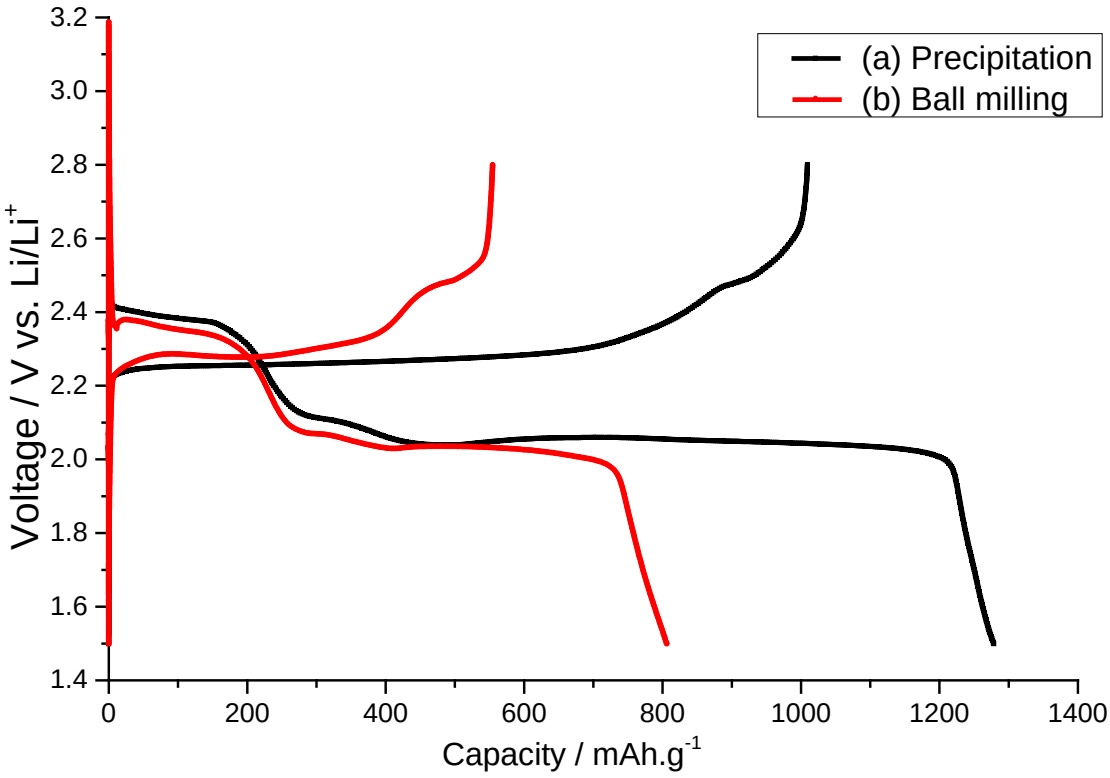

Figure 4.10 Discharge/charge profiles for S/AB composites (30 wt% S) prepared by (a) precipitation and (b) Ball milling methods, using 1M of LiTFSI in TEGDME/DOL at a C rate of 0.1 h^{-1}.

There is no significant different between the first plateau length during the first discharge for the precipitation and ball milling methods as clearly shown in Figure 4.10. On the other hand, the second plateau length for precipitation method is longer than that for ball milling method. The second plateau is corresponding to the generation of solid product Li_2S_2 and then Li_2S at the end of the discharge, which will deposited on the electrode surface, and the thicker the passivation layer can prevent further reduction of polysulfides, thus accelerate the end of discharge, as mentioned before. Using precipitation method to prepare S/AB composite will give an intimate contact with AB by making sulfur particles well-dispersed in the carbon matrix, providing a more electronically conductive network. Also, it reduces sulfur particle size and gives smaller particles, and thus increases the surface area of the electrode as well as increase the contact area between sulfur and acetylene black. Higher electrode surface area leads to thinner passivation layer, and thus increases the capacity and delay the end of discharge.[3]

Moreover, the smaller particles of sulfur lead to smaller pores that form after the complete dissolution of elemental sulfur into the electrolyte during the discharge. Smaller pores would have the more favourable structure for confining and absorbing the soluble lithium polysulfide species,[5] thus it can decrease the diffusion of lithium polysulfide species away from the cathode, resulting in the enhancement of the capacity and a better use of sulfur as an active material.

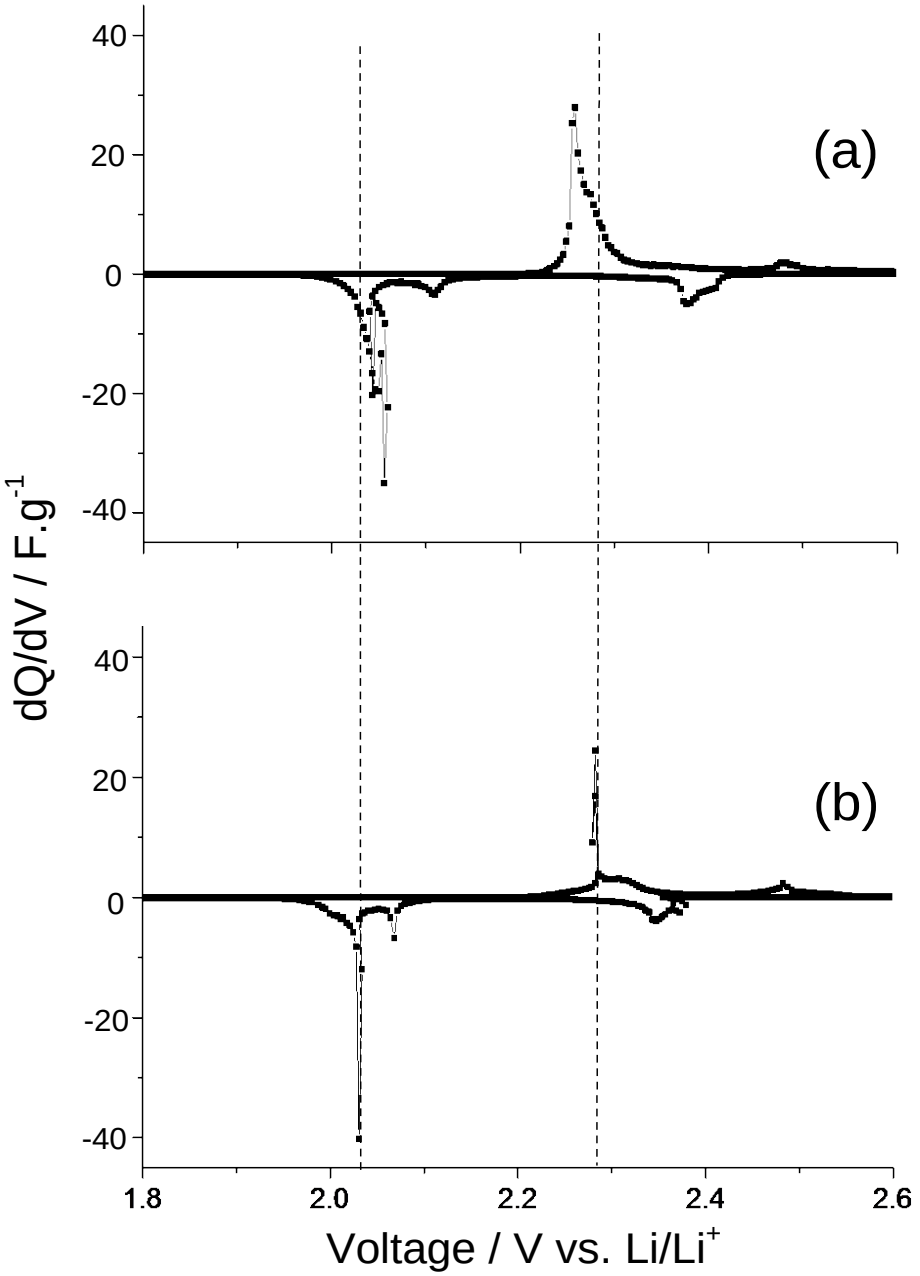

Figure 4.11 Differential capacity vs. voltage for S/AB composites (30 wt% S) prepared by (a) precipitation and (b) Ball milling methods, in 1 M LiTFSI in TEGDME/DOL, reproduced from the 1st discharge/charge curves.

The differential capacity (dQ/dV) versus voltage for sulfur electrodes prepared by precipitation and Ball milling method reproduced from Figure 4.10 are presented in Figure 4.11. It is clearly seen that the differential capacity curve for S/AB composite prepared by ball milling method shows five peaks, two peaks at 2.48 and 2,28 V during the charge, and three peaks at 2.37, 2.04 and 2.03 V during the discharge (Figure 4.11b). It can be observed that for S/AB composite prepared by precipitation method, the peak corresponding to 2.28 V plateau during charge move slightly to lower voltage, and the peaks corresponding to 2.03 and 2.04 V plateaus during discharge significantly shifts to higher voltage (Figure 4.11a), resulting in an improvement in the reversibility of the reaction. The S/AB composite prepared by precipitation method shows better reversibility and higher discharge capacity compare to the ball milling method.

4.5.3 Galvanostatic cycling

The cycle life performance of S/AB composites prepared by precipitation and ball milling methods, using 1M of LiTFSI in TEGDME/DOL as an electrolyte cycled at a C rate of 0.1 h^{-1} are shown in Figure 4.12. The first discharge capacity showed about 800 and 1280 $mAh.g^{-1}$ of S for ball milling and precipitation methods, respectively. At subsequent cycles, discharge capacity was rapidly decreased at 2nd cycle, and then the capacity fading was relatively slow and remained relatively stable after the 10th cycle, and show about 120 and 320 $mAh.g^{-1}$ of S at 50^{th} cycles for ball milling and precipitation methods, respectively.

The rapid decrease in the capacity during the first 10 cycles can be attributed to the loss of the active material during discharge resulted from deposition of Li_2S on the positive electrode, which prevent the further reduction of sulfur and causes the early end of the discharge.[6,7] Also, the uncompleted conversion of polysulfide species to elemental sulfur during charge participated in the rapid decrease in the capacity over the subsequent cycles.[8,9]However, there is a decrease in the capacity during cycling for S/AB composites prepared by these two methods due to irreversible capacity loss, the

composite prepared by precipitation method had a better cycle performance. It shows 25 % of the capacity retention after 50th cycles. This indicates that the composite structure of the S/AB prepared by precipitation method can effectively confine polysulfide species in the carbon matrix and reduce their diffusion in the electrolyte.

On the contrary, S/AB composite prepared by ball milling method show a poor cycle life and give about 15 % of the capacity retention after 50th cycles. It is hard to maintain the structural stability during the discharge and charge process, since the sulfur is not well-dispersed in the carbon matrix.

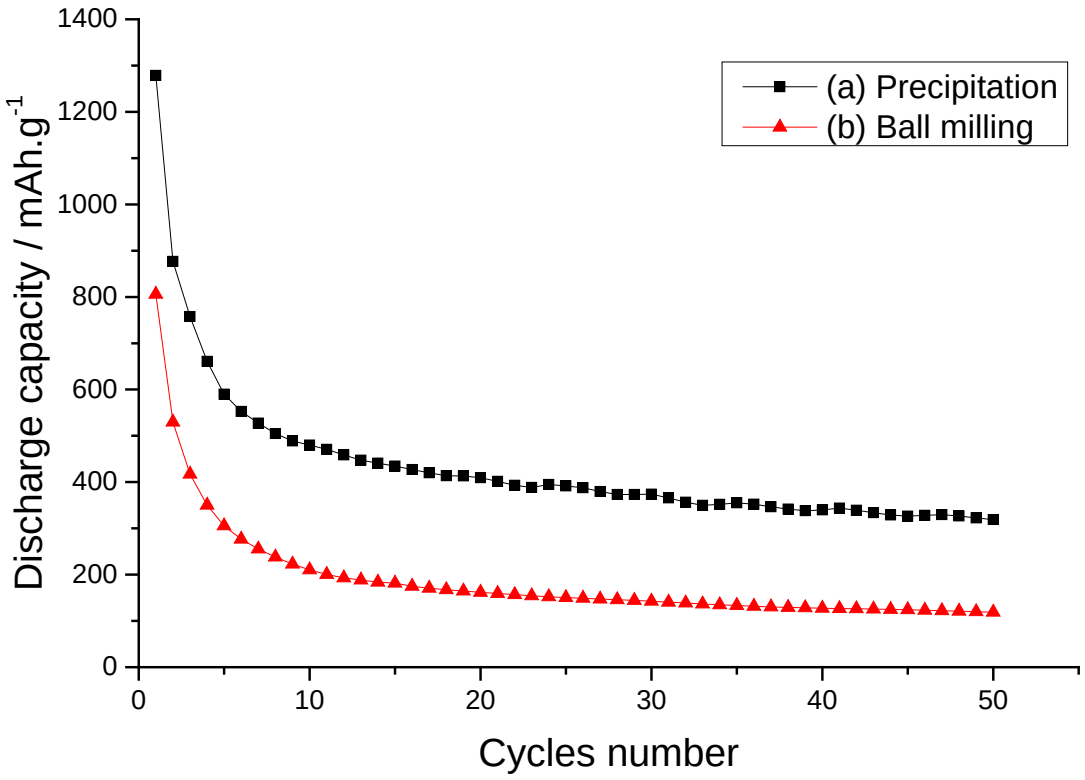

Figure 4.12 Cycle performance of for S/AB composites (30 wt% S) prepared by (a) precipitation and (b) Ball milling methods, and using LiTFSI in TEGDME/DOL at a C rate of 0.1 h^{-1}.

The precipitation method gives advantageous effects on the enhancement of discharge capacity and cycle performance by improvement of electrical contact and adsorption of lithium polysulfides. The S/AB composite prepared by precipitation method had a greater performance than that prepared by ball milling, and precipitation method is more effective in providing an overall stable cycle performance.

4.6 Conclusions

S/AB composites were simply prepared via a direct precipitation method, and the effect of the amount of AB in the composites on the electrochemical performance of the cells was studied. The results show that using the surfactant, and adding AB after the reaction between sodium thiosulfate and hydrochloric acid, help to reduces sulfur particles size, and thus increases the electrode surface area which provide a better electrical contact between sulfur and acetylene black.

The investigation on the first discharge capacity revealed that changing the ratio of AB to the total mass of the electrode has no effect on the first plateau length. On the other hand, the second plateau length in the first discharge capacity was significantly affected by the amount of AB in the electrode. As the AB content in the electrode increases, the electrode surface area is also increases. Larger surface area leads to thinner passivation layer formed from the deposition of insoluble products on the surface of the sulfur electrode, and thus delaying the end of the discharge.

The comparison between the direct precipitation method and the ball milling method reveals that the precipitation method gives beneficial effects on the enhancement of discharge capacity and cycle life performance of lithium/sulfur cell. The smaller particles of sulfur, as well as the well-distributed AB on the surface of sulfur particles resulted from participation method would provide the uniform and more conductive sulfur/AB composite with a larger surface area. Higher electrode surface area leads to formation of thinner passivation layer, and reduces the diffusion of lithium polysulfide species away from the cathode due to the smaller pores that form after the complete dissolution of elemental sulfur into the electrolyte during the discharge. Thus, increases the capacity and the utilization of sulfur as an active material. This indicates that the S/AB composite prepared by precipitation method had a greater performance than that prepared by ball milling.

4.7 References

(1) Chaudhuri, R. G.; Paria, S. *J. Colloid Interface Sci.* **2010**, *343*, 439–44.

(2) Shim, J.; Striebel, K. a.; Cairns, E. J. *J. Electrochem. Soc.* **2002**, *149*, A1321.

(3) Barchasz, C.; Leprêtre, J.-C.; Alloin, F.; Patoux, S. *J. Power Sources* **2012**, *199*, 322–330.

(4) Kolosnitsyn, V. S.; Karaseva, E. V; Amineva, N. A.; Batyrshina, G. A. *Russ. J. Electrochem.* **2002**, *38*, 329–331.

(5) Choi, Y. S.; Kim, S.; Choi, S. S.; Han, J. S.; Kim, J. D.; Jeon, S. E.; Jung, B. H. *Electrochim. Acta* **2004**, *50*, 833–835.

(6) Kolosnitsyn, V. S.; Karaseva, E. V; Seung, D. Y.; Cho, M. D. *Russ. J. Electrochem.* **2002**, *38*, 1314–1318.

(7) Cheon, S.-E.; Choi, S.-S.; Han, J.-S.; Choi, Y.-S.; Jung, B.-H.; Lim, H. S. *J. Electrochem. Soc.* **2004**, *151*, A2067.

(8) Cheon, S.-E.; Ko, K.-S.; Cho, J.-H.; Kim, S.-W.; Chin, E.-Y.; Kim, H.-T. *J. Electrochem. Soc.* **2003**, *150*, A796.

(9) Barchasz, C.; Molton, F.; Duboc, C.; Leprêtre, J.-C.; Patoux, S.; Alloin, F. *Anal. Chem.* **2012**, *84*, 3973–80.

Chapter 5:

A simple, experiment-validated model of the self-discharge of Li/S cells

5.1 Introduction

One of the main challenges in the development of lithium/sulfur batteries is the so-called "shuttle mechanism", which involves the diffusion of polysulfides from the sulfur electrode to the lithium electrode, where they are reduced via the chemical reactions with lithium. In order to achieve their full potential, the discharge reaction of lithium/sulfur batteries should involve the full conversion of sulfur into Li_2S,[1]

$$S_{8(s)} + 16\,Li^+ + 16\,e^- \rightarrow 8\,Li_2S \tag{5.1}$$

However, within the pathway of sulfur reduction, lithium polysulfides of variable chain length, Li_2S_n, are formed:[2–7]

$$\frac{n}{8}S_8 + 2\,Li^+ + 2\,e^- \rightarrow Li_2S_n \tag{5.2}$$

Li_2S_n can diffuse to the lithium electrode, where it can be chemically reduced to shorter-chain polysulfide Li_2S_m,

$$Li_2S_n + \left(\frac{2n}{m} - 2\right)Li \rightarrow \frac{n}{m}\,Li_2S_m \tag{5.3}$$

It has been shown that Li_2S_m with $m > 2$ has a high solubility,[8] and therefore, it could diffuse back to the sulfur electrode, where it would be reduced further to Li_2S,

$$Li_2S_m + (2m - 2)\,Li^+ + (2m - 2)\,e^- \rightarrow m\,Li_2S \tag{5.4}$$

Since the reduction of polysulfide at the lithium electrode does not involve the passage of electrons through the external circuit, an important effect of the shuttle mechanism is to decrease the capacity delivered by the battery (the addition of equations (5.2) to (5.4) shows that the total number of electrons involved per mole of S_8 equals 16 x (1 + 1/n - 1/m), which is lower than the 16 electrons involved in reaction (5.1), since $m < n$).

The shuttle mechanism is also the cause of battery self-discharge. Sulfur from the sulfur electrode will dissolve in the electrolyte and diffuse to the lithium electrode. There, sulfur will be reduced to polysulfides, which will travel back to the sulfur electrode. The increase in polysulfide concentration at the sulfur electrode (as formed from the consumption of sulfur) produces a decrease in the potential of the sulfur electrode that

can be understood from the Nernst equation. For instance, if Li_2S_8 is the main shuttle species, the potential of the sulfur electrode would be given by:

$$E = E^{o}_{S_8/Li_2S_8} + \frac{RT}{2F}\ln a_{S_8} - \frac{RT}{2F}\ln a_{Li_2S_8} \quad (5.5)$$

where a_{S_8} and $a_{Li_2S_8}$ are the activities of sulfur and Li_2S_8. Therefore, the dissolution and reaction of sulfur via the shuttle mechanism produces a decrease in the battery voltage and capacity that resembles the effect of discharging the battery by applying a current.

The aim of this work is to develop a simple model of the self-discharge that is able to reproduce experimental data very well under a range of conditions. It will be demonstrates that the rate of self-discharge is markedly affected by the rate of sulfur and polysulfide diffusion, and an estimation of their diffusion coefficients has been provided. It will be shown that the rate of self-discharge is markedly affected by the carbon content of the electrode, since the change of the electrode potential due to the increase in polysulfide concentration is buffered by the capacitive behaviour of carbon.

Only a few studies have addressed the quantitative analysis of the shuttle phenomenon. In 2004, Mikhaylik and Akridge[9] developed a simple model of the polysulfide shuttle, which they used to simulate experimental data of charge and discharge voltage profiles, battery self-discharge and thermal effects. This model could explain all these processes in terms of one global parameter, i.e. the shuttle constant, which reflects the rate at which long-chain polysulfides are consumed on the lithium electrode. In this work, a more detailed physical meaning of this "shuttle constant" will be given, and will relate it to the rate of diffusion of polysulfide between the sulfur and lithium electrodes.

More complicated models were developed later. Kumaresan *et al.*[10] developed a complete model of a lithium/sulfur cell that included the effects of precipitation, electrode kinetics, diffusion, migration, etc. Fronczek and Bessler[11] used a similar approach and extended the analysis to simulate impedance spectra. Neidhardt *et al.* developed a mathematical framework that was used to model not only lithium/sulfur batteries, but also lithium/oxygen batteries, solid oxide fuel cells and polymer electrolyte membrane fuel cells.[12]

More recently, Hofmann *et al.*[13] developed a detailed mechanistic model of the lithium/sulfur cell that was validated with experimental data. And very recently, Moy *et al.*[14] developed an experimental method to measure the shuttle current by chronoamperometry and they simulated the experimental data with a 1-D diffusion model. There is no doubt that all these models are very powerful, but as it will be shown in this study, our simple model is capable of reproducing the experimental data very well and provides a quantitative understanding of the shuttle phenomenon.

5.2 Experimental details

Sulfur/acetylene black (1:3) composite electrodes were prepared as described in Chapter 3, using the ball milling method. The thickness of the pellets varied between 0.6 and 0.9 mm. Sulfur loading in each electrode was about 1.7 mg/cm^2. Prior to the electrochemical experiments, the pellets were dried at 50ºC under vacuum overnight. No significant sulfur loss was caused by the drying process, since the weight of the pellets did not change significantly.

1M LiTFSI dissolved in a (1:1) mixture of TEGDME and DOL was used as an electrolyte. In order to examine the effect of the pre-saturation with sulfur, the sulfur-saturated electrolyte was prepared by adding an excess of elemental sulfur to this electrolyte, and stirring the solution for three days. The supernatant, sulfur-saturated electrolyte (concentration of about 4 mM) was used in the cell. All electrolyte preparation was done in an argon-filled glove box. The cell was assembled as described in Chapter 2. Cells were assembled with a varying number of glass fibre separators (Whatman, ca. 0.3 mm thick) soaked with the electrolyte. OCV measurements were carried out for the Li/S cells using Multichannel potentiostat galvanostat (MPG, BioLogic Science Instruments) at 25 °C.

5.3 Self-discharge model of the lithium/sulfur cells

A sketch of the lithium/sulfur cells self-discharge model is presented in Figure 5.1. It is comprised of an S/AB composite positive electrode, from now on called the sulfur electrode, a lithium electrode and a separator that determines the distance between the electrodes. The aim of the model is to predict the first self-discharge following the fabrication of the cell for a range of parameters, such as the separator thickness, etc. The principle of the model is to simulate the diffusion of the shuttle species, Li_2S_n, across the separator and their reactions at the two electrodes and to derive the sulfur electrode potential from the surface concentrations by taking into account the capacitive behaviour of the sulfur electrode.

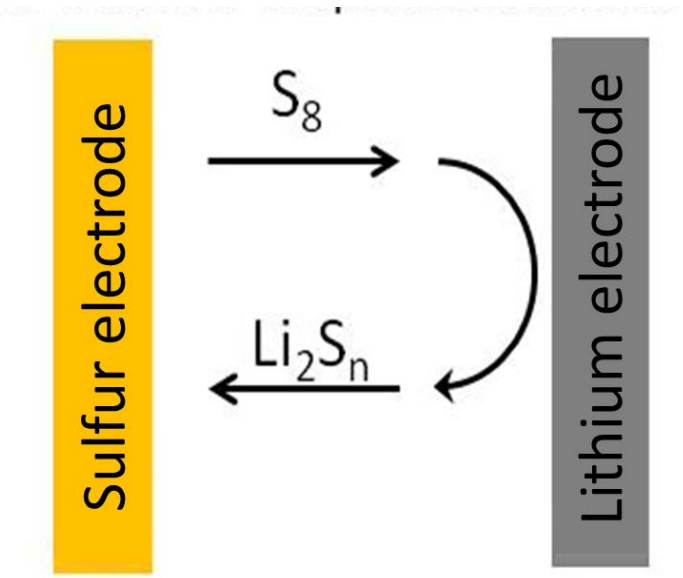

Figure 5.1 Sketch of the lithium-sulfur cells self-discharge model.

To simplify the model, the porosity of the sulfur electrode was ignored and the reactions at the sulfur electrode assumed to occur at its interface with the separator. Also, the dissolution of sulfur in the electrolyte assumed to be very fast, that the sulfur electrode acts as an infinitely large reservoir of sulfur and that the surface concentration of sulfur at the sulfur electrode is therefore pinned to the solubility of sulfur (4 mM in 1 M LiTFSI in TEGDME according to ref.[15]).

We have check that, under the conditions of the simulations performed here, the amount of sulfur consumed by dissolution in the electrolyte (ca. 0.3 mg cm^{-2}) is much smaller than the experimental sulfur loading (> 1 mg cm^{-2}). This is because, in the experiments analysed here, cells were assembled with > 2 glass fibre separators, which results in a relatively large distance between the two electrodes, producing smooth sulfur concentration gradients, which results in relatively slow sulfur diffusion (will be addressed later).

Another assumption is that the sulfur electrode has a total capacitance, C, equal to the specific capacity of carbon at approximately 0.01 F/mg (as estimated from voltammetric measurements of composite electrodes containing only AB and binder) times the carbon content (between 5 and 6.5 mg, depending on the experiment). The distance between the two electrodes is assumed to be given by the number of separators times the thickness of one separator (which, in the case of the glass fibre separators used here, is around 0.3 mm).

Only two species are considered, sulfur as S_8 and the product of its reaction at the lithium electrode, S_8^{2-}. Transport within the separator is assumed to involve diffusion only, so the concentration changes are defined by Fick's second law of diffusion:

$$\frac{\partial c_{S_8}}{\partial t} = D_{S_8} \frac{\partial^2 c_{S_8}}{\partial x^2} \tag{5.6}$$

$$\frac{\partial c_{S_8^{2-}}}{\partial t} = D_{S_8^{2-}} \frac{\partial^2 c_{S_8^{2-}}}{\partial x^2} \tag{5.7}$$

At the sulfur electrode ($x = 0$) the concentration of S_8 is set as a constant equal to the solubility limit of S_8 in the electrolyte (ca. 4 mM)[15]

$$c_{S_8}(0, t) = c_{S_8}^{sat} \tag{5.8}$$

At the lithium electrode ($x = L$), S_8 is assumed to be completely consumed by the reaction with lithium forming S_8^{2-} such that

$$c_{S_8}(L, t) = 0 \tag{5.9}$$

and the fluxes of S_8 and S_8^{2-} are taken to be equal and opposite

$$D_{S_8^{2-}} \frac{\partial c_{S_8^{2-}}}{\partial x}\bigg|_L = -D_{S_8} \frac{\partial c_{S_8}}{\partial x}\bigg|_L \tag{5.10}$$

The potential of the sulfur electrode is assumed to be given by the Nernst equation and unity activity coefficients are considered:

$$E(t) = E^0_{S_8/S_8^{2-}} + \frac{RT}{2F}\ln\left(\frac{c_{S_8}(0,t)}{c_{S_8^{2-}}(0,t)}\right) = E^0_{S_8/S_8^{2-}} + \frac{RT}{2F}\ln c_{S_8}^{sat} - \frac{RT}{2F}\ln c_{S_8^{2-}}(0,t) \tag{5.11}$$

The initial concentration of sulfur and polysulfides in the electrolyte could not be set to zero, because that produced a numerical error in the calculation. So trace amounts of sulfur and polysulfides were considered (concentrations lower than 10^{-20}M) and the ratio of concentrations of sulfur and polysulfides was set so that the initial potential was equal to the experimental value, 3.2 V vs. Li^+/Li. We confirmed that changing the values of the initial trace concentration did not produce any significant changes in the simulation results.

The variation of the surface concentration of S_8^{2-} at the sulfur electrode is calculated by taking into account the capacitive behaviour of carbon. S_8^{2-} will be oxidized to S_8 at a rate that is related to the value of the total capacitance of the electrode. To describe the self-discharge we can write:

$$n\,S_8^{2-} \rightarrow n\,S_8 + 2n\,e^- \tag{5.12}$$

where n is number of moles of S_8^{2-} consumed or number of moles of S_8 created.

The infinitesimal amount of charge is:

$$dQ = -2F dn_{S_8^{2-}} \tag{5.13}$$

This corresponds to the change in the charge capacitor according to:

$$dQ = CdE \tag{5.14}$$

Where C is the capacitance (F) and dE is change in potential on the capacitor. Therefore,

$$-2F\frac{dn_{S_8^{2-}}}{dt} = C\frac{dE}{dt} \tag{5.15}$$

$$\frac{dn_{S_8^{2-}}}{dt} = -\frac{C}{2F}\frac{dE}{dt} \tag{5.16}$$

The above equation is obtained by acknowledging that the net current at the electrode is zero. Therefore, the current due to S_8^{2-} oxidation should be equal to the reduction current associated with transferring electrons to the carbon surface:

$$|I| = 2F\frac{dn_{S_8^{2-}}}{dt} = C\left|\frac{dE}{dt}\right| \tag{5.17}$$

Therefore, the flux of S_8^{2-} at the sulfur electrode will be given by:

$$nFAD_{S_8^{2-}}\frac{\partial c_{S_8^{2-}}}{\partial x}\bigg|_0 = C\frac{dE}{dt} \tag{5.18}$$

After rearranging, the following boundary condition for S_8^{2-} at the composite electrode is obtained:

$$D_{S_8^{2-}}\frac{\partial c_{S_8^{2-}}}{\partial x}\bigg|_{x=0} = \frac{RTC}{4F^2A}\left(\frac{1}{c_{S_8}}\frac{dc_{S_8}}{dt} - \frac{1}{c_{S_8^{2-}}}\frac{dc_{S_8^{2-}}}{dt}\right) \tag{5.19}$$

The equations were numerically solved by Dr Guy Denuault using the finite element method using COMSOL Multiphysics 4.4. The following model parameters were selected as described in Table 1: A, C, $c_{S_8}(x,0)$, $c_{S_8}^{sat}$, D_{S_8}, $D_{S_8^{n-}}$, $E(0)$, $E^0_{S_8/S_8^{n-}}$, and L. The sulfur electrode potential was calculated from the Nernst equation as a function of time during the simulation.

For the simulations performed considering that S_4^{2-} were the main shuttle species, the following equations were used:

$$D_{S_4^{2-}}\frac{\partial c_{S_{84}^{2-}}}{\partial x}\bigg|_L = -2\,D_{S_8}\frac{\partial c_{S_8}}{\partial x}\bigg|_L \tag{5.20}$$

$$E(t) = E^0_{S_8/S_4^{2-}} + \frac{RT}{4F}\ln c_{S_8}^{sat} - \frac{RT}{2F}\ln c_{S_4^{2-}}(0,t) \tag{5.21}$$

$$D_{S_4^{2-}}\frac{\partial c_{S_4^{2-}}}{\partial x}\bigg|_{x=0} = \frac{RTC}{4F^2A}\left(\frac{1}{2c_{S_8}}\frac{dc_{S_8}}{dt} - \frac{1}{c_{S_4^{2-}}}\frac{dc_{S_4^{2-}}}{dt}\right) \tag{5.22}$$

Table 1 Parameters used in the simulations of the diffusion of the shuttle species.

Symbol	Unit	Description	Value used in the simulations
A	cm^2	geometric areas of electrodes	0.785 cm^2
C	F	total capacitance of sulfur electrode	0.03 to 0.06 F
$c_{S_8}(x,t)$	mol cm^{-3}	concentration of sulfur	
$c_{S_8}(x,0)$	mol cm^{-3}	initial concentration of sulfur	10^{-20} M
$c_{S_8}(0,t)$	mol cm^{-3}	concentration of sulfur at the sulfur electrode	
$c_{S_8}(L,t)$	mol cm^{-3}	concentration of sulfur at the lithium electrode	
$c_{S_8}^{sat}$	mol cm^{-3}	solubility limit of sulfur	4 mM
$c_{S_8^{2-}}(x,t)$	mol cm^{-3}	concentration of polysulfide	
$c_{S_8^{2-}}(0,t)$	mol cm^{-3}	concentration of polysulfide at the sulfur electrode	
D_{S_8}	cm^2 s^{-1}	diffusion coefficient of sulfur	2×10^{-6} to 4×10^{-6} cm^2/s
$D_{S_8^{2-}}$	cm^2 s^{-1}	diffusion coefficient of polysulfide	2×10^{-6} to 4×10^{-6} cm^2/s
$E(0)$	V	initial sulfur electrode potential	3.2 V vs. Li/Li^+
$E(t)$	V	sulfur electrode potential	
$E^0_{S_8/S_8^{2-}}$	V	standard potential for sulfur/polysulfide couple	2.45 V vs. Li/Li^+
L	cm	separator thickness	0.6 to 1.5 mm
t	s	time	
x	cm	distance along battery axis	

5.4 The study of the rate of self-discharge in lithium/sulfur cell

5.4.1 The effect of the distance between the electrodes on the rate of self-discharge

The evolution of the open circuit voltage (solid lines) of Li/S batteries containing a different number of separators between the lithium and sulfur electrodes is displayed in Figure 5.2. It can be clearly seen that as the number of separators in the Li/S cell increases, the distance between the electrodes also increases, and the self-discharge becomes slower. This is evidence of the fact that the rate of self-discharge is influenced by the rate of diffusion of sulfur and polysulfides.

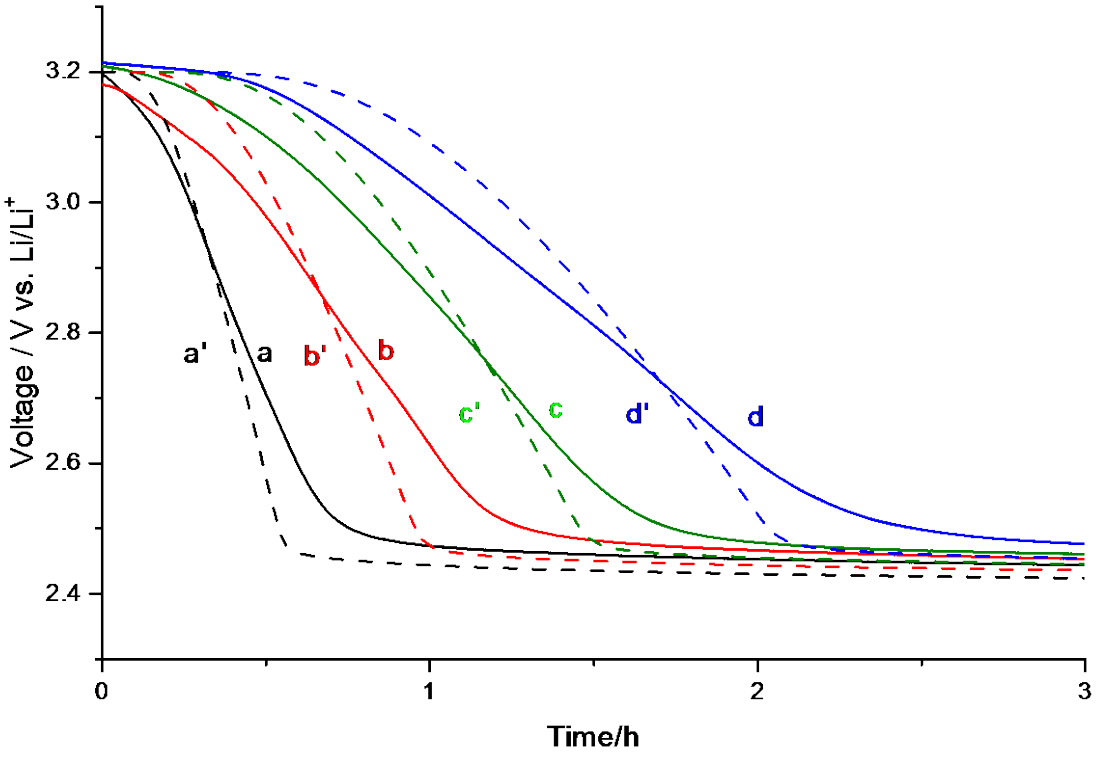

Figure 5.2 Evolution of the open circuit voltage of Li/S cells containing 2 (a), 3 (b), 4 (c) and 5 (d) glass fibre separators (solid lines). Sulfur loading: ca. 1.7 mg/cm^2, carbon loading: ca. 5 mg/cm^2. Electrolyte: 1 M LiTFSI in DOL:TEGDME (1:1). The corresponding simulations (dashed lines) are performed with a distance between the two electrodes equal to 0.6 (a'), 0.9 (b'), 1.2 (c') and 1.5 mm (d').

Since each glass fibre separator is around 0.3 mm thick, the simulations has been performed where the distance between the electrodes is set to 0.3 mm times the number of separators (see the details of the model in section 5.3). The results of the simulations are included in Figure 5.2 (dashed lines). A good agreement between the experiment and simulation is observed, despite the simplicity of the model employed here. The only free parameters of this model are the diffusion coefficients of sulfur and polysulfide species, and for simplicity, we have considered that both diffusion coefficients have the same values, 3×10^{-6} cm^2/s. These values are comparable to the diffusion coefficient of sulfur, 2.6×10^{-6} cm^2/s, as measured with a rotating ring-disc electrode in DOL/DME with 1 M LiTFSI.[3] These diffusion coefficients also compare well with the values used in more detailed models of Li/S cells, which were assumed to vary between 10^{-6} and 10^{-5} cm^2/s.[10,11,13,14]

We believe that our present estimate of the diffusion coefficient is accurate due to the simplicity of the model and the very high sensitivity of the self-discharge rate on the rate of diffusion. We compare the experimental data with simulations performed with values of the diffusion coefficient equal to 2×10^{-6} cm^2/s (Figure 5.3) and 4×10^{-6} cm^2/s (Figure 5.4). It is clear that the agreement with the experiments is much less. The small disagreement between the simulations and the experiments in Figure 5.2 could be attributed to the fact that the model only considers one “shuttle species”, with a single value of the diffusion coefficient. The simulation results in Figure 5.2 were obtained considering that the shuttle species is S_8^{2-}.

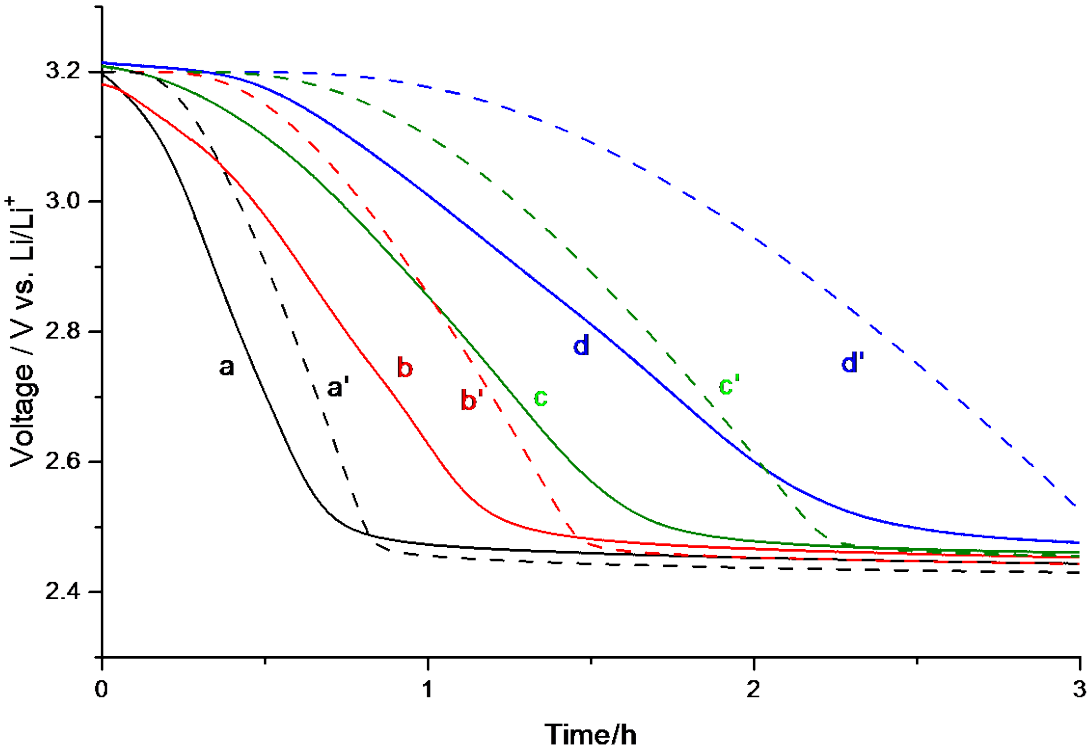

Figure 5.3 As in figure 5.2 in the main text, but simulations were performed with a value of the diffusion coefficient of sulfur and polysulfide equal to 2×10^{-6} cm^2/s (instead of 3×10^{-6} cm^2/s).

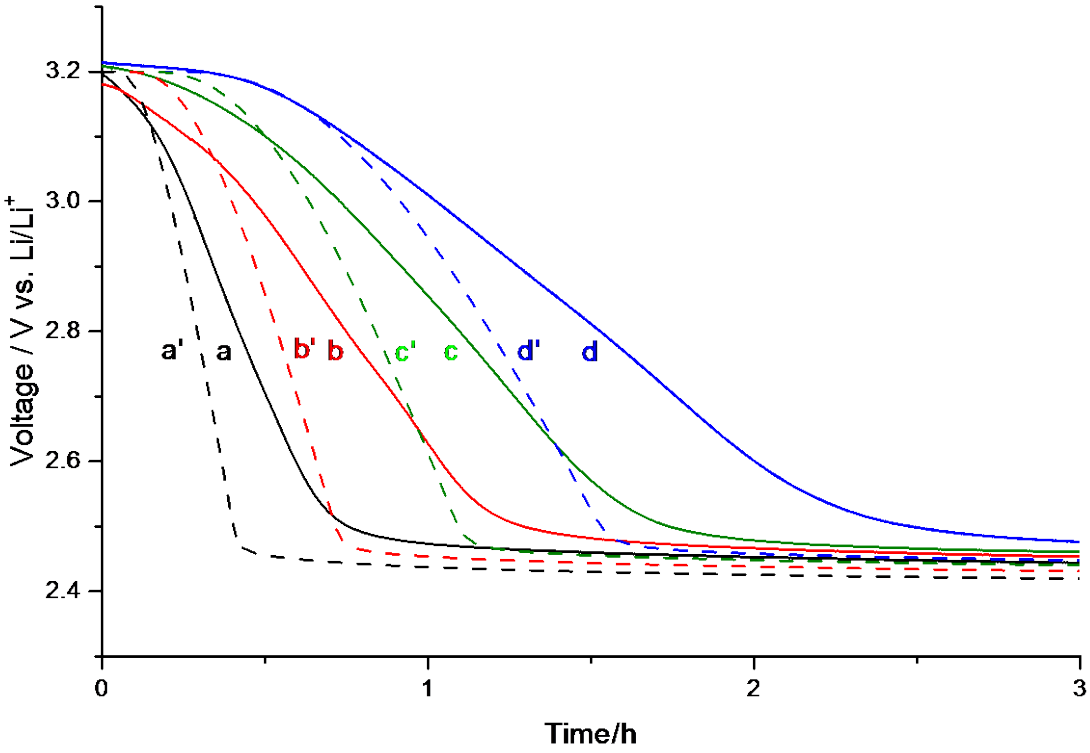

Figure 5.4 As in figure 5.2 in the main text, but simulations were performed with a value of the diffusion coefficient of sulfur and polysulfide equal to 4×10^{-6} cm^2/s (instead of 3×10^{-6} cm^2/s).

Nearly identical results can be obtained considering that the shuttle species is S_4^{2-} with a diffusion coefficient of 2.3×10^{-6} cm^2/s, as shown in Figure 5.5, which is in reasonable agreement with the diffusion coefficient of 3×10^{-6} cm^2/s used in Figure 5.2. However, in reality, a range of polysulfides with different chain lengths are probably involved in the shuttle mechanism, and polysulfides with different lengths (and charge) are expected to have different values of diffusion coefficient.

Another simplification of the present model is considering that the reaction of sulfur on the lithium electrode is mass-transport controlled. This assumption was also used in previous modelling studies, but it would need to be tested, since if the reaction of sulfur on the lithium electrode is limited by the reaction kinetics, the present approach would lead to an overestimation of the values of the diffusion coefficient.

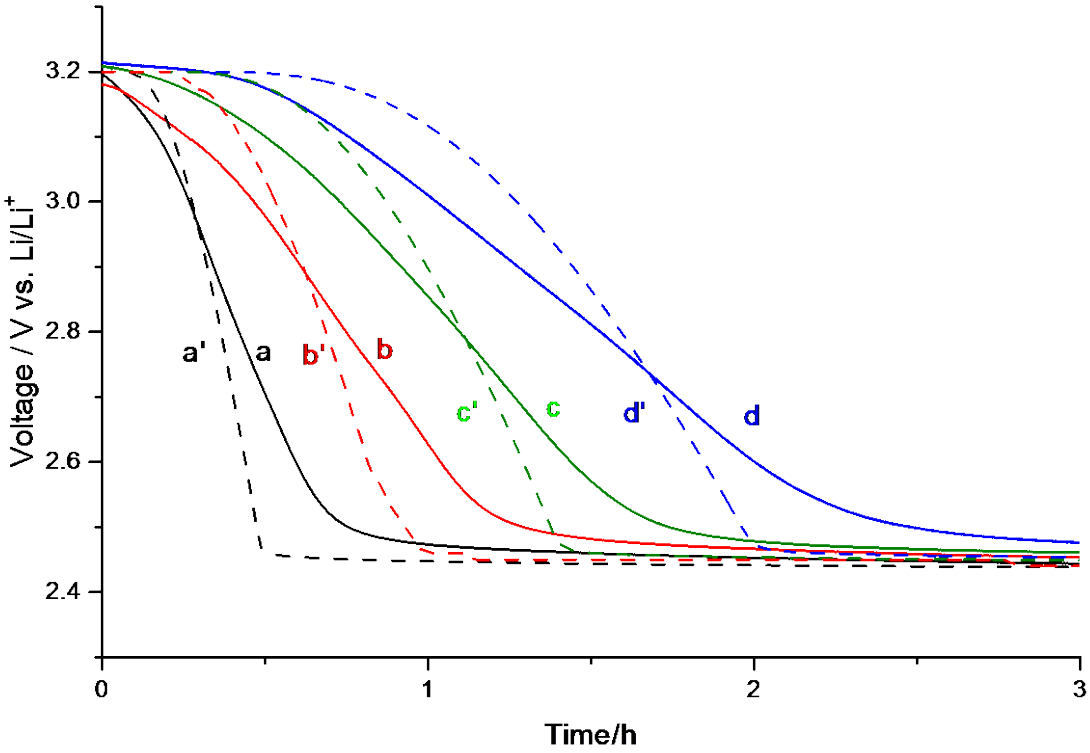

Figure 5.5 As in figure 5.2 in the main text, but simulations were performed considering a shuttle species S_4^{2-} (instead of S_8^{2-}) with a diffusion coefficient of $2.3x10^{-6}$ cm^2/s (instead of $3x10^{-6}$ cm^2/s).

5.4.2 The effect of the acetylene black content on the rate of self-discharge

Figure 5.6 shows the self-discharge of Li/S batteries containing different amounts of conductive AB additive (solid lines). The specific capacitance of AB in the composite is around 0.01 F/mg, and therefore the simulations has been performed where the total capacitance of the sulfur electrode is set to 0.01 F/mg times the carbon content. The results of the simulations are included in Figure 5.6 (dashed lines).

The effect of the carbon content on the rate of self-discharge can be understood as follows. Once polysulfides reach the sulfur electrode, they will undergo a partial oxidation that is coupled to the capacitive charging of the carbon-electrolyte interphase. In this process, polysulfides transfer electrons to the carbon surface:

$$C+\frac{\lambda}{2}S_n^{2-} \rightarrow C^{\lambda-}+\frac{n\lambda}{16}S_8 \qquad (5.23)$$

As a result, the potential of the sulfur electrode decreases, but the decrease is smoother than if the electrode had no carbon.

The simulations in Figure 5.6 demonstrate that the capacitive behaviour of carbon leads to slower self-discharge. However, the agreement with the experiments is not very good, demonstrating that additional factors need to be taken into account. It is likely that the presence of additional carbon will slow down the diffusion of sulfur and polysulfides, by either adsorption or by increasing the effective diffusion length due to the porous carbon structure.

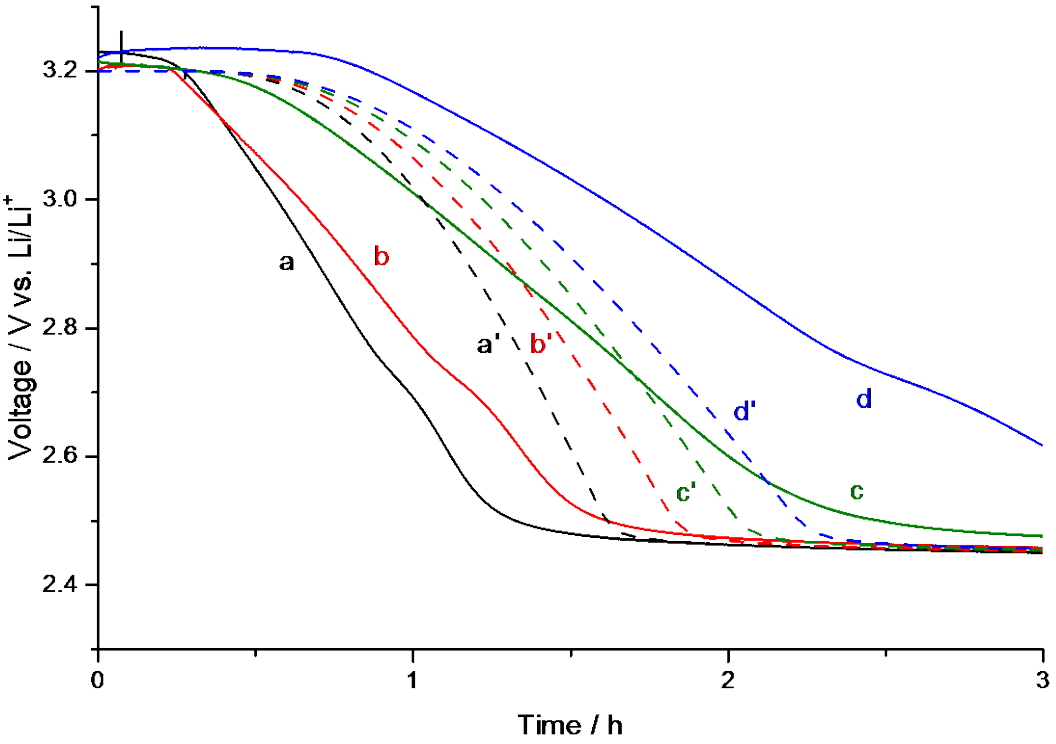

Figure 5.6 Evolution of the open circuit voltage of Li/S cells with the following AB content: 3 (a), 4 (b), 5 (c) and 6 (d) mg/cm^2 (solid lines). Sulfur loading: ca. 1.7 mg/cm^2. Electrolyte: 1 M LiTFSI in DOL:TEGDME (1:1). The corresponding simulations (dashed lines) are performed by varying the total capacitance of the S/AB composite electrode: 0.03 (a'), 0.04 (b'), 0.05 (c'), and 0.06 F (d'). The distance between the two electrodes equals 1.5 mm.

5.4.3 The effect of a sulfur-saturated electrolyte on the rate of self-discharge

In this section, we studied the effect of using a sulfur-saturated electrolyte in the Li/S cell. The evolution of the open circuit voltage of Li/S cells without (a) and with (b) sulfur dissolved in the electrolyte at saturation (solid lines), is shown in Figure 5.7. It can be observed that the self-discharge in the cell with the sulfur-saturated electrolyte is faster than that without sulfur dissolved in the electrolyte. The rate of self-discharge in the cell with the sulfur-saturated electrolyte would expect to be higher, because the step of diffusion of sulfur from the sulfur electrode to the lithium electrode is no longer required. The simulations (dashed line, curve b') also show a faster self-discharge when sulfur is dissolved in the electrolyte, but the effect is more marked than in the experiments.

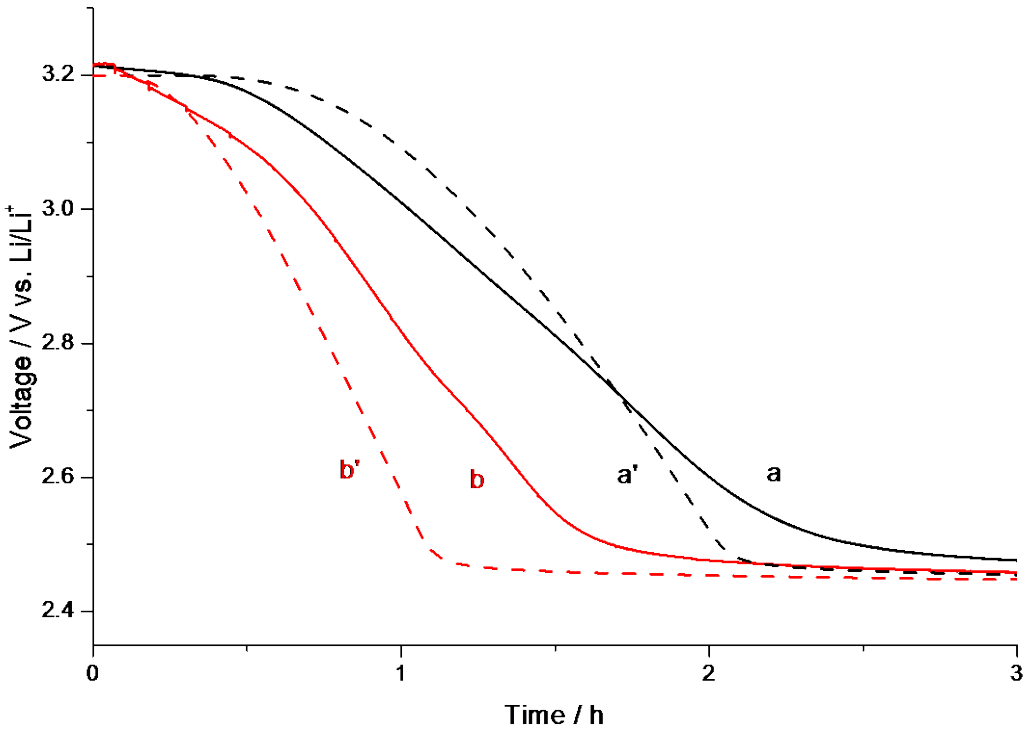

Figure 5.7 Evolution of the open circuit voltage of Li/S cells without (a) and with (b) sulfur dissolved in the electrolyte at saturation (solid lines). Sulfur loading: ca. 1.7 mg/cm^2, AB loading: ca. 5 mg/cm^2, number of glass fibre separators: 5. Electrolyte: 1 M LiTFSI in DOL:TEGDME 1:1. Simulations (dashed lines) were performed considering that the sulfur concentration in the electrolyte is negligible (a') or 4 mM (b').

5.5 Conclusion

We have proposed a new, simple model that provides a detailed understanding of the rate at which the polysulfide shuttling in lithium/sulfur batteries leads to battery self-discharge. The model explains quantitatively why increasing the distance between the sulfur and lithium electrodes decreases the rate of self-discharge, since the sulfur and polysulfides have to travel over a longer distance. The model also explains why increasing the amount of AB in the sulfur electrode slows down the self-discharge: the decrease in the open circuit voltage is "buffered" by the capacitive behaviour of AB. Once polysulfides reach the sulfur electrode, they undergo a partial oxidation to sulfur, which is coupled with charging the AB interface with a negative surface charge. Finally, the model is also able to reproduce experimental data on the rate of self-discharge in sulfur containing electrolytes, where the self-discharge is faster, because the step of diffusion of sulfur from the sulfur electrode to the lithium electrode is no longer required.

By comparing the simulation results with experimental data, we have been able to evaluate the diffusion coefficient of sulfur and the main polysulfide species. Given the simplicity of the model, this latter value of the diffusion coefficient cannot be ascribed to a particular polysulfide species of a given length. However, we believe that this value of the diffusion coefficient is, in a way, more relevant than the individual diffusion coefficients of all polysulfide species, since our result provides a direct measurement of the overall mass transport rate of the main shuttle species generated in Li/S batteries.

This model clearly shows that there are two mechanisms of sulfur lost from the sulfur electrode: dissolution across a concentration gradient and reaction with polysulfides formed at the lithium electrode. The equations derived in this work allow a comparison of the rate of self-discharge of Li/S cells with different geometries (electrode areas, distance between the electrodes, etc.) and a discussion on the differences in terms of the shuttle constant or rate of loss of sulfur.

5.6 References

(1) Ji, X.; Nazar, L. F. *J. Mater. Chem.* **2010**, *20*, 9821.

(2) Xu, R.; Belharouak, I.; Zhang, X.; Chamoun, R.; Yu, C.; Ren, Y.; Nie, A.; Shahbazian-yassar, R.; Lu, J.; Li, J. C. M.; Amine, K. **2014**.

(3) Lu, Y.-C.; He, Q.; Gasteiger, H. A. *J. Phys. Chem. C* **2014**, *118*, 5733–5741.

(4) Patel, M. U. M.; Demir-Cakan, R.; Morcrette, M.; Tarascon, J.-M.; Gaberscek, M.; Dominko, R. *ChemSusChem* **2013**, *6*, 1177–81.

(5) Park, J.-W.; Yamauchi, K.; Takashima, E.; Tachikawa, N.; Ueno, K.; Dokko, K.; Watanabe, M. *J. Phys. Chem. C* **2013**, *117*, 4431–4440.

(6) Cuisinier, M.; Cabelguen, P.-E.; Evers, S.; He, G.; Kolbeck, M.; Garsuch, A.; Bolin, T.; Balasubramanian, M.; Nazar, L. F. *J. Phys. Chem. Lett.* **2013**, *4*, 3227–3232.

(7) Gao, J.; Lowe, M. A.; Kiya, Y.; Abruna, D. *J. Phys. Chem.* **2011**, *115*, 25132–25137.

(8) Rauh, R. D.; Shuker, F. S.; Marston, J. M.; Brummer, S. B. *J. Inorg. Nucl. Chem.* **1977**, *39*, 1761–1766.

(9) Mikhaylik, Y. V.; Akridge, J. R. *J. Electrochem. Soc.* **2004**, *151*, A1969.

(10) Kumaresan, K.; Mikhaylik, Y.; White, R. E. *J. Electrochem. Soc.* **2008**, *155*, A576.

(11) Fronczek, D. N.; Bessler, W. G. *J. Power Sources* **2013**, *244*, 183–188.

(12) Neidhardt, J. P.; Fronczek, D. N.; Jahnke, T.; Danner, T.; Horstmann, B.; Bessler, W. G. *J. Electrochem. Soc.* **2012**, *159*, A1528–A1542.

(13) Hofmann, A. F.; Fronczek, D. N.; Bessler, W. G. *J. Power Sources* **2014**, *259*, 300–310.

(14) Moy, D.; Manivannan, A.; Narayanan, S. R. *J. Electrochem. Soc.* **2014**, *162*, A1–A7.

(15) Park, J.-W.; Ueno, K.; Tachikawa, N.; Dokko, K.; Watanabe, M. *J. Phys. Chem. C* **2013**, *117*, 20531–20541.

Chapter 6:

Electrochemical study of Li/S cells using galvanostatic intermittent titration technique

6.1 Introduction

The galvanostatic intermittent titration technique (GITT) which combines transient and steady-state measurements, is one of the most useful electrochemical methods that has been used to obtain the lithium ion diffusion coefficient within the intercalation electrode materials for rechargeable lithium ion batteries.[1] GITT was firstly proposed by Weppner and Huggins to obtain the diffusion coefficient of lithium ion in electrode active materials in Li_3Sb.[2]

The potential change during the pulse maybe expressed as:

$$\Delta E = k\frac{t^{1/2}}{D^{1/2}} \tag{6.1}$$

where k is a constant. Based on the Fick's second law of diffusion and through a series of assumptions and simplifications, the Diffusion coefficient *D* can be determined from the equation below when using a small current:[2,3]

$$D = \frac{4}{\pi}\left(\frac{m_B V_m}{M_B S}\right)^2 \left(\frac{\Delta E_s}{\tau\left(\frac{dE}{d\sqrt{t}}\right)}\right)^2, \quad t \ll \frac{L^2}{D} \tag{6.2}$$

where V_m is the molar volume of the compound, M_B is the molecular weight of the active material, m_B is the mass of the active material, S is the total contact area between the electrolyte and the electrode, ΔE_s is the change of the steady-state voltage of the cell resulting from the current pulse, L is the electrode thickness, and τ is the time interval for which a constant current is applied.

The essential principle of the GITT technique is to interrupt the current and observe the resulting voltage transient.[3] The significant experimental feature of the GITT technique is the voltage step which is interpreted as the IR drop (current-resistance product) due to the current flux of the mobile species across the electrode-electrolyte interface in the cell. The IR drop is always time independent, and is merely shifts the measured voltage by a constant value. This does not change the geometrical shape of the voltage-time curve.[4,5]

Another, more significant feature is the transient response over the pulse duration, which is ideally a monotonic curve. A slow change in the voltage with the time should be take place, in order to preserve a constant concentration gradient at the surface as required by Fick's constant current. The final features are the reverse IR drop and the relaxation which again should be a monotonic curve, where a slow change in the voltage will occur in order to reach the equilibrium voltage.

This study is believed to be the first example of a GITT investigation of the Li/S cell. It has rarely been used to study the diffusion behaviour in Li/S batteries, due to sulfur reduction steps which involve producing many polysulfide species during the discharge process.

In this study, GITT was employed in order to perform discharge/charge with current interruptions, and measuring E vs. time throughout, and to analyse the transient and categorize the changes during discharge/charge.

6.2 Experimental details

The sulfur/acetylene black (1:3) composite was synthesized as described in Chapter 3, using the ball milling method. The GITT was carried out for the Li/S cells using MPG (BioLogic Science Instruments) at 25 °C. Pulses at C/10 for 5 min. followed by open circuit relaxation were repeated until a cut-off voltage of 1.5 V was reached. At the beginning of the study, it was not known what is the optimum pulse and relaxations would be. Therefore, a series of five experiments were performed, as shown in Figure 6.1, and the cells were discharged at C/10 rate for 5 min. followed by open circuit relaxation for 1, 5, 10, 20, and 60 min., respectively.

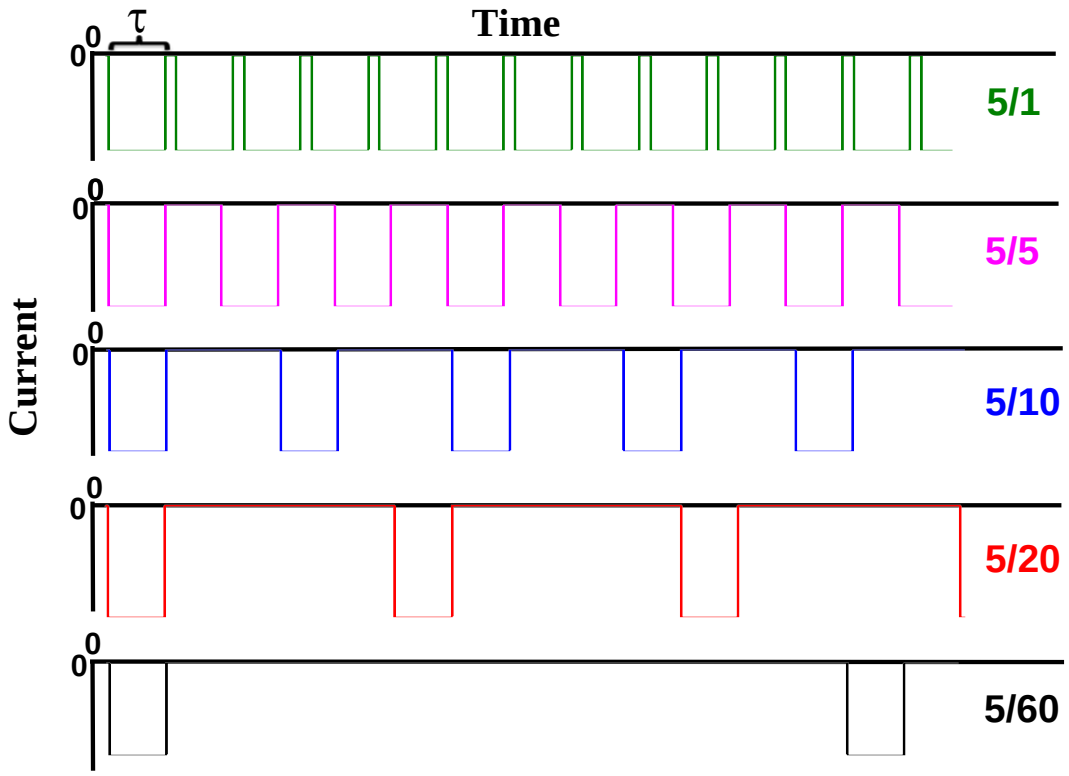

Figure 6.1 The current-time schematics.

The GITT experiment simultaneously discharges the battery at two C rates. The pulse C rate refers to the kinetics and it deviates far from equilibrium; it is calculated using the applied current, as described in Chapter 2. While, the average C rate is low and is close to equilibrium; it is calculated using the average current applied during the pulse and the relaxation. The experimental details applied for the GITT experiments are shown in Table 2.

Table 2 Experimental details that were used for the GITT experiments.

Experiment	**τ (min.)**	**Relaxation (min.)**	**Pulse C rate**	**Average C rate**
5/1	**5**	**1**	**1/10**	**1/12**
5/5	**5**	**5**	**1/10**	**1/20**
5/10	**5**	**10**	**1/10**	**1/30**
5/20	**5**	**20**	**1/10**	**1/50**
5/60	**5**	**60**	**1/10**	**1/130**

During the pulses, the following variations in potential were observed: firstly, the initial rapid change was usually ascribed to the IR drop or ohmic potential drop; secondly, a longer and slower change in potential with time. This may be described as a polarization region. The overall difference in potential (ΔE_t) defines the polarization region.

In all electrochemical testing, cells were assembled as described in Chapter 2, using 1 M of LiTFSI in TEGDME:DOL (1:1). The repeated experiments show a good reproducibility of the potentials measured with about ± 5 mV.

6.3 The general form of GITT results

The GITT profile for the first discharge of Li/S cell using 5 min. pulse and 10 min. relaxation (cell 5/10) can be shown in Figure 6.2. This figure was employed as an example of the way that we followed for describing the detailed behaviour in each region of the whole profile of the GITT measurements. These regions were selected depending on the change in the voltage behaviour at different states of the cell discharge.

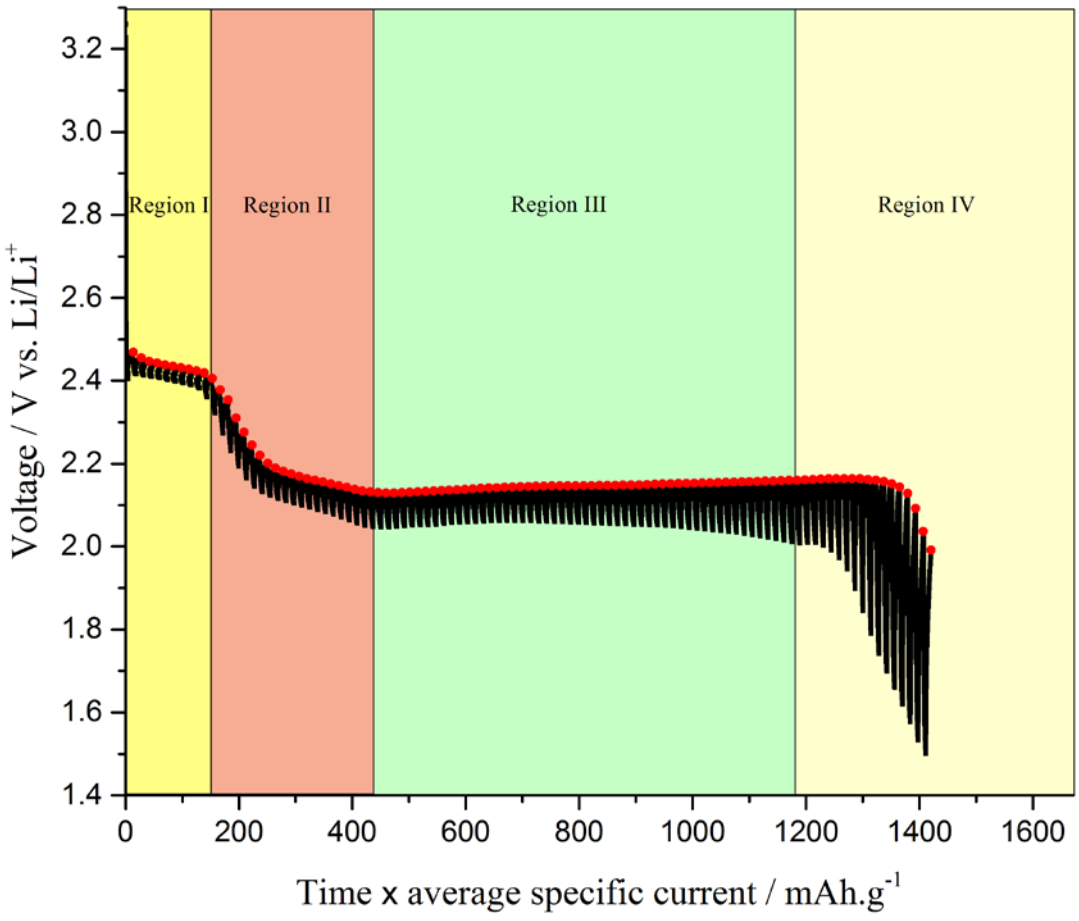

Figure 6.2 GITT profile for first discharge of Li/S cell using 5 min. pulse and 10 min. relaxation (5/10), with 1M LiTFSI in TEGDME/DOL. The red circles represent the last data point at the end of each relaxation period at discharge states of Li/S cell.

Region I in the discharge curve can be related to the reduction of elemental sulfur at the cathode with lithium ions to form the high order polysulfide Li_2S_8 which occurs between OCV and 2.4 V. This step involves two-phase reduction, where the active material transfers from solid phase to the liquid phase.

$$S_{8(s)} + 2\,Li^+ + 2\,e^- \rightarrow Li_2S_{8(soln.)} \quad (6.3)$$

The slight change in the voltage within this region (almost plateau) corresponds to an increase in the concentration of high order polysulfide according to Nernst equation:

$$E = E° + \frac{RT}{nF}\ln\frac{[S_8]}{[Li_2S_8]} \quad (6.4)$$

In region II, Li_2S_8 will be reduced to low order polysulfides (Li_2S_n, $n \geq 4$), which occurs in the liquid phase and between 2.4 – 2.1 V.

$$Li_2S_{8(soln.)} + 2\,Li^+ + 2\,e^- \rightarrow 2\,Li_2S_{4(soln.)} \quad (6.5)$$

Region III in the discharge curve representing the third reduction stage. According to the literature,[6–8] this region involves two-phase reduction where all dissolved Li_2S_4 in the positive electrode will be gradually converted to insoluble Li_2S and possibly Li_2S_2.

$$Li_2S_{4(soln.)} + 4\,Li^+ + 4\,e^- \rightarrow Li_2S_{2(s)} + 2\,Li_2S_{(s)} \quad (6.6)$$

In region IV, Li_2S_2 that generated in the cathode cannot diffuses to the electrolyte due to its low solubility in the organic solvents, and will precipitate in the electrode, and then reduced to Li_2S at the final reduction stage.

$$Li_2S_{2(s)} + 2\,Li^+ + 2\,e^- \rightarrow 2\,Li_2S_{(s)} \quad (6.7)$$

The GITT profiles of Li/S cells with 1M LiTFSI in TEGDME/DOL measured at the current density of 167.2 mA/g of S (C rate of 0.1 h^{-1}) are displayed in Figure 6.3. These measurements were token while applying the current for 5 min. followed by potential relaxation step for 1, 5, 10, 20, and 60 min (5/1, 5/5, 5/10, 5/20, and 5/60, respectively).

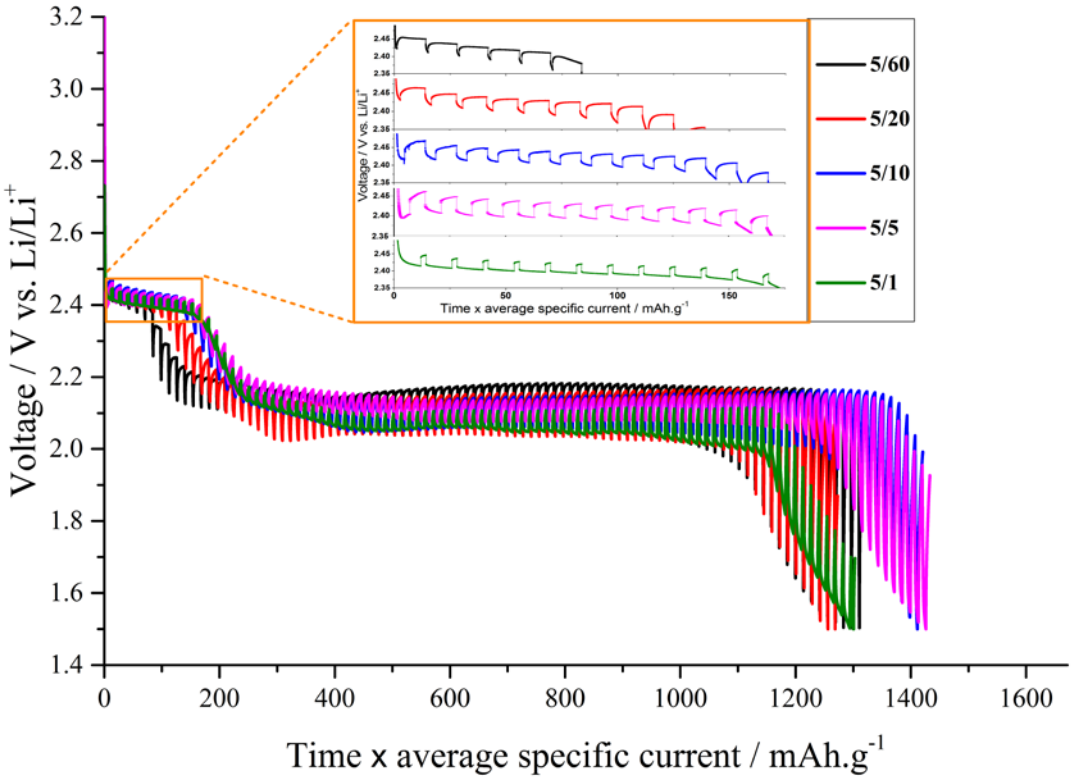

Figure 6.3 GITT profiles of Li/S cells with 1M LiTFSI in TEGDME/DOL measured at a C rate of 0.1 h^{-1} , using 5 min. pulses and different relaxation times.

It can be observed that the polarization at the high voltage region is smaller than the polarization at the end of the lower voltage region. This is in agreement with what was observed by Watanabe *et al.*, where they state that the electrode kinetics for the high voltage region of the discharge is relatively fast. Also, the slow kinetics of the solid-state reaction at the end of the discharge, as well as the rise of the mass-transport resistance of the electrolyte within the pores of the positive electrode, can led to a larger polarization at the end of the lower voltage region.[9]

The study of Watanabe *et al.* does not describe the voltage behaviour within the individual pulses. This work includes GITT experiments with a very fine time resolution, and gives far more detail of the reaction than what was previously known.

At shorter relaxation times 1, 5 and 10 min, the length of the region I (first plateau) is almost the same, and it delivers about 170 mAh.g^{-1} of S. However, the length of the first plateau in longer relaxation times 20 and 60 min is smaller than this value and it gives about 125 and 80 mAh.g^{-1} of S respectively. The decrease in the length of the region I with the relaxation time can be seen clearly in Figure 6.3 (insert). As the relaxation time increases, the length of the first plateau decreases. Li_2S_8 that generated from the reduction of elemental sulfur, is a highly soluble product in the organic solvents.[9] Li_2S_8 that produced during applying the current can diffuse from the cathode to the electrolyte, and migrate to the lithium electrode and reacts directly with the lithium to generate lower order polysulfides. And can also reduce to the final product Li_2S without any charge passing throw the cell, and thus initiate the self-discharge.

The lower order polysulfide species can also diffuse back to the sulfur cathode due to concentration gradient,[10] creating what called the shuttle mechanism.[11] These lower order polysulfide species may increase the self-discharge by reacting with elemental sulfur in the cathode and generate high order polysulfide species, and as a result the amount of sulfur that participated in the first reduction step would be lower, resulting in reducing the capacity of the first plateau due to decreasing the utilization of the active material. Increasing the relaxation time would allow more high order polysulfide species to diffuse away from the positive electrode, and react with lithium electrode, and increasing the polysulfides shuttling through the electrolyte. This could explain why the length of first plateau for long relaxation time is shorter.

The overall discharge capacity of the cells with shorter relaxation times 5/5 and 5/10 (about 1400 mAh.g^{-1} of S) is higher than that for the cells with longer relaxation times 5/20 and 5/60 (about 1300 mAh.g^{-1} of S), except cell 5/1 which deliver almost the same as the cells with longer relaxation times. As mentioned earlier, the self-discharge that rises due to the shuttle reaction would decrease the length of the first plateau and thus lower the overall capacity of the cells with longer relaxation times. For cell 5/1, the average C rate is high (C rate of 1/12) and the GITT process occurs in a much shorter time. This means that there is no enough time for polysulfides to diffuse and form a shuttle effectively inside the cathode. Therefore, solid reduction product would form and encapsulate the cathode and would block the access of the electrolyte, and thus accelerate the end of the discharge.

6.4 The potential response during the GITT for the first discharge

The GITT profile during the first discharge of the Li/S cell measured using 5 min. pulses and 10 min. relaxation time (5/10) is shown in Figure 6.4. A single step of the GITT process for the regions in different states of discharge is displayed in the inserts. The voltage current shapes during each region show almost the same voltage behaviour. Therefore, each single step has been selected depending on the most repeated results having the same voltage behaviour within that region.

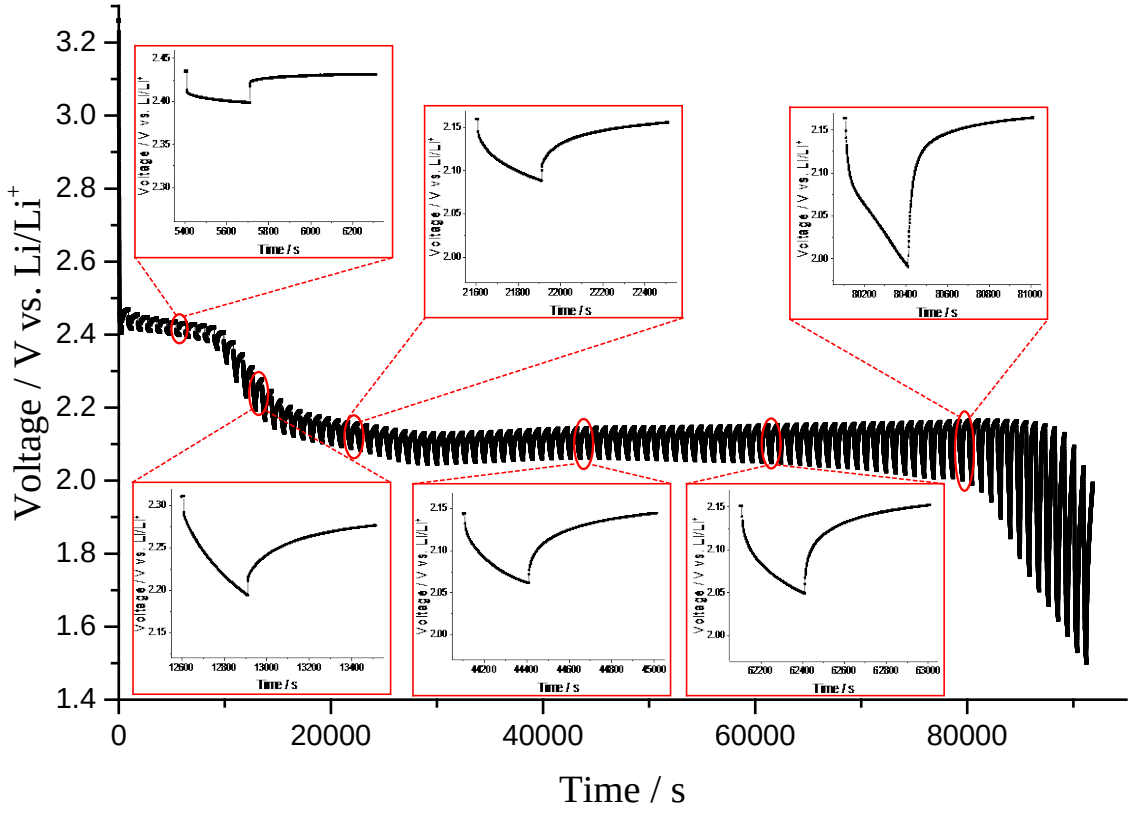

Figure 6.4 GITT profile during the first discharge of the Li/S cell measured using 5 min. pulses and 10 min. relaxation time (5/10). The inserts represent a single step of the titration process for different regions in different states of discharge.

The first observation of the discharge curve was a fast decrease in the voltage at the initial state of the discharge. The voltage was decreased quickly from the OCV which is about 3.25 V to about 2.45 V in the first 100 seconds of the discharge. Cell 5/10 was used as an example to show the voltage behaviour for the approach to the first plateau, as can be seen in Figure 6.5 (a).

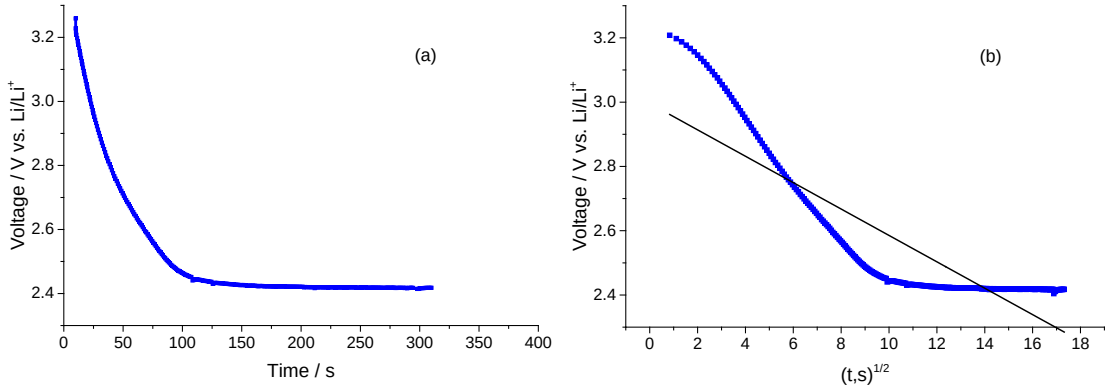

Figure 6.5 1st pulse of cell 5/10 (a) Voltage-time response, and (b) Voltage vs. $t^{1/2}$ plot. Straight line fit is displayed by the black line.

Figure 6.5 (b) represents the variation of cell voltage as a function of the square root of the time, during the first pulse of cell 5/10. It can be seen that the linear relationship was distorted and the potential does not follow the $t^{1/2}$ profile. This happened because the double layer capacitance on the nanoporous carbon electrode of about 0.01 F/mg (see Chapter 5) subtracts a significant current from the constant current applied, and therefore the expected $t^{1/2}$ profile is distorted.

The voltage-time response during the first relaxation of a single step of the GITT for the Li/S cells with different relaxation times is shown in Figure 6.6. During relaxation time (OCV), equilibration occurs by high order polysulfides diffusion, causing a change in voltage over time. The change in voltage directly correlates with the change in polysulfides concentration. For cells 5/20 and 5/60 which use longer relaxation times, it can be observed that the voltage start decreases again and the relaxation curve then becomes non-monotonic, as shown in Figure 6.6 (a). It means that there is an increase in the concentration of high order polysulfides, which is responsible for this decline in the voltage. This behaviour is presumably due to the shuttle reaction which increases the self-discharge (see Chapter 5 for more details on the self-discharge).

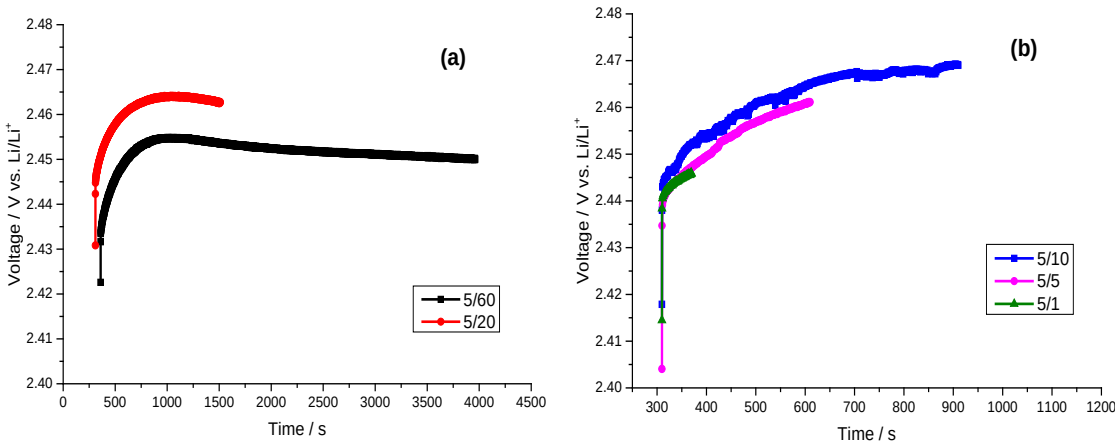

Figure 6.6 Voltage-time response during 1st relaxation of a single step of the GITT for (a) cells 5/20 and 5/60, (b) cells 5/1, 5/5, and 5/10. Note: the scale difference.

On the other hand, Figure 6.6 (b) displays the relaxation curves for shorter relaxation times during the first step of the GITT. The change of the voltage within the relaxation time for cells 5/1, 5/5 and 5/10 show a monotonic increase, however the relaxation times are very short for normal GITT interpretation, and the relaxation curves are far from reaching equilibrium potential.

6.4.1 The potential response within region I

The variation of cell voltage as a function of the square root of the time within region I, during the pulse of a single step of GITT measurements for the cells with different relaxation times, is shown in Figure 6.7. It can be seen that the voltage change has a good linearity with the square root of discharge time. This indicates that region I is following the diffusion condition for all the experiments, and the relaxation time does not affect the linear relationship of the $t^{1/2}$ profile.

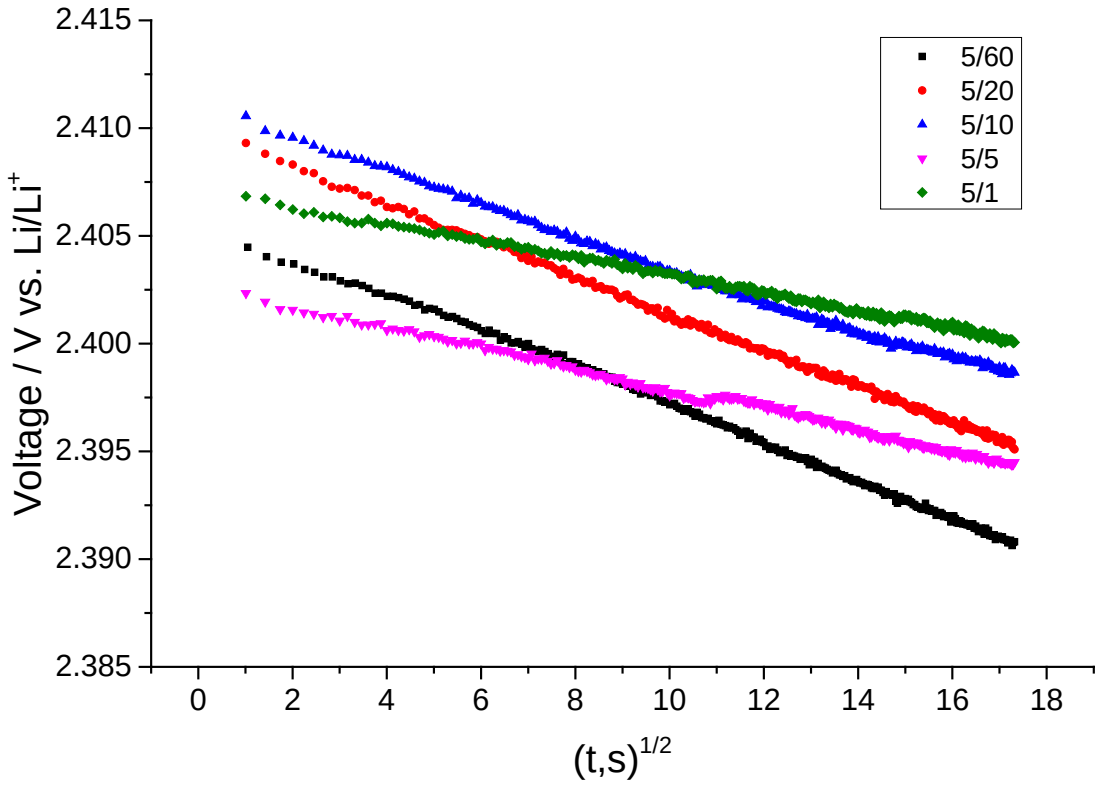

Figure 6.7 The transient voltage changes E vs. $t^{1/2}$ of region I during the pulse of a single GITT process for cells 5/1, 5/5, 5/10, 5/20, and 5/60.

Figure 6.8 represents the variation of cell voltage as a function of the time for region I, during the relaxation of a single step of GITT measurements for the cells with different relaxation times. In order to achieve a more detailed overview, the values of the times are normalized and the values of the voltages are corrected by IR drop.

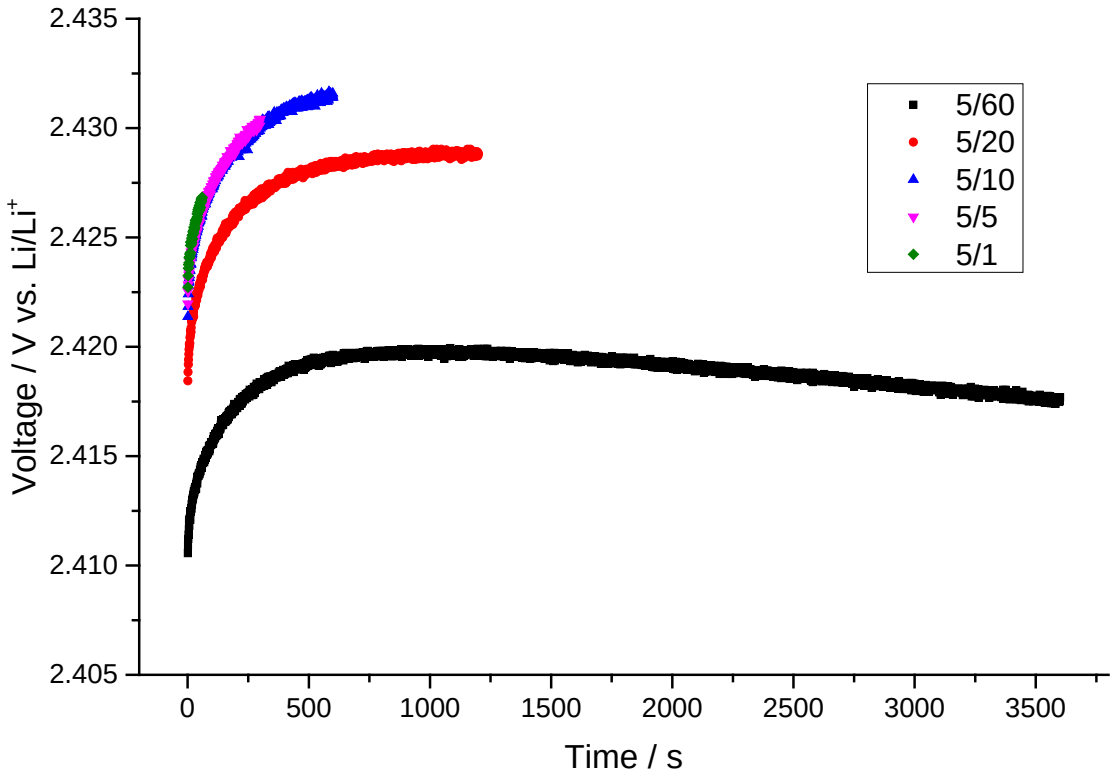

Figure 6.8 Voltage-time response of region I during the relaxation of a single GITT process for cells 5/1, 5/5, 5/10, 5/20, and 5/60. Note: the values of the times are normalized and the values of the voltages are corrected by IR drop.

For the long relaxation time of cell 5/60, a monotonic curve is not shown, but it shows a voltage decline which makes it difficult to achieve an equilibrium potential. This is attributed to the shuttle mechanism which increases the self-discharge (see Chapter 5 for more details on the self-discharge). In the case of the shorter relaxation times of cells 5/1, 5/5 and 5/10, monotonic curves are shown because the relaxation time is not long enough for the self-discharge to take place. The self-discharge that was observed after the first pulse of cell 5/20 has now disappeared, and a good relaxation curve is shown.

The voltage differences between the cells show that in this region the voltage is very sensitive to the electrode composition, and because there is some self-discharge during long relaxation (cell 5/60), there will be more time for self-discharge to occur. Therefore, the overall voltage for cell 5/60 is lower than the others.

6.4.2 The potential response within region II

In region II, high order polysulfide will be reduced to low order polysulfides. It can be observed that in this region the voltage decreases in two steps, as shown in Figure 6.2. The first part involves a fast decline in the voltage from 2.38 – 2.15 V. The variation of cell voltage as a function of the square root of the time for the first part of region II, during the pulse of a single step of GITT measurements for the cells with different relaxation times, is shown in Figure 6.9. In all cases, the transient measurements did not show linearity of the potential with the square root of time over the entire range of the pulse. It is unclear why this happened, but it presumably because the diffusion coefficient varied substantially during the course of the pulse.

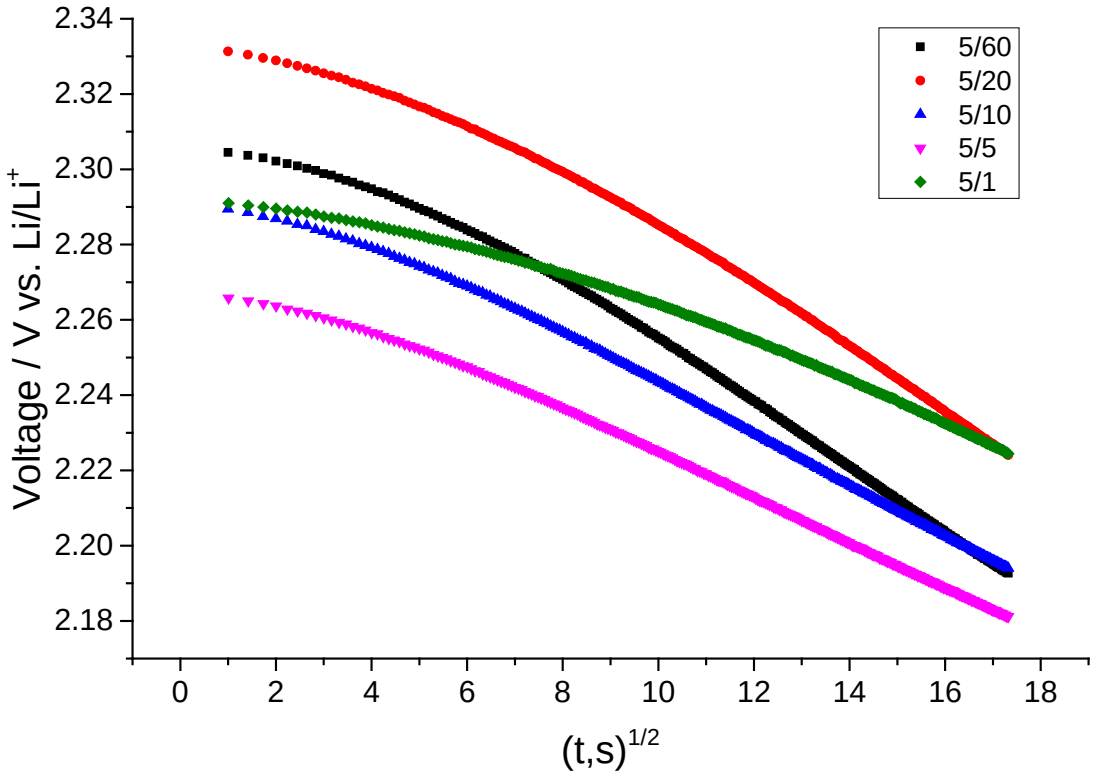

Figure 6.9 The transient voltage changes E vs. $t^{1/2}$ of the 1st part of region II during the pulse of a single GITT process for cells 5/1, 5/5, 5/10, 5/20, and 5/60.

Figure 6.10 displays the voltage changes for the first part of region II during the relaxation of a single GITT titration process using different relaxation times. Each cell shows a monotonic increase in the voltage over the entire time of the relaxation, exept cell 5/60 where a non-monotonic curve was also observed, which corresponds to the self-discharge.

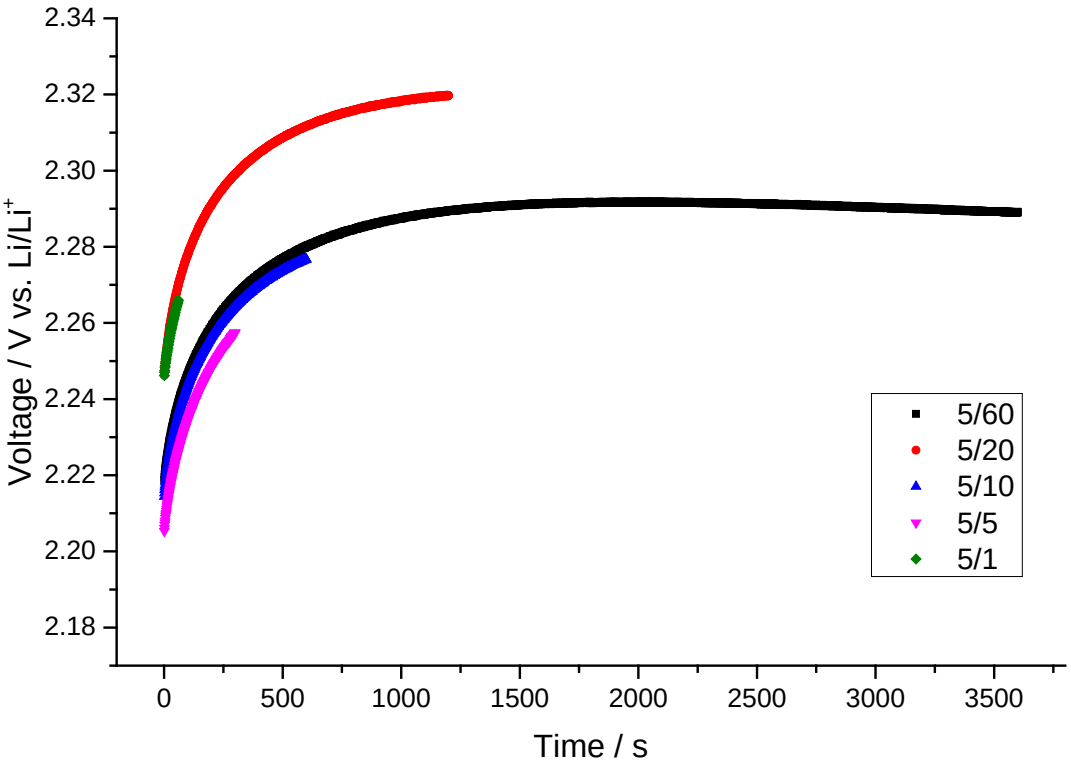

Figure 6.10 Voltage-time response of the 1st part of region II during the relaxation of a single GITT process for cells 5/1, 5/5, 5/10, 5/20, and 5/60. Note: the values of the times are normalized and the values of the voltages are corrected by IR drop.

On the other hand, the second step of region II exhibits a slower decrease in the voltage from 2.15 – 2.05 V, and the E vs. $t^{1/2}$ plot gives almost a straight line behaviour over the entire time of each pulse as can be seen in Figure 6.11.

The variation of cell voltage as a function of the time shows a monotonic curve during the relaxation of each cell, as shown in Figure 6.12. No voltage decline that refers to the self-discharge was observed for cell 5/60, and the curve becomes more monotonic which could reach a better equilibrium potential. This may occur as a result of the precipitation of the solid products on the lithium anode. It is possible that as the discharge proceeds, it is more likely that a passivation layer will form on the lithium surface to develop a solid-electrolyte interface (SEI) layer after some time, which can prevent any further reaction between the lithium and soluble polysulfides,[12] and thus suppress the shuttle reaction.

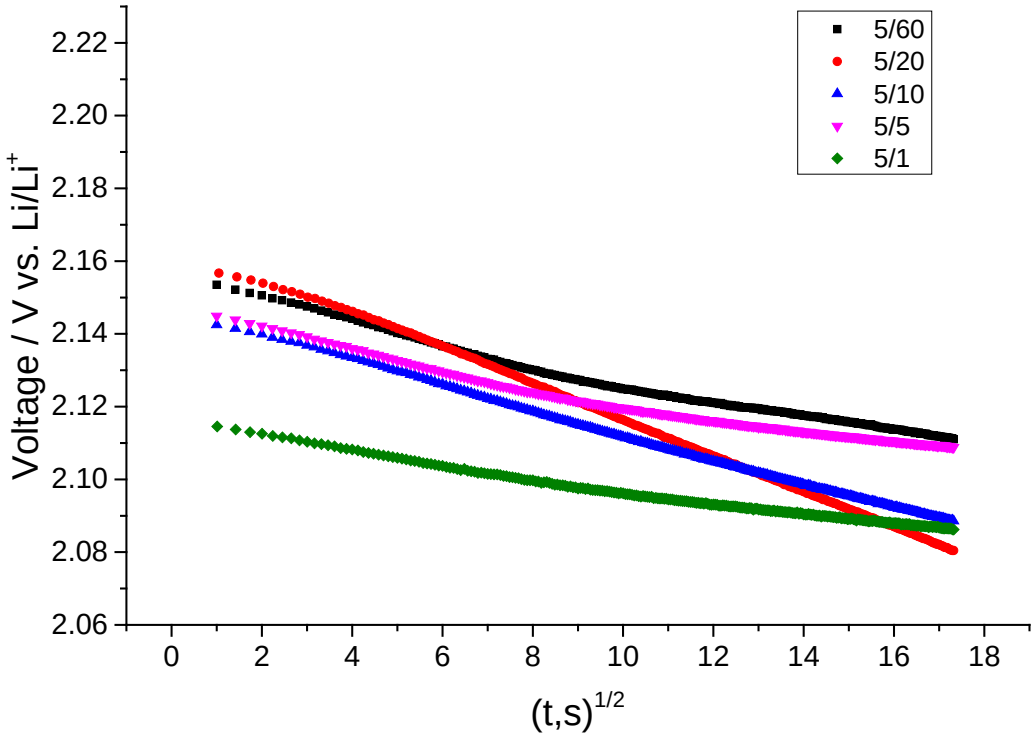

Figure 6.11 The transient voltage changes E vs. $t^{1/2}$ of the 2nd part of region II during the pulse of a single GITT process for cells 5/1, 5/5, 5/10, 5/20, and 5/60.

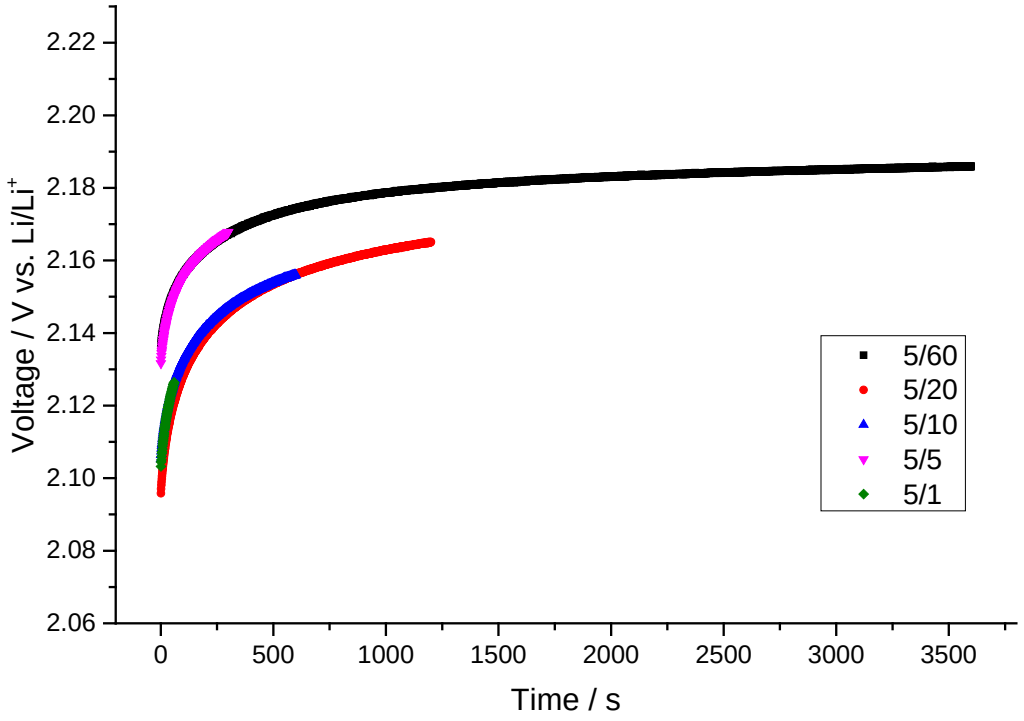

Figure 6.12 Voltage-time response of the 2nd part of region II during the relaxation of a single GITT process for cells 5/1, 5/5, 5/10, 5/20, and 5/60. Note: the values of the times are normalized and the values of the voltages are corrected by IR drop.

6.4.3 The potential response within region III

Two voltage behaviours were also observed in region III. Firstly, the voltage start increases slowly for the first part of region III from 2.05 – 2.06 V (see Figure 6.2). The variation of cell voltage as a function of the square root of the time for the first part of region III, during the pulse of a single step of GITT measurements for the cells with different relaxation times, is shown in Figure 6.13. In this part it can be seen that the E vs. $t^{1/2}$ plot gives almost a straight line over the entire time of each pulse except for the shorter relaxation times of cells 5/1 and 5/5, which shows a combination of linear relationship over the time domain from 1 to 100 s of each pulse and a little tendency at the end of the pulse, which can also be referred as an incomplete relaxation of these cells.

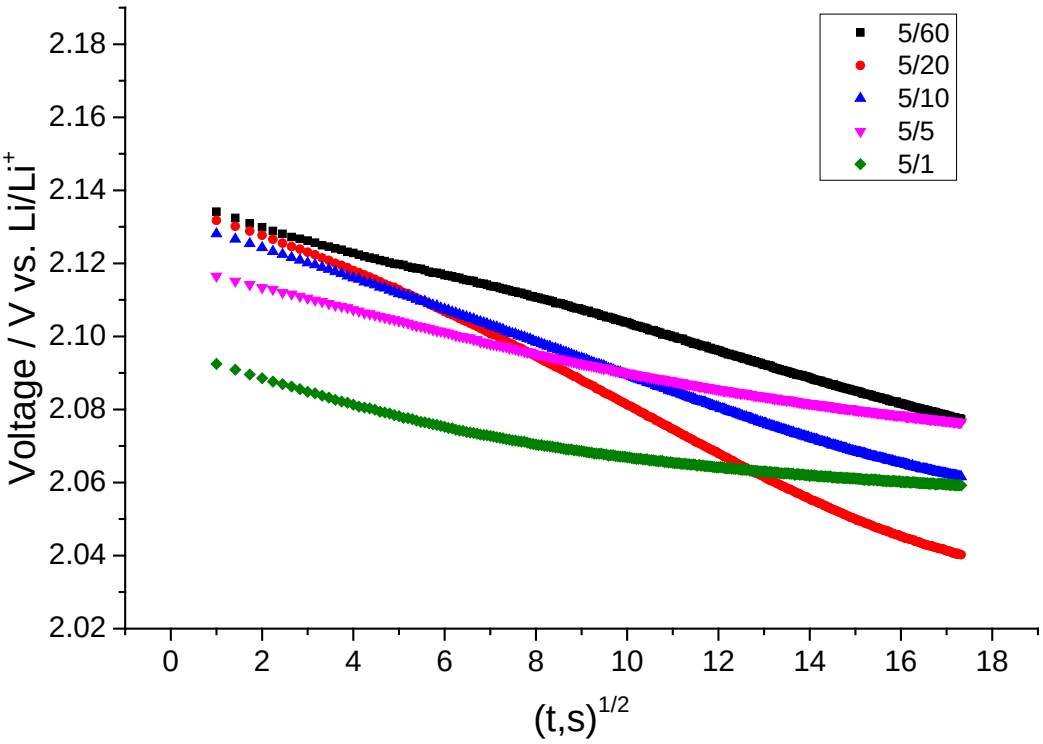

Figure 6.13 The transient voltage changes E vs. $t^{1/2}$ of the 1st part of region III during the pulse of a single GITT process for cells 5/1, 5/5, 5/10, 5/20, and 5/60.

Figure 6.14 displays the transient voltage changes for the first part of region III during the relaxation of a single GITT titration process using different relaxation times. Each cell shows a monotonic increase in the voltage over the entire time of the relaxation.

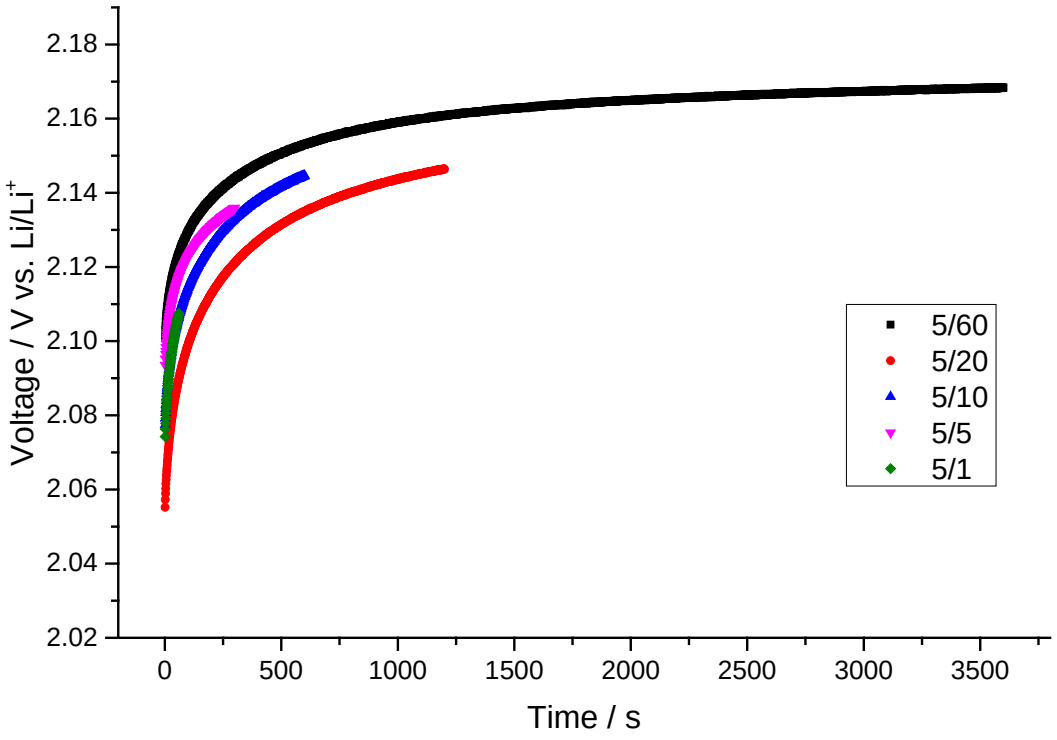

Figure 6.14 Voltage-time response of the 1st part of region III during the relaxation of a single GITT process for cells 5/1, 5/5, 5/10, 5/20, and 5/60. Note: the values of the times are normalized and the values of the voltages are corrected by IR drop.

The second part of region III exhibits a slow decrease in the voltage from 2.06 – 2 V. In this part it can be seen that the E vs. $t^{1/2}$ plot gives a straight line over the entire time for each pulse in cells 5/10, 5/20 and cell 5/60; however, cells 5/1 and 5/5 show a combination of linear relationship over the time domain from 1 to 100 s of each pulse and a tendency at the end of the pulse, which can also be attributed to an incomplete relaxation of these cells, as shown in Figure 6.15. Moreover, a monotonic increase in the voltage was also observed during the relaxation of each cell, as shown in Figure 6.16.

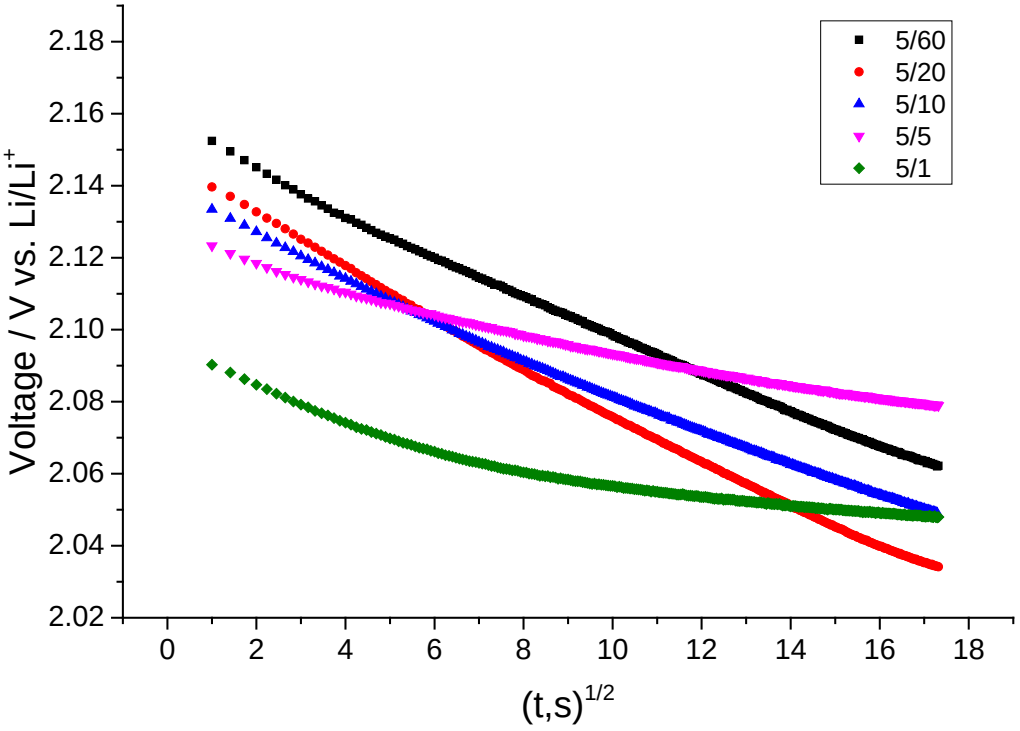

Figure 6.15 The transient voltage changes E vs. $t^{1/2}$ of the 2nd part of region III during the pulse of a single GITT process for cells 5/1, 5/5, 5/10, 5/20, and 5/60.

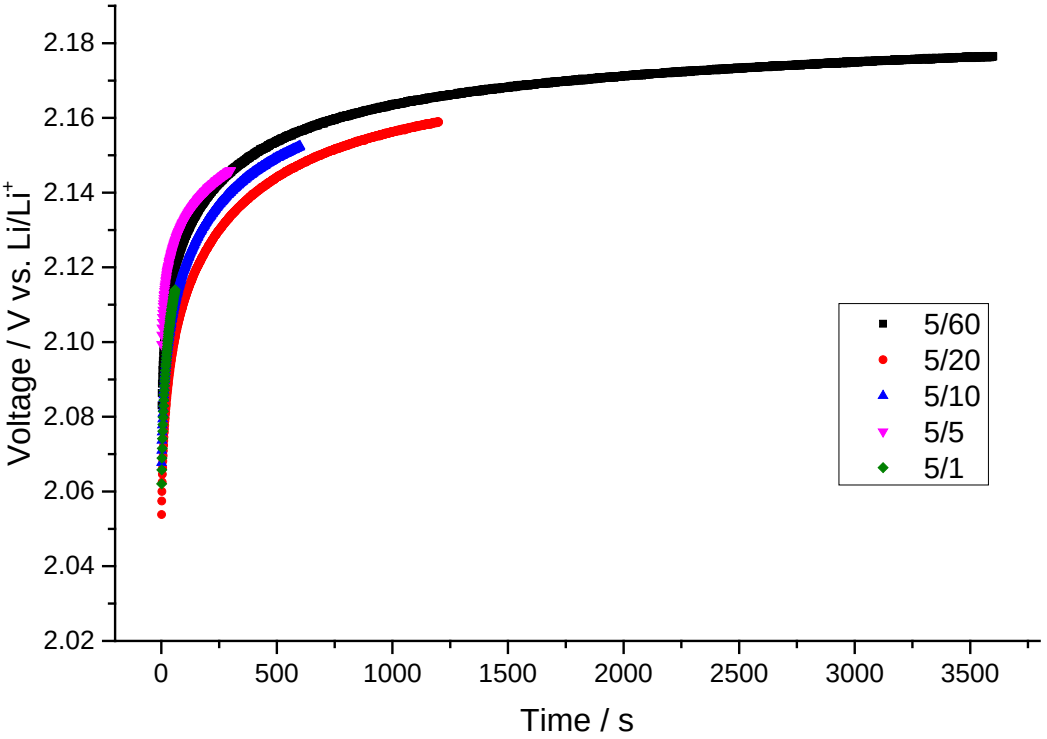

Figure 6.16 Voltage-time response of the 2nd part of region III during the relaxation of a single GITT process for cells 5/1, 5/5, 5/10, 5/20, and 5/60. Note: the values of the times are normalized and the values of the voltages are corrected by IR drop.

6.4.4 The potential response within region IV

Region IV represents the final stage of the GITT measurement. In this region a fast decrease in the voltage was observed from 2 – 1.5 V. Figure 6.17 displays the variation of cell voltage as a function of the square root of the time within region IV, during the pulse of a single step of GITT measurements for the cells with different relaxation times. It can be seen that the E vs. $t^{1/2}$ plot was distorted from the linearity, and the potential does not follow the $t^{1/2}$ profile. This distortion may occur as a result of the electrode composition, where a large amount of solid was formed in this region, according to Equation 6.7. Therefore, it may precipitate on the electrode surface and block the diffusion path.

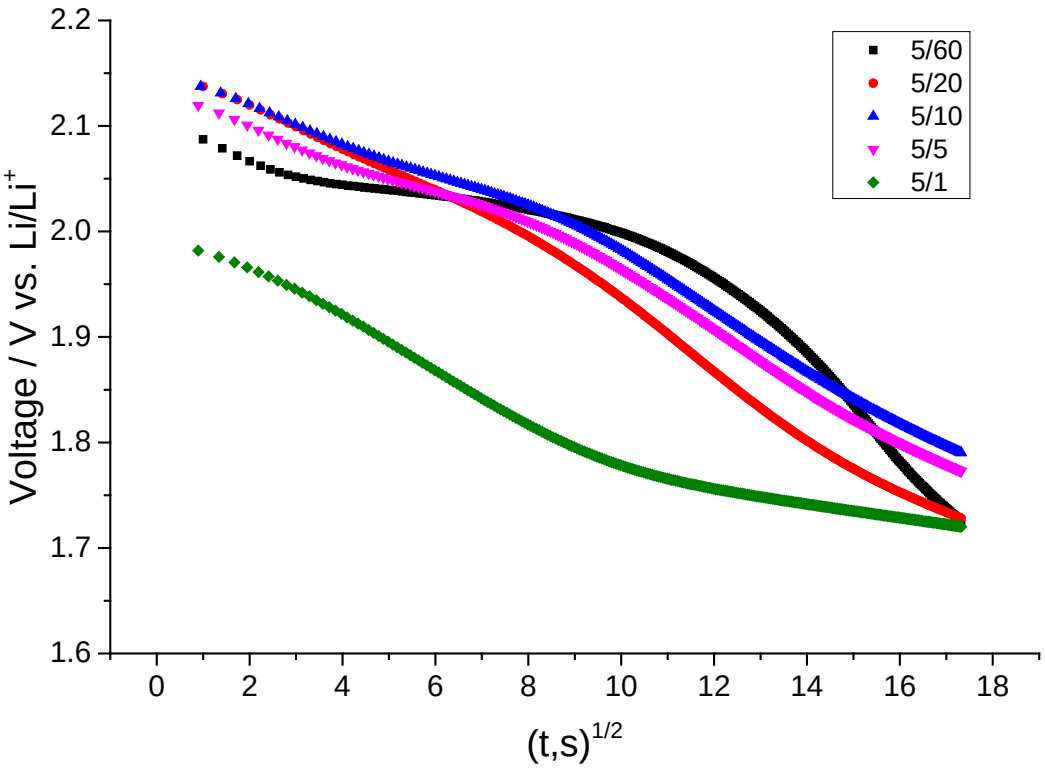

Figure 6.17 The transient voltage changes E vs. $t^{1/2}$ of region IV during the pulse of a single GITT process for cells 5/1, 5/5, 5/10, 5/20, and 5/60. Note: the scale compares to Figure 6.16.

During the relaxation, each cell shows a monotonic voltage increase with a combination of a fast increase in the voltage over the time domain from 1 to 100 s for each relaxation, and a slow increase for the rest of the relaxation, except cell 5/1, which shows only a fast increase in the voltage over the entire time due to the short relaxation time of the cell, as shown in Figure 6.18.

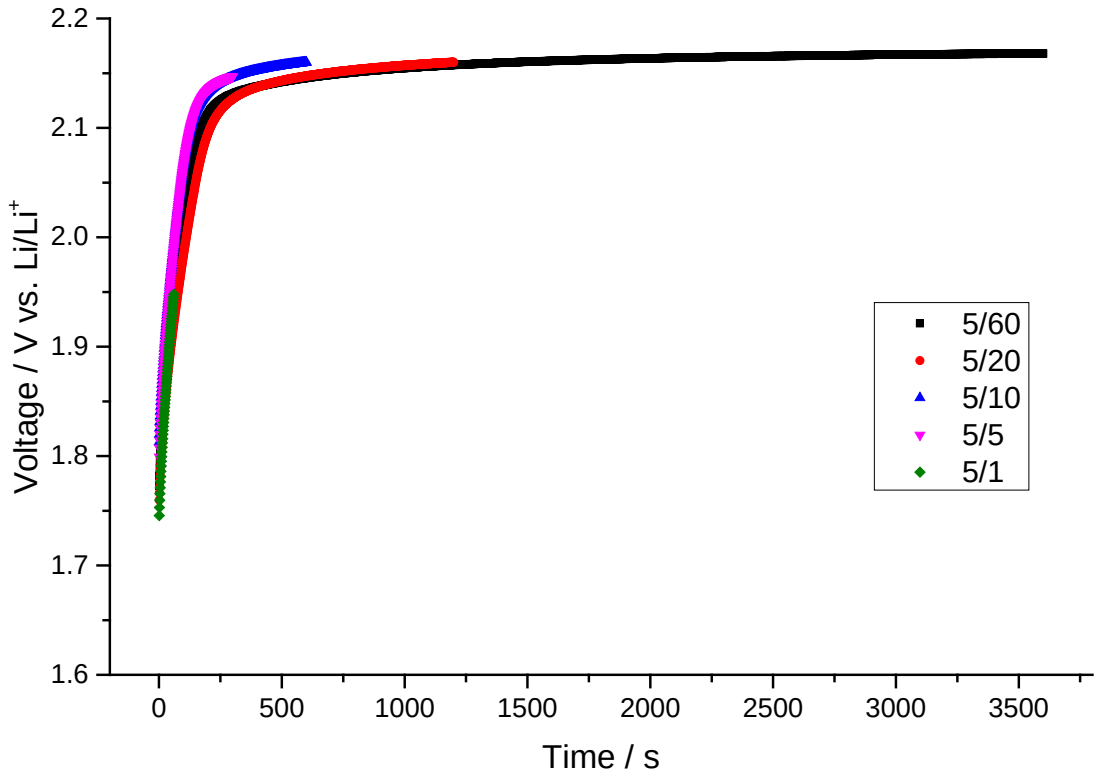

Figure 6.18 Voltage-time response of region IV during the relaxation of a single GITT process for cells 5/1, 5/5, 5/10, 5/20, and 5/60. Note: (1) the scale compares to Figure 6.16. (2) the values of the times are normalized and the values of the voltages are corrected by IR drop.

6.5 The potential response during the GITT for the first charge

The GITT profile during the first charge of cell 5/10 is shown in Figure 6.19. A single step of the GITT process for the regions in different states of charge is displayed in the inserts. These regions were selected depending on the change in the voltage at different states of the cell charge. Region V can be related to the oxidation of Li_2S to Li_2S_4,

$$4\ Li_2S_{(s)} \rightarrow Li_2S_{4(s)} + 6\ Li^+ + 6\ e^- \quad (6.8)$$

Li_2S_4 can be oxidized in region VI to produce high order polysulfide,

$$2\ Li_2S_{4(soln.)} \rightarrow Li_2S_{8(soln.)} + 2\ Li^+ + 2\ e^- \quad (6.9)$$

Region III in the charge curve represents the final stage of the oxidation which occurs at a high voltage region, where high order polysulfide will be gradually converted to elemental sulfur,

$$Li_2S_{8(soln.)} \rightarrow S_{8(s)} + 2\ Li^+ + 2\ e^- \quad (6.10)$$

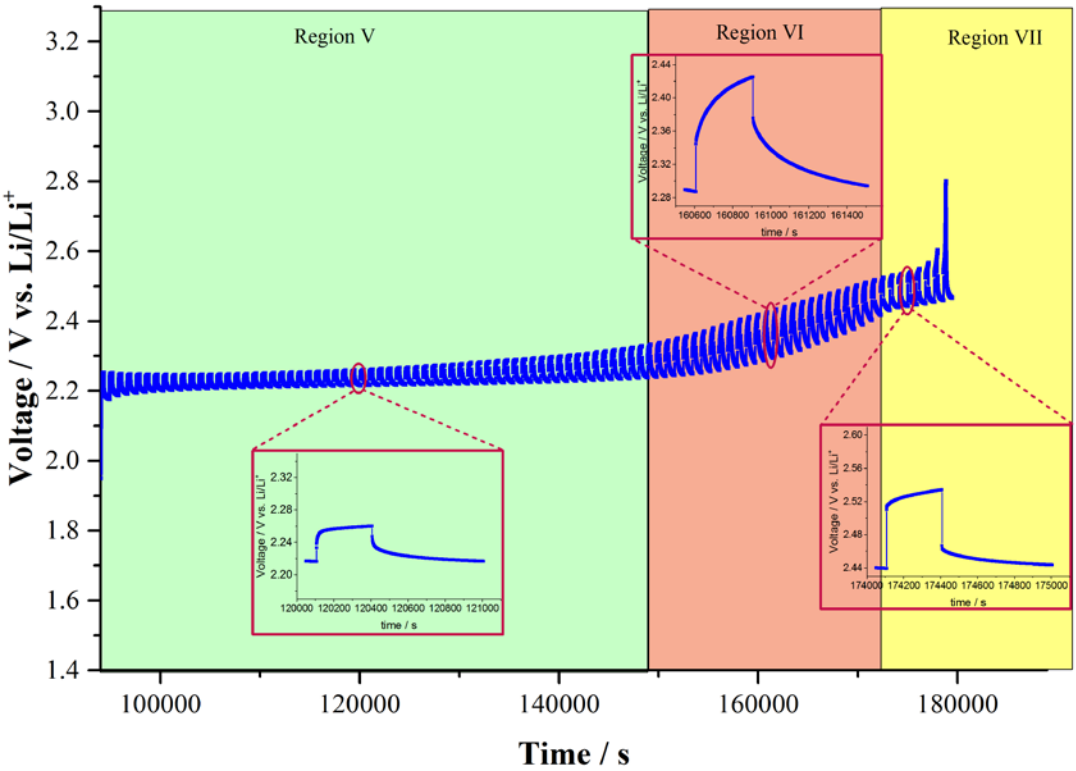

Figure 6.19 GITT profile during the first discharge of Li/S cell measured using 5 min. pulses and 10 min. relaxation time (5/10). The inserts represent a single step of the titration process for different regions in different states of charge.

6.5.1 The potential response within region V

This region represents the combination of the reverse of regions III and IV in the discharge curve. It involves two-phase reaction, where the active material transfers from solid phase (Li_2S) to the liquid phase (Li_2S_4), and according to Nernst equation the slight change in the voltage within this region as shown in Figure 6.19, can be attributed to the increase in the concentration of soluble Li_2S_4.

Figure 6.20 displays the variation of cell voltage as a function of the square root of the time within region V, during the pulse of a single step of GITT measurements for the cells with different relaxation times. For the long relaxation times cells 5/20 and 5/60, It can be seen that the E vs. $t^{1/2}$ plot gives almost a straight line over the entire time of each pulse, as shown in Figure 6.20 (a). While for short relaxation times the transient voltage change was distorted from the linearity and shows a combination of straight line over the time domain from 1 to 100 s of each pulse and a tendency for the rest of the pulse, which can be attributed to the incomplete relaxation of these cells, as shown in Figure 6.20 (b).

In addition, a monotonic decrease of the voltage with the relaxation time was observed for each cell, as shown in Figure 6.21.

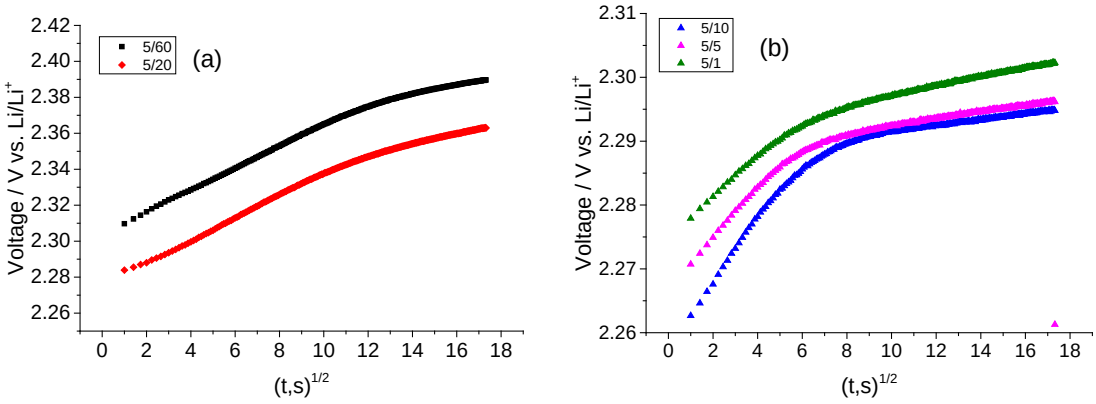

Figure 6.20 The transient voltage changes E vs. $t^{1/2}$ of region V during the pulse of a single GITT process for (a) cells 5/20 and 5/60, and (b) cells 5/1, 5/5, and 5/10. Note: the scale difference.

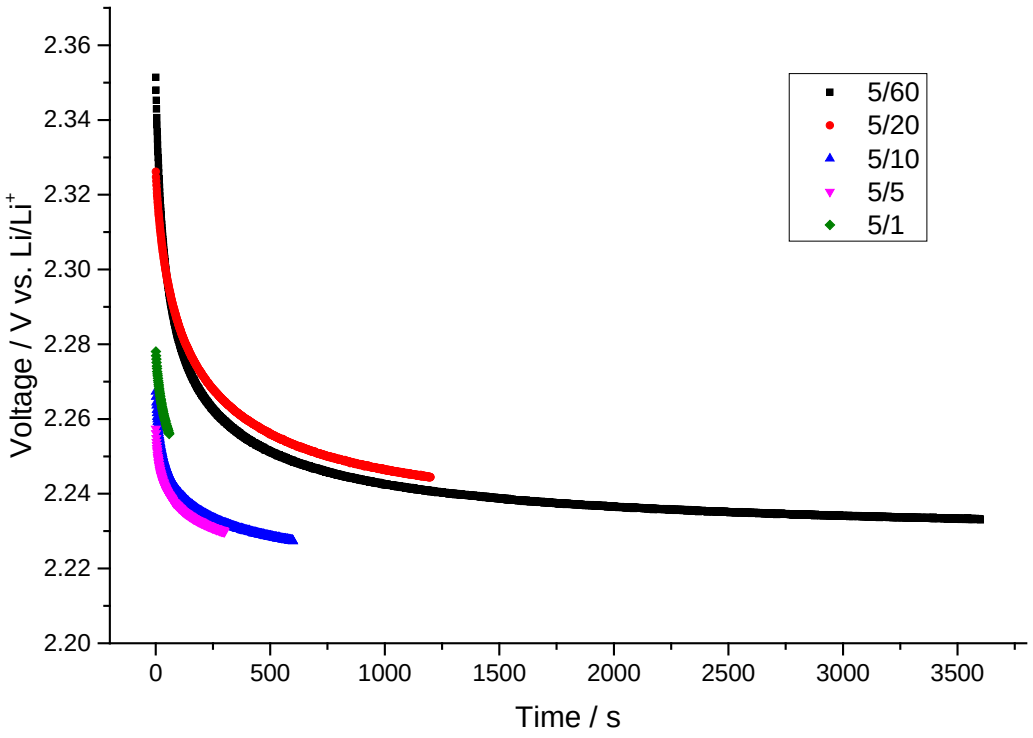

Figure 6.21 Voltage-time response of region V during the relaxation of a single GITT process for cells 5/1, 5/5, 5/10, 5/20, and 5/60. Note: the values of the times are normalized and the values of the voltages are corrected by IR drop.

6.5.2 The potential response within region VI

Region VI involves one-phase reaction, where low order polysulfide will be oxidized to high order polysulfides (Equation 6.9). The variation of cell voltage as a function of the square root of the time, during the pulse of a single step of GITT measurement, is shown in Figure 6.22. Each cell shows almost a straight line over the entire time of each pulse.

Figure 6.23 displays the voltage changes for first part of region VI during the relaxation of a single GITT titration process using different relaxation times. Each cell shows a monotonic decrease in the voltage during the relaxation time.

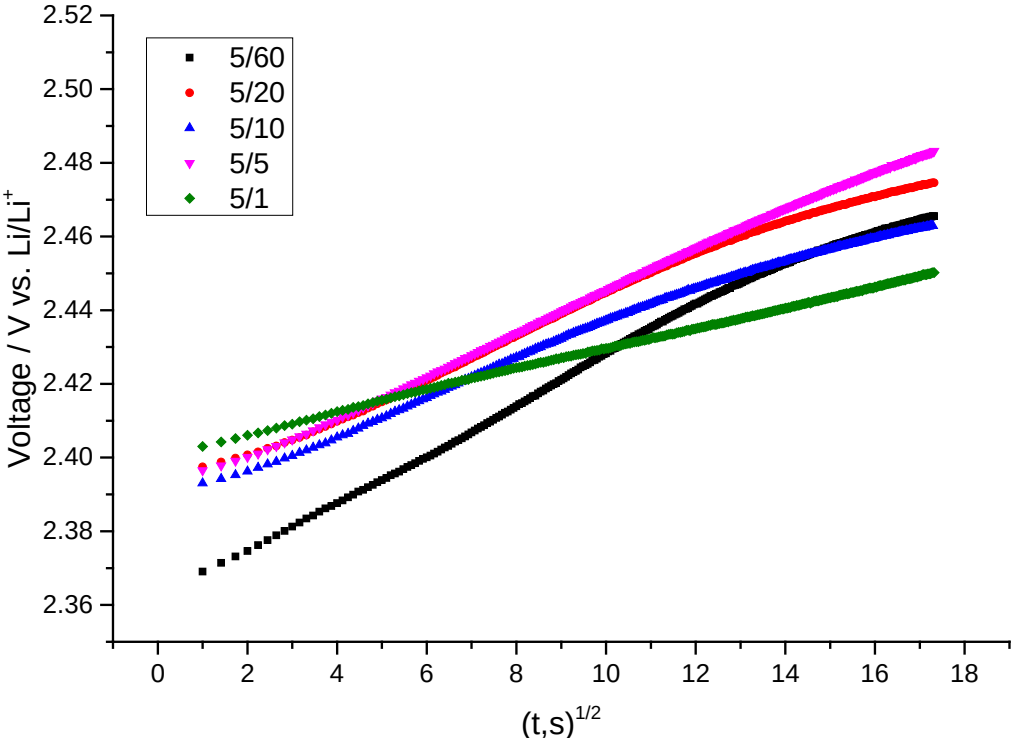

Figure 6.22 The transient voltage changes E vs. $t^{1/2}$ of region VI during the pulse of a single GITT process for cells 5/1, 5/5, 5/10, 5/20, and 5/60.

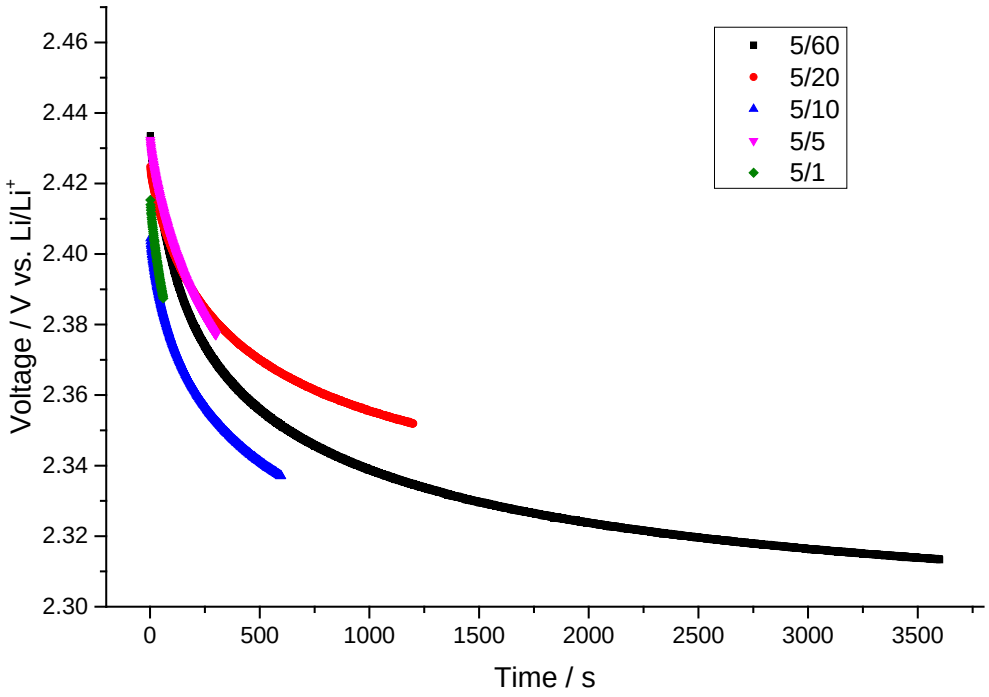

Figure 6.23 Voltage-time response of region VI during the relaxation of a single GITT process for cells 5/1, 5/5, 5/10, 5/20, and 5/60. Note: the values of the times are normalized and the values of the voltages are corrected by IR drop.

6.5.3 The potential response within region VII

This region represents the final stage of the charge as described in equation 6.10. The variation of cell voltage as a function of the square root of the time within region VII, during the pulse of a single step of GITT measurements, is shown in Figure 6.24. It can be seen that the transient voltage change has a good linearity with the square root of discharge time. This indicates that region VII is following the diffusion condition, which is compatible with the previous observation during region I in the discharge (section 6.4.1). In addition, a monotonic decrease of the voltage with the relaxation time was also observed for each cell, as shown in Figure 6.25.

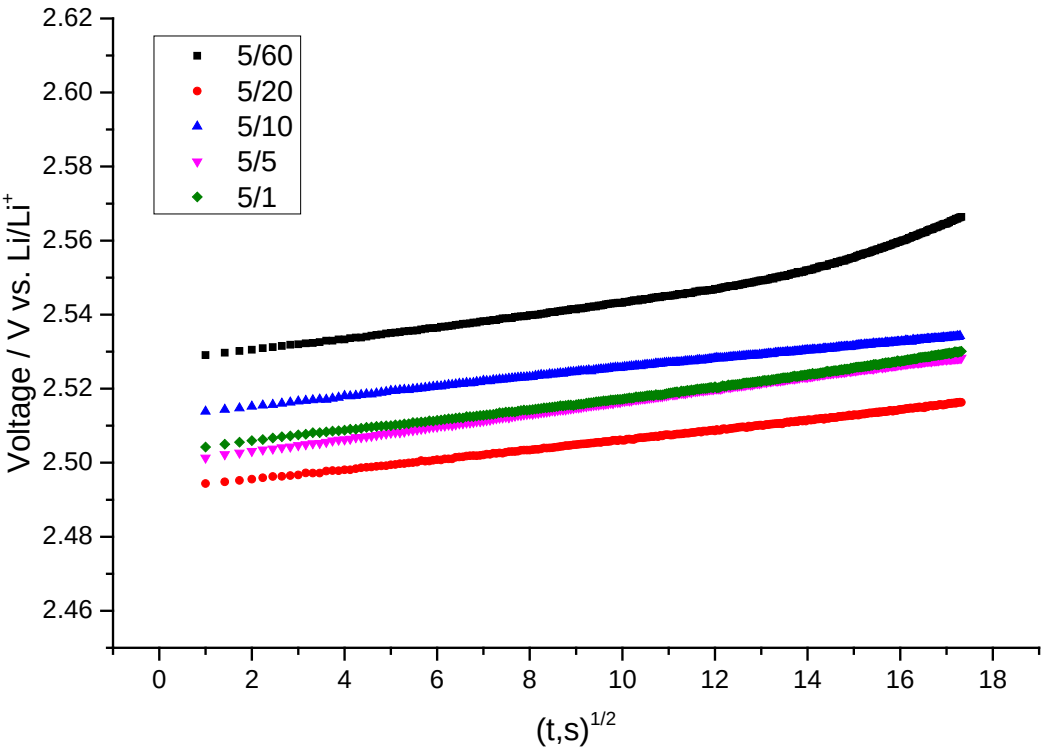

Figure 6.24 The transient voltage changes E vs. $t^{1/2}$ of region VII during the pulse of a single GITT process for cells 5/1, 5/5, 5/10, 5/20, and 5/60.

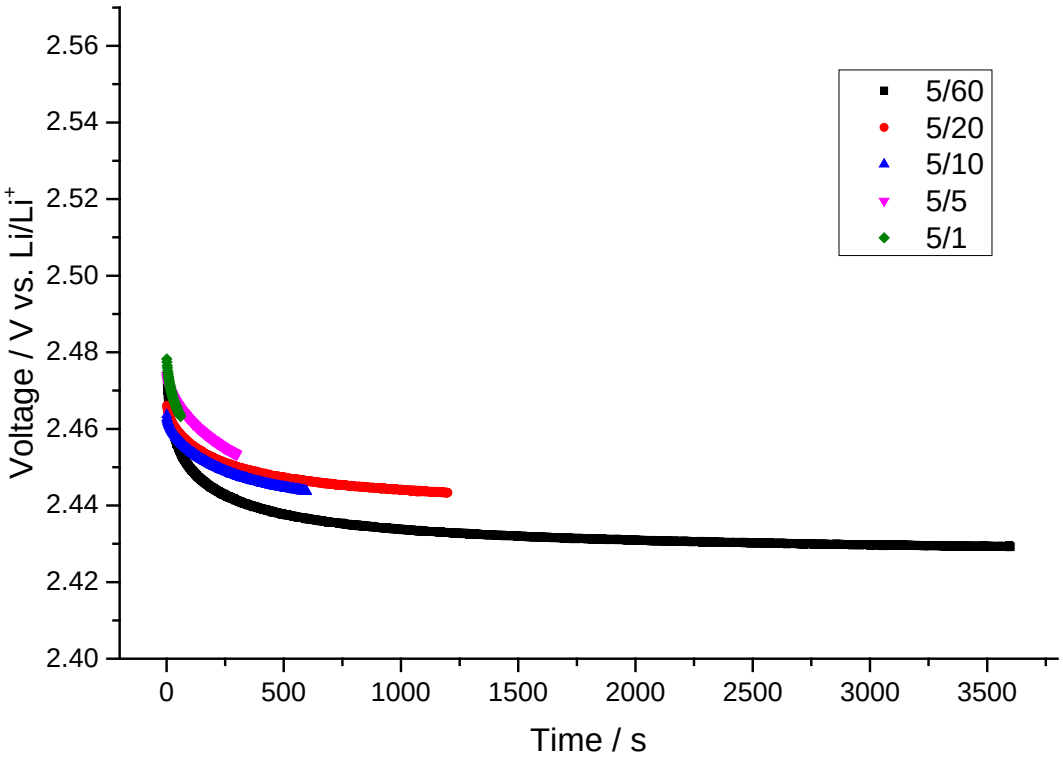

Figure 6.25 Voltage-time response of region VII during the relaxation of a single GITT process for cells 5/1, 5/5, 5/10, 5/20, and 5/60. Note: the values of the times are normalized and the values of the voltages are corrected by IR drop.

6.6 The potential response during the GITT for the second discharge

It was noted above that self-discharge occurred during the beginning of the first discharge cycle, leading to reversal of the potential change during relaxation, whereas pulses from the second part of region II onwards showed monotonic relaxations. Results are given here for the GITT study for the second discharge using cell 5/60. In this case, normal relaxations were shown throughout the discharge process, so that the relaxations can be considered to approach the equilibrium potential before the next pulse, fulfilling the GITT requirement.

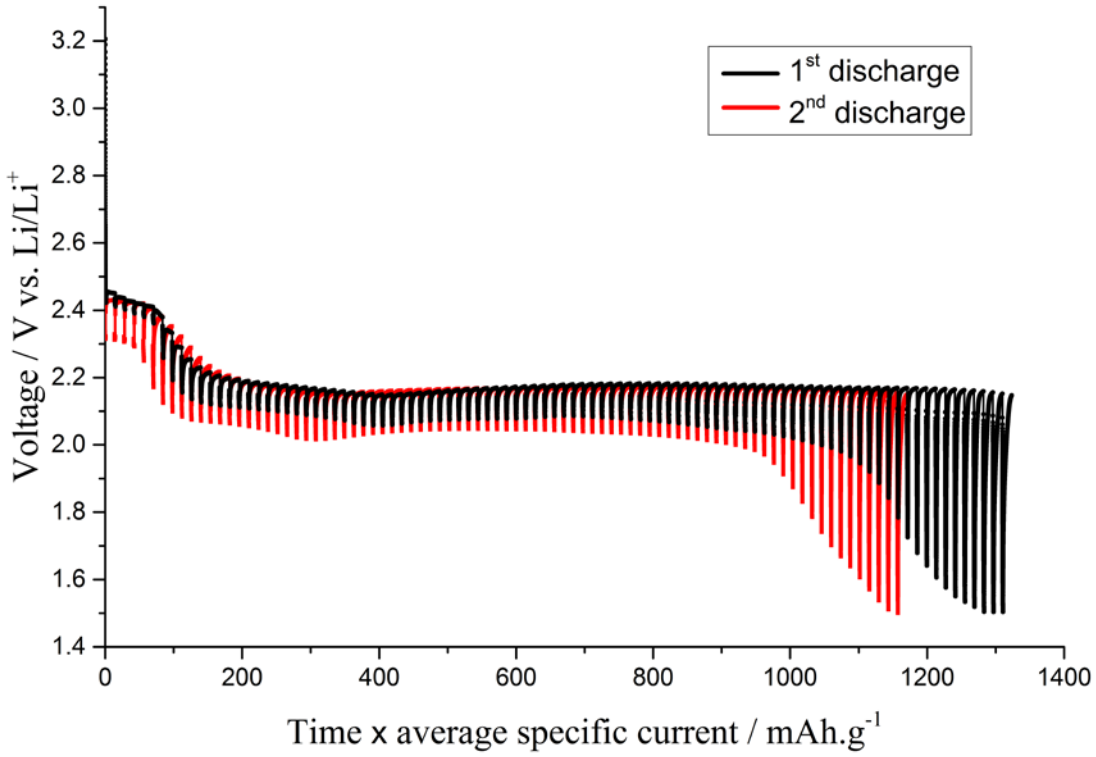

Figure 6.26 Comparison of GITT profiles during the 1st discharge (black line) and the second discharge (red line) of cell 5/60.

Figure 6.26 displays the GITT profiles during the 1st and 2nd discharges of cell 5/60. It can be observed that the overall length of the 2nd discharge is lower than that for the 1st discharge. This may occur as a result of the irreversible loss of the active material, where part of Li_2S left in the cathode at the end of the discharge is in a form that is not easily oxidized during the charging process,[13,14] so that, does contribute sulfur to the

discharge capacity at the next discharge. In addition, the incomplete charge of high order polysulfide, where it might not be fully transferred back into elemental sulfur, can lower the capacity at the next discharge.[15–17]

The initial value for the IR drop of the 1st discharge is about 22 mV as shown in Figure 6.27 (black), followed by an increase of this value during region I to reach about 33 mV at the end of this region (top peak). This might be related to the viscosity increase and corresponding conductivity decrease due to formation of high order polysulfide, which has a higher concentration in the electrolyte.[9] After that, a gradual decrease in the IR drop was observed during region II to about 14 mV corresponding to the formation of lower order polysulfides, which have a lower concentration.[9] The IR drop then starts gradually increase within the rest of the 1st discharge to become about 37 mV at the end of region IV. This is probably due to the change of the cross section area of the positive electrode surface as a result of the passivation layer of Li_2S_2 and Li_2S, which would reduce the cross section area, and thus increase the resistance of the cell.

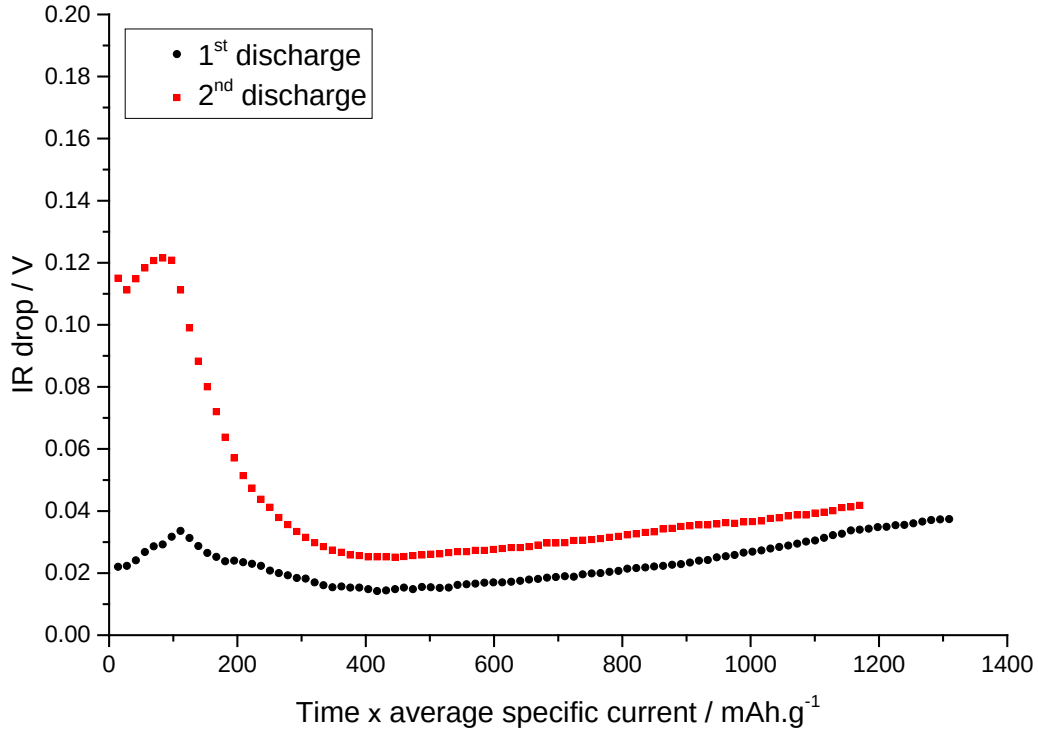

Figure 6.27 IR drop within the GITT profiles during the 1st discharge (black) and the second discharge (red) of cell 5/60.

During the 2nd discharge, it can clearly see that the change in the IR drop behave in similar way to that observed within the 1st discharge, but with a much higher values especially during regions I and II, where it has a highest value of about 120 mV, as shown in Figure 6.27 (red). The reason behind that might also be attributed to the reduction of the cross section area of the cathode resulted from deposition of elemental sulfur at the end of the charge, which also contributes to the rise in the resistance of the cell. Then the increase in the IR drop previously attributed to the electrolyte is similar to that observed in 1st discharge. After that, a large decline in the IR drop can be seen within region II, which is probably due to the dissolution of part of the solid active materials that deposited on the positive electrode surface during the first cycle. A gradual increase in the IR drop was then observed within the rest of the 2nd discharge, which also attributed to the decrease in the cross section area previously described in the 1st discharge.

Moreover, the values of the OCV are almost the same during each discharge process, except in the regions that it suffer from self-discharge in the 1st discharge. The non-monotonic voltage change that was observed in the 1st discharge is disappeared in the 2nd discharge. This can be attributed to the SEI layer that formed on the lithium electrode during the 1st discharge, which can suppress the shuttle reaction during the 2nd discharge, and thus suppress the self-discharge.

The variation of cell voltage as a function of the square root of the time within region I, during the pulse of a single step of GITT measurement is shown in Figure 6.28 (a). It can be seen that there is some distortion of the potential transient from the linearity, which might be due to the passivation layer on the cathode surface, as mentioned above. Also, A monotonic increase in the voltage was observed during the relaxation of this region which can get closer to a better equilibrium potential, as shown in Figure 6.28 (b), attributed to the formation of the SEI layer as previously described.

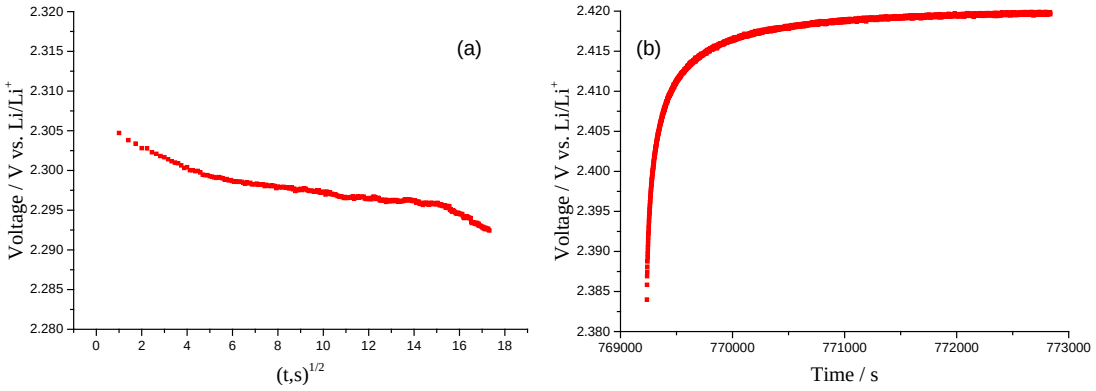

Figure 6.28 The voltage response for the second discharge of cell 5/60 during a single GITT process in region I, (a) Voltage vs. $t^{1/2}$ plot during the pulse, and (b) Voltage-time response during the relaxation. Note: the values of the voltages are corrected by IR drop.

Two voltage behaviours were also observed in region II during the 2nd discharge. The first part involves a fast decline in the voltage, where the linear relationship of the voltage with $t^{1/2}$ was distorted and the potential does not follow the $t^{1/2}$ profile during the entire time of each pulse, as shown in Figure 6.29 (a). It is unclear why this distortion happened in this region, but it may be due to the variation of the diffusion coefficient during the course of the pulse as mentioned in the 1st discharge. Also, a monotonic increase in the voltage during the relaxation time was observed during this part of region II, as shown in Figure 6.29 (b).

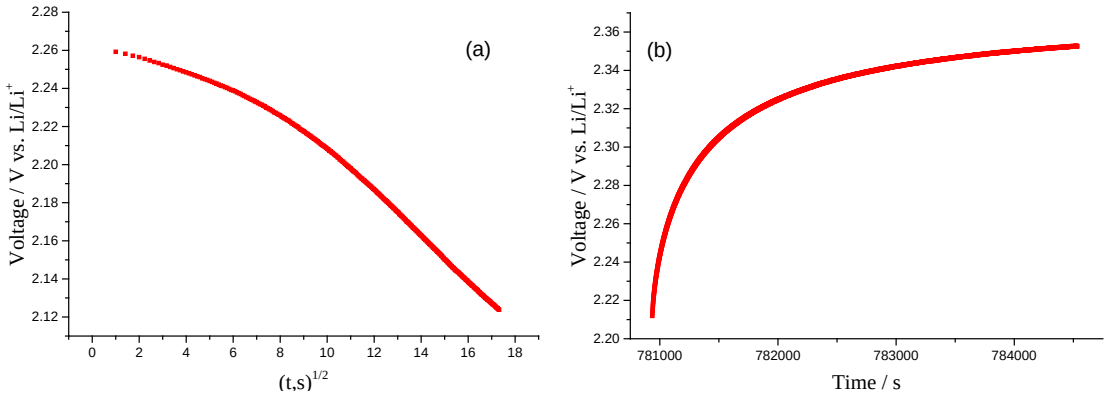

Figure 6.29 The voltage response for the second discharge of cell 5/60 during a single GITT process of the 1st part of region II, (a) Voltage vs. $t^{1/2}$ plot during the pulse, and (b) Voltage-time response during the relaxation. Note: the values of the voltages are corrected by IR drop.

On the other hand, in the second part of region II, which exhibits a slower decrease in the voltage, the variation of transient voltage as a function of the square root of the time gives a straight line over the entire time of each pulse, as can be seen in Figure 6.30 (a), which indicates that a diffusion condition can be achieved during this part of region II. In addition, a monotonic increase in the voltage during the relaxation time was also observed during this part of region II, as shown in Figure 6.30 (b).

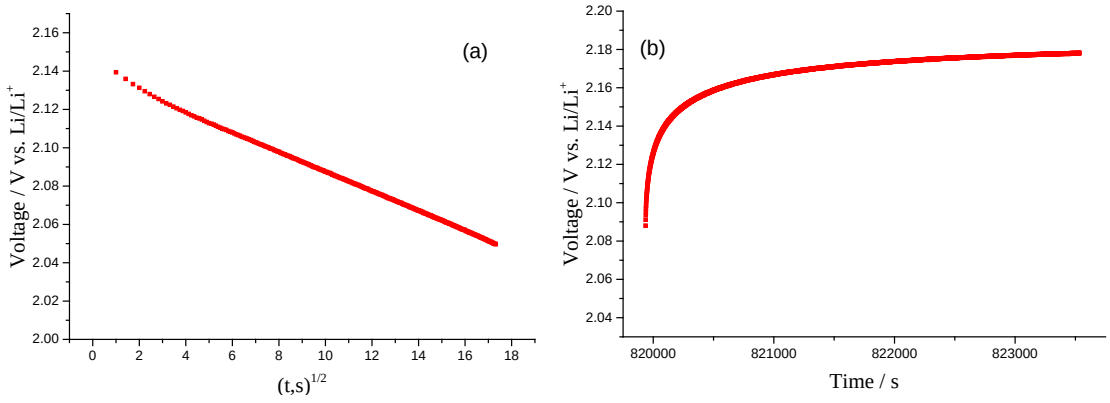

Figure 6.30 The voltage response for the second discharge of cell 5/60 during a single GITT process of the 2nd part of region II, (a) Voltage vs. $t^{1/2}$ plot during the pulse, and (b) Voltage-time response during the relaxation. Note: the values of the voltages are corrected by IR drop.

Two voltage behaviours were also observed in region III. A slow increase in the voltage in the first part, and then a slow decrease in the voltage were observed in the second part within this region. The variation of cell voltage as a function of the square root of the time for first part of region III, during the pulse of a single step of GITT measurement, is shown in Figure 6.31 (a). It can be seen that the E vs. $t^{1/2}$ plot gives a straight line over the entire time of each pulse. In addition, a monotonic increase in the voltage during the relaxation time was also observed during this part of region III, as shown in Figure 6.31 (b).

In addition, a linear relationship between the transient voltage changes with the square root of the time during the second part of region III was also observed, as shown in Figure 6.32 (a). Moreover, a monotonic increase in the voltage during the relaxation time was also observed during this part of region III, as shown in Figure 6.32 (b).

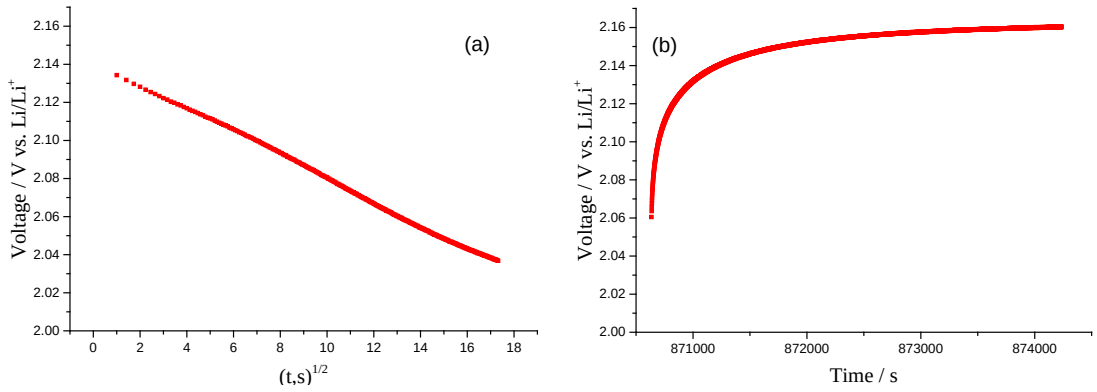

Figure 6.31 The voltage response for the second discharge of cell 5/60 during a single GITT process of the 1st part of region III, (a) Voltage vs. $t^{1/2}$ plot during the pulse, and (b) Voltage-time response during the relaxation. Note: the values of the voltages are corrected by IR drop.

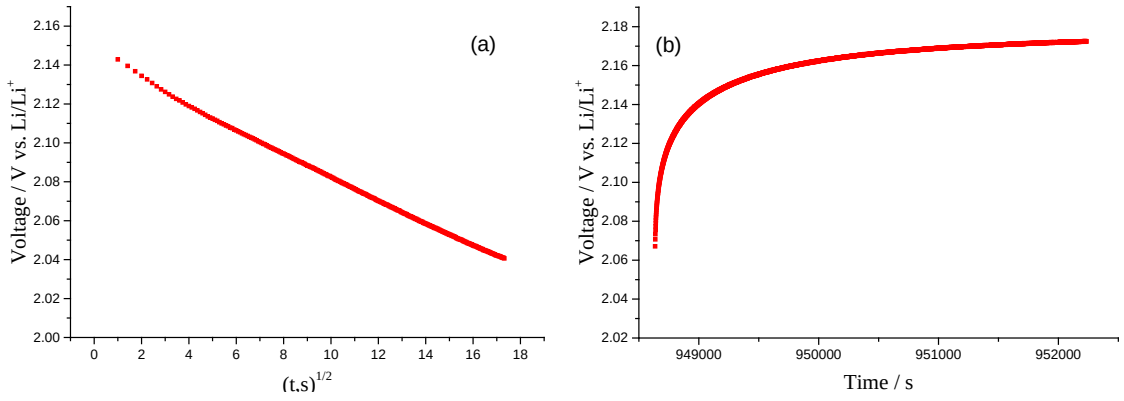

Figure 6.32 The voltage response for the second discharge of cell 5/60 during a single GITT process of the 2nd part of region III, (a) Voltage vs. $t^{1/2}$ plot during the pulse, and (b) Voltage-time response during the relaxation. Note: the values of the voltages are corrected by IR drop.

Region IV in the second discharge exhibits a fast decrease in the voltage from 2 – 1.5 V. Figure 6.33 (a) represents the variation of cell voltage as a function of the square root of the time for region IV, during the pulse of a single step of GITT measurement of cell 5/60. It can be seen that there is some distortion of the voltage transient from the linearity. The electrode composition which contains a large amount of solid generated in this region may cause this distortion by blocking the diffusion path, as mentioned earlier in section 6.4.4. In addition, a monotonic increase in the voltage during the relaxation time was also observed in this region, as shown in Figure 6.33 (b).

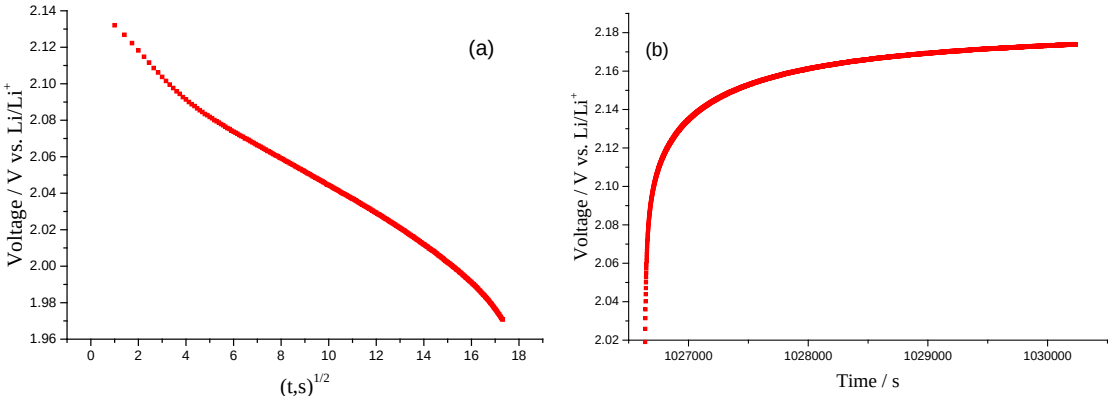

Figure 6.33 The voltage response for the second discharge of cell 5/60 during a single GITT process of region IV, (a) Voltage vs. $t^{1/2}$ plot during the pulse, and (b) Voltage-time response during the relaxation. Note: the values of the voltages are corrected by IR drop.

6.7 Conclusion

The analysis of the GITT experiments with a very fine time resolution can provide a closer look at the reactions that occur inside the Li/S cell. Analysis of the transient and classifying the voltage behaviour within the individual pulses at different states of discharge/charge was achieved in this chapter. It is difficult to define which species is diffusing since the electrochemical processes in Li/S cells are complicated and it involves the formation of more than one species. However, we can here define an effective diffusion coefficient for the species whose diffusion limits the discharge rate.

A series of five experiments with different relaxations were performed in order to determine the optimum relaxation time.The transient voltage change as a function of the square root of the time shows a straight line behaviour during region I, the second part of region II, and region III for each cell except for the shorter relaxation times for cells 5/1 and 5/5, which shows a combination of linear relationship over the time domain from 1 to 100 s and a little tendency at the end of the pulse which can be attributed to the incomplete relaxation of these cells. This linear relationship indicates that the diffusion condition can be achieved during these regions and there is no significant effect of the relaxation time on the linear relationship, except for cells 5/1 and 5/5 during region III.

On the other hand, the 1st part of region II and region IV exhibits some distortion from the linearity. This means that this distortion can only take place within a one-phase reaction, which involves a fast decrease in the voltage. It is unclear why this happened during the 1st part of region II, but during region IV it might have occurred due to blocking the diffusion path, which resulted from the deposition of insoluble products on the cathode surface.

At the shorter relaxation times for cells 5/1, 5/5 and 5/10, the relaxation time was insufficient to allow the cell voltage to reach its steady-state value. For long relaxations, the cells suffer from self-discharge which is directly associated with the shuttle reaction that was initiated in an early stage of the discharge. The self-discharge was shown only during the first pulse of cell 5/20, and then it disappeared, while for cell 5/60, the self-discharge was observed during region I and the first part of region II, and is responsible

for shortening the length of region I in this cell. After that, the cell shows a good relaxation curve with a monotonic behaviour for the rest of the discharge process.

In addition, the transient voltage change as a function of the square root of the time during the charge shows straight line behaviour during the whole charge curve for cells with a long relaxation time. Also, cells with short relaxation times show a good linear relationship during the charge curve, except in region V which shows a distortion from the linearity and this might be due to the incomplete relaxation of these cells.

Moreover, the GITT analyses during the second discharge of cell 5/60 show almost the same transient voltage behaviour as a function of the square root of the time, which was observed during the first discharge. The main and significant difference was that the self-discharge observed in the first discharge, was suppressed in the second discharge. The monotonic increase in the voltage indicates that the self-discharge was prevented during region I, and this may be attributed to the generation of an efficient SEI layer on the Li anode surface.

Although, the self-discharge that cell 5/60 underwent during the early stages of the first discharge, it shows a better relaxation time which can get closer to the equilibrium potential with a monotonic increase in the voltage that is required to accomplish the GITT requirement. Therefore, suppressing the shuttle mechanism is very important to obtain an optimum relaxation time with the monotonic curve, which is required in order to get closer to a true potential equilibrium.

6.8 References

(1) Markevich, E.; Levi, M. D.; Aurbach, D. *J. Electroanal. Chem.* **2005**, *580*, 231–237.

(2) Weppner, W.; Huggins, R. A. *J. Electrochem. Soc.* **1977**, *124*, 1569–1578.

(3) Mennola, T.; Mikkola, M.; Noponen, M.; Hottinen, T.; Lund, P. *J. Power Sources* **2002**, *112*, 261–272.

(4) Gellings, P. J.; Bouwmeester, H. J. M. *The CRC Handbook of Solid State Electrochemistry*; 1997.

(5) Yuan, X.; Ma, Z.-F.; Nuli, Y.; Xu, N. *J. Alloys Compd.* **2004**, *385*, 90–95.

(6) Zhang, S. S. *Electrochim. Acta* **2012**, *70*, 344–348.

(7) Zhang, S. S.; Tran, D. T. *J. Power Sources* **2012**, *211*, 169–172.

(8) Kolosnitsyn, V. S.; Kuzmina, E. V.; Mochalov, S. E. *J. Power Sources* **2013**, *252*, 28–34.

(9) Park, J.-W.; Yamauchi, K.; Takashima, E.; Tachikawa, N.; Ueno, K.; Dokko, K.; Watanabe, M. *J. Phys. Chem. C* **2013**, *117*, 4431–4440.

(10) Guo, J.; Xu, Y.; Wang, C. *Nano Lett.* **2011**, *11*, 4288–94.

(11) Mikhaylik, Y. V.; Akridge, J. R. *J. Electrochem. Soc.* **2004**, *151*, A1969.

(12) Barghamadi, M.; Kapoor, a.; Wen, C. *J. Electrochem. Soc.* **2013**, *160*, A1256–A1263.

(13) Cheon, S.-E.; Ko, K.-S.; Cho, J.-H.; Kim, S.-W.; Chin, E.-Y.; Kim, H.-T. *J. Electrochem. Soc.* **2003**, *150*, A800.

(14) Cheon, S.-E.; Ko, K.-S.; Cho, J.-H.; Kim, S.-W.; Chin, E.-Y.; Kim, H.-T. *J. Electrochem. Soc.* **2003**, *150*, A796.

(15) Akridge, J.; Mikhaylik, Y.; White, N. *Solid State Ionics* **2004**, *175*, 243–245.

(16) Ryu, H.-S.; Ahn, H.-J.; Kim, K.-W.; Ahn, J.-H.; Lee, J.-Y. *J. Power Sources* **2006**, *153*, 360–364.

(17) Barchasz, C.; Molton, F.; Duboc, C.; Leprêtre, J.-C.; Patoux, S.; Alloin, F. *Anal. Chem.* **2012**, *84*, 3973–80.

Chapter 7:

Electrochemical performance of Li/S cells using lithium ion conducting glass ceramic separator

7.1 Introduction

A great deal of effort is devoted to alleviating capacity fading which is directly related to the shuttle reaction of polysulfide species in Li/S batteries. Various porous compounds and conductive polymers have been studied to reduce the shuttle reaction through confining polysulfides at the cathode by physical or chemical absorption[1–6] Moreover, various inorganic additives, such as lithium nitrate ($LiNO_3$)[7] and phosphorous pentasulfide (P_2S_5)[8] have been investigated as an electrolyte additives to reduce the polysulfide shuttle by forming a passivation layer on the surface of the Li electrode.

Nevertheless, as long as there are any polysulfides dissolving in the electrolytes, it is reported that no known absorption strategies can perfectly eliminate the migration of polysulfides from the positive electrode.[8] Also, it is considered that an unstable and irregular passivation layer formed on the lithium anode by electrolyte additives cannot completely stop the reaction with polysulfides.[9]

Another approach to suppressing the shuttle reaction is by using a solid electrolyte instead of liquid electrolyte. Various kinds of solid electrolytes such as glass-ceramic electrolytes[10–12] have been proposed as barriers between the sulfur and lithium electrodes, and could effectively eliminate the problem of polysulfides shuttling. In spite of the considerable attempts devoted to mitigate the polysulfide shuttle between the cathode and the anode, it remains a significant challenge to the building of highly stable lithium/sulfur batteries.[13]

In order to achieve better information about the electrochemical reactions that take place inside the Li/S cell, a lithium ion conducting glass ceramic (LICGC) separator (Li_2O-Al_2O_3-SiO_2-P_2O_5-TiO_2-GeO_2) was used in this study. The LICGC separator serves to protect the Li anode through blocking the chemical reaction path with sulfur and polysulfides that diffuse from the cathode.[14]

7.2 Experimental details

The sulfur/acetylene black (1:3) composite was synthesized as described in Chapter 3, using the ball milling method, and sulfur loading in each electrode was about 1.7 mg/cm^2. Galvanostatic discharge/charge measurements were carried out using a constant current density of 168 mA g^{-1} (0.1 C) in the potential range of 1.5 to 2.8 V. EIS measurements were carried out using the frequency range between 200 kHz and 100 mHz. The GITT was carried out for the Li/S cells as described in Chapter 6, by applying the current at a C rate of 0.1 h^{-1} for 5 min. followed by open circuit relaxation for 60 min. Electrochemical measurements were performed using MPG (BioLogic Science Instruments) at 25 °C, and using 1M LiTFSI dissolved in a (1:1) mixture of TEGDME and DOL as an electrolyte.

The typical cell used for the Li/S battery test was slightly modified in order to test the cell with an LICGC separator (150 µm thickness, Ohara, Japan), as shown in Figure 7.1. The cell was assembled using 15 mm of S/AB composite as the cathode and 18 mm of lithium metal as the anode, separated by 25.4 mm of LICGC separator sandwiched between two glass fibre separators, each one soaked with 0.175 ml of electrolyte. Since the LICGC separator is not stable against Li,[14] it was separated from the Li with a glass fibre (GF) separator. The cell was sealed by screwing down the lid on the cell. The spring below the current collector piston ensures good contact between the electrodes and the electrolyte, while the Viton ring on the piston ensures there is no leakage of the electrolyte between the electrodes by keeping the electrolyte confined in the cathode side.

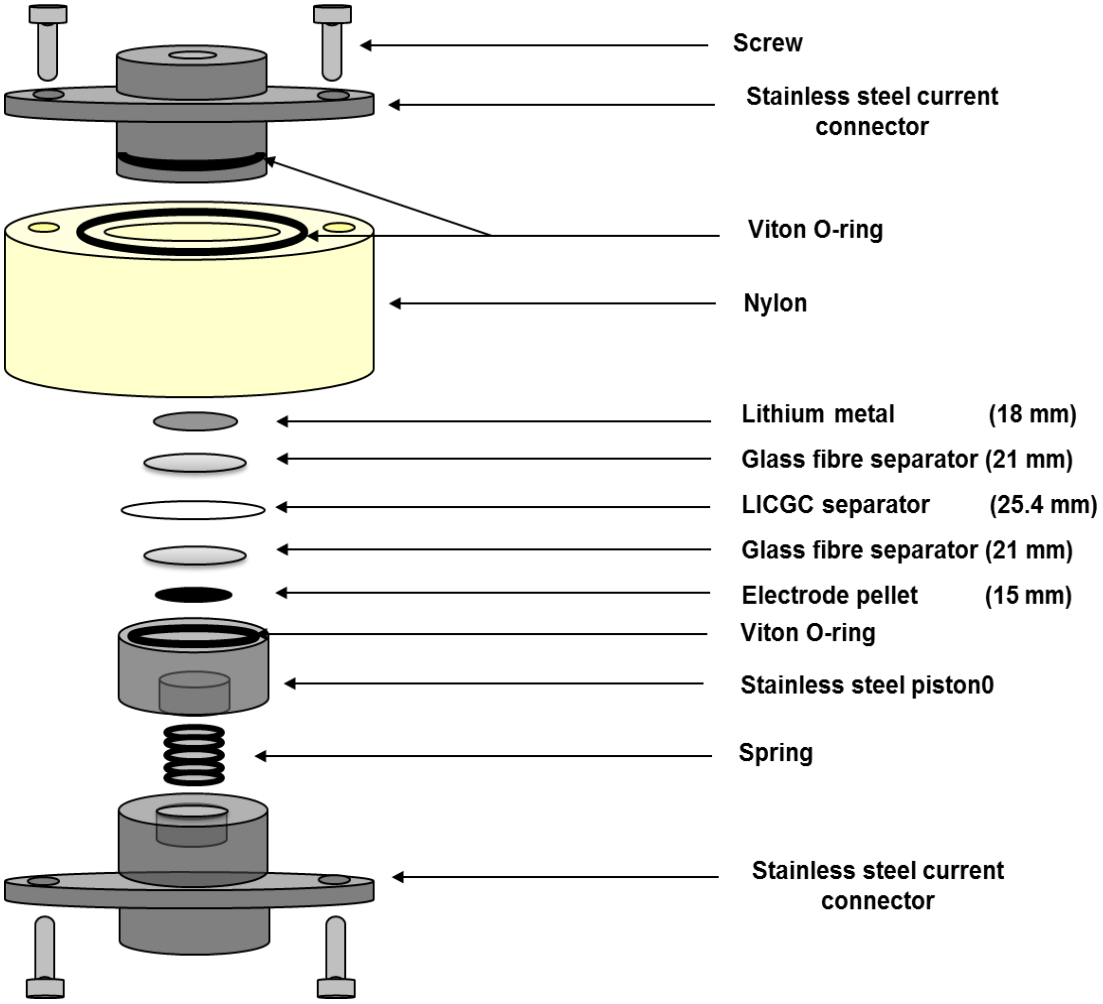

Figure 7.1 Modified cell for testing of Li/S battery materials with an LICGC separator (showing diameters).

7.3 Open circuit voltage comparison for Li/S cells with/without an LICGC separator

The open circuit voltages of Li/S cells using 1 M LiTFSI in TEGDME/DOL (1:1), and containing two GF with LICGC separators (red line), and two GF separators (black line), between the sulfur and lithium electrodes are shown in Figure 7.2.

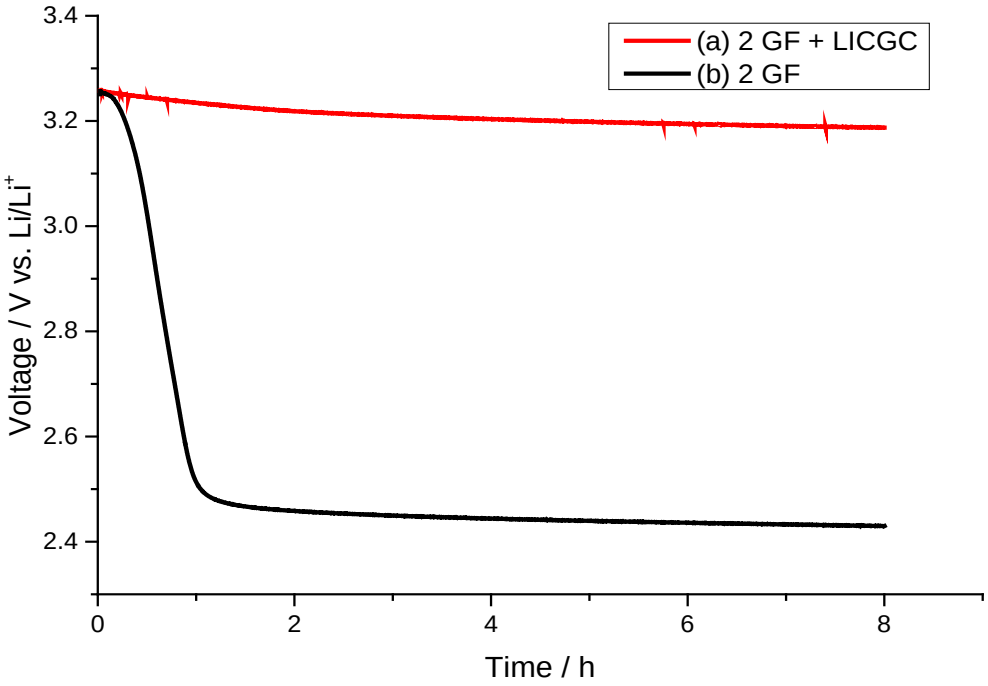

Figure 7.2 The open circuit voltages of Li/S cells using 1 M of LiTFSI in TEGDME/DOL (1:1), and containing (a) 2 GF + LICGC separators (red line), and (b) 2 GF separators (black line).

It can clearly be seen that the OCV for each cell is about 3.26 V. A fast decrease in the voltage was observed for the normal cell with only GF separators which reached 2.5 V in 1 h. This decrease in the voltage was attributed to the self-discharge resulting from sulfur and polysulfides diffusion between the cathode and the anode, as explained in Chapter 5. After that, the voltage was slightly decreased to 2.43 V after 8 h. On the other hand, the cell containing the LICGC separator shows a more stable voltage, with a non-significant decrease in the voltage from its initial value of 3.26 V to about 3.19 V after 8 h. The slight voltage difference of about 0.07 V is negligible in comparison to 0.83 V for the normal cell with only GF separators. This indicates that the diffusion of sulfur and polysulfide species from one electrode to the other was prevented, and the self-discharge was suppressed using the LICGC separator.

7.4 Effect of the LICGC separator on the capacity of Li/S cells

The S/AB electrodes were galvanostatically discharged and charged between 1.5 V and 2.8 V vs. Li/Li^+ at the current density of 167.2 $mA.g^{-1}$ (C rate of 0.1 h^{-1}), using 1M of LiTFSI in TEGDME/DOL (1:1) as an electrolyte, using two GF with LICGC separators (red line), and two GF separators (black line), as shown in Figure 7.3.

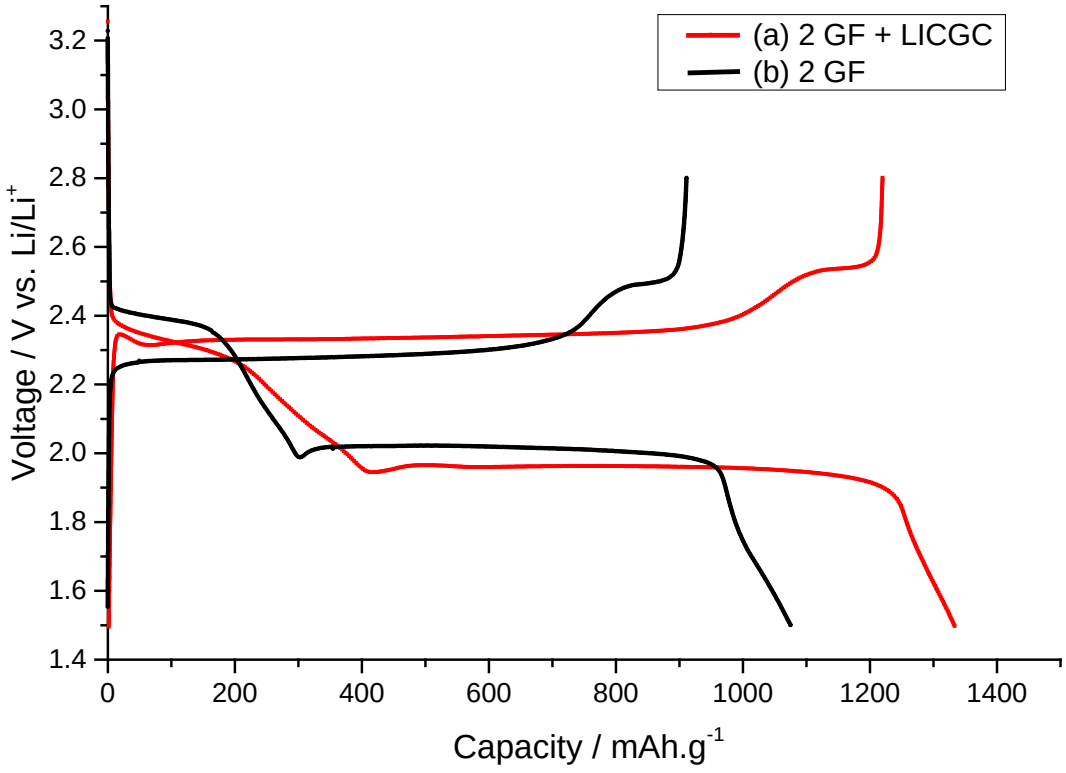

Figure 7.3 Discharge/charge profiles of Li/S cells using 1 M of LiTFSI in TEGDME/DOL (1:1), and containing (a) 2 GF + LICGC separators (red line), and (b) 2 GF separators (black line). The C rate was 0.1 h^{-1}, corresponding to a current density of about 167.2 $mA.g^{-1}$.

Two discharge plateaus are clearly shown for each cell, which are similar to those reported earlier,[15,16] corresponding to the two stages of elemental sulfur reduction first to the soluble lithium polysulfides and then to the lithium sulfide. Also, it shows two charge plateaus corresponding to the reverse reaction of lithium sulfide to sulfur.

The voltage decrease during region I (first plateau) in the discharge profile for the cell containing the LICGC separator is steeper than that which uses only the GF separator. Also, the discharge capacity obtained during region I in the normal cell is about 180 $mAh.g^{-1}$ of S, which is less than that obtained by the one using the LICGC separator at approximately 200 $mAh.g^{-1}$ of S. This decrease in the discharge capacity for the normal cell is directly correlated to the self-discharge resulting from the polysulfide shuttle (see Chapter 5).

Moreover, a gradual decrease in the voltage was observed during region II in the discharge profile for the cell with an LICGC separator, while the voltage decrease during region II in the normal cell without an LICGC separator shows a steeper decrease in the voltage with a lower discharge capacity. Again, this can be attributed to the polysulfide shuttle between the positive and negative electrodes.

The overall discharge capacity of the normal cell that uses only two GF separators is about 1075 $mAh.g^{-1}$ (64% of the theoretical capacity based on the complete reduction of sulfur to Li_2S). On the other hand, the cell with the LICGC separator produces a higher discharge capacity than the normal cell, about 1340 $mAh.g^{-1}$ (80% of the theoretical capacity), which is about 25% higher than that delivered by the normal cell. This clearly shows that using an LICGC separator in the Li/S cell would give a beneficial effect for confining the soluble lithium polysulfide species, thus it can prevent the diffusion of sulfur and lithium polysulfide species away from the cathode to the anode, resulting in the enhancement of the capacity and a better use of sulfur as an active material. In addition, the polysulfide shuttle effect in the normal cell was also observed during the charge, where it shows a lower charge capacity than that using an LICGC separator.

Although an LICGC separator would enhance the capacity of the Li/S cell by suppressing the shuttle reaction, the cell is still far from reaching the theoretical capacity (1672 $mAh.g^{-1}$ of S). This result could be attributed to the deposition of solid products Li_2S_2 and Li_2S generated during regions III and IV on the cathode surface, which would block further reduction of lithium polysulfides, and thus accelerate the end of the discharge.

One of the effects of the LICGC separator on the discharge profiles of the Li/S cells is the impact on the IR drop. The IR drop on the cell using the LICGC separator is higher than that for the discharge profiles of the normal cell without an LICGC separator when exposed to the same discharge current. A higher resistance resulting from the LICGC separator leads to a lower cell voltage.

EIS spectroscopy is a valuable tool for comparing the resistance of the cell containing the LICGC separator with the normal cell that uses only GF separators. Figure 7.4 displays the Nyquist plots of Li/S cells containing (a) 2 GF with LICGC separators (red line), and (b) 2 GF separators (black line). The x-axis intercept at high frequency shows the uncompensated resistance (R_u) of the cell with the LICGC separator at about 42 Ω, which is higher than that without the LICGC separator at about 10 Ω, as would be expected. The difference between the two intercepts is interpreted as the additional resistance of the LICGC. The semicircles in each case signify the parallel combination of R_{ct} and C_{dl}. The additional resistance in R_{ct} when using LICGC has not increased significantly using LICGC separator. In both cases the sloped line illustrates the Warburg impedances signifying mass transfer resistance. It may be noted that for the LICGC separator there is a small additional resistance between the extrapolation of the Warburg and the second semicircle.

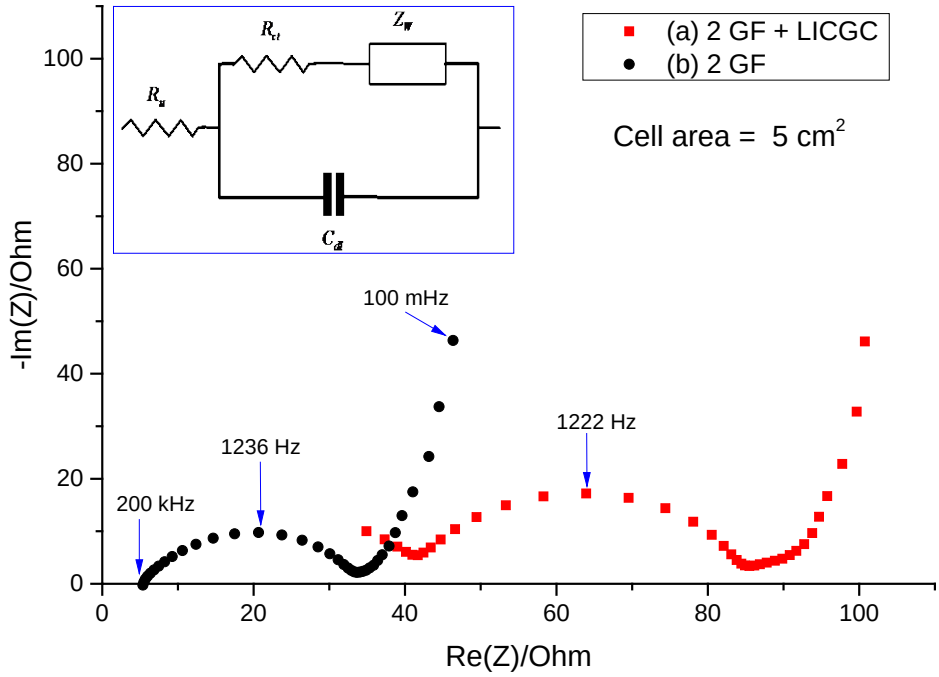

Figure 7.4 Nyquist plots of Li/S cells containing (a) 2 GF + LICGC separators (red line), and (b) 2 GF separators (black line) in the frequency range of 100 mHz – 200 kHz, using 1M of LiTFSI in TEGDME/DOL (1:1) electrolyte.

7.5 GITT analysis for Li/S cells with/without an LICGC separator

The main problem with the GITT measurements on Li/S cells is the distortion of the GITT results that sometimes occurs at long relaxation times, presumably due to the shuttle reaction (see Chapter 6). This results in a non-monotonic voltage variation which obscures observation of the approach to equilibrium. In order to achieve better information about the electrochemical behaviour of the Li/S system, GITT experiments were carried out using an LICGC separator. The LICGC separator is very important for eliminating the shuttle reaction, which is required to get closer to a true equilibrium potential.

Because using an LICGC separator would increase the IR drop due to its resistance, the cell with the LICGC separator was discharged/charged using a higher voltage range, i.e. between 1 – 3.2 V. The GITT profile for the discharge of Li/S cell with an LICGC separator were divided into four regions, as shown in Figure 7.5. These regions were selected depending on the change in the voltage behaviour at different states of the cell discharge.

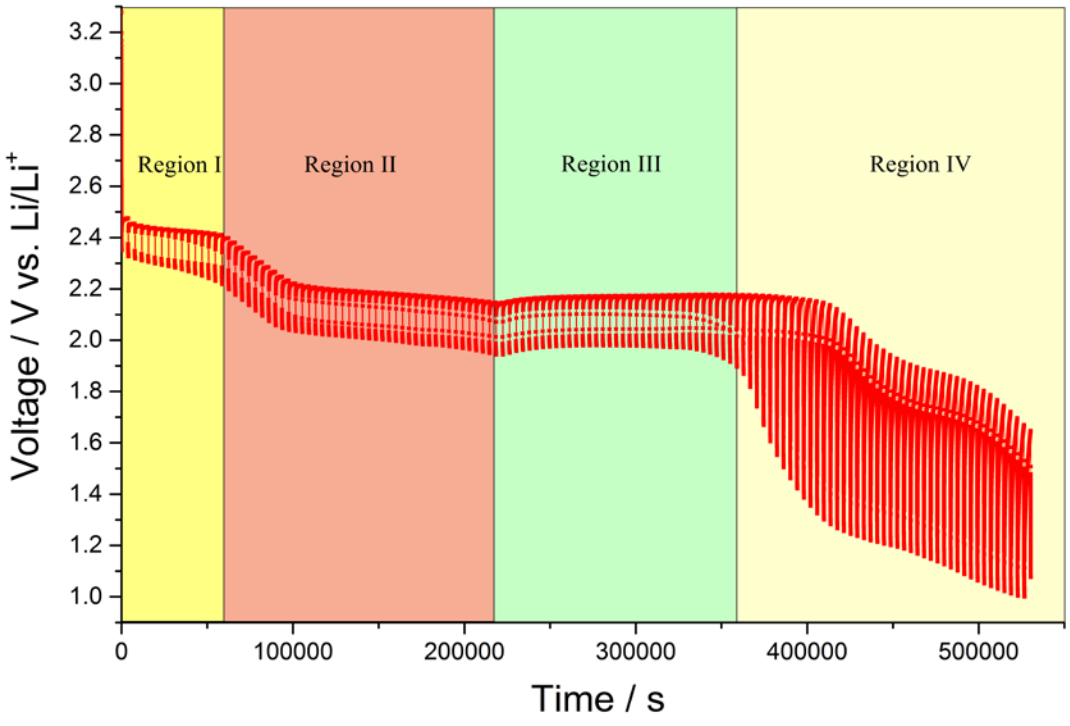

Figure 7.5 GITT profile for first discharge of Li/S cell with LICGC separator, measured at 0.1 h^{-1} C rate, and using a 5 min pulse followed by a 60 min relaxation.

7.5.1 The potential response during the GITT for the first discharge

The GITT profiles during the first discharge of Li/S cells containing (a) 2 GF with LICGC separators (red line), and (b) 2 GF separators (black line), and using 1M LiTFSI in TEGDME/DOL (1:1) measured at a C rate of 0.1 h^{-1}, are displayed in Figure 7.6. These measurements were taken while applying the current for 5 min. followed by a potential relaxation step for 60 min.

As in Chapter 6, it can be also observed that the polarization at the high voltage region is smaller than the polarization at the end of the lower voltage region for both cells. This has been attributed to the fast electrode kinetics at the high voltage region, and to the rise of the mass-transport resistance of the electrolyte within the pores of the positive electrode and the slow kinetics of the solid-state reaction at the end of the lower voltage region.[17]

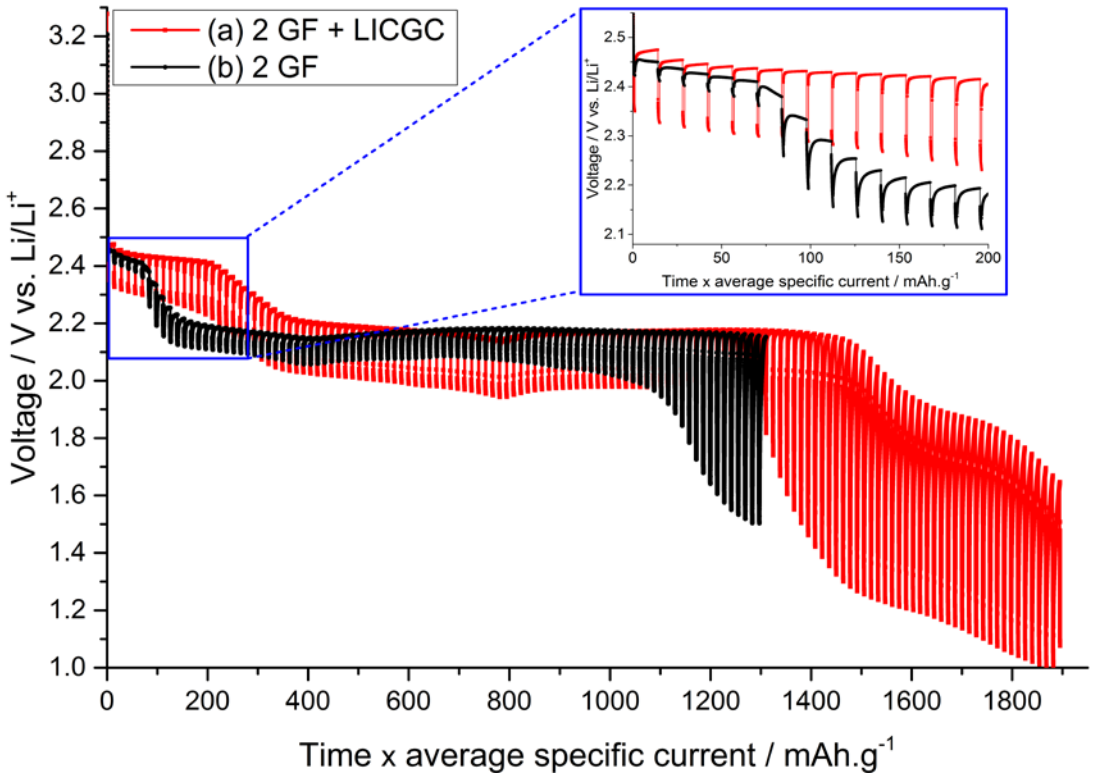

Figure 7.6 GITT profiles during the first discharge of Li/S cells containing (a) 2 GF + LICGC separators (red line), and (b) 2 GF separators (black line). Using 1 M of LiTFSI in TEGDME/DOL (1:1), measured at a C rate of 0.1 h^{-1}, and using a 5 min pulse followed by a 60 min relaxation.

Region I in the GITT profile of the Li/S cell containing the LICGC separator (red line) is longer than that for the cell using only GF separators (black line), as shown in the Figure 7.6 insert. This is probably the result of eliminating of self-discharge due the shuttle reaction which reduced the length of region I in the normal cell (see Chapter 6).

The first part of region II is also lengthened compared with the normal cell. Here, the elimination of the shuttle reaction is shown by more gradual decrease in the voltage within in the GITT profile for the cell with an LICGC separator.

The second part of region II, ending in a plateau in the relaxed potential at about 400 $mAh.g^{-1}$ of S, was attributed to the complete reduction of Li_2S_8 to form Li_2S_4 for the GF separated cell. In case of the cell containing the LICGC separator, the second part of region II ended with a local minimum value at approximately 800 $mAh.g^{-1}$ of S, close to half of the theoretical capacity of 1672 $mAh.g^{-1}$ based on the full conversion of sulfur to Li_2S (equation 7.1) and therefore corresponding to an average positive electrode composition of Li_2S_2 (equation 7.2),

$$S_{8(s)} + 16\,Li^+ + 16\,e^- \rightarrow 8\,Li_2S \qquad (7.1)$$

$$S_{8(s)} + 8\,Li^+ + 8\,e^- \rightarrow 4\,Li_2S_2 \qquad (7.2)$$

Little is known about of Li_2S_2, although it is expected to have a low solubility and has been reported as a solid in many publications. No crystal structure information can be found for Li_2S_2, and it is possible that this is a metastable phase that can disproportionate into Li_2S and another species with a higher sulfur content.

Region III, the second plateau, in the LICGC cell corresponds to Li/S stoichiometries greater than one, where precipitation of Li_2S is most likely. The remainder of the composition may be dissolved polysulphides such as Li_2S_4, possibly mixed with solid Li_2S_2.

During the first discharge of the cell with the membrane, a local minimum may be seen between regions II and III. The origin of this interesting phenomenon is not understood, although it is characteristic of a supersaturation / nucleation process, for example the formation of a non-stoichiometric $Li_{2+x}S_2$ phase followed by nucleation and growth of crystalline Li_2S.

The last part within region IV of the GITT process in the LICGC cell shows a strange behaviour, where a continuous increase in the capacity was observed even after reaching the theoretical capacity of 1672 mAh.g^{-1} of S. The reason for this is not clear but might be regarding to discharging the cell to lower voltage of 1 V compared to 1.5 V for the normal cell. But the majority of this behaviour might be related to some other reactions that could occur at a low voltage discharge, e.g. the electrolyte decomposition.

The IR drop values within the GITT profiles during the first discharge of Li/S cells using two GF with LICGC separators (red), and two GF separators (black), are shown in Figure 7.7. It can be clearly seen that the IR drop for the cell with the LICGC separator is much higher than that for the cell without the LICGC separator. The IR drop for the cell with the LICGC separator is expected to be higher due to its higher resistance, with an initial value of about 115 mV compared to about 22 mV for the cell without LICGC separator. An irregular increase in the IR drop was observed during the GITT process for the cell containing LICGC separator, which is different than that observed for the cell without LICGC separator (see Chapter 6).

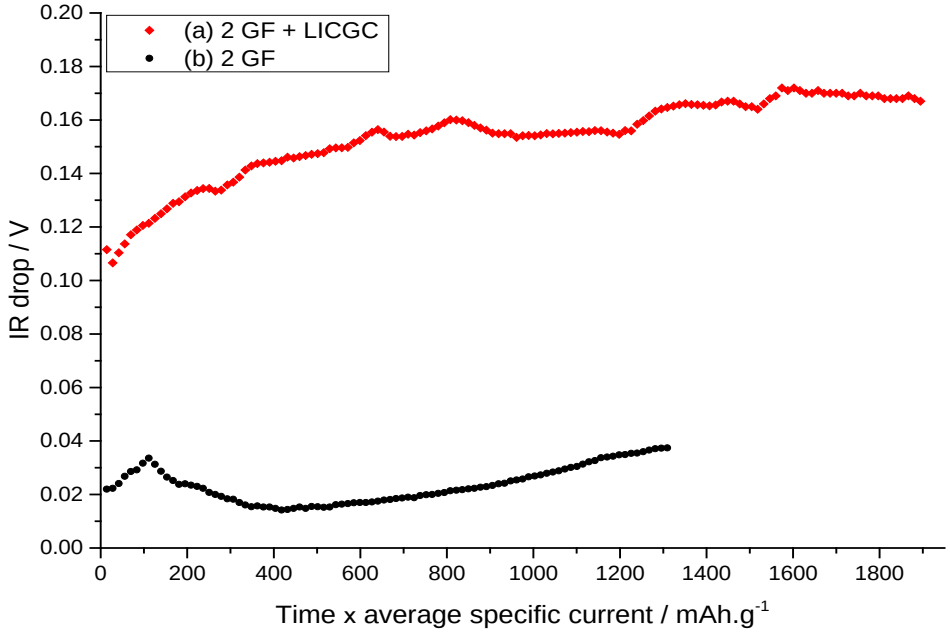

Figure 7.7 IR drop within the GITT profiles during the first discharge of Li/S cells cells containing (a) 2 GF + LICGC separators (red), and (b) 2 GF separators (black).

To explain the variation of the IR drop during the discharge in the two cases above, it may be suggested that this is mainly due to the high viscosity of high order polysulfides which are more prevalent in the case of LICGC separator than for conventional separator, in which polysulfides may be quickly reduced by the shuttle reaction.

7.5.2 Individual pulse responses

In this section the change in potential during the pulse is analysed as a function of the square root of time to check the validity of the GITT expression arising from the assumption of Fick's laws under a constant flux.

7.5.2.1 The potential response during region I

The variation of cell voltage as a function of the square root of the time within region I, during the pulse of a single step of GITT measurements for the Li/S cells using two GF with LICGC separators (red line), and two GF separators (black line), is shown in Figure 7.8. It can be seen that the E vs. $t^{1/2}$ plot gives a relatively straight line over the entire time for each pulse in the cell using the LICGC separator, as well as for the cell using only two GF separators. This indicates that the simple diffusion analysis is valid within region I in the GITT profile.

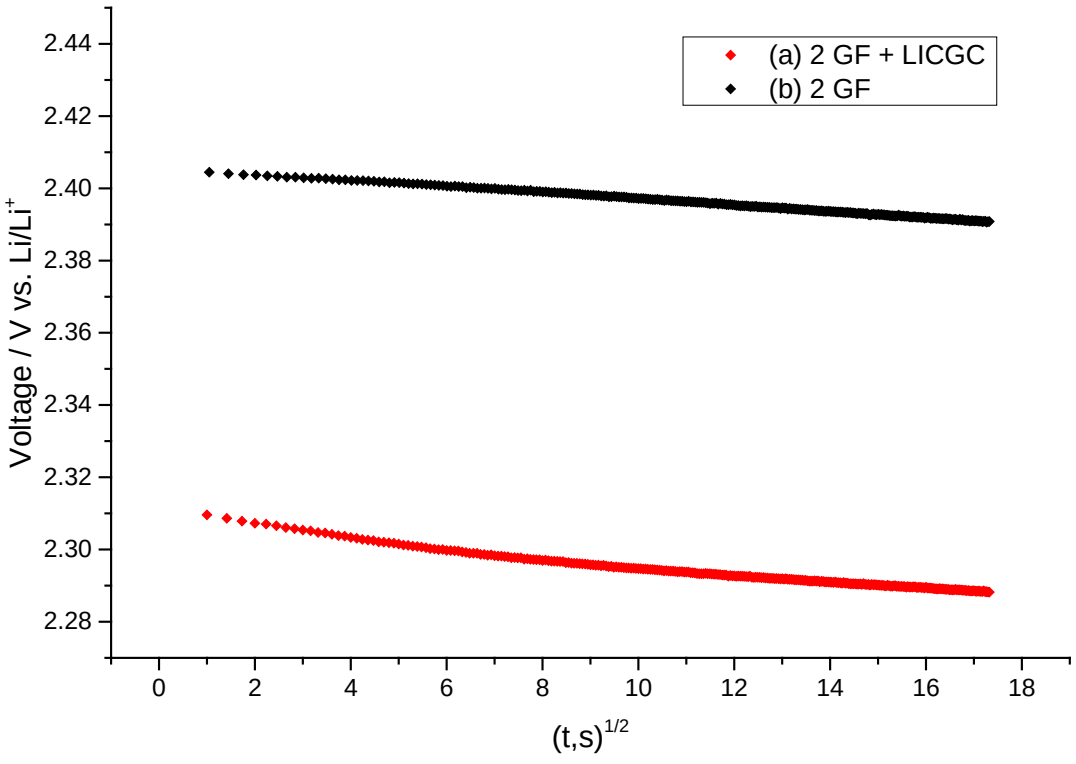

Figure 7.8 The transient voltage changes E vs. t1/2 of region I during the pulse of a single GITT process for Li/S cells containing (a) 2 GF + LICGC separators (red line), and (b) 2 GF separators (black line).

Figure 7.9 represents the variation of cell voltage as a function of the time for region I, during the relaxation of a single step of GITT measurements for the Li/S cells using two GF with LICGC separators (red line), and two GF separators (black line). In order to achieve a more detailed overview, the values of the times are normalized and the values of the voltages are corrected by IR drop.

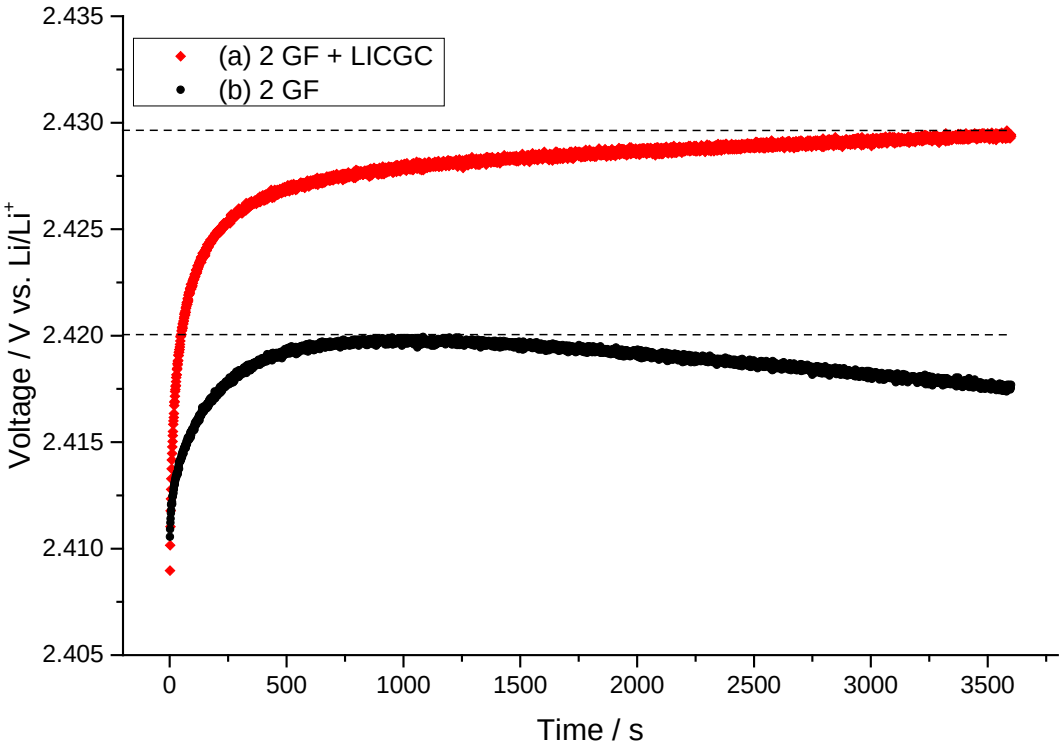

Figure 7.9 Voltage-time response of region I during the relaxation of a single GITT process for the Li/S cells containing (a) 2 GF + LICGC separators (red line), and (b) 2 GF separators (black line). Note: the values of the times are normalized and the values of the voltages are corrected by IR drop.

The most significant observation of the voltage behaviour during the relaxation is the voltage decline that occurs in the normal cell that uses only GF separators, as shown in Figure 7.9 (black line). The voltage decline which is attributed to the shuttle reaction between the sulfur and lithium electrodes makes it difficult to achieve an equilibrium potential in the normal cell. In contrast, this voltage decline has disappeared in the cell containing the LICGC separator, and a monotonic increase in the voltage was observed within this region which can get closer to a better equilibrium potential. This indicates that using the LICGC separator prevents the shuttle reaction effectively. Therefore, no self-discharge would be present in the Li/S cells that use the LICGC separator.

7.5.2.2 The potential response during region II

Two voltage behaviours were observed during the GITT process within region II. The first part involves a fast decline in the voltage, where the linear relationship of the voltage with $t^{1/2}$ was distorted for the cell without an LICGC separator (see Chapter 6); however, the cell with the LICGC separator shows a straight line over the entire time for each pulse, as shown in Figure 7.10, which indicates that this part of region II is following the diffusion condition for the cell with the LICGC separator.

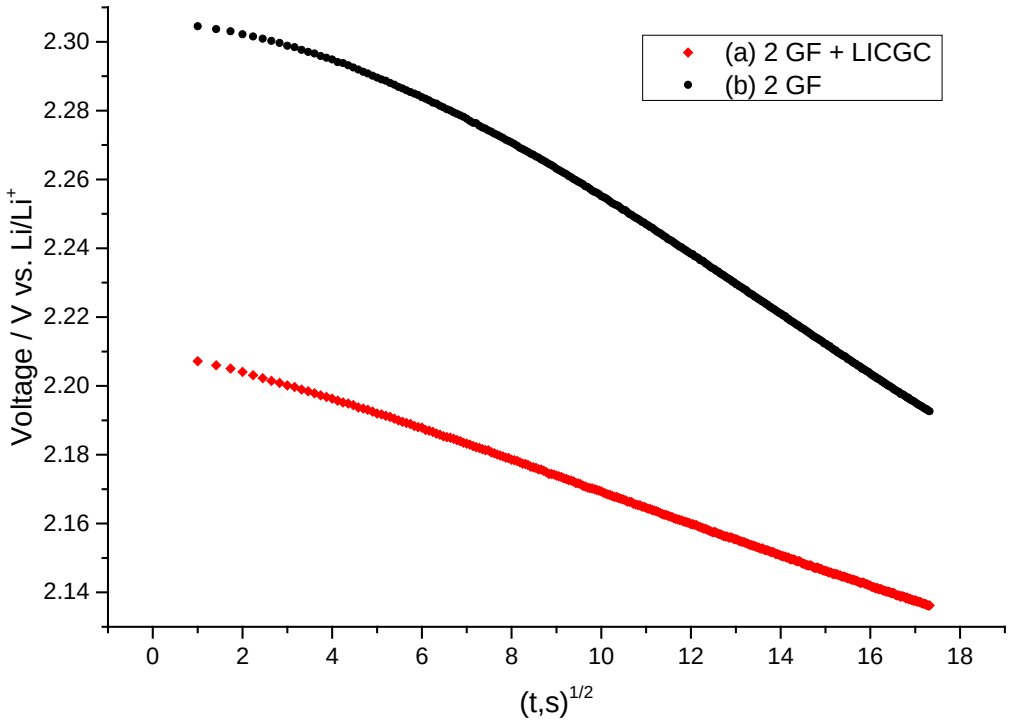

Figure 7.10 The transient voltage changes E vs. $t^{1/2}$ of the 1st part of region II during the pulse of a single GITT process for Li/S cells containing (a) 2 GF + LICGC separators (red line), and (b) 2 GF separators (black line).

Figure 7.11 displays the voltage changes for the first part of region II during the relaxation of a single step of the GITT measurements for the Li/S cells using two GF with LICGC separators (red line), and two GF separators (black line). It shows a voltage decrease during the relaxation time resulted from the self-discharge of the cell using only GF separators. On the other hand, a monotonic increase in the voltage with the time was observed during this part of region II for the cell with the LICGC separator, as shown in Figure 7.11 (red line), which also indicates suppressing the shuttle reaction using the LICGC separator.

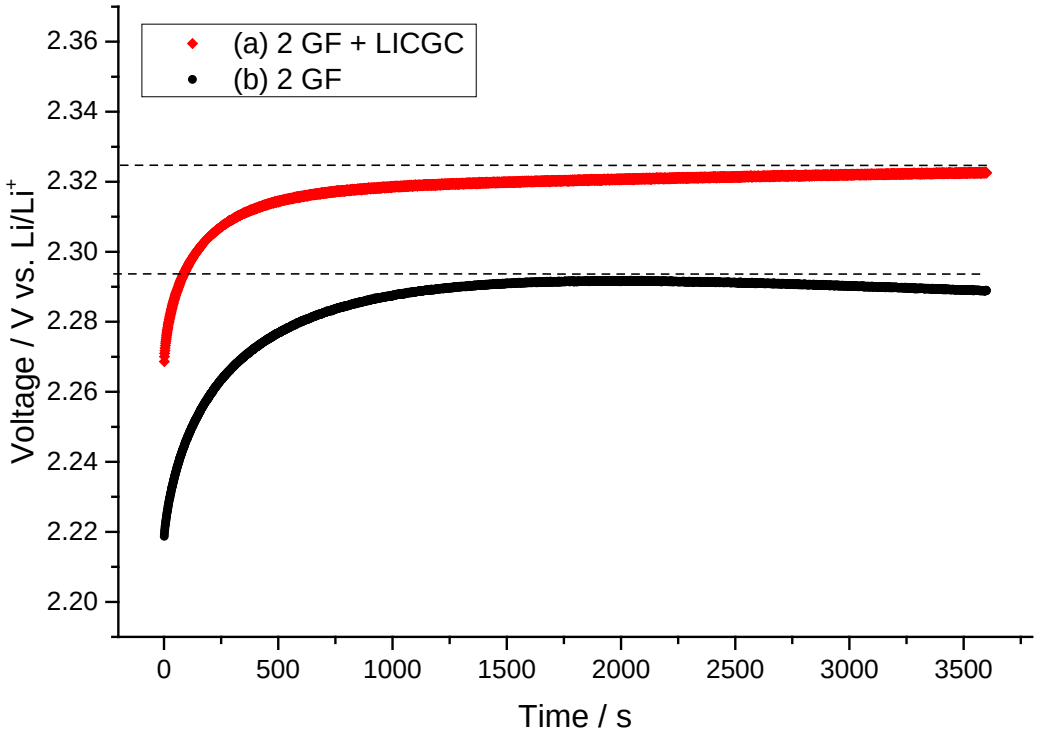

Figure 7.11 Voltage-time response of the 1st part of region II during the relaxation of a single GITT process for the Li/S cells containing (a) 2 GF + LICGC separators (red line), and (b) 2 GF separators (black line). Note: the values of the times are normalized and the values of the voltages are corrected by IR drop.

The second step of region II exhibits a slower decrease in the voltage. The variation of cell voltage as a function of the square root of the time for the second part of region II, during the pulse of a single step of the GITT measurements for the Li/S cells using two GF with LICGC separators (red line), and two GF separators (black line), is shown in Figure 7.12. A linear relationship of the voltage with $t^{1/2}$ was observed for each cell and the potential does follow the $t^{1/2}$ profile well.

Moreover, no voltage decline during the relaxation time was observed during the relaxation time within the second part of region II, as shown in Figure 7.13. Each cell with and without an LICGC separator shows a monotonic increase in the voltage with the time, which could reach a better equilibrium potential. This indicates that there is no more self-discharge to be found during this part of region II, even for the cell with only GF separators. This may occur as a result of the formation of the SEI layer on the surface of the lithium electrode, as described in Chapter 6.

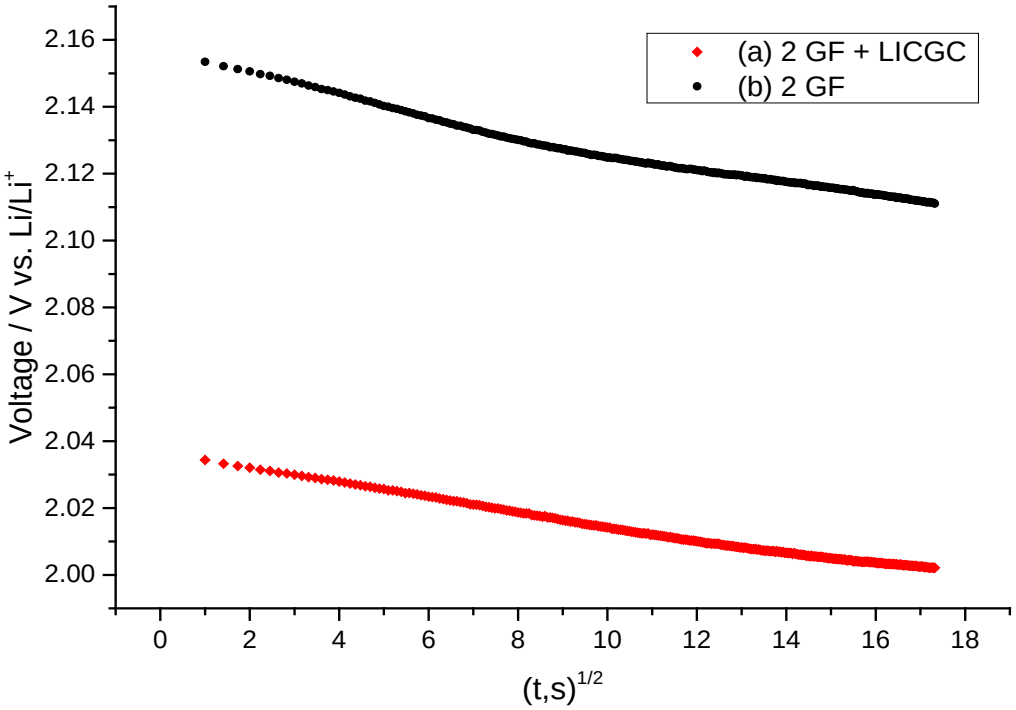

Figure 7.12 The transient voltage changes E vs. $t^{1/2}$ of the 2nd part of region II during the pulse of a single GITT process for Li/S cells containing (a) 2 GF + LICGC separators (red line), and (b) 2 GF separators (black line).

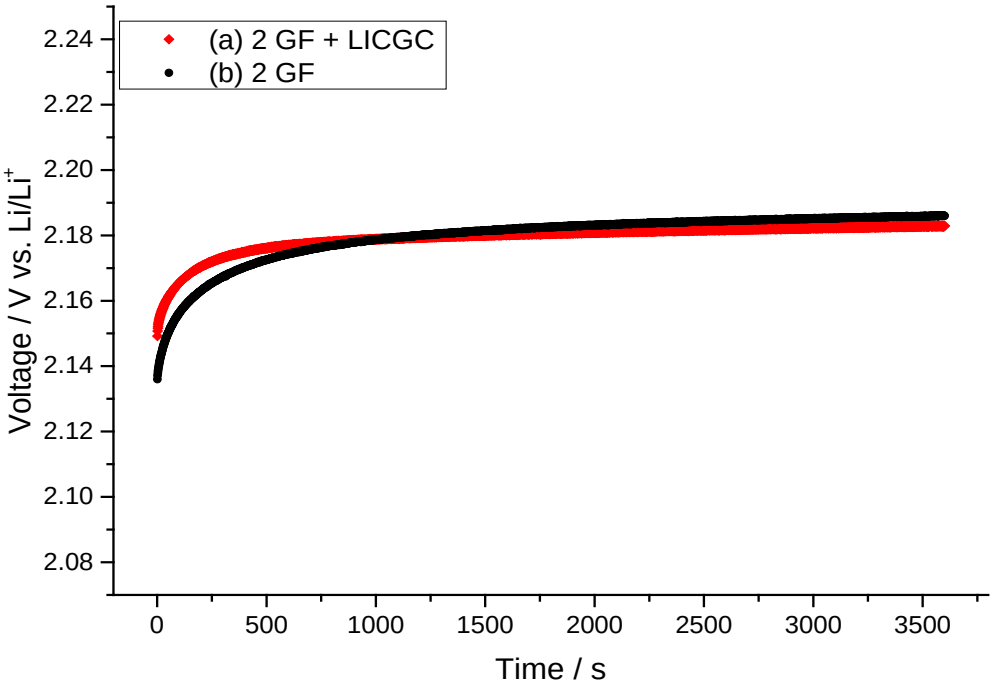

Figure 7.13 Voltage-time response of the 2nd part of region II during the relaxation of a single GITT process for the Li/S cells containing (a) 2 GF + LICGC separators (red line), and (b) 2 GF separators (black line). Note: the values of the times are normalized and the values of the voltages are corrected by IR drop.

7.5.2.3 The potential response during region III

Two voltage behaviours were also observed in region III: a slow increase in the voltage in the first part followed by a slow decrease in the voltage in the second part within this region. The variation of cell voltage as a function of the square root of the time for the first part of region III, during the pulse of a single step of the GITT measurements for the Li/S cells using two GF with LICGC separators (red line), and two GF separators (black line), is shown in Figure 7.14. It can be seen that the E vs. $t^{1/2}$ plot for each cell with and without the LICGC separator gives a straight line over the entire time of each pulse. This linear relationship is also observed during the transient voltage changes for the second part of region III (Figure 7.15). This indicates that the diffusion conditions can be achieved within region III.

In addition, a monotonic increase in the voltage with the time was also observed during the first and second parts of region III for each cell, as shown in Figures 7.16 and 7.17, respectively.

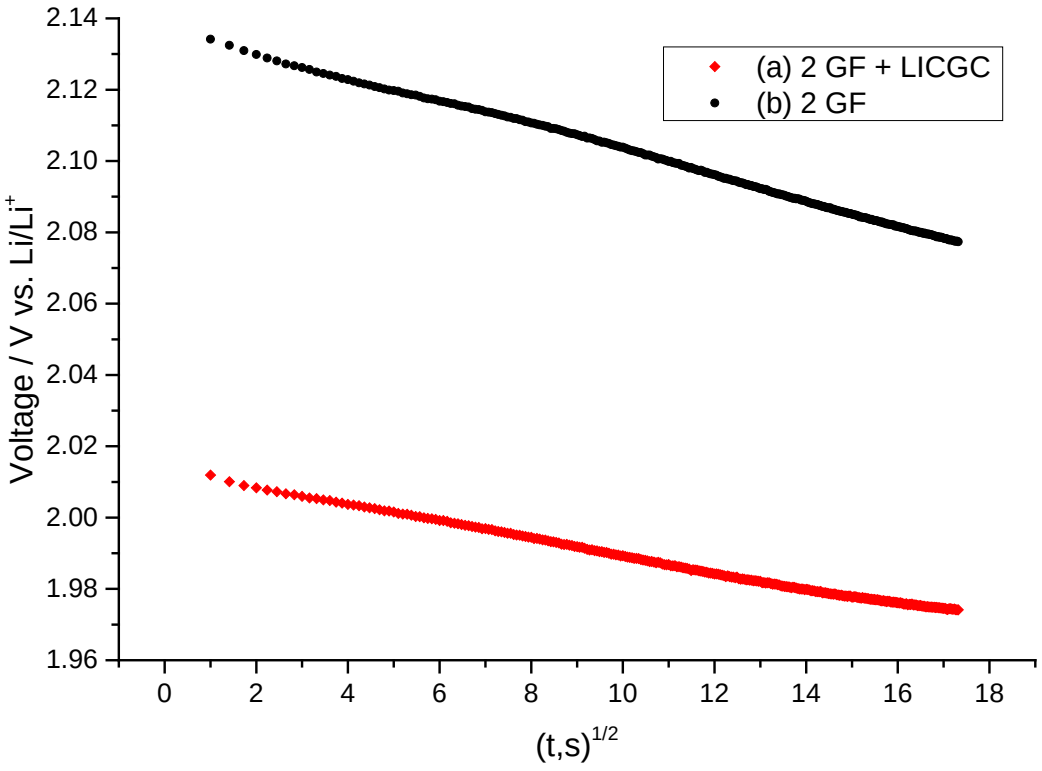

Figure 7.14 The transient voltage changes E vs. $t^{1/2}$ of the 1st part of region III during the pulse of a single GITT process for Li/S cells containing (a) 2 GF + LICGC separators (red line), and (b) 2 GF separators (black line).

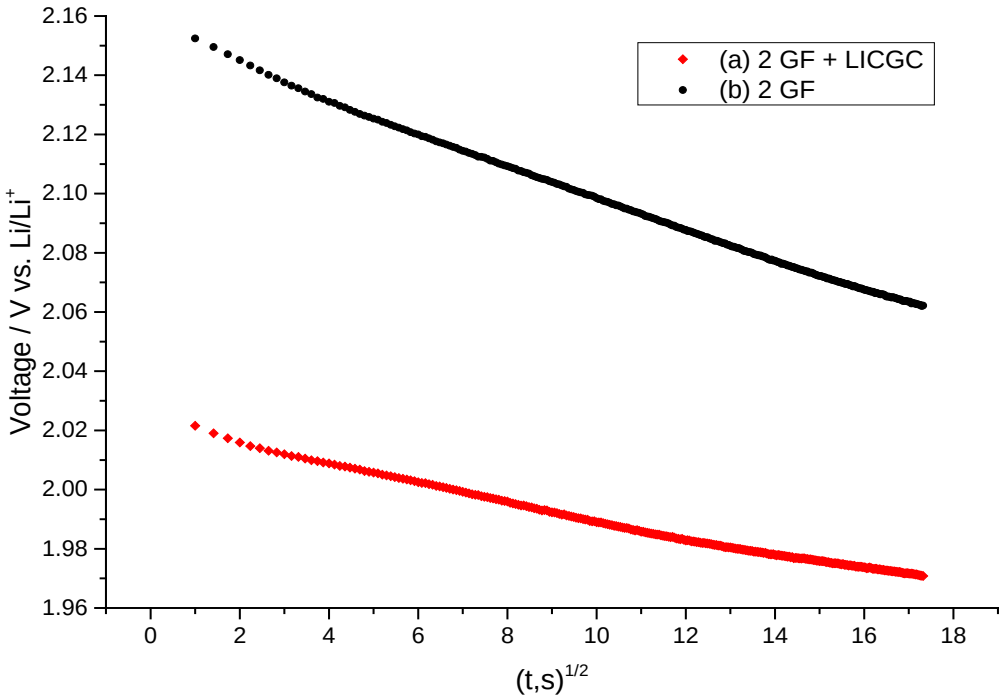

Figure 7.15 The transient voltage changes E vs. $t^{1/2}$ of the 2nd part of region III during the pulse of a single GITT process for Li/S cells containing (a) 2 GF + LICGC separators (red line), and (b) 2 GF separators (black line).

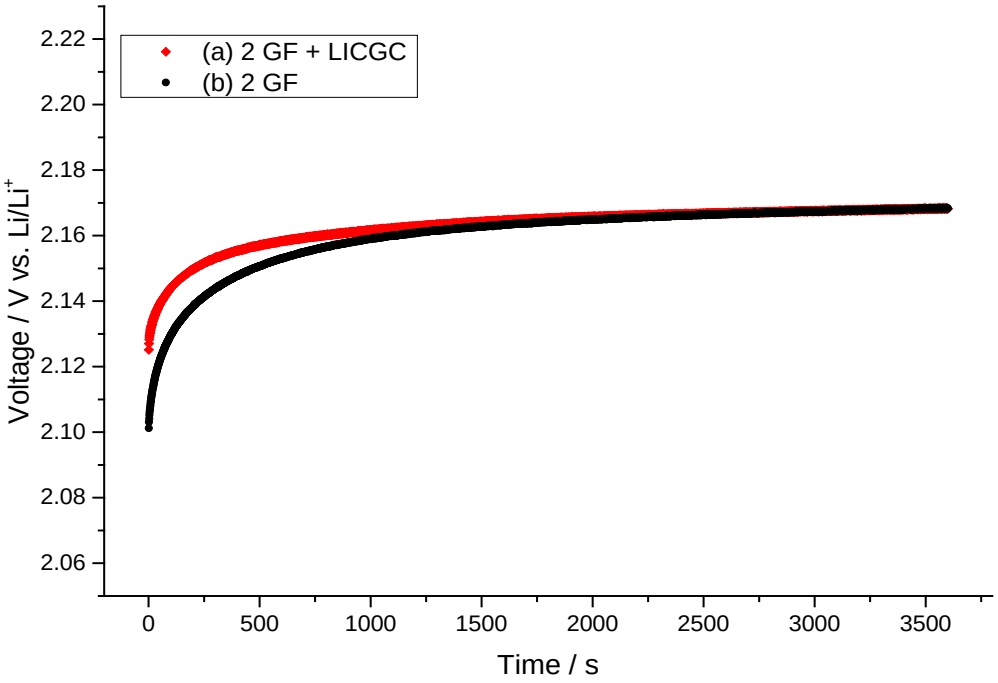

Figure 7.16 Voltage-time response of the 1st part of region III during the relaxation of a single GITT process for the Li/S cells containing (a) 2 GF + LICGC separators (red line), and (b) 2 GF separators (black line). Note: the values of the times are normalized and the values of the voltages are corrected by IR drop.

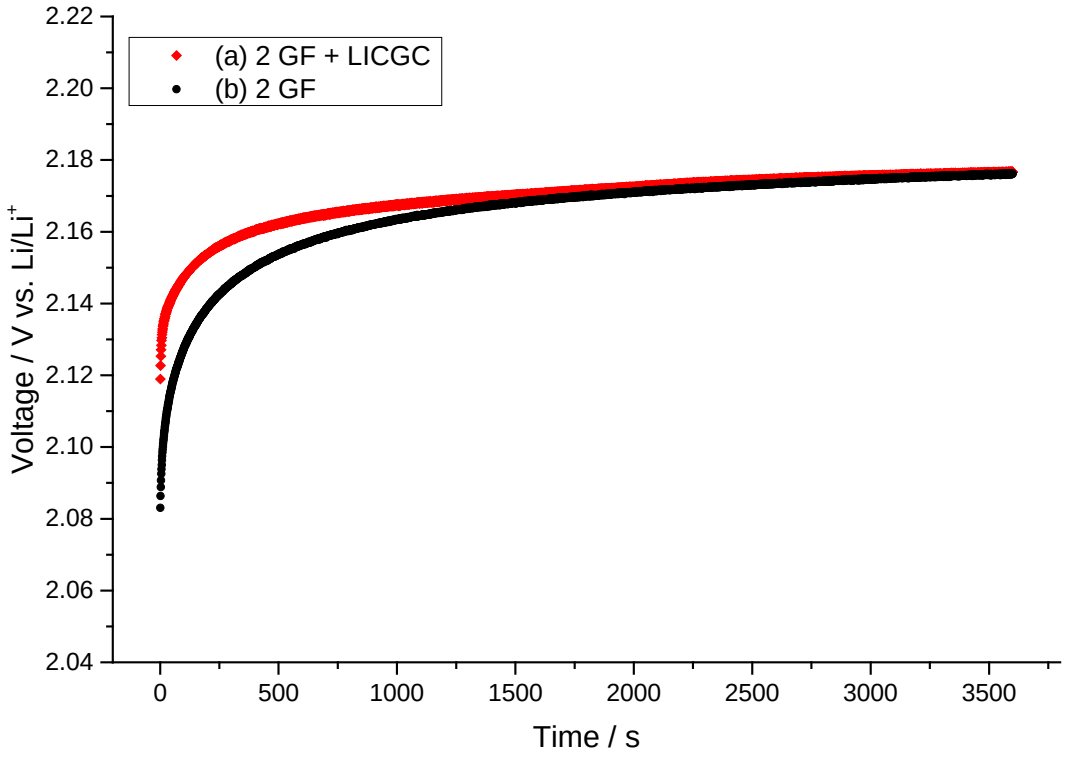

Figure 7.17 Voltage-time response of the 2nd part of region III during the relaxation of a single GITT process for the Li/S cells containing (a) 2 GF + LICGC separators (red line), and (b) 2 GF separators (black line). Note: the values of the times are normalized and the values of the voltages are corrected by IR drop.

7.5.2.4 The potential response during region IV

Region IV in the discharge profile referred to the final reduction stage, which exhibits a fast decrease in the voltage. Figure 7.18 represents the variation of cell voltage as a function of the square root of the time within region IV, during the pulse of a single step of the GITT measurements for the Li/S cells using two GF with LICGC separators (red line), and two GF separators (black line). It can be seen that there is a distortion of the voltage transient from the linearity for each cell. This distortion might be occurring as a result of the electrode composition, which involves the generation of a large amount of solid products within this region, which might be deposited on the positive electrode surface and block the diffusion path.

During the relaxation, each cell shows monotonic voltage behaviour where there is a combination of a fast increase in the voltage over the time domain from 1 to 100 s for each relaxation, and a slow increase in the voltage for the rest of the relaxation, as shown in Figure 7.19.

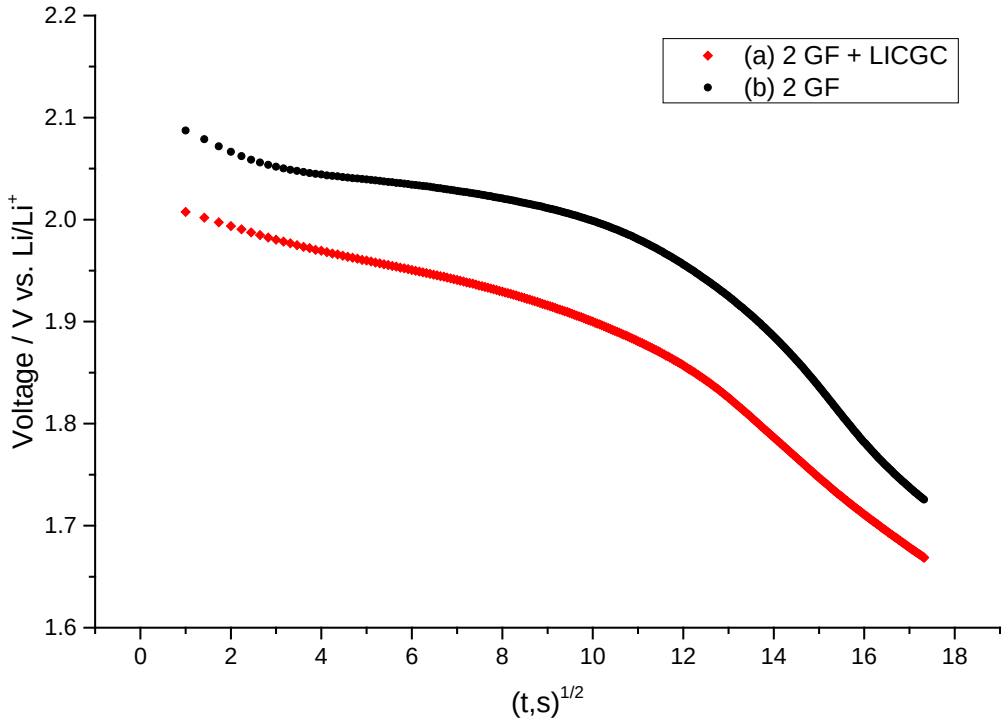

Figure 7.18 The transient voltage changes E vs. $t^{1/2}$ of region IV during the pulse of a single GITT process for Li/S cells containing (a) 2 GF + LICGC separators (red line), and (b) 2 GF separators (black line).

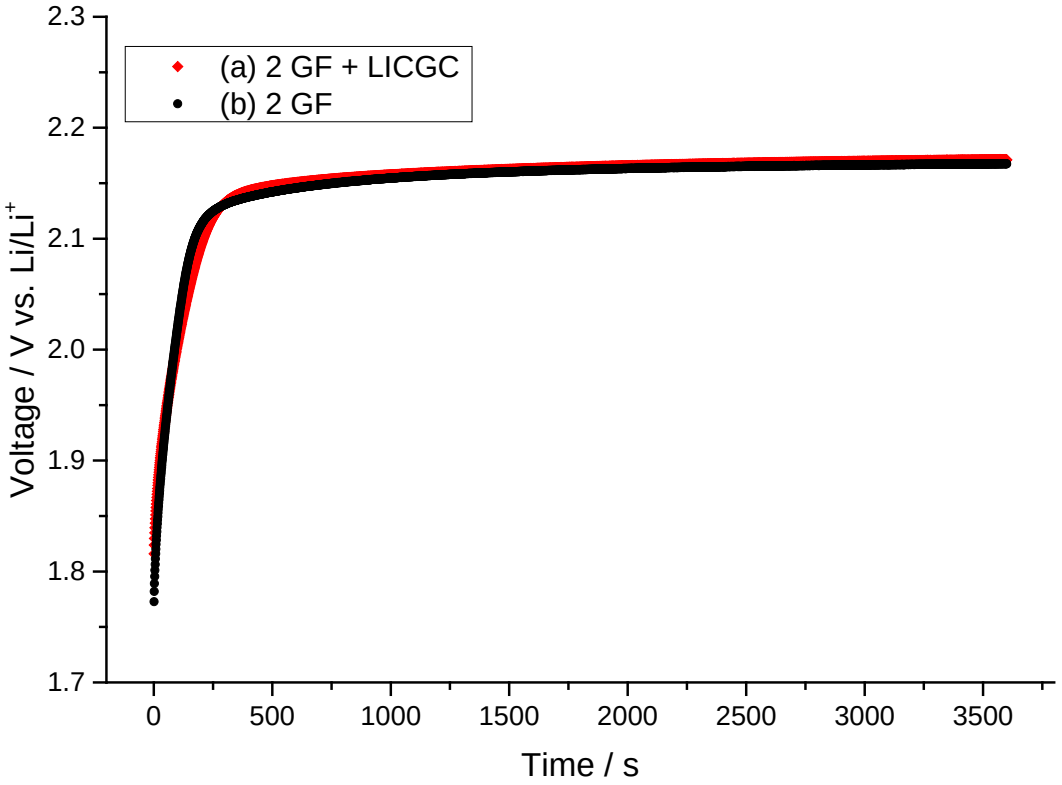

Figure 7.19 Voltage-time response of region IV during the relaxation of a single GITT process for the Li/S cells containing (a) 2 GF + LICGC separators (red line), and (b) 2 GF separators (black line). Note: the values of the times are normalized and the values of the voltages are corrected by IR drop.

7.5.3 The potential response during the GITT for the first charge

The GITT profiles during the first charge of Li/S cells containing (a) 2 GF with LICGC separators (red line), and (b) 2 GF separators (black line), and using 1M LiTFSI in TEGDME/DOL (1:1) measured at a C rate of 0.1 h^{-1}, are displayed in Figure 7.20. The charge profiles were divided into three regions (see Chapter 6 section 6.5).

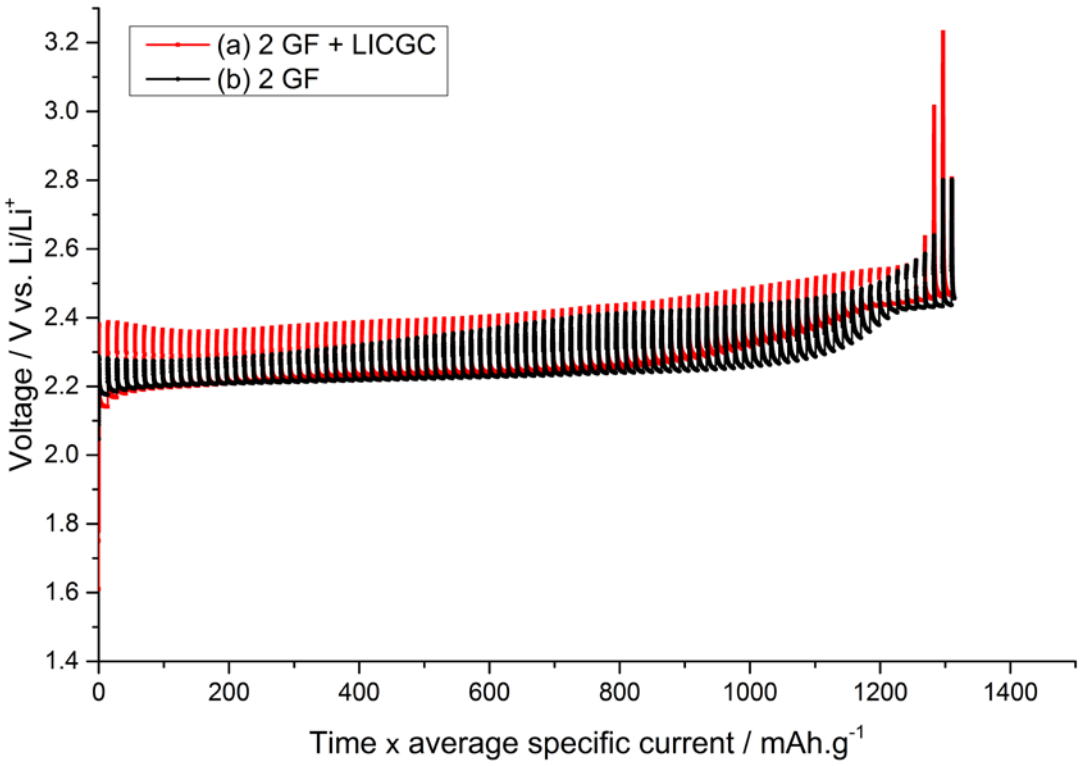

Figure 7.20 GITT profiles during the first charge of Li/S cells containing (a) 2 GF + LICGC separators (red line), and (b) 2 GF separators (black line). Using 1 M of LiTFSI in TEGDME/DOL (1:1), measured at a C rate of 0.1 h^{-1}, and using a 5 min pulse followed by a 60 min relaxation.

During the charge, a higher IR drop was also observed for the cell containing the LICGC separator (red line) related to the higher resistance of LICGC separator. In addition, the overall length of the GITT profile of the cell with the LICGC separator is almost the same as that for the cell without the LICGC separator. This is unexpected, because the length of the first discharge using the LICGC separator is longer than that for the normal cell. Therefore, it is expected that the charge will also be longer for the cell using the LICGC separator. The reason for this is not clear but could be related to the electrolyte decomposition that might occur in the cell with the LICGC separator during discharging the cell at a lower voltage.

7.5.3.1 The potential response during region V

A slow voltage increase is observed during this region in the charge profiles. Figure 7.21 displays the variation of cell voltage as a function of the square root of the time within region V, during the pulse of a single step of the GITT measurements for the Li/S cells using two GF with LICGC separators (red line), and two GF separators (black line). It can be seen that the E vs. $t^{1/2}$ plot for each cell gives almost a linear relationship over the entire time of each pulse. Moreover, a monotonic decrease in the voltage with the relaxation time was observed during region V for each cell, as shown in Figure 7.22.

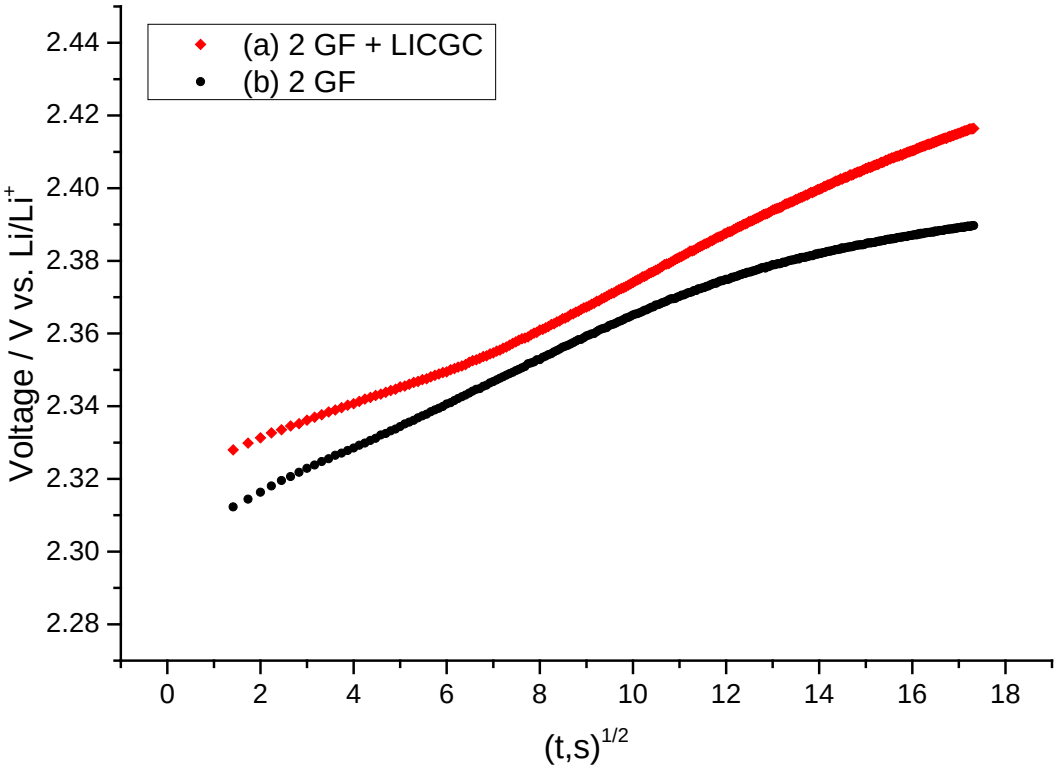

Figure 7.21 The transient voltage changes E vs. $t^{1/2}$ of region V during the pulse of a single GITT process for Li/S cells containing (a) 2 GF + LICGC separators (red line), and (b) 2 GF separators (black line).

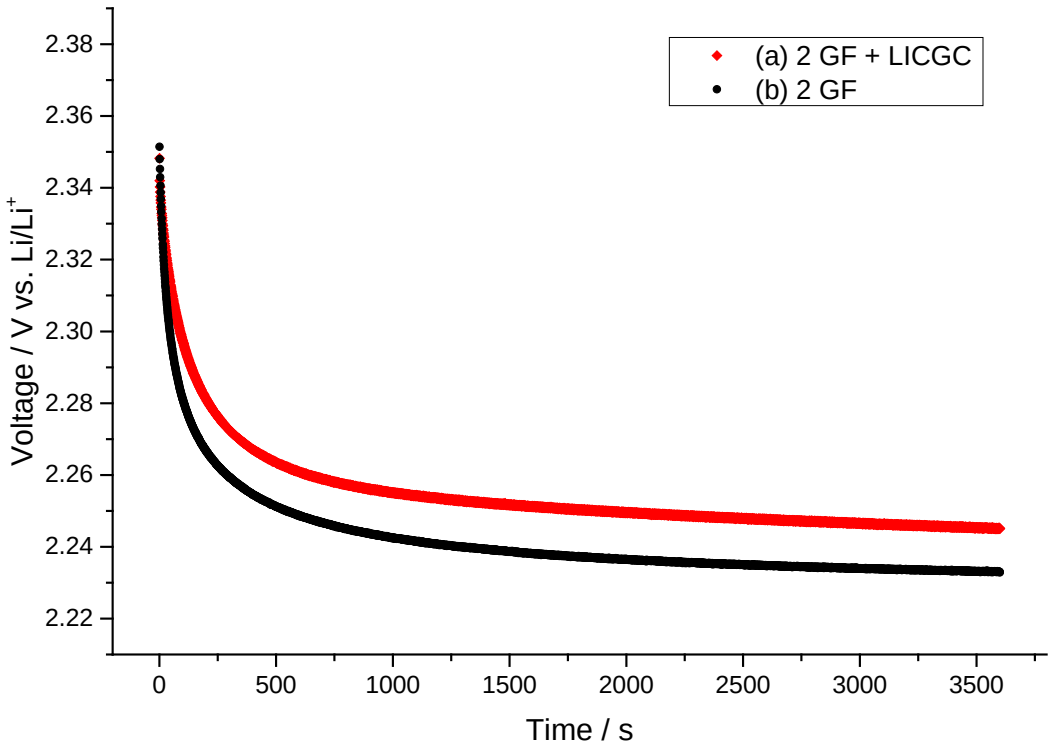

Figure 7.22 Voltage-time response of region V during the relaxation of a single GITT process for the Li/S cells containing (a) 2 GF + LICGC separators (red line), and (b) 2 GF separators (black line). Note: the values of the times are normalized and the values of the voltages are corrected by IR drop.

7.5.3.2 The potential response during region VI

The transient voltage change as a function of the square root of the time within region VI for each cell with and without the LICGC separator shows an almost straight line over the entire time of each pulse, as shown in Figure 7.23, which indicates that region VI is following the diffusion condition. In addition, each cell shows a monotonic decrease in the voltage with the relaxation time during region VI, as shown in Figure 7.24.

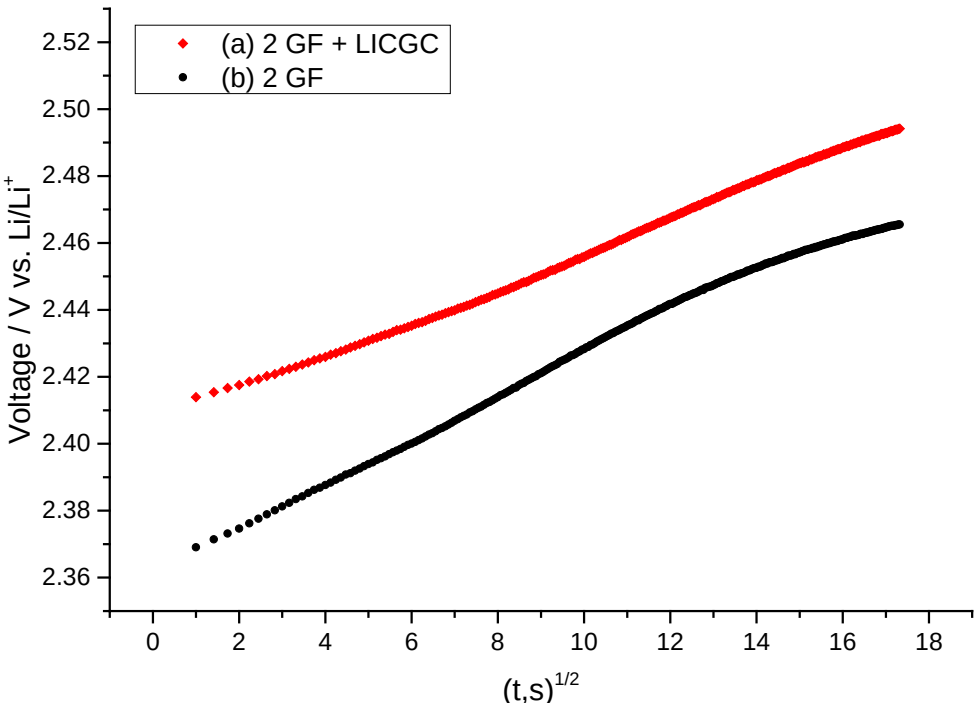

Figure 7.23 The transient voltage changes E vs. $t^{1/2}$ of region VI during the pulse of a single GITT process for Li/S cells containing (a) 2 GF + LICGC separators (red line), and (b) 2 GF separators (black line).

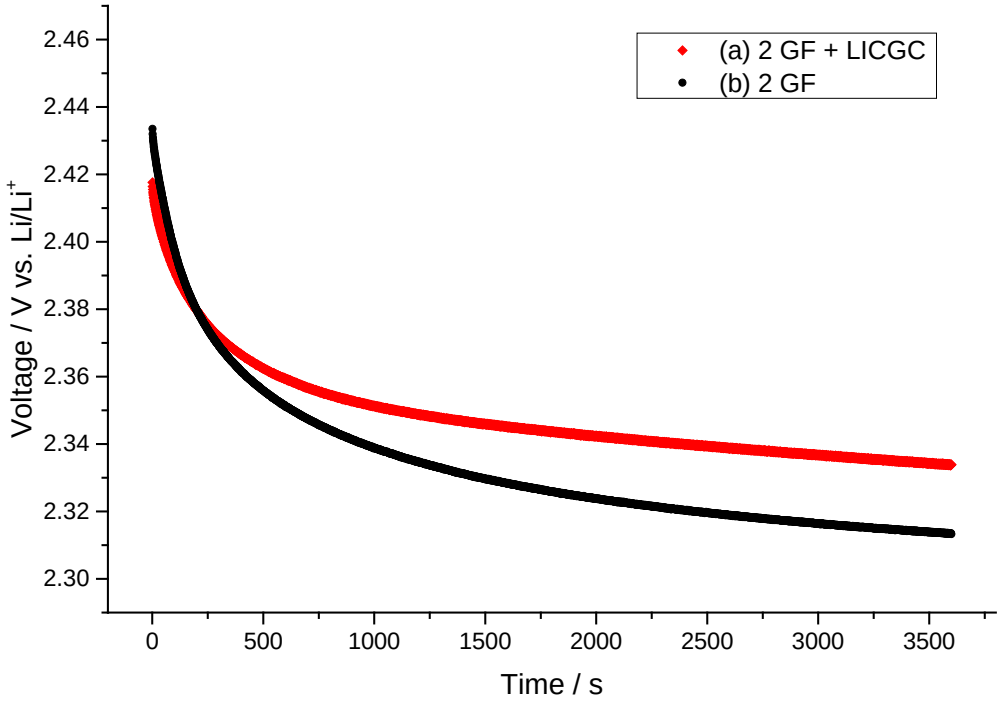

Figure 7.24 Voltage-time response of region VI during the relaxation of a single GITT process for the Li/S cells containing (a) 2 GF + LICGC separators (red line), and (b) 2 GF separators (black line). Note: the values of the times are normalized and the values of the voltages are corrected by IR drop.

7.5.3.3 The potential response during region VII

This region represents the final stage of the charge, which involves the production of elemental sulfur. The variation of cell voltage as a function of the square root of the time within region VII, during the pulse of a single step of the GITT measurements for the Li/S cells using two GF with LICGC separators (red line), and two GF separators (black line), is shown in Figure 7.25. It can be seen that the transient voltage change for each cell has a good linearity with the square root of charge time within this region. This indicates that region VII is following the diffusion condition. In addition, a monotonic decrease of the voltage with the relaxation time was also observed for each cell, as shown in figure 7.26.

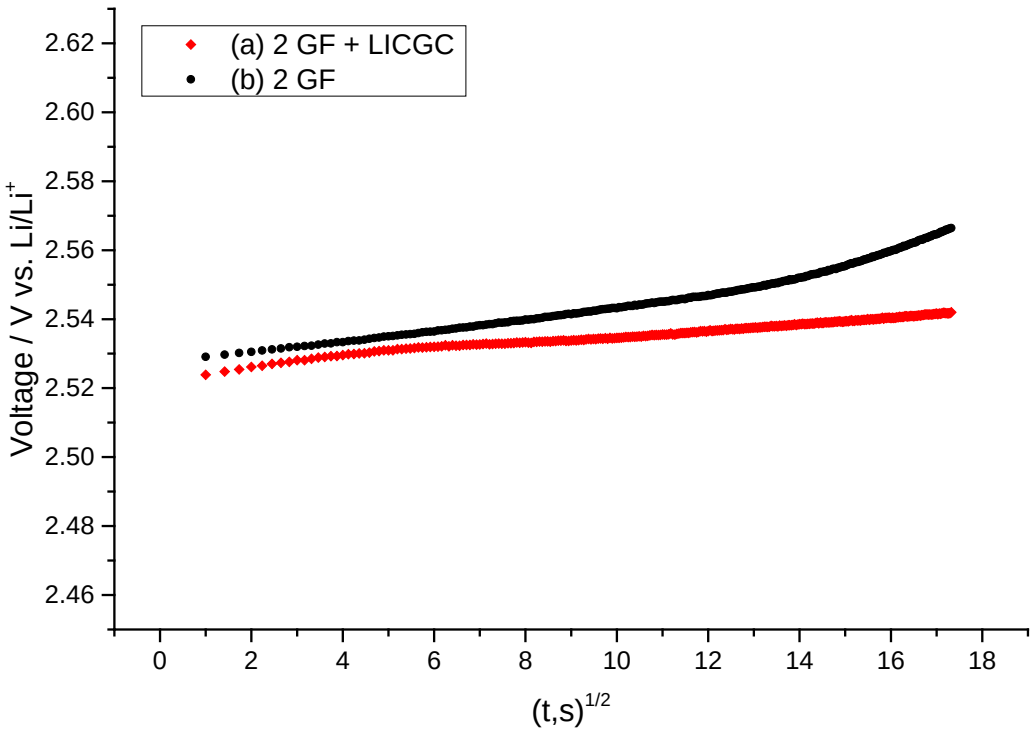

Figure 7.25 The transient voltage changes E vs. $t^{1/2}$ of region VII during the pulse of a single GITT process for Li/S cells containing (a) 2 GF + LICGC separators (red line), and (b) 2 GF separators (black line).

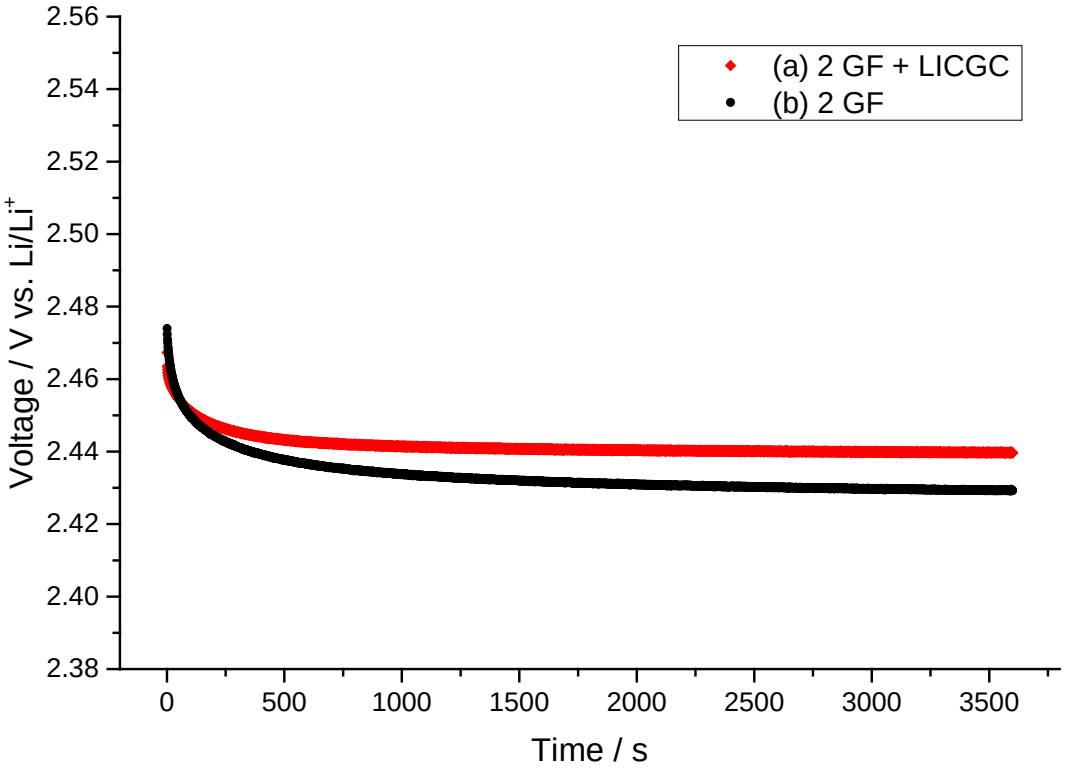

Figure 7.26 Voltage-time response of region VII during the relaxation of a single GITT process for the Li/S cells containing (a) 2 GF + LICGC separators (red line), and (b) 2 GF separators (black line). Note: the values of the times are normalized and the values of the voltages are corrected by IR drop.

7.5.4 Determination of the diffusion coefficients of Li/S cells

The diffusion coefficients calculated from the GITT profiles during the discharge of Li/S cells using two GF with LICGC separators (red line), and two GF separators (black line), are shown in Figures 7.27. These values were calculated using the equation below:[18]

$$D = \frac{4L^2}{\pi\tau}\left(\frac{\Delta E_s}{\Delta E_t}\right)^2 \qquad (7.3)$$

It can be see that the diffusion coefficient determined at the start of the GITT experiment are about 2.6 × 10^{-7} $cm^2.s^{-1}$ for the cell using only GF separators, which is higher than that reported recently by Yang *et. al.*,[19] with a diffusion coefficient start from about 10^{-10} $cm^2.s^{-1}$ using 1 M LiTFSI in DOL/DME (1:1). After that, the cell shows a fast decrease in the diffusion coefficient within region I to become about 8.4 × 10^{-9} $cm^2.s^{-1}$ at the end of region I, which might be associated with the rise of the viscosity resulting from the high lithium polysulfide formation within this region.

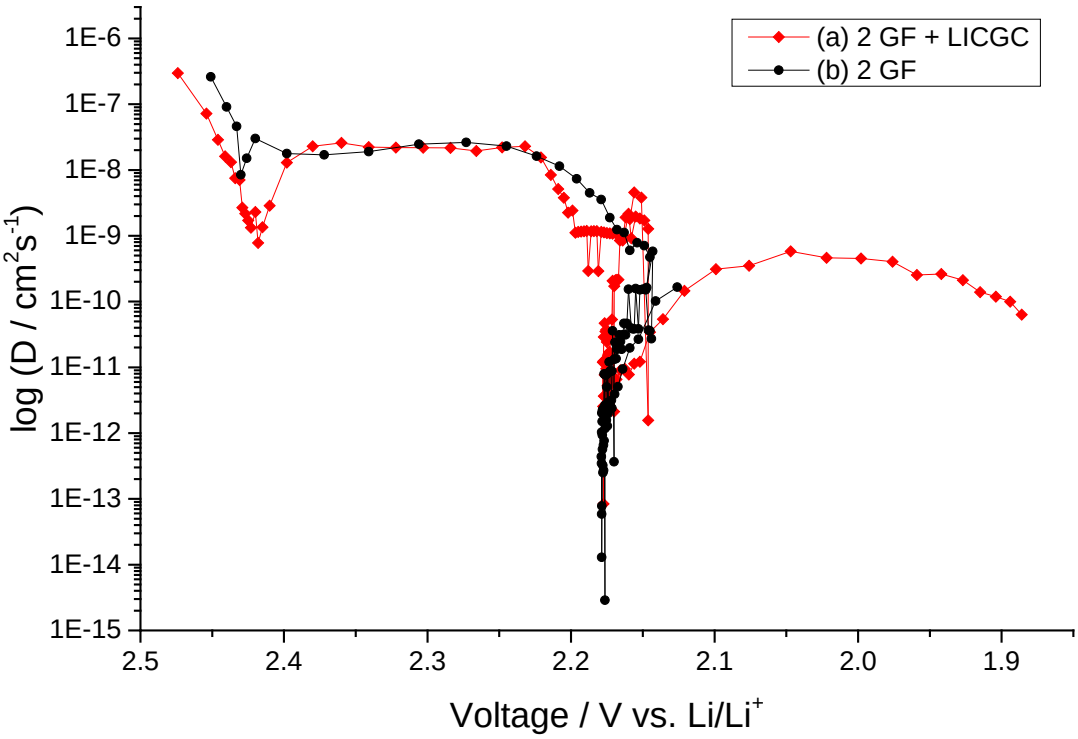

Figure 7.27 The diffusion coefficients as a function of discharge voltage derived from GITT date in the first discharge of Li/S cells containing (a) 2 GF + LICGC separators (red line), and (b) 2 GF separators (black line).

Then the diffusion coefficient start to increase and stabilise within the first part of region II at about 2.5×10^{-8} $cm^2.s^{-1}$ as low order polysulfides start being generated, followed by a gradual decrease within the second part of region II. The gradual decrease continued within region III to reach the lowest value of about 6×10^{-14} $cm^2.s^{-1}$ at the end of region III, as shown clearly in Figure 7.28, which displays the diffusion coefficients as a function of x Li_2S. This decrease in the diffusion coefficient can be attributed to the deposition of solid products, which might hinder the diffusion path. During region IV, the diffusion starts increase again to reach about 1.66×10^{-10} $cm^2.s^{-1}$ at the end of the discharge process.

On the other hand, the cell containing the LICGC separator shows initial diffusion coefficient of about 2.97×10^{-7} $cm^2.s^{-1}$, which is very close to that observed for the cell without LICGC separator. This indicates that there is no significant effect of the LICGC separator on the diffusion at the beginning of the GITT measurements, and fast diffusion can be observed at the start of the reduction. A fast decline in the diffusion was also observed within region I similar to that observed for the normal cell but with lower value of about 7.8×10^{-10} $cm^2.s^{-1}$. It may be suggested that this is mainly due to the high viscosity of high order polysulfides which are more prevalent in the case of LICGC separator than for conventional separator, which may reduce the polysulfides by the shuttle reaction.

After that, the diffusion coefficient start rises again during the first part of region II and stabilise for the rest of this part at about 2.5×10^{-8} $cm^2.s^{-1}$, which correspond to the formation of low order polysulfides with lower viscosity. Then, the diffusion coefficient starts decrease again to about 1.1×10^{-9} $cm^2.s^{-1}$ and stabilised at this value within the second part of region II. During region III, the diffusion increases a little and then decreases to reach its lowest value of about 2×10^{-12} $cm^2.s^{-1}$,

Moreover, an increase of the diffusion followed by decrease of the diffusion was observed during region IV. This might be due to the decrease of the electrolyte viscosity resulted from precipitation of solid product in the first phase and then a thick deposition layer formation in the second. It may be noted that the very low values of the effective diffusion coefficients may arise from a true plateau in the relaxed potential ΔE_s , related to two-phase equilibrium where the usual GITT equation is inapplicable.

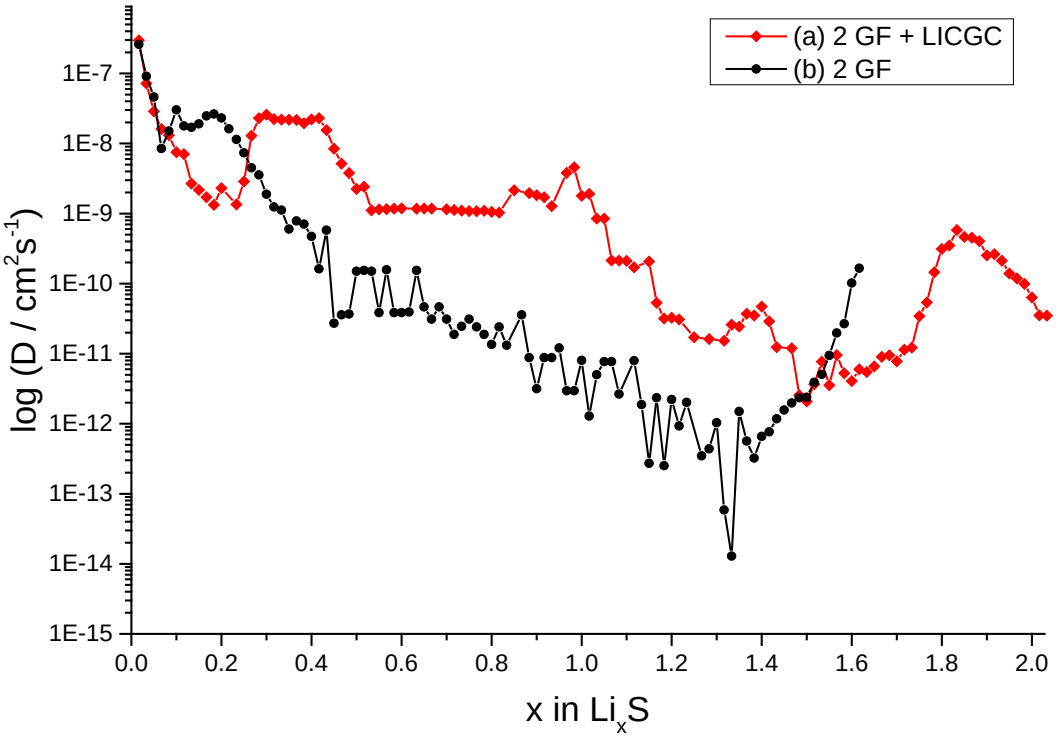

Figure 7.28 The diffusion coefficients as a function of of x in Li_2S derived from GITT date in the first discharge of Li/S cells containing (a) 2 GF + LICGC separators (red line), and (b) 2 GF separators (black line).

7.6 Conclusion

The electrochemical performance of Li/S cells with the LICGC separator shows a higher discharge capacity of about 1340 $mAh.g^{-1}$ of S compared to 1075 $mAh.g^{-1}$ of S for the cell that uses only GF separators. The much poorer capacity of the cell without the LICGC separator compared to that with the LICGC separator is believed to be associated with the diffusion of the sulfur and polysulfide species between the positive and negative electrodes, which cause the self-discharge of the cell. This is commensurate with the OCV results which reveal that using the LICGC separator effectively prevents the shuttle reaction and thus eliminates the self-discharge.

A good agreement with the above results was also observed during the GITT measurements. The voltage decline resulted from the self-discharge that was observed in the early stages of the discharge (region I and the 1^{st} part of region II) in the normal cell using only GF separators, disappeared in the cell uses the LICGC separator and a monotonic increase in the voltage was observed, which indicates the elimination of the self-discharge. The biggest success of the LICGC separator is to allow the GITT experiment to be interpreted in a normal way without any distortion caused by the shuttle reaction.

Analysis of the GITT experiments for Li/S cells with/without an LICGC separator reveals that the linear relationship of the transient voltage changes as a function of the square root of the time is successfully achieved using an LICGC separator, which indicates that the diffusion condition can be accomplished in an Li/S battery containing an LICGC separator. The linear relationship was observed within the whole GITT process, except in region IV, which shows a distortion from linearity, possibly occurring as a result of the deposition of solid products on the cathode surface, and thus blocking the diffusion path.

In addition, the diffusion coefficient using LICGC separator was calculated, and it show an initial value of about 2.97×10^{-7} $cm^2.s^{-1}$ which similar to that calculated for the normal cell. Also, the diffusion coefficient varied during the GITT experiment using LICGC separator, but this variation is more severe for the normal cell.

7.7 References

(1) Ji, X.; Lee, K. T.; Nazar, L. F. *Nat. Mater.* **2009**, *8*, 500–6.

(2) Jayaprakash, N.; Shen, J.; Moganty, S. S.; Corona, A.; Archer, L. A. *Angew. Chem.* **2011**, *123*, 6026–6030.

(3) Demir-Cakan, R.; Morcrette, M.; Nouar, F.; Davoisne, C.; Devic, T.; Gonbeau, D.; Dominko, R.; Serre, C.; Férey, G.; Tarascon, J.-M. *J. Am. Chem. Soc.* **2011**, *133*, 16154–60.

(4) Yang, Y.; Yu, G.; Cha, J. J.; Wu, H.; Vosgueritchian, M.; Yao, Y.; Bao, Z.; Cui, Y. *ACS Nano* **2011**, *5*, 9187–93.

(5) Qiu, L.; Zhang, S.; Zhang, L.; Sun, M.; Wang, W. *Electrochim. Acta* **2010**, *55*, 4632–4636.

(6) Xiao, L.; Cao, Y.; Xiao, J.; Schwenzer, B.; Engelhard, M. H.; Saraf, L. V; Nie, Z.; Exarhos, G. J.; Liu, J. *Adv. Mater.* **2012**, *24*, 1176–81.

(7) Aurbach, D.; Pollak, E.; Elazari, R.; Salitra, G.; Kelley, C. S.; Affinito, J. *J. Electrochem. Soc.* **2009**, *156*, A694.

(8) Lin, Z.; Liu, Z.; Fu, W.; Dudney, N. J.; Liang, C. *Adv. Funct. Mater.* **2013**, *23*, 1064–1069.

(9) Lin, Z.; Liang, C. *J. Mater. Chem. A* **2015**, *3*, 936–958.

(10) Hayashi, A.; Ohtsubo, R.; Ohtomo, T.; Mizuno, F.; Tatsumisago, M. *J. Power Sources* **2008**, *183*, 422–426.

(11) Nagao, M.; Hayashi, A.; Tatsumisago, M. *Electrochim. Acta* **2011**, *56*, 6055–6059.

(12) Nagao, M.; Imade, Y.; Narisawa, H.; Watanabe, R.; Yokoi, T.; Tatsumi, T.; Kanno, R. *J. Power Sources* **2013**, *243*, 60–64.

(13) Huang, J.-Q.; Zhang, Q.; Peng, H.-J.; Liu, X.-Y.; Qian, W.-Z.; Wei, F. *Energy Environ. Sci.* **2014**, *7*, 347.

(14) Hagen, M.; Dörfler, S.; Althues, H.; Tübke, J.; Hoffmann, M. J.; Kaskel, S.; Pinkwart, K. *J. Power Sources* **2012**, *213*, 239–248.

(15) Shim, J.; Striebel, K. a.; Cairns, E. J. *J. Electrochem. Soc.* **2002**, *149*, A1321.

(16) Kolosnitsyn, V. S.; Karaseva, E. V. *Russ. J. Electrochem.* **2008**, *44*, 506–509.

(17) Park, J.-W.; Yamauchi, K.; Takashima, E.; Tachikawa, N.; Ueno, K.; Dokko, K.; Watanabe, M. *J. Phys. Chem. C* **2013**, *117*, 4431–4440.

(18) Wen, C. J.; Boukamp, B. A.; Huggins, R. A.; Weppner, W. *J. Electrochem. Soc.* **1979**, *126*, 2258–2266.

(19) Yang, C.-P.; Yin, Y.-X.; Guo, Y.-G.; Wan, L.-J. *J. Am. Chem. Soc.* **2015**, *137*, 2215–2218.

Chapter 8:

Conclusions and Further work

8.1 Conclusions

This research has looked at the electrochemical performance of sulfur/acetylene black composite prepared via the ball milling method, in different electrolyte systems. It was found that for sulfolane-based electrolytes there is no significant difference in the cyclic voltammetry and discharge capacity results with the change of lithium salt. On the contrary, changing the solvent has important effect on the electrochemical performance of the lithium/sulfur cell. Highest discharge capacity and better reversibility were achieved by the electrolyte containing 1,3-dioxolane. The viscosity difference between these electrolytes explains these results in terms of their penetration into the sulfur electrode structure as well as the diffusion rate of lithium ion and the dissolution rate of the solid active materials.

Sulfur/acetylene black composites were simply prepared using the direct precipitation method, and the effect of the S/AB ratio in the composites on the electrochemical performance of the cells was investigated. It was found that using the surfactant, and adding acetylene black after the reaction, helps to reduce the size of the sulfur particles, and thus increase the electrode surface area which provide a better electrical contact between sulfur and acetylene black. The results also show a dependence of the discharge capacity on the amount of AB. Increasing the AB content in the electrode effectively increases the discharge capacity of the cell, as a result of increase the contact area between sulfur and acetylene black and also enhances the electronic the conductivity of the electrode.

The investigation on the first discharge capacity revealed that changing the ratio of acetylene black to the total mass of the electrode has no effect on the length of the first plateau in the potential. On the other hand, as the amount of acetylene black decreased, the length of the second plateau decreased. This result was explained by the increase in the passivation layer thickness and/or the decrease in available electrochemical surface area.

The comparison between the direct precipitation method and the ball milling method was also investigated. It was found that the precipitation method gives beneficial effects on the enhancement of discharge capacity and cycle life performance of lithium/sulfur cell. The precipitation method is more effective for a good distribution of sulfur with

acetylene black and obtaining a uniform S/AB composite, and providing smaller particles that lead to more conductive composite material. Higher electrode surface area leads to formation of a thinner passivation layer, and reduces the diffusion of lithium polysulfide species away from the cathode due to the smaller pores that form after the complete dissolution of elemental sulfur into the electrolyte during the discharge. Thus increases the capacity and the utilization of sulfur as an active material. Although, the precipitation method improves the cycle life performance of S/AB composite, it does not completely eliminate capacity loss of the material due to irreversible capacity loss upon cycling.

A simple model of the self-discharge has been proposed that is capable to reproduce experimental data very well under a range of conditions. This model clearly shows that there are two mechanisms of sulfur loss from the sulfur electrode: dissolution across a concentration gradient and reaction with polysulfides formed at the lithium electrode. The model explains quantitatively why increasing the distance between the sulfur and lithium electrodes decreases the rate of self-discharge, since the sulfur and polysulfides have to travel over a longer distance. The model also explains why increasing the amount of carbon in the sulfur electrode slows down the self-discharge: the decrease in the open circuit voltage is “buffered” by the capacitive behaviour of carbon. Once polysulfides reach the sulfur electrode, they undergo a partial oxidation to sulfur, which is coupled with charging the carbon interface with a negative surface charge. Finally, the model is also able to reproduce experimental data on the rate of self-discharge in sulfur containing electrolytes, where the self-discharge is faster, because the step of diffusion of sulfur from the sulfur electrode to the lithium electrode is no longer required.

The GITT technique was used in Li/S cell and a series of five experiments with different relaxations were performed in order to determine the optimum relaxation time. Analysis of the transient voltage change within the individual pulses at different states of discharge/charge reveals that the straight line of the E versus $t^{-1/2}$ plot cannot be obtained within the whole GITT measurements. It was found that for short relaxation times, the distortion from linearity might be related to the incomplete relaxation of these cells and the relaxation time was insufficient to allow the cell voltage to reach its steady-state value. By contrast, using long relaxation times shows a better relaxation

during which the electrode potential can get closer to the equilibrium condition that is required to validate the analysis procedure; however, under this condition the charge measurement will be affected by self-discharge during the early stages of the first discharge. However, no self-discharge was found through the analysis of the GITT measurement during the second discharge of cell 5/60. This indicates that the shuttle reaction was prevented within the second discharge, which might be attributed to the generation of an effective SEI layer on the Li anode surface.

The lithium ion conducting glass ceramic (LICGC) separator was successfully utilised as a shield to eliminate the shuttle reaction inside the Li/S cells. The electrochemical performance of Li/S cells with LICGC separator was investigated. It was found that there is no significant change in the cell voltage along the OCV experiment, which indicated insignificant self-discharge and that the shuttle reaction was effectively prevented using the LICGC separator. This is in good agreement with the galvanostatic discharge/charge results of Li/S cells with the LICGC separator, which delivered a higher discharge capacity than the normal cell using only glass fibre separators.

The Li/S cell with LICGC separator was also investigated using the GITT technique. No self-discharge was observed in this case, fulfilling the objective of using the LICGC separator. The analysis of the GITT experiment shows that a controlled diffusion condition can be achieved in a Li/S battery containing LICGC separator, since the change in the voltage as a function of the square root of the pulse time give a linear relationship within the whole GITT experiment, except in the final stage, which showed a distortion from linearity due to the precipitation of solid products on the cathode surface, an thus blocking the diffusion path.

8.2 Further work

Further work should improve the model for self-discharge in order to incorporate experiment-based data on the reaction of sulfur and polysulfide on the lithium electrode, as well as elucidating the length of the main shuttle species by analytical techniques. The effect of the acetylene black content on the rate of self-discharge demonstrate that additional factors may slow down the diffusion of sulfur and polysulfides between the electrodes (e.g. adsorption property of AB and the effective diffusion length due to the porous AB structure). More work is recommended in order to study these effects quantitatively.

During this work, a good understanding of the shuttle reaction and its effects on the electrochemical performance of Li/S cells has been obtained using LICGC separator. However, further investigation into the GITT technique using longer relaxation time would be useful in order to get very closer to equilibrium potential.

Finally, the theoretical analysis of the GITT should be complemented by automated analysis of the complex data set presented in a single cycle. This will require further mathematical curve fitting and software development.